Discovery of antibodies against PTH1R, a class B GPCR: Characterisation of their binding and impact on PTH1R function

Kaushik Sarkar

Department of Life Sciences

Imperial College London

Thesis submitted for the degree of Doctor of Philosophy
2018

Declaration

I declare that the work described within this thesis has been carried out by myself, unless stated otherwise. All sources of information within this thesis have been acknowledged.

Rabbit immunisation was performed by members of special facility unit (SFU) at UCB. Mass-spectrometry experiments and data analyses were performed by Dr Rebecca Burnley (UCB). Surface plasmon resonance (SPR) experiments with full-length receptors and subsequent data analyses were carried out by Dr Marta Westwood. Cryo-EM data collection and analysis was performed by Dr Jun He.

The copyright of this thesis rests with the author and is made available under a Creative Commons Attribution Non-Commercial No Derivatives licence. Researchers are free to copy, distribute or transmit the thesis on the condition that they attribute it, that they do not use it for commercial purposes and that they do not alter, transform or build upon it. For any reuse or redistribution, researchers must make clear to others the licence terms of this work.

Abstract

Parathyroid hormone receptor 1 (PTH1R) belongs to the Secretin or Class B family of the G-protein coupled receptor (GPCR) superfamily and natively binds parathyroid hormone (PTH) and parathyroid hormone related peptide (PTHrP). Ligand binding to PTH1R is a two-step process, which first involves binding to a large extracellular domain (ECD) and then to the extracellular loops (ECL). This in turn causes activation of the receptor by inducing conformational changes in the transmembrane domains. PTH1R plays a crucial role in bone metabolism and calcium homeostasis, signalling mainly through G_s and $G_{q/11}$ G-proteins. Here, we used phage display technology and immunisation followed by B-cell screening and isolation, to discover PTH1R-specific antibodies (mAbs) against the ECD and the ECL respectively. Antibody binding to the receptor was confirmed using ELISA, flow-cytometry and confocal microscopy. Intracellular cyclic AMP (cAMP) assay revealed that antibody binding had no effect on G-protein mediated signalling by the PTH1R. However, β-arrestin recruitment was down-regulated by the ECD specific antibody indicating that this antibody acts as a biased antagonist. These studies also highlighted that the ECL specific antibody acted as a neutral allosteric ligand (NAL). Affinity measurements by surface plasmon resonance using full-length receptor, solubilised in styrene-maleic acid copolymer (SMA), revealed binding affinities (K_D) of ~ 4 nM and ~0.9 nM for ECD and ECL specific antibodies respectively. Epitope mapping using hydrogen-deuterium exchange-mass spectrometry (HDX-MS) indicated that the ECD antibody binding site had some overlap with the known PTH binding region of the ECD. HDX-MS also indicated that the ECL specific mAb bound to ECL-1. To the best of our knowledge, the ECD binding antibody is the first PTH1R antibody showing antagonism of β-arrestin recruitment. The ECL specific antibody, although not exhibiting function in the range assays tested, is anticipated to be a useful tool for PTH1R structural studies using cryo-electron microscopy (cryo-EM) and/or X-ray crystallography.

Table of content

Declaration ---- 2
Abstract ---- 3
Table of content ---- 4
Table of Figures ---- 8
Table of table ---- 12
Abbreviations ---- 13
Acknowledgements ---- 17
1. Introduction ---- 19
1.1 G-protein coupled receptors ---- 20
1.1.1 Classification of GPCRs ---- 21
1.1.2 GPCR Ligands ---- 23
1.1.3 G-protein mediated signalling ---- 25
1.1.4 Structural elucidation of GPCR-G-protein binding ---- 26
1.1.5 GPCR β-arrestin interaction ---- 28
1.1.6 Structural characteristics of arrestin binding and desensitisation ---- 29
1.2 Secretin Family (Class B) GPCR ---- 32
1.2.1 Secretin family ---- 32
1.2.2 Structural insights into the class B-secretin family ---- 35
1.3 Parathyroid hormone receptor family ---- 42
1.3.1 Physiological importance of PTH1R ---- 43
1.3.2 Structural insights into PTH binding ---- 45
1.3.3 PTH1R activation ---- 47
1.3.4 PTH1R desensitisation and role of arrestins ---- 47
1.3.5 Other GPCR interacting proteins (GIP) modulating PTH1R ---- 49
1.4 GPCR expression and stabilisation ---- 51
1.4.1 Expression systems ---- 51
1.4.2 Receptor stabilisation and extraction methods ---- 52
1.5 Antibodies as therapeutics ---- 60
1.5.1 Generation of therapeutic antibodies ---- 61
1.6 Antibodies against GPCR targets ---- 66
2. Antibody generation against PTH1R extra-cellular domain (ECD) using phage display technology ---- 75
2.1 Introduction ---- 75
2.2 Material and Methods ---- 78

2.2.1 Constructs ---- 78
2.2.2 ECD expression purification and characterisation ---- 79
2.2.3 Phage display against PTH1R ECD ---- 82
2.2.4 Screening for phage binders ---- 84
2.2.5 Medium-scale expression of selected phage hits as scFv-Fc ---- 87
2.2.6 Binding of purified scFv-hFc to PTH1R expressing cells using Flow cytometry 88
2.2.7 Kinetics of ECD binding using Surface Plasmon Resonance (SPR) ---- 88
2.2.8 Functional characterisation of phage derived antibodies ---- 89
2.3 Results ---- 91
2.3.1 Constructs ---- 91
2.3.2 PTH1R ECD is pure and functional ---- 92
2.3.3 Phage display outcome and sequence diversity analysis ---- 95
2.3.4 A selection of ECD binders also bind to full-length PTH1R on cells. ---- 97
2.3.5 Final selection based on cell surface binding and PTH competition using HTFC ---- 99
2.3.6 Binding confirmation of purified scFv-huFc using flow-cytometry ---- 102
2.3.7 PD12 has low nanomolar affinity for soluble ECD ---- 104
2.3.8 PD12 exhibits weak cAMP antagonism ---- 106
2.4 Discussion ---- 107

3. Antibody generation against PTH1R extracellular loops using UCB core discovery approach ---- 111

3.1 Introduction to Core discovery approach ---- 111
3.2 Materials and Methods ---- 115
3.2.3 Materials ---- 115
3.2.4 PTH1R construct generation ---- 115
3.2.5 Rabbit fibroblast transfection and surface expression analysis using flow cytometry ---- 117
3.2.6 Rabbit immunisation ---- 118
3.2.7 B-cell culture set up ---- 120
3.2.8 Primary screening using fluorescence cytometry (Mirrorball) ---- 122
3.2.9 Secondary screening using FMAT ---- 122
3.2.10 B-cell foci picking using cell expressing receptor ---- 123
3.2.11 Primary, secondary and TAP PCR ---- 124
3.2.12 FMAT analysis of TAP products and selection of binders ---- 125
3.2.13 Sequencing and cloning of final hits ---- 126
3.2.14 Expression and purification of a selected rabbit IgG ---- 126
3.2.15 Cell surface expressed PTH1R binding using flow-cytometry ---- 127

3.3 Results---------- 128
3.3.1 Immunisation constructs ---------- 128
3.3.2 Immunogen design and surface expression analysis ---------- 129
3.3.3 Rabbit sera titre analysis confirms immune response to PTH1R---------- 130
3.3.4 Primary screening to identify PTH1R-positive wells ---------- 132
3.3.5 Specific B-cell isolation using FMAT and fluorescent-foci picking---------- 133
3.3.6 Low diversity – one predominant sequence family ---------- 139
3.3.7 CoreAb1 IgG was purified to homogeneity ---------- 139
3.3.8 CoreAb1 IgG binds to the extracellular loop of PTH1R---------- 140
3.4 Discussion ---------- 142
4. PTH1R over-expression, extraction using SMA and detergents---------- 147
4.1 Introduction ---------- 147
4.2 Materials and methods---------- 152
4.2.1 PTH1R constructs for expression and purification ---------- 152
4.2.2 Over-expression using suspension cell line (Expi293)---------- 154
4.2.3 Surface expression analysis using flow cytometry and fluorescence microscopy ---------- 154
4.2.4 Functional characterisation using cAMP assay---------- 155
4.2.5 Large scale PTH1R construct expression and membrane preparation -------- 155
4.2.6 SMA extraction of PTH1R constructs from Expi293 membranes ---------- 156
4.2.7 Detergent extraction of PTH1R constructs from Expi293 membranes--------- 157
4.2.8 Affinity purification of solubilised receptor---------- 157
4.2.9 Size exclusion chromatography (SEC) purification of Strep-Tactin XT® purified receptor---------- 159
4.2.10 Characterisation using SDS-PAGE and analytical SEC chromatography --- 159
4.3 Results---------- 159
4.3.1 Full-length and ECD-truncated PTH1R shows successful surface expression and trafficking ---------- 159
4.3.2 Expression constructs are functional and modulate cAMP ---------- 163
4.3.3 WT2 and ΔN2 expression constructs are unstable and exhibit poor SMA solubilisation---------- 165
4.3.4 Surface expression and in vitro function of C-terminal truncated constructs remain unaffected ---------- 168
4.3.5 Strep-Tactin XT improves purification of both SMA and detergent solubilised ΔC29-491 and ΔNΔC171-491 constructs ---------- 171
4.3.6 Generation of pure ΔNΔC171-491 PTH1R construct ---------- 173

4.4 Discussion ---------- 175

5. Biophysical and functional analysis of phage and core antibodies binding to full-length PTH1R ---------- 180

5.1 Introduction ---------- 180

5.1.1 PTH1R signalling ---------- 180

5.1.2 Hydrogen-Deuterium Exchange – Mass spectrometry (HDX-MS) as a tool for epitope mapping ---------- 181

5.1.3 Emerging role of CryoEM in GPCR structural biology ---------- 183

5.2 Material and methods ---------- 185

5.2.1 Functional characterisation of ECD binding (ECD-mAb) and core-derived loop binding (ECL-mAb) antibody ---------- 185

5.2.2 Binding kinetics of ECD-mAb and ECL-mAb using surface plasmon resonance (SPR) ---------- 186

5.2.3 Reformatting ECD-mAb and ECL-mAb to Fab format ---------- 187

5.2.4 ECD-mAb and ECL-mAb Fab expression and purification ---------- 188

5.2.5 Hydrogen-Deuterium Exchange- Mass spectrometry (HDX-MS) analysis of ECD-mAb and ECL-mAb antibody ---------- 189

5.2.6 ECL-mAb Fab and DDM stabilised ΔNΔC171-491 complexing and purification ---------- 191

5.2.7 Cryo-EM analysis of ECL-mAb Fab binding to DDM stabilised ΔNΔC171-491 ---------- 192

5.3 Results ---------- 192

5.3.1 ECD-mAb is a weak cAMP antagonist ---------- 192

5.3.2 ECD-mAb antagonises β-arrestin recruitment ---------- 194

5.3.3 ECL-mAb is a neutral allosteric ligand (NAL) ---------- 195

5.3.4 ECD-mAb and ECL-mAb binds the full-length receptor with high affinity ---------- 197

5.3.5 ECD-mAb binds to the N-terminal region of PTH1R ECD ---------- 199

5.3.6 ECL-mAb binds to the extra-cellular loop -1 of PTH1R ---------- 201

5.3.7 Cryo-EM allows visualisation of ECL-mAb: ΔNΔC171-491 complex ---------- 203

5.4 Discussion ---------- 207

6. Discussion and future work ---------- 213

Bibliography ---------- 220

Supplementary data ---------- 246

Table of Figures

Figure 1-1: A snake plot representation of the human β_2-adrenergic receptor, a widely studied receptor from GPCR superfamily. 20
Figure 1-2: Summary of G-protein mediated GPCR signalling cascades..... 21
Figure 1-3: A schematic plot showing the effects of agonists on biological response mediated by a GPCR..... 24
Figure 1-4: Overall topology of an inactive GDP-bound form of a heterotrimeric G-protein (PDB 1GOT (Lambright et al., 1996). 26
Figure 1-5: Crystal structure of activated β_2-AR in complex with heterotrimeric G-protein ... 27
Figure 1-6: Schematic representation of β-arrestin mediated receptor desensitisation..... 29
Figure 1-7: High resolution structure of visual arrestin in complex with activated Rhodopsin 31
Figure 1-8: Sequence alignment of the ECD of secretin-family receptors..... 33
Figure 1-9: Sequence alignment of extracellular loops, TM4 and 6 for the members of Secretin sub-family 34
Figure 1-10: Crystal structure of the CRF and GCGR transmembrane domains (TMDs)..... 36
Figure 1-11: Cryo-EM structure of salmon calcitonin (sCT) activated calcitonin receptor (CTR) bound to heterotrimeric G-protein..... 38
Figure 1-12 : Cryo-EM structure of GLP1-activated GLP1R in complex with heterotrimeric G-protein..... 40
Figure 1-13: The orthosteric binding site of GLP1R..... 41
Figure 1-14: Key residues of GLP1R ECL-1 interacting with GLP. 42
Figure 1-15: Snake diagram of PTH1R 43
Figure 1-16: PTH binding to the PTH1R ECD binding. 46
Figure 1-17: Arrestin-selective PTH1R agonism..... 48
Figure 1-18: GPCR interacting protein (GIP) interaction sites. 50
Figure 1-19: Nanobody and Fab as crystallographic chaperones..... 57
Figure 1-20: A schematic representation of SMALP stabilisation 60
Figure 1-21: Schematic representation of phage library panning..... 63
Figure 1-22: Schematic representation of hybridoma technology 64
Figure 1-23: mAb discovery workflow..... 72
Figure 1-24: Receptor expression, purification and mAb characterisation workflow. 73
Figure 2-1: A brief overview of discovery and screening pipeline used for the antibody discovery against PTH1R ECD using phage display. 77
Figure 2-2: A schematic representation of the cAMP assay in agonist and antagonist mode. 90

Figure 2-3: PTH1R and PTH1R-ECD constructs used for phage display and selection process. 91
Figure 2-4: SDS-PAGE analysis of fractions from ECD purification 92
Figure 2-5: Western blot detection and effect of deglycosylation of purified ECD. 93
Figure 2-6: LC/MS analysis of ECD sample for molecular weight determination 94
Figure 2-7: Isothermal Titration Calorimetry data showing binding of ECD and PTH (1-34). 95
Figure 2-8: Phage ELISA results and a schematic representation of specific and non-specific binding 96
Figure 2-9: A schematic diagram of the TAP method and agarose gel analysis of TAP products. 97
Figure 2-10: FMAT assay to test expression and cell-surface binding of TAP products..... 98
Figure 2-11: iQue analysis of shortlisted ECD binders 100
Figure 2-12: Selection of final ECD-binding clones based on cell-surface binding and PTH competition 101
Figure 2-13: Sequence alignment and SDS-PAGE analysis of selected scFv-Fc 102
Figure 2-14: Cell-surface binding confirmation of purified scFv-hFc using flow-cytometry . 103
Figure 2-15: Immobilisation strategy for ECD-binding kinetics measurement and representative sensorgrams. 104
Figure 2-16: Cyclic-AMP (cAMP) regulation by ECD binders on CHOK1 cells stably expressing PTH1R. 106
Figure 3-1: UCB Core discovery platform for high-throughput mAb discovery and screening 113
Figure 3-2: A brief overview of the work-flow for discovering loop-binding antibodies against PTH1R post immunisation..... 114
Figure 3-3: PCR-mediated deletion of PTH1R extra-cellular domain (ECD). 116
Figure 3-4: Schematic representation of three constructs used for rabbit immunisation 128
Figure 3-5: Flow-cytometry analysis of PTH1R cell surface expression in transiently transfected rabbit fibroblast cells. 129
Figure 3-6: Rabbit immunisation with cells expressing PTH1R receptor and sera titre analysis. 131
Figure 3-7: A schematic representation of mirroball fluorescence cytometry assay 132
Figure 3-8: Primary screening of the cultured B-cells for cell-surface binding using Mirrorball. 133
Figure 3-9: FMAT assay set up and final data for a selection of supernatants. 134
Figure 3-10: Foci picking using Expi293 cells expressing ΔN PTH1R constructs. 136
Figure 3-11: Foci picking strategy and agarose gel analysis of secondary PCR products . 137

Figure 3-12: Representative FMAT data using TAP products to confirm successful sequence isolation, antibody expression and cell-surface binding 138
Figure 3-13: CDR sequence diversity among the selected clones..... 139
Figure 3-14: Protein A purification and SDS-PAGE gel analysis of CoreAb1 rabbit IgG. ... 140
Figure 3-15: Flow cytometry analysis of CoreAb1 IgG..... 141
Figure 3-16: Alignment showing sequence diversity between human and rabbit PTH1R ECL sequence 143
Figure 4-1: Detergent micelle formation and membrane protein solubilisation..... 149
Figure 4-2: PTH1R expression, extraction and purification workflow. 151
Figure 4-3: Overlap extension PCR coupled with site-directed mutagenesis to generate WT2 and ΔN2 constructs..... 153
Figure 4-4: Schematic representation of WT1, 2 and ΔN2 constructs 160
Figure 4-5: PTH1R WT2 and ΔN2 construct expression by flow-cytometry 161
Figure 4-6: Fluorescence microscopy to determine receptor localisation..... 162
Figure 4-7: Functional characterisation of PTH1R WT2 and ΔN2 constructs using cAMP assay 164
Figure 4-8: Variability in the PTH concentration-dependent responses between stable and transiently transfected cells 165
Figure 4-9: SMA solubilisation and IMAC purification of WT2 construct. 166
Figure 4-10: SMA extraction and IMAC purification of ΔN2 construct..... 167
Figure 4-11: DISOPRED 3 analysis of PTH1R and C-terminal tail truncated construct schematic..... 168
Figure 4-12: Expression and cell-surface localisation of the C-terminal tail truncated receptor using flow-cytometry and fluorescence microscopy..... 169
Figure 4-13: Functional characterisation of PTH1R ΔC29-491 and ΔNΔC171-491 constructs using cAMP assay 170
Figure 4-14: SDS-PAGE analysis of Talon (Co^{2+}) and Strep-Tactin XT enriched ΔC29-491 and ΔNΔC171-491 PTH1R constructs. 172
Figure 4-15: SDS-PAGE analysis of Strep-Tactin XT purified DDM and LMNG solubilised ΔC29-491 and ΔNΔC171-491 constructs. 173
Figure 4-16: Affinity and gel-filtration purification of ΔNΔC171-491 construct..... 174
Figure 5-1: Schematic representation of HDX-MS analysis and its use in epitope mapping. 182
Figure 5-2: The variable and constant domains of ECD-mAb (A) and ECL-mAb (B) Fab fragment..... 188
Figure 5-3: cAMP antagonism by ECD-mAb scFvFc 193

Figure 5-4: β-arrestin recruitment agonism and antagonism by ECD-mAb scFvFc and Fab. 195
Figure 5-5: cAMP agonism and antagonism by loop binding ECL-mAb IgG 196
Figure 5-6: β-arrestin recruitment agonism and antagonism by ECL-mAb IgG 197
Figure 5-7: Binding kinetics analysis of ECD and ECL-mAb binding to purified PTH1R receptor constructs. 198
Figure 5-8: HDX-MS analysis of PTH1R ECD bound to ECD-mAb scFvFc 200
Figure 5-9: HDX-MS analysis of ECL-mAb binding to ΔNΔC171-491 201
Figure 5-10: Sequence coverage map and difference chart for ECD-mAb and ECL-mAb epitope mapping by HDX-MS 203
Figure 5-11: ΔNΔC171-491 – ECL-mAb complex purification using gel-filtration and fraction analysis using SDS-PAGE and Western blotting. 205
Figure 5-12: Cryo-EM micrographs showing receptor-Fab complex 206
Figure 5-13: Comparison of ΔNΔC171-491: ECL mAb particle size on cryo-EM grid with published structures. 211
Figure 6-1: A schematic summarising the function of ECD and ECL-mAb. 216

Table of table

Table 1-1: Summary of Secretin family receptors. Table adapted from (Hoare, 2007)..... 32
Table 1-2: Expression system to facilitate GPCR structure-function studies..... 51
Table 1-3: Fusion proteins used in GPCR stabilisation (Milić et al., 2015)..... 53
Table 1-4: A representative table of widely used detergents used for receptor solubilisation and structural studies..... 58
Table 1-5: Table summarising immunogen formats commonly used in mAb discovery against membrane-bound proteins. Table adapted from Hutchings et al., 2017..... 61
Table 1-6: FDA-approved mAbs derived using hybridoma technology (Arruebo et al., 2011; Zhang, 2012) 65
Table 1-7:mAbs against GPCR targets in clinical development..... 68
Table 2-1: A list of constructs used in this study..... 78
Table 2-2: Primers used for performing TAP PCR..... 85
Table 2-3: A table summarising the affinity measurement of scFv-hFc..... 105
Table 3-1: Primer sequences used for ECD deletion..... 116
Table 3-2: A summary of components added for culturing B-cell using UCB's core discovery automation..... 121
Table 3-3: A table of consolidated positive hits from the FMAT assay..... 135
Table 4-1: A summary of PCR primers used for overlap extension PCR..... 152
Table 4-2: Composition for wash and elution buffer used for Strep-Tactin XT purification . 158
Table 5-1: Table summarising the affinity measurement of ECD-mAb and ECL-mAb IgG binding to SMA-stabilised PTH1R constructs. 198

Abbreviations

µl	Microlitre
µM	Micromolar
µm	Micrometer
ADCC	Antibody-Dependent Cellular Cytotoxicity
ADCP	Antibody-Dependent Cellular Phagocytosis
Apols	Amphipols
ASPA	Animals Scientific Procedures Act
AT1AR	Angiotensin II type 1A receptor
ATP	Adenosine triphosphate
AWERB	Animal Welfare and Ethical Review Body
BCA	Bicinchoninic acid assay
B-cells	B-lymphocyte cells
BLyS	B Lymphocyte Stimulator
BMC	Blomstrand Chondrodysplasia
BMD	Bone Mineral Density
BRET	Bioluminescence resonance energy transfer
BRIL	Apocytochrome b_{562}RIL
BSA	Bovine Serum Albumin
cAMP	Cyclic-AMP
CDC	Complement-Dependent Cytotoxicity
CDR	Complementarity-Determining Regions
cfu	Colony Forming Units
CHO	Chinese Hamster Ovary
CHS	Cholesterol hemisuccinate
CRF1R	Corticotropin-relasing factor receptor -1
CV	Column Volume
DDM	Dodecyl Maltoside
DMSO	Dimethylsulphoxide
DTT	Dithiothreitol
Dvl	Dishevelled
E3KARP	Exchanger 3 kinase A regulatory protein
ECD	Extracellular Domain
ECL	Extracellular Loops
EDTA	Ethylenediaminetetra acetic acid

EFC	Enzyme fragment complementation technology
EGF	Epidermal Growth Factor
ELISA	Enzyme-linked immunosorbent assay
ERK	Extracellular signal–regulated kinases
Fab	Fragment antigen-binding
FBS	Fetal bovine serum
Fc	Crystallisable fragment
FcRn	Neonatal Fc receptor
FCS	Fetal calf serum
FDA	Food and drug administration
FITC	Fluorescein isothiocyanate
FMAT	Flurorescent microvolume assay technology
FSC	Forward scatter
Fv	Fragment variable
FZD	Frizzled
GCGR	Glucagon receptor
GDP	Guanosine diphosphate
GPCR	G-protein coupled receptor
GRK	G-protein receptor kinases
GTP	Guanosine triphosphate
HAT	Hypoxanthine-aminopterin-thymidine
HCl	Hydrochloric acid
HDX	Hydrogen-deuterium exchange
HEK293	Human embryonic kidney 293
HPLC	High performance liquid chromatography
HTFC	High throughput flow cytometry
HTRF	Homogenous time-resolved fluorescence
IBMX	3-isobutyl-1-methylxanthine
ICL	Intra-cellular loop
IgG	Immunoglobulin G
IMAC	Immobilised metal affinity chromatography
IMP	integral membrane protein
ITC	Isothermal titration calorimetry
JMC	Jansen’s metaphyseal chondrodysplasia
JNK	c-Jun N-terminal kinase

kDa	Kilodalton
LC/MS	Liquid chromatography- coupled to mass spectrometer
LMNG	Lauryl-maltose neopentyl glycol
mAb	Monoclonal antibody
MAPK	Mitogen- activated protein kinases
MOI	Multiplicity of infection
MWCO	Molecular weight cut-off
NAL	Neutral allosteric ligand
NAM	Negative allosteric modulator
NEM	N-ethyl maleimide
NHERF-2	Sodium hydrogen exchanger regulatory factor 2
nM	Nanomolar
nM	Nanomolar
Npols	Neutral amphipols
PAM	Positive allosteric modulator
PBS	Phosphate buffered saline
PCR	Polymerase Chain Reaction
PD	Pharmacodynamics
PK	Pharmacokinetics
PLC	Phospholipase C
PTH	Parathyroid hormone
PTH1R	Parathyroid hormone receptor- 1
PTHrP	Parathyroid hormone related peptide
scFv	Single-chain fragment variable
SDS-PAGE	Sodium dodecyl sulphate poly-acrylamide gel electrophoresis
SEC	Size exclusion chromatography
SLE	Systemic lupus erythematosus
SMA	Styrene-maleic acid
SMALP	Styrene-maleic acid lipid particles
SPR	Surface plasmon resonance
SSC	Side scatter
TAP	Transcriptionally-active PCR
TBS	Tris-buffered saline
TEV	Tobacco etch virus
TM	Transmembrane

TMD	Transmembrane domain
V2R	Human V2 vasopressin receptor
VFT	Venus-fly trap
WNT	Wingless and Int-1
WT	Wild-type
XFEL	X-ray free electron laser

Acknowledgements

Firstly, and most importantly, this work would not have been possible without the support of my three research supervisors: Prof Bernadette Byrne (Imperial College London), Dr Michael Wright (UCB, VRDE) and Dr David McMillan (UCB, PEP). Their unconditional support and guidance has been amazing and made my PhD journey much more enjoyable! Also, a special thanks to my PRPs: Dr Konstantinos Beis (Imperial) and Dr Karen Polizzi (Imperial).

Special thanks to Rebecca M for her help with immunisation and B-cell screening, Lisa for her help and guidance with receptor expression and purification, Marta for help with SPR and Rebecca B for her expertise and help with HDX-MS work. You have all played a key role in shaping this work and I'm very grateful for your time and help.

I'm also grateful to a lot of amazing people at UCB, who were very generous with their time, skills and ideas: Alison Turner, Andy Popplewell, Alistair Henry, Gill Holdsworth, Nicolas Basse, Dan Lightwood, Kerry Tyson, Simon Tickle, Ash Hudson, Sarfaraj Topia, Prash Mori, Neesha Dedi, Neha Dhami, Catherine Simpson, Omar Qureshi, Dave Cook, Anthony-Scott Tucker, Marianne Bergin, Jeff Kennedy, Emily Barry, Jun He, Oliver Durrant & Oliver Mace.

I would also like to convey my gratitude to UCB for funding the project and UCB fellows: Alastair Lawson, Henrik Klitgaard, Jiye Shi, Martyn Robinson, & Terry Baker for their help and support.

I'm thankful to Prof Mark Wheatley, Naomi Pollock and Richard Logan of University of Birmingham for giving me the opportunity to visit their lab and teaching me SMA solubilisation.

Lastly, a huge thanks to my family. Thanks, Maa and Baba for all your support; without your love and blessings none of this would have been possible. Thanks to my in-laws Kedarnath and Pankajini, my sister, Tanaya and brothers-in-law, Saurav and Prasanta. Finally, I would like to express my heartfelt gratitude to my wife, Meera for being a constant source of support and inspiration. I'll always be very grateful for all your help. Thanks a lot, Meera!

Chapter 1: Introduction

1. Introduction

Synopsis

G-protein coupled receptors mediate the cellular responses to a wide range of biologically active molecules including hormones and neurotransmitters (Latorraca, Venkatakrishnan and Dror, 2016). They are also a major drug target and over ~34% of all currently prescribed drugs act through GPCRs (Hauser *et al.*, 2018). A large proportion of the drugs against GPCRs are small molecules and exhibit variable efficacy and off-target effects (Allen and Roth, 2011; Huggins, Sherman and Tidor, 2012). Secretin family members play a key role in physiological processes such as regulating appetite, serum sugar and calcium levels etc. by binding to peptide hormones (Lagerström and Schiöth, 2008). This receptor family is also implicated in various diseases such as osteoporosis, diabetes, cancer and neurodegeneration (Bortolato *et al.*, 2014). The majority of approved drugs which target this receptor family are of peptide origin and include fragments and analogues of the endogenous ligands (Bortolato *et al.*, 2014). This is mainly because efforts to design small molecules against secretin family receptors have been largely unsuccessful (Hutchings, Koglin and Marshall, 2010; Poyner and Hay, 2012). A major contributory factor to these failures has been the lack of structural data for secretin family members. However the situation is starting to change as a number of high-resolution structures of secretin family members in a range of conformational states have recently become available (Hollenstein *et al.*, 2013; Liang *et al.*, 2017; Liang *et al.*, 2018; Zhang *et al.*, 2018).

An emerging field in GPCR therapeutics are functional antibodies, antibodies with the ability to not only recognise and bind the receptor but also modify receptor activity (Hutchings *et al.*, 2017). Antibody and antibody-derived fragments also play a key role in structure determination, as crystallographic chaperones and as research reagents for use in protein detection and localisation (Griffin and Lawson, 2011; Lawson, 2012; Groff, Brown and Clippinger, 2015; Gong, Murray and Trimmer, 2016). This thesis describes attempts to generate antibodies that can be used to modify receptor function and as an aid to structural

studies. The target receptor is the parathyroid hormone receptor 1 (PTH1R), which plays a key role in calcium (Ca^{2+}) homeostasis and bone mineralisation (Datta and Abou-Samra, 2009). PTH1R is a well-validated target for bone disorders including osteoporosis and current available treatment options include Teriparatide®, the N-terminal fragment of parathyroid hormone (Mahon and J. Mahon, 2012) and Abaloparatide, a PTHrP analogue (Doyle *et al.*, 2017). The current therapeutics are both peptide based and therefore presents an opportunity for generating mAbs against PTH1R.

1.1 G-protein coupled receptors

The G-protein coupled receptor (GPCR) superfamily is comprised of approximately 800 members playing crucial roles in cellular signal transduction and communication (Fredriksson *et al.*, 2003). Members of this superfamily share a common seven α-helical transmembrane (7TM) architecture with extracellular N- and intracellular C-terminal domains (Figure 1-1).

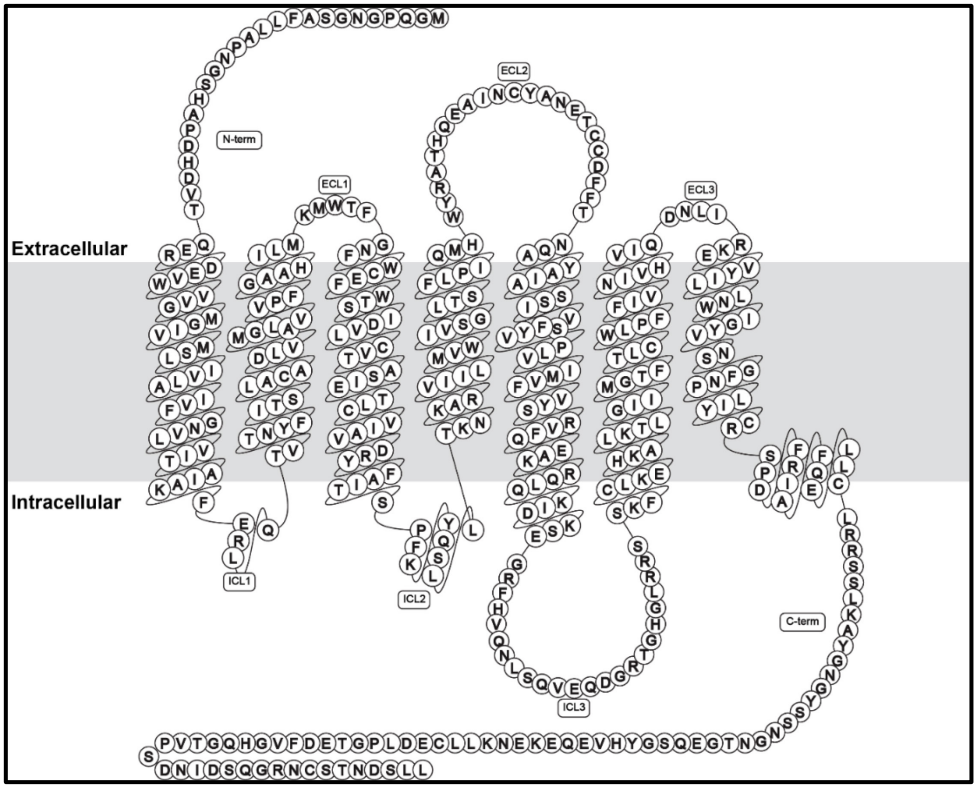


Figure 1-1: A snake plot representation of the human β_2-adrenergic receptor, a widely studied receptor from GPCR superfamily.

The plot highlights the extracellular N-terminal domain (ECD), seven transmembrane helices (TM) and intracellular C-terminal domain (ICD) conserved topology of GPCRs. The length and complexity of the ECD varies between different families of GPCR. Snake plot generated using GPCRDB (Vroling *et al.*, 2013)

GPCRs have an extraordinary ability to bind to a wide variety of extracellular ligands such as neurotransmitters, ions, lipids, proteins, peptides, hormones, and respond to light, taste, odour and pain (Venkatakrishnan *et al.*, 2013). Extracellular binding of a cognate ligand activates the receptor which in turn activates a heterotrimeric G-protein (Hamm, 1998). The activated Gα subunit dissociates from the Gβγ complex and interacts with a second messenger molecule e.g. adenylate cyclase to elicit a cellular response (Pierce, Premont and Lefkowitz, 2002) (Figure 1-2).

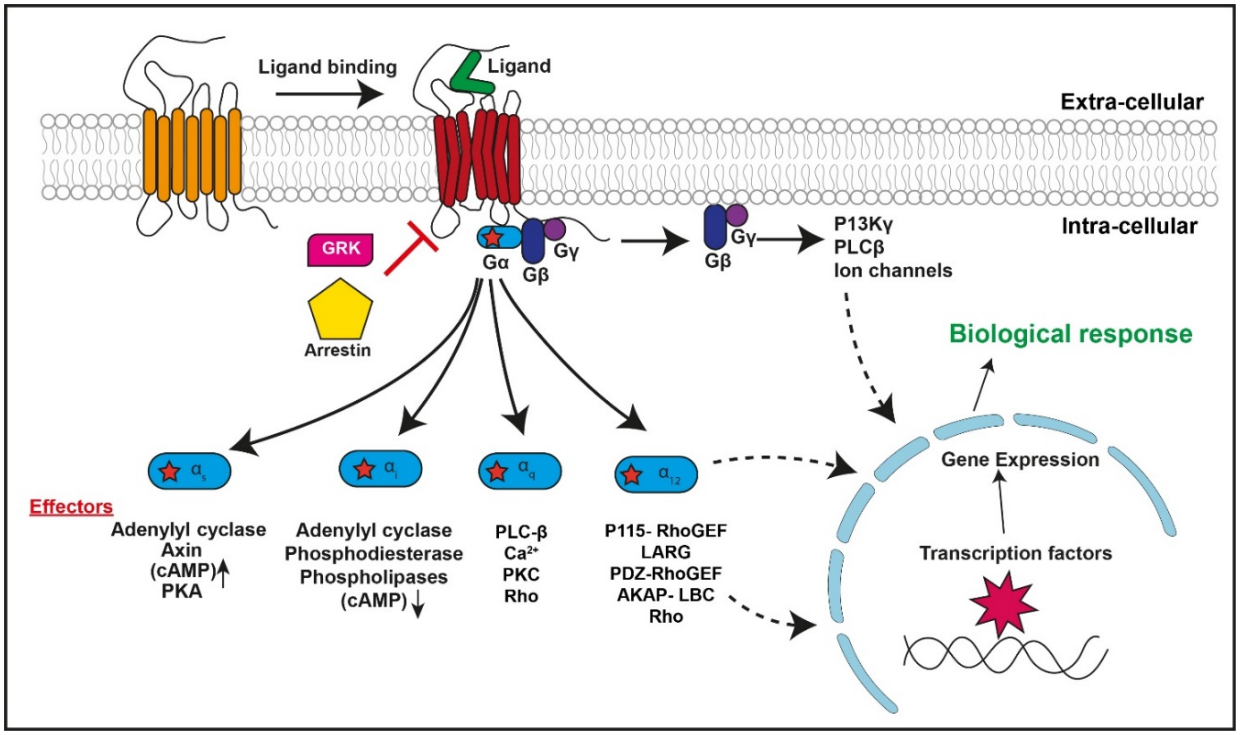


Figure 1-2: Summary of G-protein mediated GPCR signalling cascades.

Upon ligand-induced activation, the GPCR activates the G-protein, causing nucleotide exchange in the Gα subunit. This in turn results in dissociation of the Gα subunit from the β and γ heterodimer. The Gα is then free to interact with a second messenger molecule (listed by Gα subtype). The effector molecules initiate a downstream signalling cascade leading to cellular changes (e.g. an increase in intracellular Ca^{2+}) and alteration in gene-expression. G-protein receptor kinases (GRKs) play a key role in receptor phosphorylation, crucial for β-arrestin recruitment. Arrestin molecules bind to phosphorylated GPCRs causing receptor desensitisation and recycling. The βγ heterodimer is also able to bind to and activate other effector molecules with specific cellular consequences. Figure adapted from (Dorsam and Gutkind, 2007).

1.1.1 Classification of GPCRs

The GPCR superfamily can be broadly classified in to 6 major classes but in humans an accepted classification, the GRAFS classification, divides the superfamily into 5 main

groups: Glutamate (also class C) receptors, Rhodopsin (class A), Adhesion (class B), Frizzled/taste2 and Secretin-like (class B) (Schiöth and Fredriksson, 2005).

The class A or rhodopsin family contains the largest number of receptors in the GPCR superfamily and includes some of the best studied and most well understood receptors (Tehan *et al.*, 2014). Most class A receptors contain conserved sequence motifs crucial for receptor activation and G-protein binding (Kristiansen, 2004). Almost all the members that have been studied in this family possess an "NSxxNPxxY" motif in helix 7 and a "E/DRY" motif at the cytoplasmic side of helix 3 (Rovati, Capra and Neubig, 2007; Lagerström and Schiöth, 2008). The "E/DRY" motif gives rise to the so called "ionic lock", a well-known feature key in class A receptor activation and signalling (Mitchell *et al.*, 1998; Ballesteros *et al.*, 2001). The glutamate/aspartate residue of the motif maintains the receptor's ground state and mutation of these residues have been found to increase receptor constitutive activity (Rovati, Capra and Neubig, 2007). The arginine residue forms stabilising interactions with the neighbouring glutamate/aspartate and/or with other charged residues in helix 6 (Ballesteros *et al.*, 1998, 2001)

In contrast to the rhodopsin family receptors with short, largely unstructured N-terminal regions, the other GPCR families possess large N-terminal extracellular domains (ECD) with varying levels of complexity (Fredriksson *et al.*, 2003). The glutamate family receptors contain large ECDs consisting of two lobes, referred to as the Venus-fly Trap (VFT) domain, largely responsible for ligand binding (Kunishima *et al.*, 2000).

The secretin family receptors also have a large ECD which varies from 60-100 amino acids in length and contains conserved cysteine residues and glycosylation sites (Grauschopf *et al.*, 2000; Hofmann *et al.*, 2001; Bazarsuren *et al.*, 2002). In this case, ligand binding is bimodal, with the ECD playing a crucial role in the initial engagement of the ligand binding and its subsequent docking into the orthosteric site. The docking of the ligand into the orthosteric site, generally located in the transmembrane domain (TMD) causes structural changes which in turn activates the receptor (Pioszak and Xu, 2008).

The Frizzled (FZD) family in humans is comprised of 10 members which bind to Wingless and Int-1 (Wnt), a cysteine-rich glycoprotein with crucial roles in cell proliferation, differentiation and migration (Anastas and Moon, 2013). The binding of Wnt is mediated through FZD's cysteine-rich N-terminal extracellular domain (Dann *et al.*, 2001).

The Adhesion family is comprised of 33 receptors in humans. They contain large N-terminal extracellular regions containing functional domains found in other protein families such as integrin, cadherins and tyrosine kinases (Bjarnadóttir, Fredriksson and Schiöth, 2007). Members of the adhesion family contain motifs such as epidermal growth factor (EGF) and mucin-like repeats and play an important role in cell adhesion (Stacey *et al.*, 2000; Kristiansen, 2004).

1.1.2 GPCR Ligands

The binding site for a cognate ligand is termed the orthosteric site of the receptor (Neubig *et al.*, 2003). Molecules binding at the orthosteric sites, called orthosteric ligands, can be broadly classified into agonists, antagonists and inverse agonists (Figure 1-3). An agonist molecule can bind to and activate a receptor, up-regulating intracellular signalling pathways. A full-agonist elicits maximum response in the selected pathway and in general, cognate ligands are full-agonists (Neubig *et al.*, 2003). Partial agonists on the other hand elicit submaximal response even at very high concentrations (Neubig *et al.*, 2003). Antagonists inhibit ligand induced downstream signalling whereas inverse agonists inhibit constitutive receptor activity (Prather, 2004).

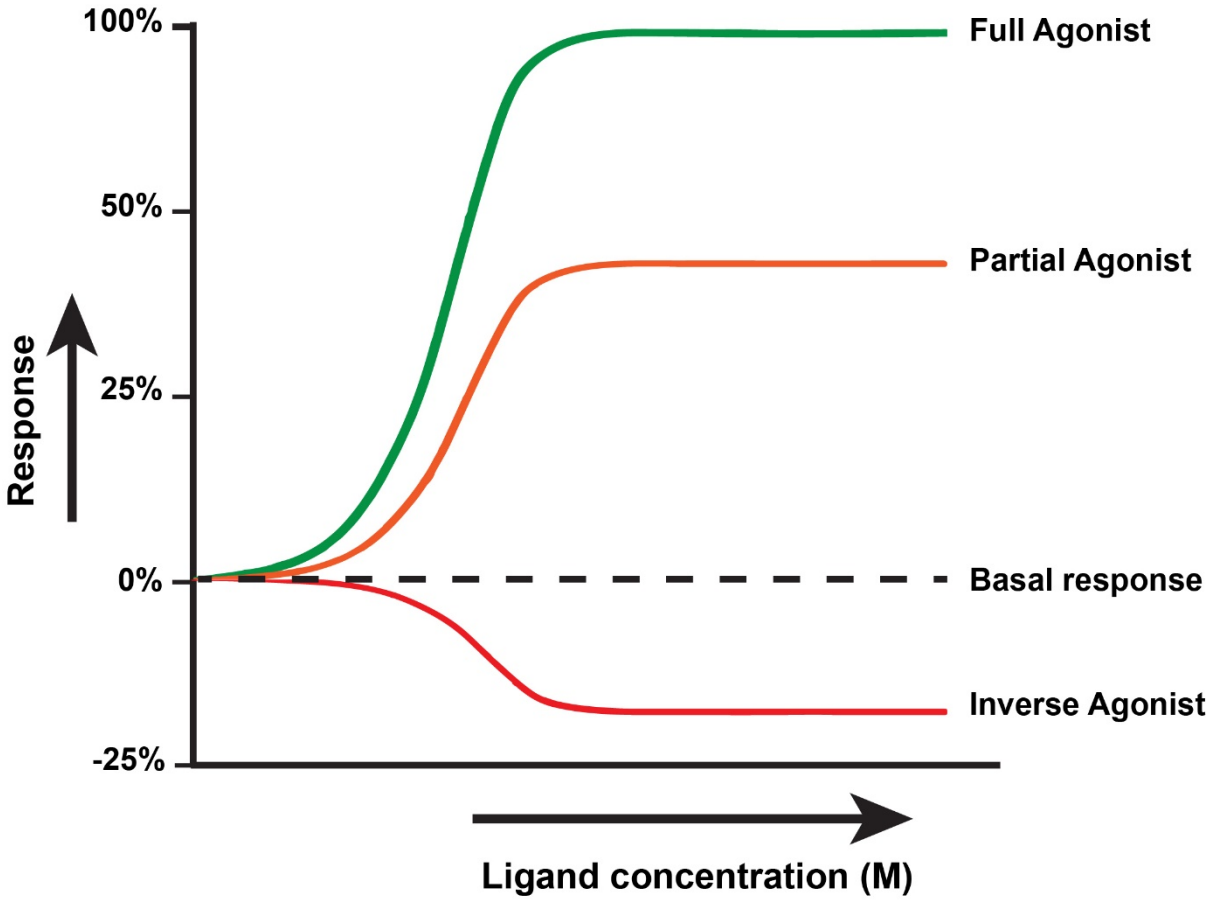


Figure 1-3: A schematic plot showing the effects of agonists on biological response mediated by a GPCR.

The dotted line represents basal activity (if any) and any response above this is stimulated by an agonist. Full-agonists (green) exert the maximum response as generally seen with the cognate ligand, whereas a partial agonist (orange) does not elicit the maximum response. Inverse agonists (red) block both ligand-induced receptor activity and inhibit constitutive receptor activity upon binding to the orthosteric sites. The direction of arrows represent increase in response and ligand concentration. Figure adapted from (Tate, 2012).

Certain classes of ligands are able to bind sites distinct from the orthosteric binding pocket and these are classed as allosteric ligands (Christopoulos *et al.*, 2014). Allosteric ligands can modulate cognate ligand binding and receptor activity and therefore present a novel means of targeting certain receptors (Christopoulos *et al.*, 2014). These types of ligands can be further divided into positive allosteric modulators (PAMs) and negative allosteric modulators (NAMs). PAMs increase receptor activity in response to an orthosteric ligand binding whereas NAMs decrease receptor activity (Lane *et al.*, 2017). Recently, there has been a lot of interest in generating allosteric modulators of GPCRs as therapeutics due to their benefits over orthosteric ligands such as better subtype-selectivity (Christopoulos *et al.*, 2014).

The sub-type selectivity can arise from the higher sequence diversity in allosteric sites or due to selective cooperativity for a certain subtype over others (Jeffrey Conn *et al.*, 2009).

1.1.3 G-protein mediated signalling

Binding of a ligand to a GPCR initiates a very intricate and tightly-controlled signalling cascade. The other major player in this signalling cascade is the G-protein. G-proteins are heterotrimers comprised of α, β and γ subunits (Cabrera-Vera *et al.*, 2003). These hetero-trimeric proteins are further subdivided into 4 main subclasses based on the Gα subunit: $G_{\alpha s}$, $G_{\alpha i}$, $G_{\alpha q}$ and $G_{\alpha 12}$ (Simon, Strathmann and Gautam, 1991) (Figure 1-2). Although GPCRs are large in number and bind to a wide array of ligands, they signal largely via binding to this relatively small number of G-proteins (Oldham and Hamm, 2008).

High resolution crystal structures of G-proteins in a range of conformational states have provided important insights into this class of protein and their role in signal transduction (Noel, Hamm and Sigler, 1993; Lambright *et al.*, 1996). The α subunit is comprised of a Ras-like GTPase domain and an α-helical domain (Figure 1-4). The GTPase domain is highly conserved and performs the crucial role of GDP-GTP exchange as well as mediating binding to the Gβγ dimer, activated GPCR and other effector proteins (Oldham and Hamm, 2008). The GTPase domain of the Gα subunits also contains three loops termed switch I, II, and III, shown to play a crucial role in GPCR binding and nucleotide exchange (Oldham and Hamm, 2008). Crystal structures reveal that these flexible loops become rigid and ordered in a GTP bound G-protein (Noel, Hamm and Sigler, 1993; Lambright *et al.*, 1996). Six α helices form the other half of the Gα subunit and these act as lids, opening and closing to facilitate exchange of the nucleotide (Cabrera-Vera *et al.*, 2003). The Gβ subunit has a seven-bladed β-propeller structure composed of seven WD40 sequence repeats (Lambright *et al.*, 1996; Duc, Kim and Chung, 2015). The GDP-bound Gα subunit forms a high affinity association with the Gβγ, but binding of GTP to the Gα following receptor activation, reduces the affinity of the interaction and induces dissociation from the Gβγ (Tesmer, 2010).

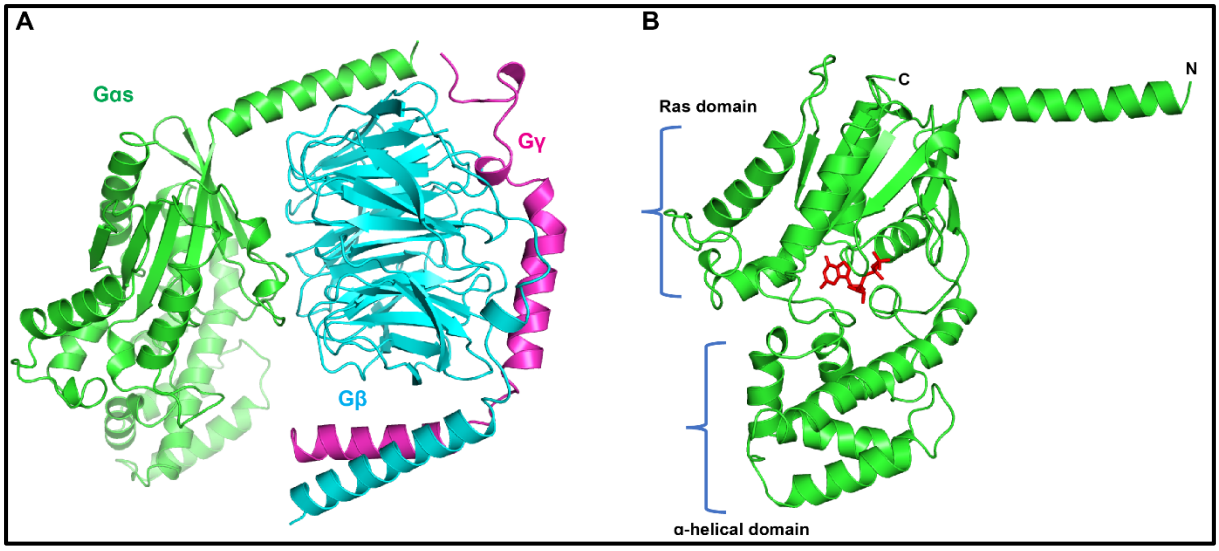


Figure 1-4: Overall topology of an inactive GDP-bound form of a heterotrimeric G-protein (PDB 1GOT (Lambright *et al.*, 1996).

A) The overall structure of the G-protein heterotrimer with the Gα, Gβ and Gγ subunits shown in green, cyan and magenta respectively. The structure also illustrates that all the interactions between the Gα and the Gβγ dimer are mediated by the Gβ subunit only. B) The Ras-like and α helical domain (in green) of the Gα are indicated. The nucleotide is shown in the red stick model bound to the Gα Ras domain.

The ligand-induced activation of a GPCR causes structural changes in the Gα subunit, exchange of GDP for GTP and thus dissociation of the Gβγ subunit. The activated G-protein subunits (α.GTP and βγ) are then free to associate with downstream effector molecules (Ritter and Hall, 2009) (See Figure 1-2).

1.1.4 Structural elucidation of GPCR-G-protein binding

A 3.2 Å resolution structure of the human β_2-adrenergic receptor in complex with the heterotrimeric G-protein gave the first insights into the molecular details of G-protein binding to an activated GPCR (Rasmussen *et al.*, 2011). Crystallisation of the complex was facilitated by a number of receptor modifications such as addition of T4 Lysozyme, a highly crystallisable protein, to the N-terminus of the receptor which improved the crystal contacts and use of a nanobody to stabilise the heterotrimeric G-protein complex (Rasmussen *et al.*, 2011) (Figure 1-5, A). The structure highlights the docking of the Gα subunit into the C-terminal face of the receptor. When compared with the inactive structure of β_2AR, it was found that the TM6 of G-protein bound β_2-AR exhibits a 14 Å outward movement (Figure 1-5, B). In addition, in the

active structure, TM5 extends by 2 helical turns compared to the inactive structure (Figure 1-5, B).

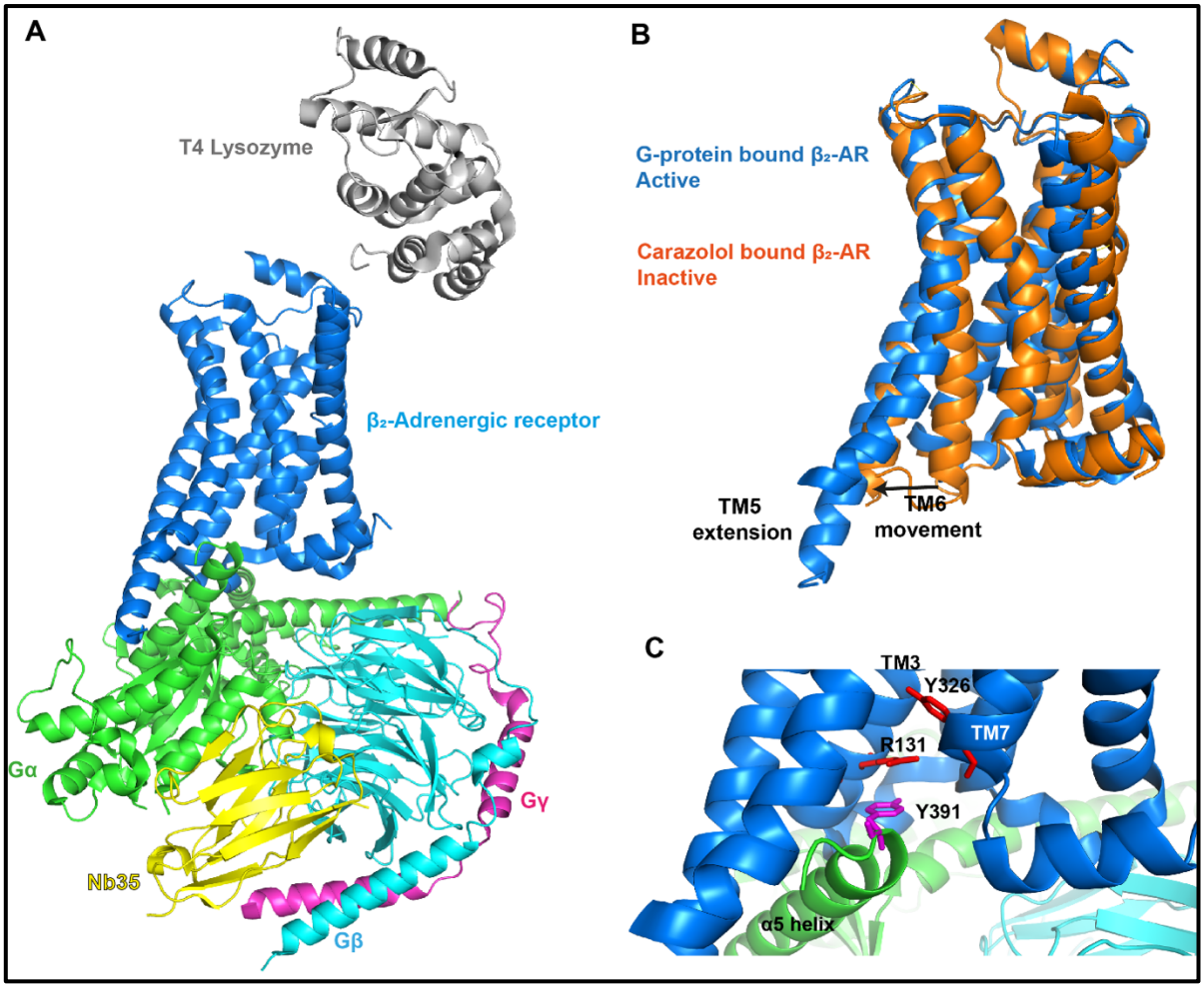


Figure 1-5: Crystal structure of activated β_2-AR in complex with heterotrimeric G-protein

A) The overall structure of the complex. The T4L used to stabilise the complex and provide soluble crystal contacts is shown in grey, the β_2-AR in blue, Gα in green, Gβ in cyan and Gγ in magenta. The nanobody, Nb35, used to stabilise the G-protein is shown in yellow. B) The superposition of active G-protein-bound receptor (blue) shows a marked extension of TM5 and large outward movement of TM6 compared to the inactive carazolol-bound β_2-AR (orange). C) Key interactions between the α5 helix of G-protein and TM interface is shown. The G-protein residue Y391 is coloured in magenta while receptor residues are shown in red.

The α5 helix of the G-protein Ras domain makes important interactions with the TM domains of β_2-AR. Y391 of the G-protein (magenta Fig 1-5C) interacts with R131 of the receptor 'DRY' motif, known to play a crucial role in receptor activation and deactivation. R131 also packs against Y326 of the conserved 'NPxxY' motif in TM7 (Figure 1-5, C). The activated receptor perturbs the N- terminus of the Gα subunit, resulting in a change in the P-loop which interacts with the phosphate group of the nucleotide. The HDX -MS analysis of the complex

indicates greater H/D exchange for the α subunit compared to the β and γ subunits confirming that it is the α subunit that undergoes large conformational changes during activation (Chung *et al.*, 2011).

1.1.5 GPCR β-arrestin interaction

Ligand-activated receptors are rapidly phosphorylated by G-protein receptor kinases (GRKs), typically at the cytoplasmic tail region allowing β-arrestin binding to the receptor. There are seven related GRKs (GRK1–GRK7) with varying tissue distribution and preferences for binding to certain receptors (Reiter and Lefkowitz, 2006; Moore, Milano and Benovic, 2007). The binding of β-arrestin to the phosphorylated receptor blocks further G-protein-mediated signalling through a steric mechanism (DeWire *et al.*, 2007).

β-arrestins were discovered in late 1980's where researchers noted that pure preparations of GRK2 were unable to desensitize activated β_2-adrenergic receptor preparations, but the receptor could be desensitised by addition of a large molar excess of visual arrestin (Benovic *et al.*, 1987). Later, molecular cloning identified two proteins, with a sequence homology of 78%, termed β-arrestin 1 and β-arrestin 2 (Lohse *et al.*, 1990; Attramadal *et al.*, 1992) which desensitise GPCRs.

The mechanism of β-arrestin-mediated receptor internalisation can vary between receptor subclasses (DeWire *et al.*, 2007). In some receptors, such as the β_2-adrenergic receptor, low affinity binding of the β-arrestin to activated receptor is associated with a rapid increase in β-arrestin concentration at the activated receptor. The overall interaction is transient, with the receptor-arrestin complex being rapidly targeted into clathrin-coated pits following which the β-arrestin is released (Shenoy and Lefkowitz, 2003) (Figure 1-6).

In contrast, class B receptors such as angiotensin II type 1A receptor (AT1AR) exhibit a much stronger binding to β-arrestin. The arrestin bound receptor can remain in complex the surface of the endocytic vesicles (Oakley *et al.*, 2000). Due to the stronger interactions between the receptor and β-arrestin, and the subsequent greater stability of the complex, class

B receptors recycle to the cell-surface much more slowly than Class A receptors (DeWire *et al.*, 2007) (Figure 1-6).

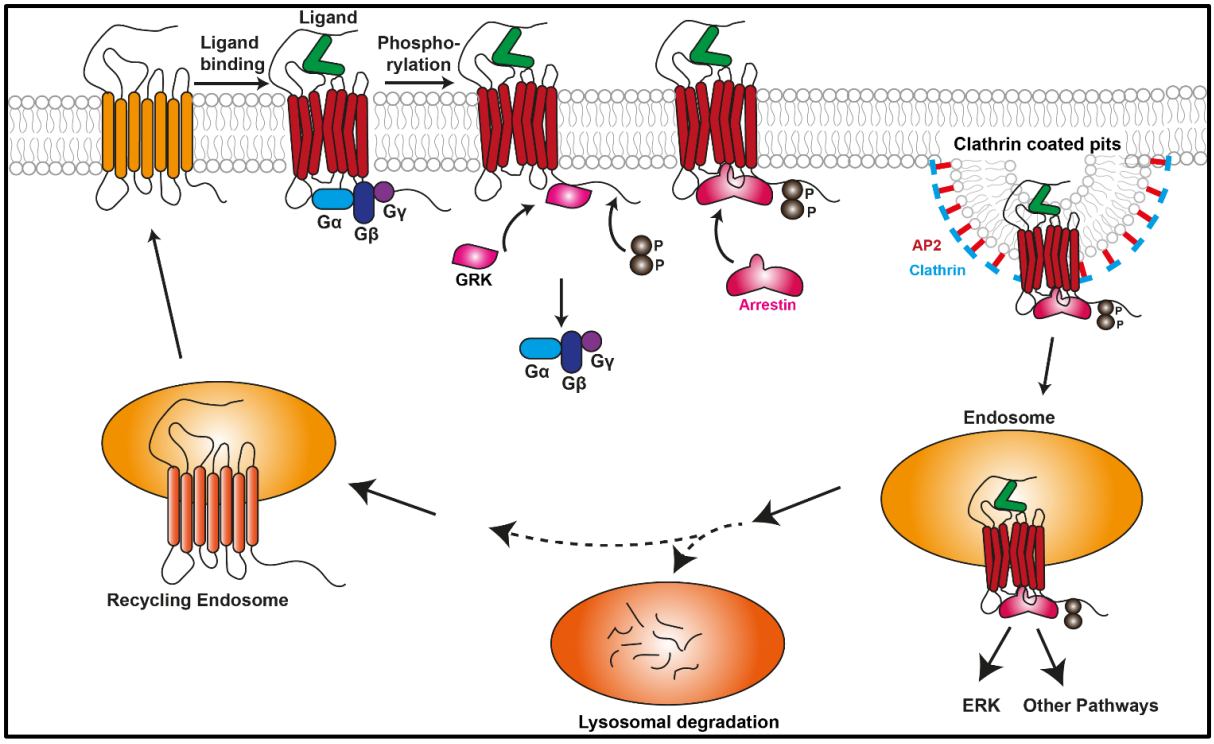


Figure 1-6: Schematic representation of β-arrestin mediated receptor desensitisation

A ligand-activated receptor is phosphorylated by G-protein receptor kinases (GRKs) shown in magenta which cause dissociation of the Gα subunit and recruitment of β-arrestin. The activated receptor is internalised by β-arrestin in clathrin coated pits which results in the formation of endosomes. Some receptors can signal through various signalling pathways from the endosomal compartments as receptor- β-arrestin complexes. From the endosome the internalised receptor either enters the lysosomal degradation pathway or is recycled back to the cell-surface. (Ritter and Hall, 2009)

The GPCR-β-arrestin interaction controls the important process of desensitization and recycling of GPCR (Hanyaloglu and von Zastrow, 2008). In addition, it is also now known that the GPCR-β arrestin complex can initiate a G-protein independent intracellular signalling cascade (see section 1.3.4). mAbs which could modulate β-arrestin recruitment and/or β-arrestin mediated signalling could prove as useful tools for further studying the receptor-arrestin interaction and potentially present a novel therapeutic angle.

1.1.6 Structural characteristics of arrestin binding and desensitisation

The mechanism of GPCR desensitisation through arrestin is well understood across different GPCR families through extensive biochemical studies and from high-resolution structures of arrestin, in various conformational states. Structures of arrestin in both active and

inactive conformations are available (Han *et al.*, 2001; Shukla *et al.*, 2013). The arrestin molecules are bi-lobed with a polar core with some key loops forming critical interactions with the intracellular surface of the GPCR. The C-terminal tail of arrestin plays a crucial role in stabilisation of the core and maintaining an inactive state in the absence of a phosphorylated GPCR (Hirsch *et al.*, 1999; Kim *et al.*, 2013).

The structure of β-arrestin in complex with a C-terminal GPCR phosphopeptide highlights some of the structural features important in arrestin binding (Shukla *et al.*, 2013). The structure was stabilised using a conformationally-selective nanobody bound to a fully phosphorylated 29 amino acid C-terminal peptide derived from the human V2 vasopressin receptor (V2Rpp). Binding of V2Rpp induced rotation of the N- and C- terminal domains relative to each other into a markedly different conformation than seen in the inactive arrestin. Binding to the receptor also induced a re-orientation of the 'lariat' loop which has previously been shown to be important for maintaining the inactive conformation (Shukla *et al.*, 2013).

More recently, a high resolution structure of visual arrestin fused to activated rhodopsin was solved using X-ray free electron laser (XFEL) techniques (Kang *et al.*, 2015). The structure shows the overall topology (Figure 1-7, A and B) of the complex and highlights the key role helices 7 and 8 of rhodopsin play in arrestin recruitment. The arrestin adopts an active conformation with a 20° rotation occurring between the two lobes, causing opening of a cleft in the arrestin molecule which accommodates the second intracellular loop of rhodopsin.

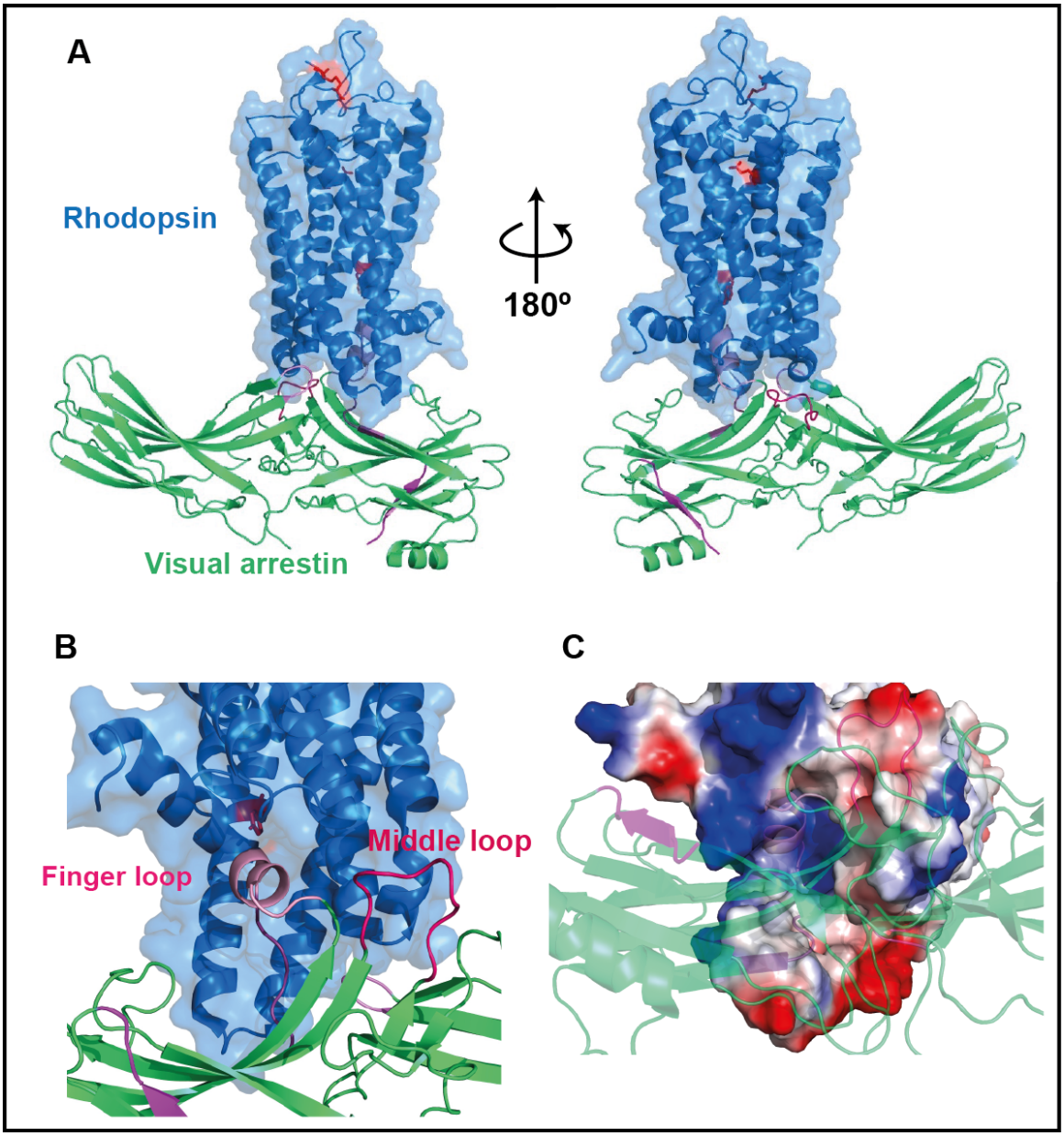


Figure 1-7: High resolution structure of visual arrestin in complex with activated Rhodopsin

A) The overall structure of the complex is shown with rhodopsin in blue and the visual arrestin in green (PDB: 4ZWJ). B) The arrestin binding interface illustrating the interactions the "finger" and "middle" loops form with the receptor's C-terminal face. C) The arrestin binding interface of the receptor is shown in surface representation and coloured by charge, highlighting the importance of charged residues in arrestin binding.

The other important aspect to note from the overall structure is that the binding of arrestin is not only mediated by shape complementarity, but also charge. The intracellular region of rhodopsin is positively charged and a pocket of positively charged residues accommodates the finger loop of arrestin (Figure 1-7, B-C), which contains 3 conserved negatively charged residues (E71, D72, and D74) (Kang *et al.*, 2015).

1.2 Secretin Family (Class B) GPCR

1.2.1 Secretin family

The Secretin family of class B GPCRs consists of 15 receptors which bind to peptide ligands and are of immense physiological importance (Lagerström and Schiöth, 2008). The members of this family are summarised in Table 1-1 below and closely-related members are colour coded.

Table 1-1: Summary of Secretin family receptors. Table adapted from (Hoare, 2007)

Receptor	Ligand	Physiological role
Calcitonin receptor (CTR)*	Calcitonin	Ca^{2+} homeostasis
Calcitonin receptor-like receptor (CRLR)*	-	
Corticotropin-releasing factor receptor – 1 (CRF1R)	CRH	Stress responses
Corticotropin-releasing factor receptor – 2 (CRF2R)	CRH	Stress responses Cardiac contractility
Glucagon receptor (GCGR)	Glucagon	Glucose homeostasis
Glucagon-like peptide -1 receptor (GLP-1R)	GLP-1	Insulin secretion
Glucagon-like peptide -2 receptor (GLP-2R)	GLP-2	Gut mucosal growth
Gastric Inhibitory peptide receptor (GIP-R)	GIP	Insulin secretion
Growth-hormone- releasing hormone receptor (GHRHR)	GRF	Growth hormone release
Secretin receptor (SCT-R)	Secretin	Pancreatic secretion
Parathyroid hormone receptor -1 (PTH1R)	PTH, PTHrP	Ca^{2+} homeostasis Developmental regulator
Parathyroid hormone receptor – 2 (PTH2R)	PTH, TIP39	Hypothalamic secretion Nociception
VPAC1 receptor (VIPR1)	VIP/PACAP	Neuroendocrine functions
VPAC2 receptor (VIPR2)	VIP/PACAP	Neuroendocrine functions
PAC1 receptor (PAC-R)	PACAP	Neuroendocrine functions

*** CTR and CRLR interact with RAMP 1-3 to form amylin (AMY) 1-3, calcitonin gene-related peptide (CGRP) and adrenomedullin (AM) 1-2 receptors**

This family was named after the secretin receptor (SCT-R), the first receptor of this family to be identified (Ishihara *et al.*, 1991). Unlike the class A receptors, the secretin family

members contain a large, soluble extracellular N-terminal domain (ECD) which plays a key role in ligand binding (DeAlmeida and Mayo, 1998; Assil *et al.*, 2001; Grace *et al.*, 2004).

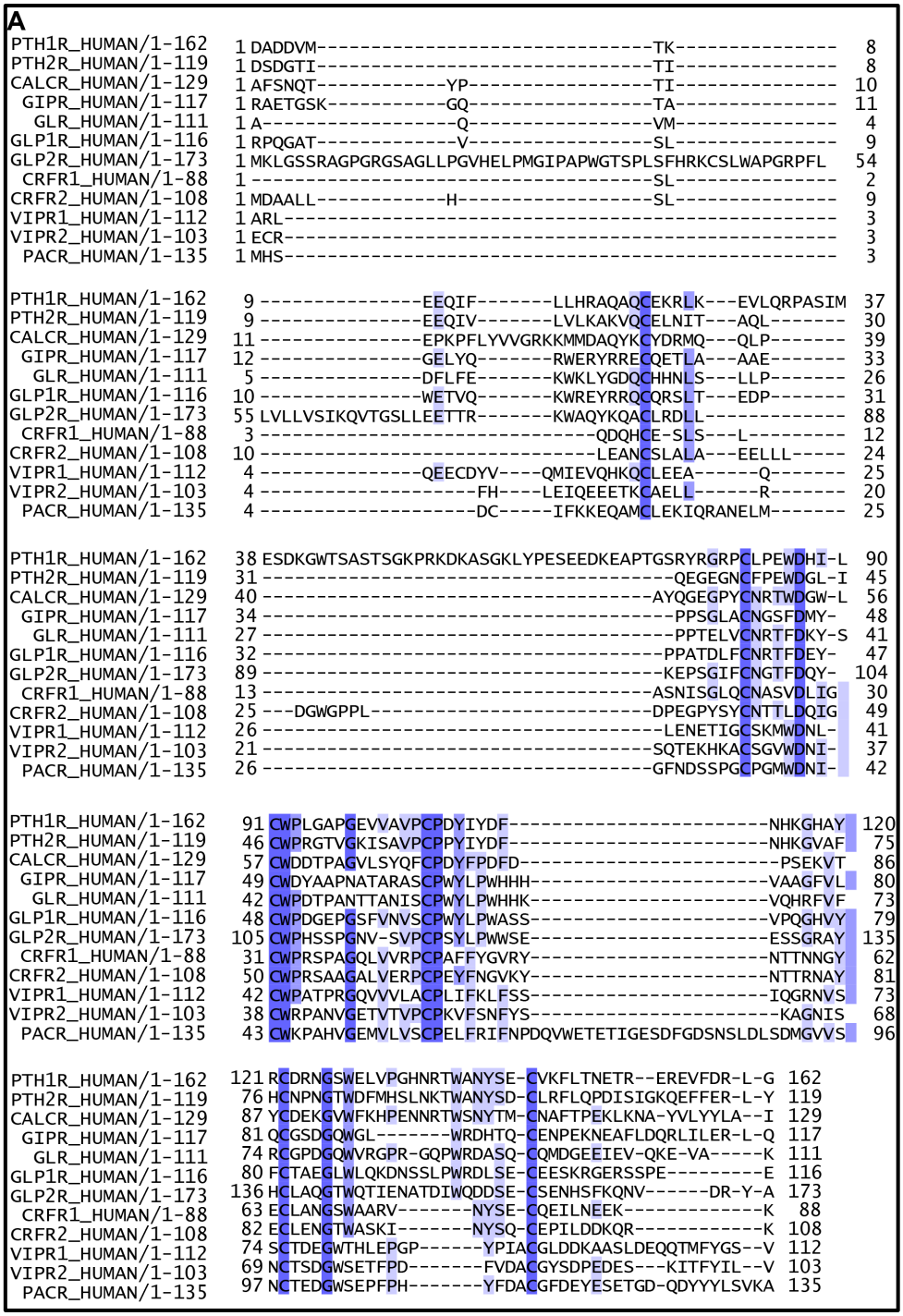


Figure 1-8: Sequence alignment of the ECD of secretin-family receptors

The sequence alignment highlights the overall lack of similarity between the members of the secretin family. All receptor ECDs however do contain a small number of conserved sequence motifs (highlighted in blue). Of particular note, are six conserved cysteines which form three disulphide bonds key in stabilising the ECD structure.

The overall sequence homology between the secretin family receptors ranges from 21 to 67% (Lagerström and Schiöth, 2008) with the N-terminal extracellular domain exhibiting the highest sequence variation (Figure 1-8). This N-terminal domain contains 6 conserved cysteine residues which form a network of three disulphide bonds key for maintaining the tertiary structure and facilitating ligand binding (Lagerström and Schiöth, 2008). The extracellular loops show very little sequence consensus with the exception of the 'CWx' motif present in ECL2 of secretin family receptors (Figure 1-9).

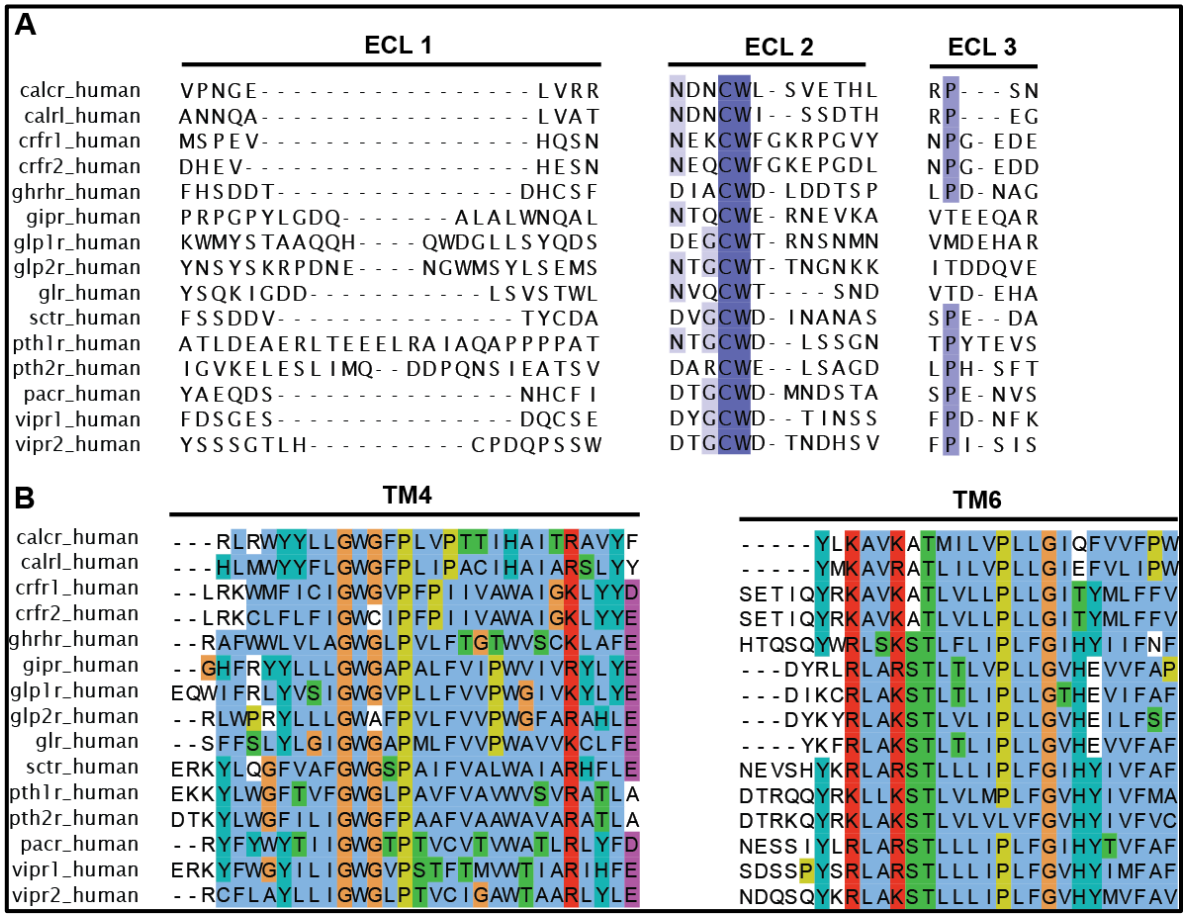


Figure 1-9: Sequence alignment of extracellular loops, TM4 and 6 for the members of Secretin sub-family

A) ECL-1 exhibits the highest variability in sequence length and composition with PTH receptors having the longest ECL1. The CWx motif of ECL2 is highly conserved among the members of the sub-family. In ECL3, a conserved proline is seen with most members except the glucagon family. B) The sequence alignment of TMs4 and 6, both known to be essential for ligand-mediated receptor activation shows conserved motifs such as "GWGxP" and "PxxG"

In addition, the receptors also contain two transmembrane motifs, 'GWGxP' in TM4 and 'PxxG' in TM6. These have been well studied and are known to play important roles in

receptor activation and signalling (Bortolato *et al.*, 2014; Hollenstein *et al.*, 2014; Culhane *et al.*, 2015; Y. Zhang *et al.*, 2017).

These receptors and their ligands are implicated in many human diseases such as diabetes, osteoporosis, cancer, neuro-degeneration, cardiovascular disease, inflammation and obesity (Bortolato *et al.*, 2014). They are therefore the targets of many pharmaceutical drugs and intense research (Hollenstein *et al.*, 2014). In contrast to the class A GPCRs, high-throughput screening approaches by various groups have not been very successful in identifying many secretin family-specific small molecules with suitable pharmacokinetics (PK), pharmacodynamics (PD) and affinity (Hoare, 2005). With better structure-function data being available this trend is now changing. In recent years, a few small molecule drugs against secretin family members such as telcagepant (Ho *et al.*, 2008), ubrogepant (Voss *et al.*, 2016), LY2409021 (Kazda *et al.*, 2016), Verucerfont (Gilligan *et al.*, 2009) and BMS-927711(Marcus *et al.*, 2013) have entered clinical trials but with varying levels of success and high attrition rates. Overall, these receptors still present a major challenge with respect to drug discovery.

1.2.2 Structural insights into the class B-secretin family

Recent technological advances in X-ray crystallography such as XFEL and more powerful Cryo-EM microscopes have allowed elucidation of 9 secretin family receptor structures in a range of conformational states.

Structure of the transmembrane domains

High resolution crystal structures of two Class B GPCRs, corticotropin-releasing hormone receptor 1 (CRF1R) and glucagon receptor (GCGR) were published in 2013 and these gave the first insights into the three dimensional structure of the secretin family (Hollenstein *et al.*, 2013; Siu *et al.*, 2013). Crystallisation of CRF1R was made possible using a thermostabilisation approach which generated a construct with increased thermostability compared to the wild-type form of the receptor and a bias towards the inactive conformation. The final construct contained 12 thermostabilising mutations, away from the antagonist

binding site. The final crystallised protein also lacked the ECD, and had a T4L inserted into intracellular loop 2 (ICL2) to aid expression and crystallisation. The structure was solved in the presence of CP-376395, a small molecule antagonist (Hollenstein *et al.*, 2013).

GCGR was crystallised using a chimera approach, where thermostable *E. coli* apocytochrome b_{562}RIL (BRIL) was fused to the N-terminus of the receptor lacking the ECD (Siu *et al.*, 2013). The receptor was also truncated at the C-terminus (at residue 432) to improve receptor yield. This final construct was crystallised in the presence of a small molecule antagonist and is therefore in an inactive conformation (Siu *et al.*, 2013).The modifications to the receptor did not alter the binding affinity for the antagonist ligand NNC0640, when compared with the wild-type (WT) receptor (Siu *et al.*, 2013).

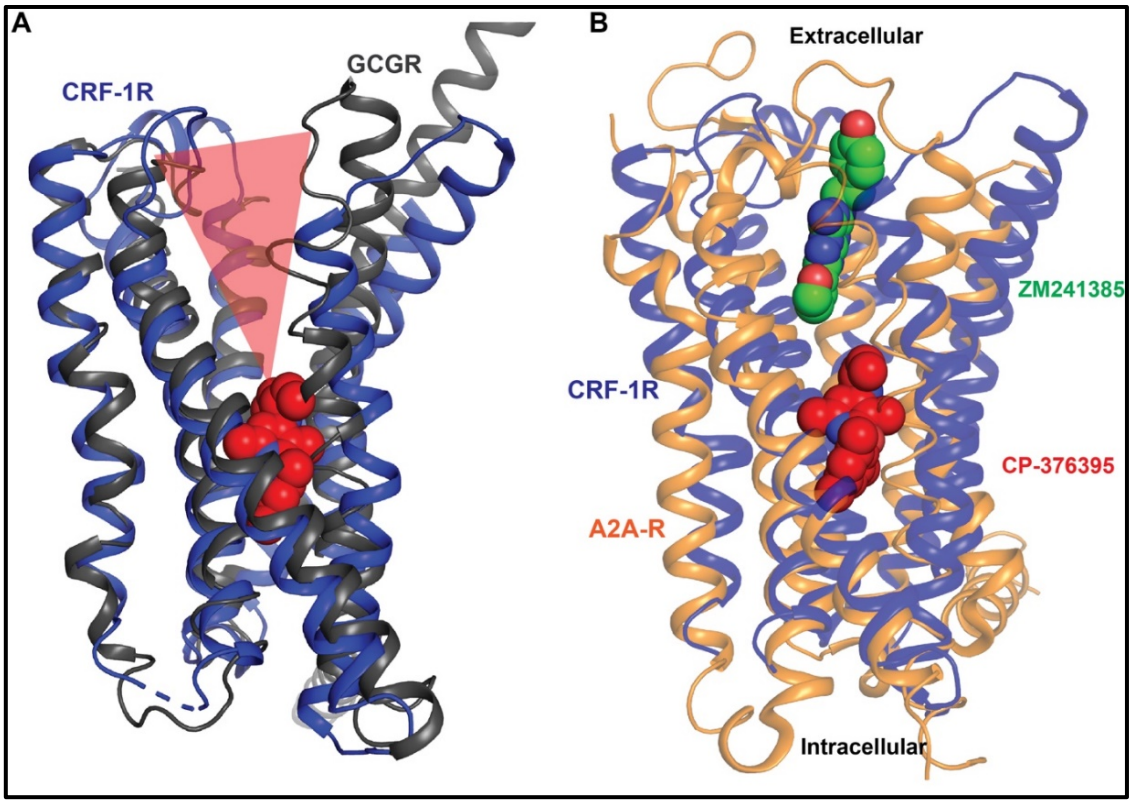


Figure 1-10: Crystal structure of the CRF and GCGR transmembrane domains (TMDs).

A) Superimposed high-resolution structure of the glucagon (4L6R) (grey) and corticotropin (4K5Y) receptors (blue) highlights the open "chalice-like" structure. The deep ligand binding site for CRF1R can be seen (CP-376395 ligand in red sphere representation). B) Superposition of ligand bound CRF-1R and A_{2A}R structure (3EML) highlights the deep ligand binding pocket of CRF-1R, where CP-376395 is shown in red spheres while the A_{2A}R binding ligand, ZM241385 is shown in green spheres (Jaakola *et al.*, 2008; Hollenstein *et al.*, 2013; Siu *et al.*, 2013)

Comparing the CRF and GCGR structures with existing class A structures confirmed that the transmembrane domains in both classes adopt the hallmark seven transmembrane

helical bundle but there are some clear differences between the structures. The overall shape of the helix bundle in the secretin family receptors is much more “open” when compared to class A receptors, which gives rise to a large solvent filled cavity (Bortolato *et al.*, 2014) (Figure 1-10, A). In addition, the secretin family contain a much deeper ligand binding pocket as illustrated by the CRF1R structure (Bortolato *et al.*, 2014) (Figure 1-10, B). The well-known “DRY motif” of the class A receptors, which gives rise to the ionic lock is missing from the secretin family molecules, but a conserved motif, ‘GWGxP’ is located in TM4 and creates a network of interactions that non-covalently links to TMs 2, 3 and 4. Similarly, a conserved S130 in TM1 interacts with conserved residues (S353, G393 and F357/L386) in TM7 which in-turn stabilises the kink in TM7 for both receptors (Hollenstein *et al.*, 2014). The conserved Y400 in GCGR forms hydrogen bonds with T351 and Q245. The equivalent interactions in class A GPCRs are known to play a key role in receptor activation and G-protein interaction (Rasmussen *et al.*, 2011). In CRF1, the thermostabilising mutation Y363A contributes to the receptor’s inactive state, further highlighting the importance of this conserved Tyr (Hollenstein *et al.*, 2014).

Full-length structures- insights into receptor activation

The CRF-1R and GCGR crystal structures provided the first insights into the overall conformation of the TMDs, as well as the structure and chemical nature of the ligand binding site of Secretin family GPCRs. However, both structures are in the inactive conformation and lack the ECD. More recently, cryo-EM structures of the full-length glucagon-like peptide -1 receptor (GLP-1R) (Zhang *et al.*, 2017; Liang *et al.*, 2018) and calcitonin receptor (CTR) (Liang *et al.*, 2017) have been obtained in complex with a heterotrimeric G-protein.

The active form of the CTR-in complex with both salmon calcitonin (sCT) and the heteromeric G-protein was structurally characterised (Figure 1-11). The construct used for this study was largely unmodified with only the native signal peptide replaced with the haemagglutinin signal peptide and a protease cleavable His tag added at the C-terminus. The structure had a global resolution of 4.1 Å and revealed some crucial aspects of peptide ligand

binding and G-protein docking (Liang *et al.*, 2017). The electron density for the ECD and the alpha helical domain of the G_s was poor and therefore were missing from the final structure. While density for the sCT was observed, accurate determination of the side chain conformations was not possible due to ambiguity in the final data. The overall structure is shown in (Figure 1-11, A). Upon receptor activation, there is a large movement in TMs 6 and 7 that allows docking of the G-protein to the intracellular face of the receptor. TM6 exhibits a 60° kink and ~15Å movement away from the TM bundle at the cytoplasmic side (Figure 1-11, A). The α5 helix of the Ras domain makes extensive contacts with the integral membrane domain through L394, L393, E392, H387 and M385 (Figure 1-11, B).

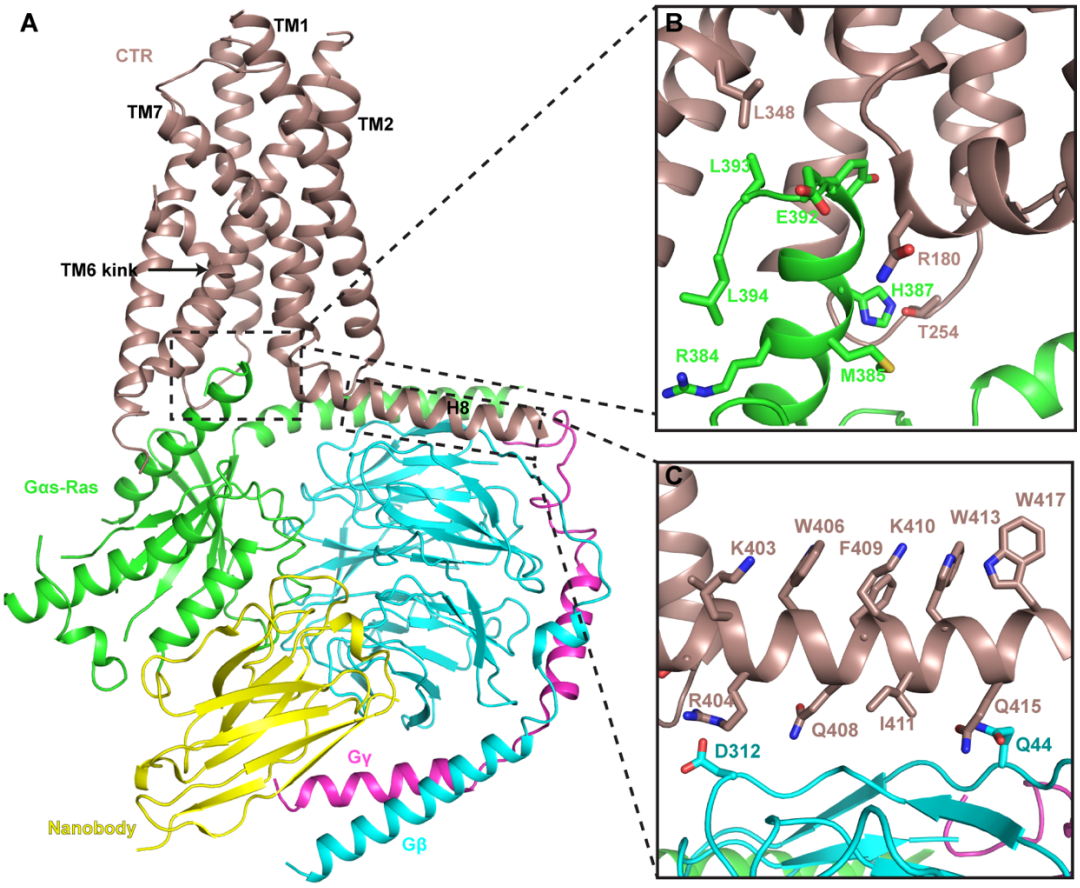


Figure 1-11: Cryo-EM structure of salmon calcitonin (sCT) activated calcitonin receptor (CTR) bound to heterotrimeric G-protein.

A) The overall structure shows sCT-activated calcitonin receptor (CTR) in complex with the heterotrimeric Gαs-protein. The molecules are shown in cartoon representation, with the receptor TMD in brown, Gα in green, Gβ in cyan and Gγ in magenta. The stabilising nanobody is shown in yellow. B) The α5 helix of G_s Ras-domain is shown docked alongside the intracellular face of the receptor. The outward movement of TM6 facilitates the G-protein binding and receptor activation C) The alpha helix following TM7, also known as helix-8, is shown to be interacting with the Gβ subunit. Figure generated using PyMOL with coordinates from PDB 5UZ7 (Liang *et al.*, 2017).

A series of bulky aromatic residues in helix 8 was found to make extensive contacts with the detergent micelle (Figure 1-11, C) and residues on the opposite side of helix 8 lie in close proximity to the Gβ subunit probably interacting via polar interactions (Figure 1-11, C).

While the structure of CTR provided information on receptor activation and G-protein binding, precise details of ligand binding and the interaction of ECD with the TMD were lacking. The structure of rabbit GLP1-R in complex with the native ligand and the heterotrimeric G-protein provided better electron density for both the ligand and the ECD (Zhang *et al.*, 2017) (Figure 1-12). Rabbit GLP1R, which shares 92% identity with the human receptor, was chosen for structure determination as it was found to express better in insect cells than the mouse and human homologues (Zhang *et al.*, 2017). GLP1R was recalcitrant to extraction by DDM or LMNG and therefore formation of the complex with the heterotrimeric G protein was done using insect cell membrane enriched for GLP1R (Zhang *et al.*, 2017). The final structure was reconstructed with a global resolution of 4.1Å, and a 3.9 Å nominal resolution in the core region including the GLP-1, TMD and the α5 helix of the G_s Ras-like domain (Zhang *et al.*, 2017).

The overall structure revealed peptide ligand binding to the orthosteric site within the TMD and ECD but no direct interaction between the TMD and ECD was observed (Zhang *et al.*, 2017). The lack of direct interactions between the ECD and the TMD implies that in the absence of ligand, the extracellular domain is flexible and this flexibility might be important for initial ligand recognition and binding (Zhang *et al.*, 2017).

GLP1R ECD was previously solved in complex with GLP1 peptide (3IOL) (Underwood *et al.*, 2009) and superposition of this structure with the full-length GLP1R structure yields an overall RMSD of ~0.75Å (Figure 1-12, B). The cryo-EM GLP1R structure reveals one additional helical turn at the N-terminal portion of the ligand compared to the ECD-GLP1 structure (Figure 1-12, B). The stabilisation and extension of the ligand N-terminal region has been shown to be important for receptor activation in some class B GPCRs (Parthier *et al.*, 2009).

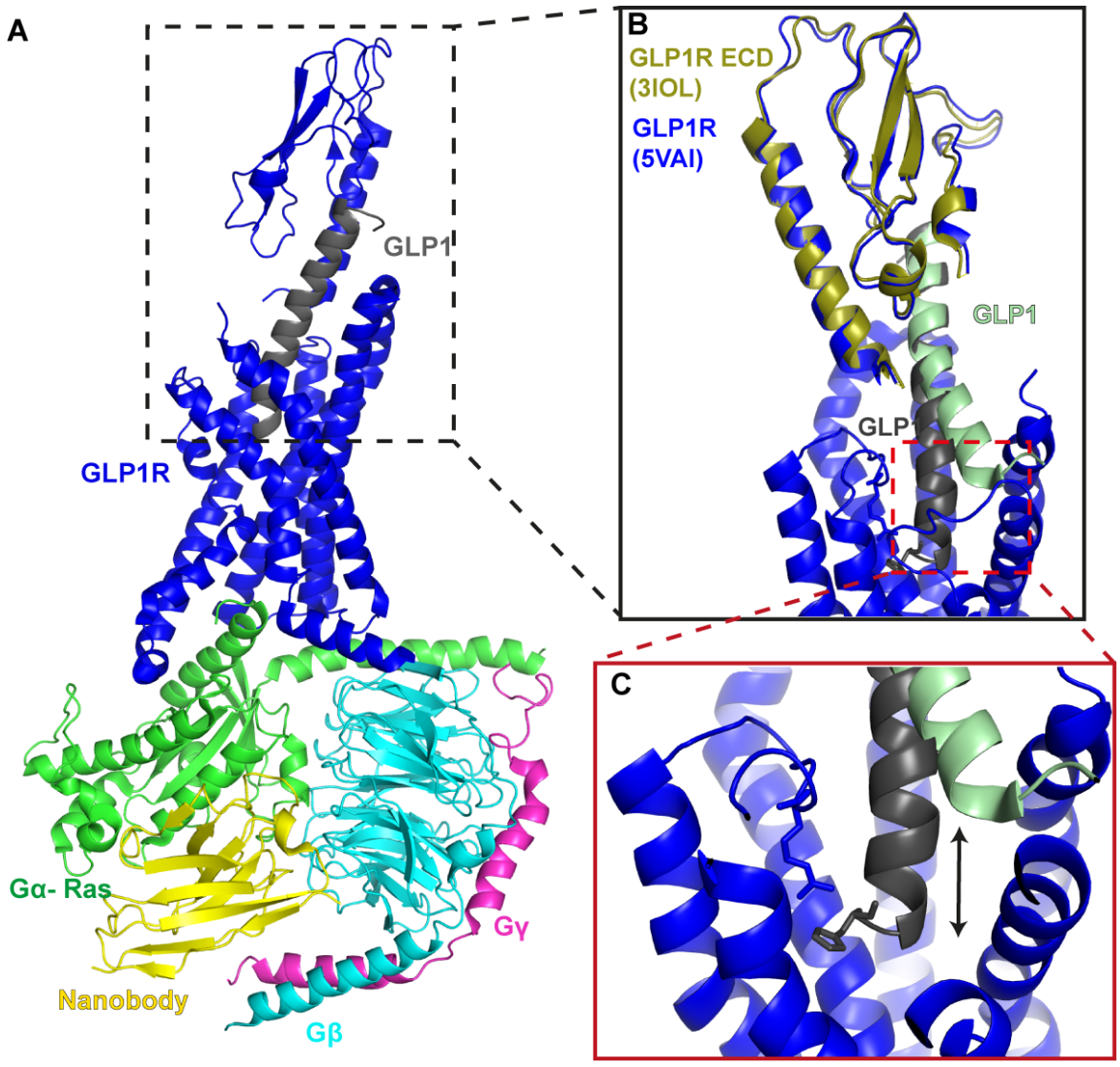


Figure 1-12 : Cryo-EM structure of GLP1-activated GLP1R in complex with heterotrimeric G-protein

A) The structure of the complex is shown in cartoon representation, where GLP1R is shown in blue, GLP1 peptide in grey, Ras-like domain of G_s subunit in green, nanobody in yellow, Gβ in cyan and Gγ in magenta. B) Superposition of GLP1R ECD from the cryo-EM structure of full-length GLP1R (blue, PDB: 5VAI) and GLP1R ECD in complex with GLP1 (olive colour, PBD: 3IOL) shows good overlay of the structural features. C) Close-up of the N-terminus of the GLP1 peptide shows stabilisation and extension of the ligand upon binding to the full-length receptor (grey) when compared to ligand bound to the ECD-only (light green).

The interaction of the ligand with residues in the TMD is key for receptor activation and signal transduction. The N-terminus of the peptide ligand makes extensive interactions with TMs 1,2,5,7, and ECL2 (Figure 1-13).

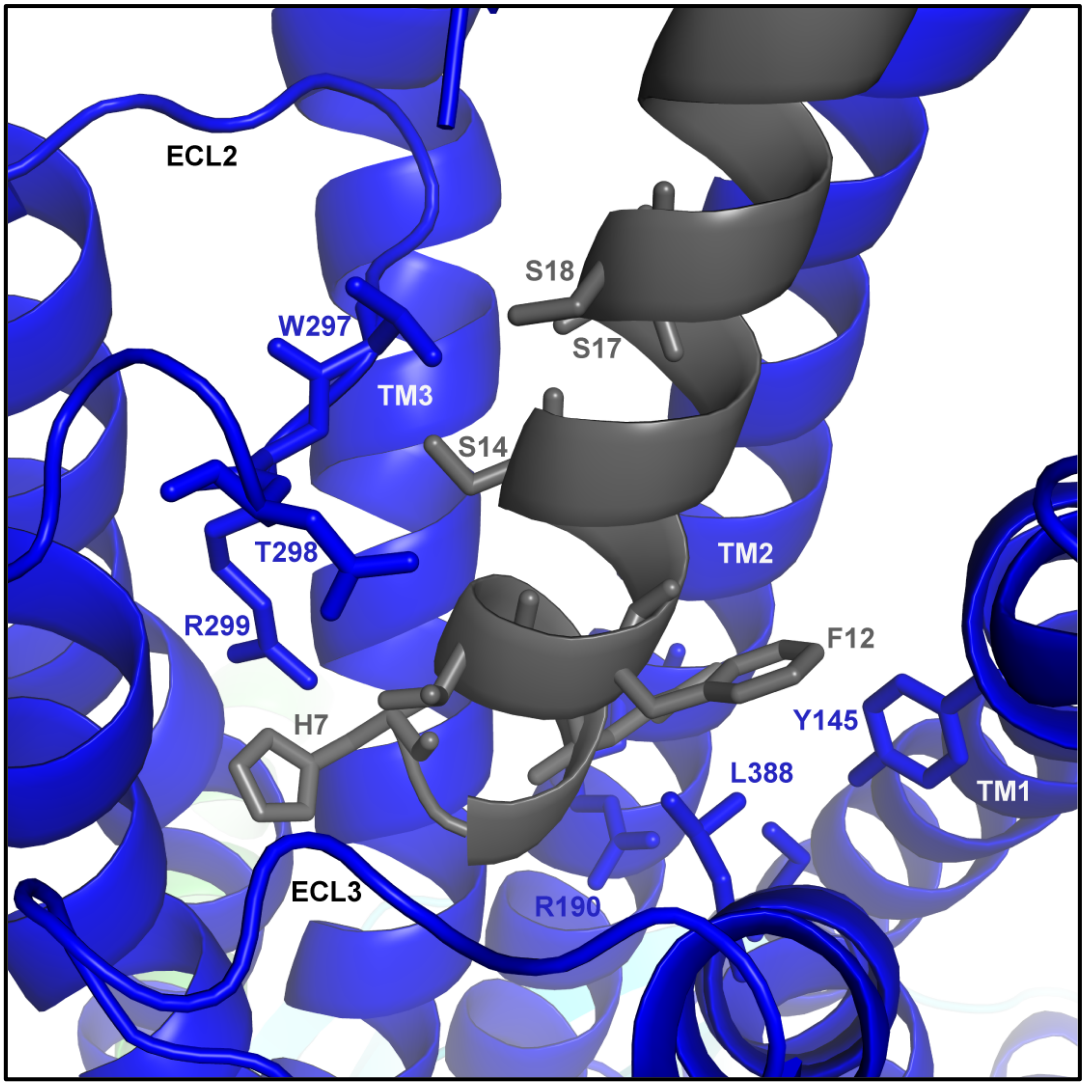


Figure 1-13: The orthosteric binding site of GLP1R

The N-terminus of the GLP1 peptide makes important interactions with residues in ECL2, TM1 and TM2. Key residues from the receptor are shown in blue stick representation and in grey stick representation for the peptide.

The H7 of the peptide ligand interacts with R299 of ECL2. The long side-chain of R299 appears to bend down towards the TMD, facilitating interaction with H7 (Figure 1-13). Similarly, E9 of GLP1 forms van der Waals interactions with L388 and S392 of TM7 and is suitably positioned to form hydrogen bonds with R190 and Y145 on TM2 and 1 respectively (Y. Zhang *et al.*, 2017). The extracellular loops also play a crucial role in ligand binding. Three serine moieties on the ligand (S14P, S17P, S18P) form polar interactions with T298, W297 and R299 on ECL2 (Figure 1-13). These interactions confirm the role ECL2 plays in ligand binding highlighted by previous studies (Koole *et al.*, 2012; Yang *et al.*, 2016). Similarly, ECL-

1 is also known to play a key role in ligand binding and receptor activation and in this case W31 of the ligand is packed against Q211 and H212 of GLP1R (Figure 1-14).

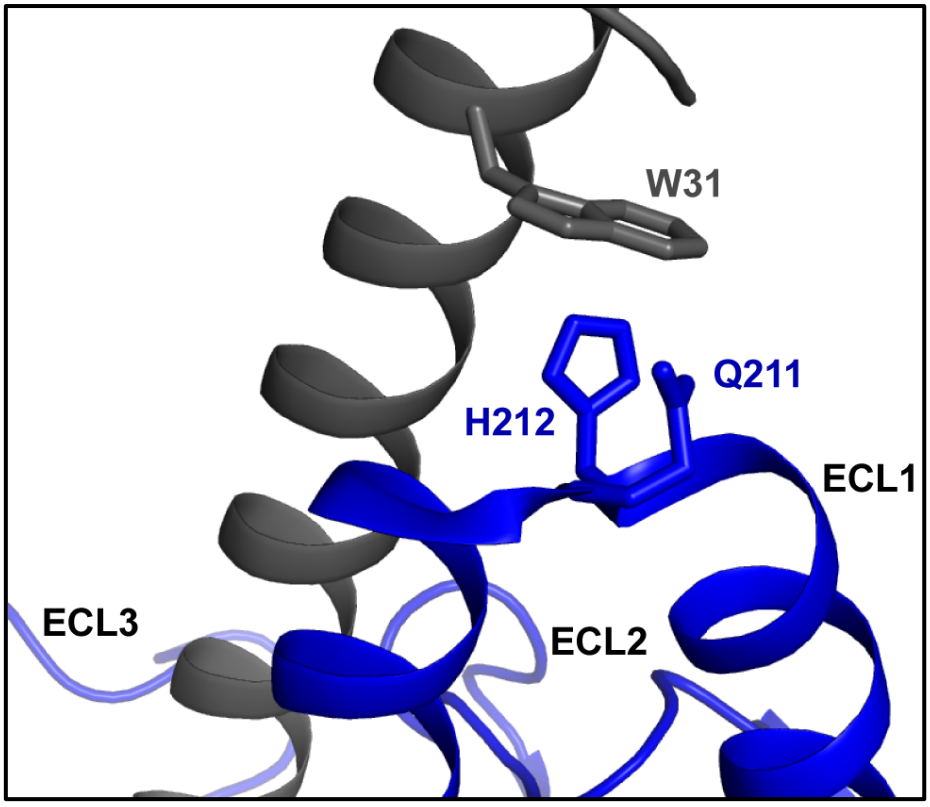


Figure 1-14: Key residues of GLP1R ECL-1 interacting with GLP.
The GLP1 peptide is shown in grey and GLP-1R is shown in blue cartoon representation

1.3 Parathyroid hormone receptor family

Parathyroid hormone receptor 1 (PTH1R) belongs to the secretin family of class B GPCRs and binds to parathyroid hormone (PTH) and parathyroid hormone-related peptide (PTHrP). PTH1R is mainly expressed in cells that are targets of PTH and PTHrP such as osteoblasts in bone and renal tubular cells of the kidney (Datta and Abou-Samra, 2009). Even though both PTH and PTHrP bind to the same receptor, they exhibit low sequence identity (~16%) (Schlüter, 1999). PTH is mainly synthesised and expressed by the parathyroid gland, whereas PTHrP expression is produced by various tissues such as skin, growth plate chondrocytes, smooth muscles, bone, kidney and neuronal and glial cells (Datta and Abou-Samra, 2009).

In humans, the PTH1R gene is located in chromosome 3, and is a multi-exonic gene with a total of 14 exons (Kong *et al.*, 1994). The mature receptor consists of 567 amino acids following cleavage of the signal peptide. The ECD contains 6 conserved cysteine residues forming 3 disulphide bridges 4 N-linked glycosylation sites (Grauschopf *et al.*, 2000) (Figure 1-15).

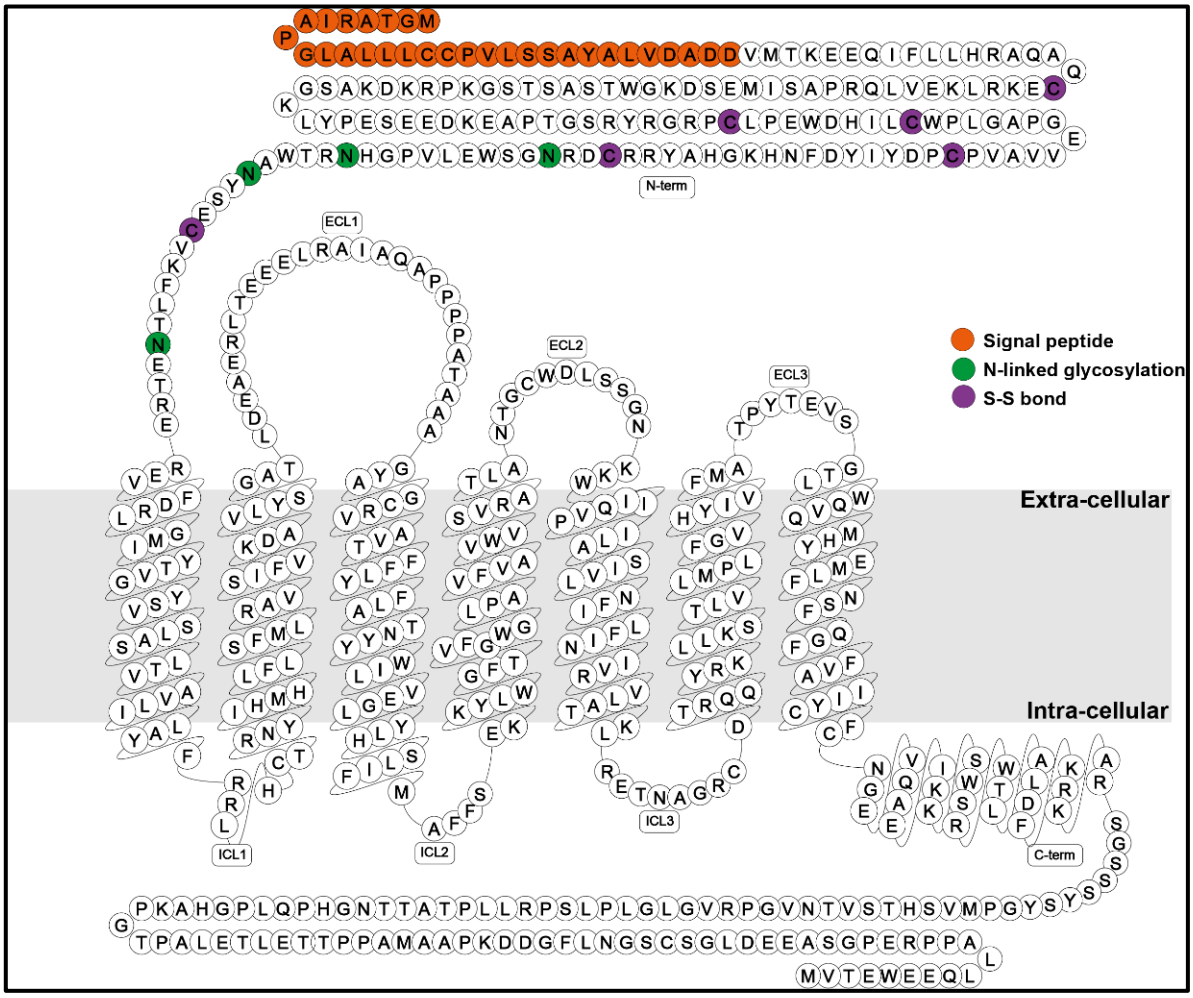


Figure 1-15: Snake diagram of PTH1R

A snake plot of PTH1R highlighting the residues of the N-terminal ECD, the transmembrane domains, extracellular and intracellular loops and the cytoplasmic C-terminal tail. The signal peptide residues are shown in orange, the disulphide bond forming cysteine residues in purple and N-linked glycosylation sites in green. Snake plot created using GPCRDB (Isberg *et al.*, 2015)**.**

1.3.1 Physiological importance of PTH1R

The importance of PTH1R in bone development and bone cell differentiation has been previously shown using homologous recombination and transgenic technology (Schipani, Kruse and Jüppner, 1995; Parfitt *et al.*, 1996; Jobert *et al.*, 1998; Lanske *et al.*, 1999).

Blomstrand chondrodysplasia (BMC) is a genetic disorder characterized by advanced endochondral bone maturation (Jobert *et al.*, 1998). BMC is caused by the presence of a missense mutation which leads to the substitution of proline for a leucine (P132L) within the ECD of the receptor (Zhang *et al.*, 1998). Cells expressing this mutant receptor exhibit severely reduced cAMP accumulation in response to PTH although receptor expression and trafficking are unaffected (Zhang *et al.*, 1998).

The activating mutations, H223R or T410P, in PTH1R causes Jansen's metaphyseal chondrodysplasia (JMC) (Schipani, Kruse and Jüppner, 1995). Patients suffering with JMC exhibit decreased tubular reabsorption of phosphate, hypercalcemia, hypophosphatemia, and increased urinary excretion of cAMP (Schipani *et al.*, 2014). *In vitro* studies using COS-7 cells showed that both mutations result in reduced expression and trafficking as well as increased constitutive activity leading to higher basal cAMP levels (Schipani *et al.*, 1997).

Currently, the bioactive N-terminal 34 residue fragment of human parathyroid hormone, PTH (1-34) (teriparatide, Forsteo®, Forteo®) is an FDA-approved drug for treating osteoporosis (Neer *et al.*, 2001). Intermittent injection of teriparatide is known to reduce fracture risk of the spine though its effect on non-vertebral bones are much less pronounced (Neer *et al.*, 2001). It should however be noted that while treatment with teriparatide induces bone matrix production by the osteoblasts, it also induces osteoclastogenesis by stimulating secretion of growth factors and cytokines such as RANKL. With chronic usage, this leads to bone resorption, even when administered intermittently (Neer *et al.*, 2001). Some other side effects of teriparatide include hypercalcemia, nausea, headache, dizziness, and leg cramps (Neer *et al.*, 2001).

Recently, a novel PTHrP analogue, abaloparatide (TYMLOS®) received FDA-approval for treatment of osteoporosis (Leder *et al.*, 2015). Abaloparatide is a PTH1R agonist which shares 41% sequence homology to PTH (1–34) (teriparatide) and 76% homology to PTHrP (Doyle *et al.*, 2017). In a recently published phase 3 clinical study, it was found that similar increases in spine bone mineral density (BMD) were induced by both abaloparatide and teriparatide, but abaloparatide increased hip and femoral neck BMD by a further 1% when

compared to teriparatide (Leder *et al.*, 2015). Interestingly, the incidence of hypercalcemia was found to be lower with abaloparatide (6.4%) when compared to teriparatide (3.4%) and therefore might offer an alternative to teriparatide (Leder, 2017). Whilst a number of treatments are available, these are sub-optimal and thus there is scope to develop other more effective therapeutics.

1.3.2 Structural insights into PTH binding

High resolution crystal structures are available for the apo-form of the N-terminal ECD of PTH1R (3L2J) (Pioszak *et al.*, 2010), the ECD in complex with PTH (3C4M) (Pioszak and Xu, 2008), and in complex with PTHrP (3H3G) (Pioszak *et al.*, 2009). In all three cases, the ECD molecule was expressed in *E. coli* with an N-terminal maltose-binding protein (MBP) tag present on the crystallised protein. The fusion protein was co-expressed with DsbC, a bacterial disulphide isomerase, to facilitate successful folding and disulphide bond formation (Bessette *et al.*, 1999).

The functional activity of the expressed ECD was determined by PTH (15-34) binding studies in an AlphaScreen binding assay, which measured the ability of PTH (15–34)-NH_2 to compete with the interaction of biotin-PTH (7–34)-NH_2 and MBP-PTH1R-ECD-His_6 along with isothermal-titration calorimetry (ITC). Both methods concluded that the binding affinity of the ligand to the expressed ECD was around 1-3 μM, comparable with other class B GPCR ECD ligand binding affinities (Pioszak and Xu, 2008).

PTH1R ECD adopts an α-β-β-α fold with a central hydrophobic core which forms the PTH binding groove (Pioszak and Xu, 2008). The single amphipathic helix of PTH (15-34) docks into the hydrophobic groove formed by the ECD domain (Figure 1-16, A). Hydrophobic interactions involving residues V21, W23, L24, L28, V31 and F34 of PTH play a key role in the PTH-PTH1R ECD binding.

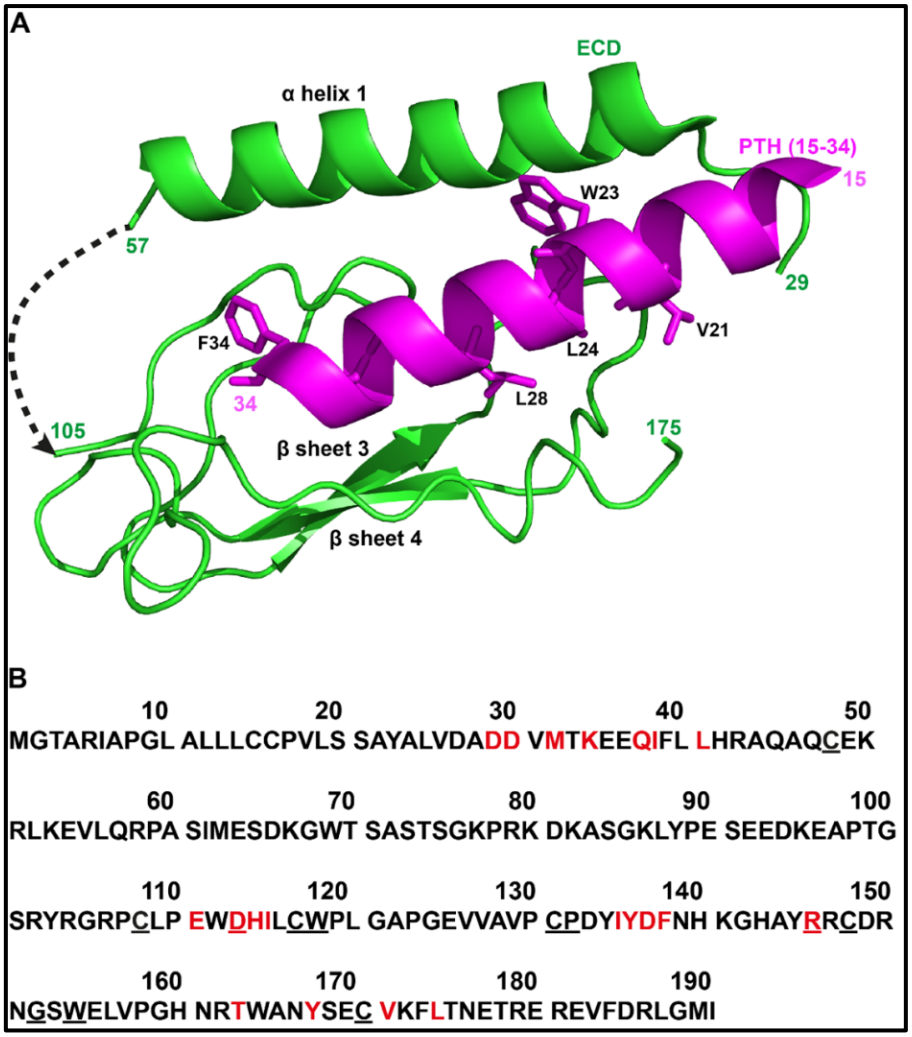


Figure 1-16: PTH binding to the PTH1R ECD binding.

A) Crystal structure of PTH (15-34) bound to PTH1R ECD shows the overall binding of the ligand to the ECD. PTH (15-34) (in magenta) binds into the hydrophobic groove formed by the ECD (shown in green). Residues V21, W23, L24, L28 and F34 of PTH (15-34) involved in binding are shown as sticks. Some ECD residues were not built due to poor density and this region is indicated by the black dashed arrow. Figure generated using PDB coordinates from 3C4M (Pioszak and Xu, 2008) B) PTH1R ECD sequence highlighting residues involved in PTH binding (red) and residues conserved in other secretin family member ECDs (underlined).

Even though the α-β-β-α fold is conserved among class B GPCR ECDs, none of the residues that form the PTH-binding groove are conserved among other members suggesting a unique surface topology for each individual receptor (Pioszak and Xu, 2008) (Figure 1-16, B). While the structure of N-terminal ECD has elucidated the ligand binding partly, a full-length structure of PTH1R is still not available, and could further help fully understand the mechanism of PTH binding and receptor activation. The structure also does not provide any information on the interactions the cognate ligand makes with the TMD, which is known to be crucial for receptor activation.

1.3.3 PTH1R activation

Parathyroid hormone receptor-1, like other class B GPCRs, has the ability to bind to more than one G-protein subclass (Schwindinger *et al.*, 1998) and thus can activate different intracellular signalling pathways. Binding to the G_s or $G_{q/11}$ subunit is mediated by the N-terminal end of the third intra-cellular loop (Huang *et al.*, 1996). Mutagenesis studies on rat PTH1R, showed that replacing the EKKY sequence in ICL2, with DSEL selectively inhibited G_{q11} binding leaving G_s coupling and signalling unaffected (Iida-Klein *et al.*, 1997) suggesting that this region is selective for G_α coupling, although the precise mechanism is not clear.

Complete removal of the C-terminal tail of PTH1R, yielded a construct with enhanced PTH-induced cAMP generation. The authors concluded that a region(s) within the C-terminal tail of PTH1R limits the efficacy with which the receptor interacts with G_s possibly as the result of fine-tuning the ligand binding affinity (Iida-Klein *et al.*, 1995). These experiments along with various other studies have shown that the intracellular loops and the C-terminal tail play a key role in not just receptor activation and deactivation but fine control of receptor signalling through alternative G-protein subclasses, and thus the cellular response to PTH.

1.3.4 PTH1R desensitisation and role of arrestins

Like most GPCRs, desensitisation of ligand-activated PTH1R starts with receptor phosphorylation of residues within the C-terminal tail region, carried out by GRKs. The phosphorylated receptor preferentially binds to β-arrestin which then initiates the receptor internalisation process. Phosphopeptide mapping and direct sequencing revealed that PTH activated PTH1R is phosphorylated at serines 489, 491, 492, 493, 495, 501 and 504. This phosphorylation motif is located at the N-terminal end of the intracellular C-terminal domain and mutating all 7 serine to alanine completely abrogates phosphorylation and internalisation (Tawfeek, Qian and Abou-Samra, 2002).

Interestingly, it is now well established that the scaffolding properties of β-arrestins can bring elements of certain signalling pathways into close proximity to the internalised receptor (Luttrell *et al.*, 1999). β-arrestin regulation has been demonstrated for an

ever-increasing number of signalling molecules, including the mitogen- activated protein kinases (MAPK), extracellular signal–regulated kinases (ERK), c-Jun N-terminal kinase (JNK), and p38 as well as Akt, PI3 kinase, and RhoA (DeWire *et al.*, 2007). Arrestin mediated signalling via the MAPK pathway is propagated by three proline rich motifs (P-XX-P) which are located at the C--terminal tail of PTH1R (Rey *et al.*, 2006).

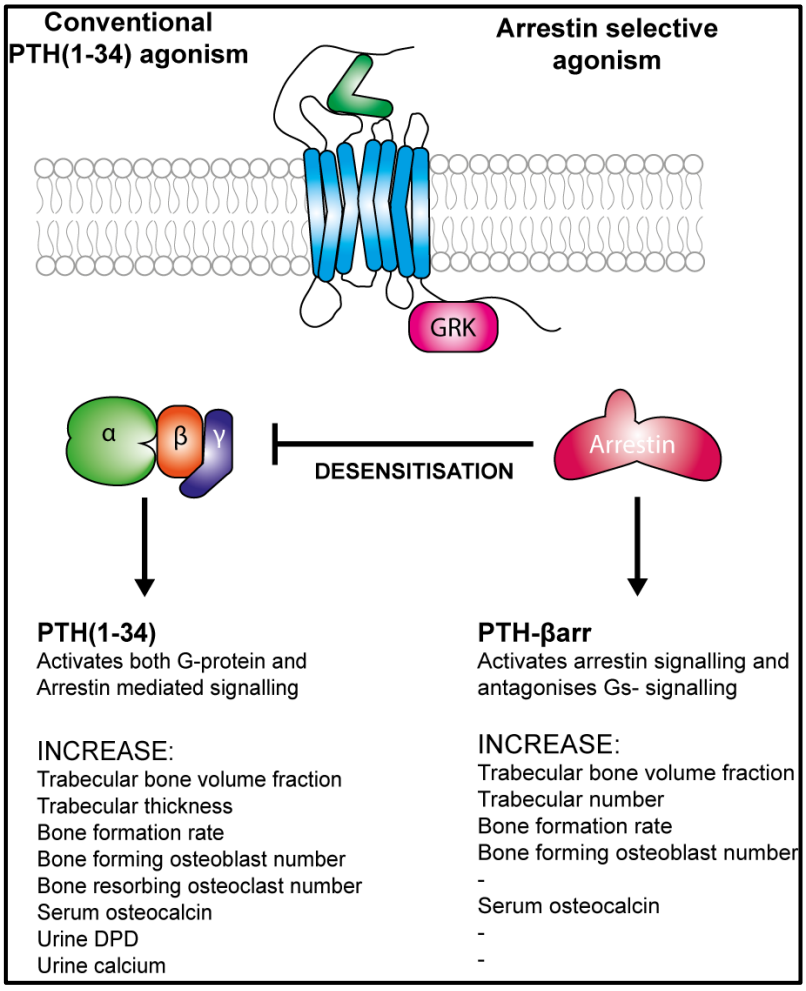


Figure 1-17: Arrestin-selective PTH1R agonism.

A schematic representation showing the effect of arrestin-mediated signalling in PTH1R. A β-arrestin biased ligand such as PTH-βarr causes anabolic bone formation in *in vivo* studies carried out in mouse. PTH (1-34) causes an increase in osteoclast number which is not seen with PTH-βarr, among other things. Figure adapted from (Gesty-Palmer and Luttrell, 2011).

The ability to signal through two distinct G-proteins, together with the additional signalling role of β-arrestin have opened up new opportunities for the design of drugs that act as “biased ligands” preferentially stimulating / inhibiting only one signalling pathway (Eason, Jacinto and Liggett, 1994; DeWire and Violin, 2011). A number of biased ligands for PTH1R have been described (Gesty-Palmer and Luttrell, 2011), such as PTH(1-31) which is G_s

selective (Whitfield and Morley, 1995), PTH (3-34) which is G_q selective (Jouishomme *et al.*, 1992) and D-Trp^{12},Tyr^{34}-PTH(7–34) which acts as an inverse G_s agonist (Gardella *et al.*, 1996), among others. PTH1R-dependent signalling through β-arrestin is said to result in bone accrual without activation of osteoclasts and a β-arrestin biased ligand D-Trp^{12},Tyr^{34}-PTH(7–34) (PTH-βarr or PTH (7-34) has been shown to induce anabolic bone formation *in vivo* (Figure 1-17) (Gesty-Palmer *et al.*, 2009). However, van der Lee et al. later showed that the β-arrestin biased agonist effects of PTH-βarr could not be replicated in human embryonic kidney (HEK293), Chinese hamster ovary (CHO) and U2OS cells indicating that drawing conclusions on *in vivo* effects of PTH(7–34) from *in vitro* pharmacology should be done with caution (van der Lee *et al.*, 2013).

1.3.5 Other GPCR interacting proteins (GIP) modulating PTH1R

In addition to G-proteins and β-arrestins, GPCRs are also known to interact with various intracellular proteins which further modify their signalling repertoire (Bockaert *et al.*, 2004). Yeast two-hybrid screening of a human kidney cDNA library using the C-terminal tails for PTH1R C-terminal tails as bait identified the sodium hydrogen exchanger regulatory factor 2 (NHERF-2, also called exchanger 3 kinase A regulatory protein, E3KARP) as a strong interacting partner (Mahon *et al.*, 2002). NHERF1 and 2 binding to PTH1R occurs at the 'ETVM' motif at the C-terminal end of PTH1R (Figure 1-18) (Mahon *et al.*, 2002). In osteoblast-like RoS 17/2.8 cells where NHERF expression is undetectable, PTH1R signals mainly by regulating adenylyl cyclase, whereas in human umbilical vein endothelial ECv304 cells, expressing high levels of both NHERF1 and 2, PTH1R signals mainly through PLCβ regulation, clearly indicating the role of NHERF in switching PTH1R's G-protein binding preference (Mahon *et al.*, 2002). PTH1R binding to NHERF illustrates the key role GIPs can play in modulating GPCR signalling.

Dishevelled (Dvl), a PDZ domain containing a key mediator of β-catenin signalling, has also been shown to directly interact with PTH1R using co-immunoprecipitation experiments (Romero *et al.*, 2010). Unlike NHERF1, however, the PDZ domain of Dvl2 does not interact

with the canonical PDZ-interaction motif (ETVM) in the C-terminal tail of the PTHR. A truncated PTH1R (at residue 480) missing the canonical PDZ binding motif can still interact with Dvl2, but a truncation at position 470 eliminates Dvl2 binding (Romero *et al.*, 2010). The Dvl2 binding motif has been suggested to be ^{472}KSWSRW, located immediately downstream of the transmembrane helix 7 of the PTH1R. This sequence is homologous to the consensus Dvl-binding motif (KTXXXW) conserved in all members of the Frizzled (Fzd) family of receptors (Figure 1-18) (Umbhauer *et al.*, 2000). The binding of Dvl2 to the PTHR has important consequences for the regulation of PTHR signalling and ablation of this interaction eliminates PTH-dependent activation of β-catenin-dependent gene expression (Romero *et al.*, 2010). Since the Wnt signalling pathway plays a major role in development, bone morphogenesis (Baron and Kneissel, 2013) and tumorigenesis (Anastas and Moon, 2013), and Dvl2 is one of the major mediators in this pathway (Gao and Chen, 2010), the cross-talk between Dvl and PTH1R merits further investigation.

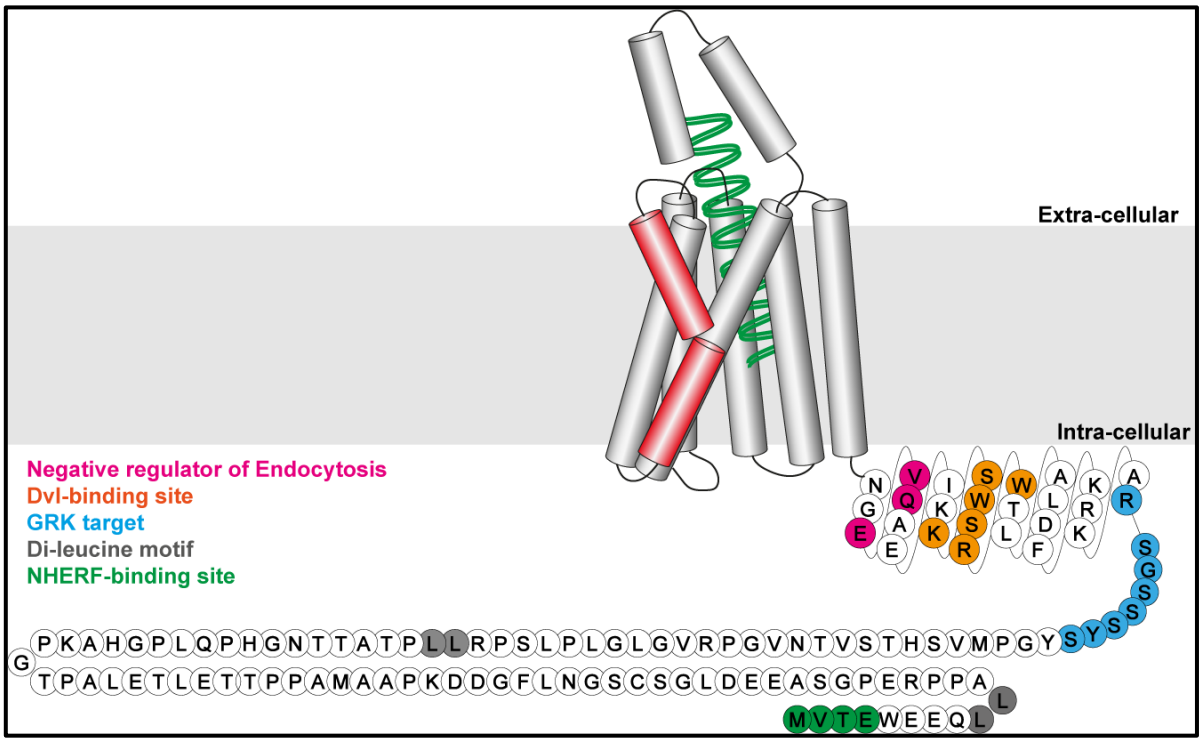


Figure 1-18: GPCR interacting protein (GIP) interaction sites.

Important motifs for PTH1R phosphorylation and internalisation (colour coded) are all located in helix 8 and the C-terminal tail and plays a crucial role in signalling modulation. Figure adapted from (Vilardaga *et al.*, 2010)

1.4 GPCR expression and stabilisation

1.4.1 Expression systems

Most of the recently solved high resolution structures of GPCRs have been obtained using protein expressed in insect cells using baculoviral based expression systems (Bertheleme, Chae, *et al.*, 2013; Milić *et al.*, 2015). Insect cells can be produced in large scale at a reasonable cost and are effective at performing the eukaryotic post-translational modifications which can be crucial for receptor folding, function and stability (Bertheleme, Chae, *et al.*, 2013). There are two examples of protein expressed in *Pichia pastoris* being successfully used to determine high resolution GPCRs structures; the human adenosine A_{2A} (Hino *et al.*, 2012) and histamine H1 receptors, both crystallised in complex with Fab fragments (Shimamura *et al.*, 2011). More recently, a 2.8Å structure of US28, a viral GPCR from human cytomegalovirus was solved, using protein expressed in HEK 293 cells (Burg *et al.*, 2015). The structure determination of CXCR1 by NMR was carried out using protein expressed in *E. coli* and then refolded from inclusion bodies (Park, Bibhuti B Das, *et al.*, 2012). *E. coli* was also used for the production of stabilised rat NTS1 (Egloff *et al.*, 2014). Table 1-2 summarises established heterologous expression systems used for GPCR structure-function studies.

Table 1-2: Expression system to facilitate GPCR structure-function studies*

Expression system	GPCR	Family	References	Advantages	Disadvantage
Natural source	Rhodopsin	A	(Palczewski *et al.*, 2000)	Extraction possible if receptor is expressed in abundance.	No sequence modifications are possible; Difficult purification without tags
	Rhodopsin	A	(Murakami and Kouyama, 2008)		
Insect cells	β_1-adrenergic receptor	A	(Warne *et al.*, 2008b)	Eukaryotic (PTM); Large scale up possible; Reasonable set-up and media cost.	Time-consuming; Requires large number of viral particles; Membrane lipid content different from mammalian cells.
	β_2-adrenergic receptor	A	(Cherezov, *et al.*, 2007)		
	D_3 receptor	A	(Chien *et al.*, 2010)		
	M_2 receptor	A	(Haga, *et al.*, 2012)		
	M_3 receptor	A	(Kruse *et al.*, 2012)		
	A_{2A} receptor	A	(Lebon *et al.*, 2011)		

	CRF1 receptor	B	(Hollenstein *et al.*, 2013)		
	Glucagon receptor	B	(Siu *et al.*, 2013)		
	$mGlu_1$ receptor	C	(Wu *et al.*, 2014)		
	$mGlu_5$ receptor	C	(Doré *et al.*, 2014a)		
	Smoothened (SMO) receptor	F	(Wang *et al.*, 2013)		
Yeast	H_1 receptor	A	(Shimamura *et al.*, 2011)	Quick growth and easy to culture; Relatively less-expensive media	Different PTMs; High ergosterol and low cholesterol in membrane.
	A_{2A} receptor	A	(Hino *et al.*, 2012)		
Bacteria	CXCR1	A	(Park *et al.*, 2012)	Easy to culture and scale up; Cheap media and set-up.	No PTM; Extraction of inclusion bodies difficult.
	NTS1 receptor	A	(Egloff *et al.*, 2014)		
Mammalian	Rhodopsin	A	(Standfuss *et al.*, 2007)	Proper post-translational modifications; Appropriate membrane lipid content	Expensive media and set-up; Generation of stable cell line is very time-consuming
	Rhodopsin	A	(Mattle *et al.*, 2018)		
	CB_1 cannabinoid receptor		(Hua *et al.*, 2016)		
	Leukotriene B4 receptor		(Hori *et al.*, 2018)		
	Smoothened (SMO) receptor	F	(Byrne *et al.*, 2016)		

*** Table is not exhaustive and attempts to provide few representative examples of GPCRs from each receptor family**

1.4.2 Receptor stabilisation and extraction methods

GPCRs, are very flexible molecules and this presents some challenges for crystallisation and structure determination efforts. A number of different approaches have been used to reduce conformational flexibility and increase the likelihood of crystallisation as detailed below.

Fusion proteins

One approach is the use of fusion proteins. T4 lysozyme (T4L) and apocytochrome b562 RIL (BRIL) are two highly stable, soluble and readily crystallisable proteins. A substantial number of GPCR structures have been structurally characterised as fusion proteins with either

T4L or BRIL (Milić *et al.*, 2015). In most cases the fusion protein has been inserted into or replaces ICL3, a typically highly flexible region of the receptor. In addition, they have both also been successfully fused to the N-terminus of a receptor (Milić *et al.*, 2015). A comprehensive study of the fusion proteins, their insertion site and loop distance was performed with a range of soluble proteins including flavodoxin, xylanase, rubredoxin as well as T4L and BRIL (Chun *et al.*, 2012).

Table 1-3: Fusion proteins used in GPCR stabilisation (Milić *et al.*, 2015)

Fusion protein	Position	Receptor	Reference
T4L	ICL3	β_2-adrenergic receptor	(Cherezov *et al.*, 2007; Hanson *et al.*, 2008; Wacker *et al.*, 2010; Rosenbaum *et al.*, 2011; Rasmussen *et al.*, 2011)
		A2A receptor	(Jaakola *et al.*, 2008; Xu *et al.*, 2011)
		D3 receptor	(Ellen Y. T. Chien *et al.*, 2010)
		CXCR4	(Wu *et al.*, 2010)
		H1 receptor	(Shimamura *et al.*, 2011)
		M2 receptor	(Haga, Andrew C Kruse, *et al.*, 2012)
		μ receptor	(Manglik *et al.*, 2012)
		κ receptor	(Wu *et al.*, 2012)
		mouse δ receptor	(Granier *et al.*, 2012)
		NTS1	(White *et al.*, 2012b)
		PAR1	(Zhang *et al.*, 2012)
		S1P1 receptor	(Hanson *et al.*, 2012)
		FFA1 receptor	(Srivastava *et al.*, 2014)
T4L	ICL2	CRF1 receptor	(Hollenstein *et al.*, 2013)
		mGlu5 receptor	(Doré *et al.*, 2014c)
T4L	N	β_2- adrenergic receptor	(Zou, Weis and Kobilka, 2012)
		β_2- adrenergic receptor	(Rasmussen *et al.*, 2011)
		β_2- adrenergic receptor	(Ring *et al.*, 2013)
BRIL	ICL3	A2A receptor	(Liu *et al.*, 2012)
		5-HT1B receptor	(Wang, Jiang, *et al.*, 2013)
		5-HT2B receptor	(Wacker *et al.*, 2017)

		P2Y12 receptor	(Zhang *et al.*, 2014)
		SMO	(Wang, Wu, Katritch, Han, X.-P. Huang, *et al.*, 2013)
BRIL	N	NOP receptor	(Thompson *et al.*, 2012)
		Glucagon receptor	(Siu *et al.*, 2013)
		SMO	(Wang, Wu, Katritch, Han, X.-P. Huang, *et al.*, 2013)
		mGlu1 receptor	(Wu, Wang, Karen J. Gregory, *et al.*, 2014)
		human δ receptor	(Fenalti *et al.*, 2014)
Rubredoxin	ICL3	CCR5	(Tan *et al.*, 2013)
PGS[1]	ICL3	OX2 receptor	(Yin *et al.*, 2014)

[1] ***P. abysii*** **glycogen synthase**

These insertions not only help by stabilising flexible loops, which can hinder the crystallisation process but also provide soluble domains key in the formation of crystal contacts (Milić *et al.*, 2015). This method is well-established and has helped with GPCR structure determination from all major families. Major truncation at ICL3 or C-terminal region and insertions of soluble domain can sometimes affect the ability of the receptor to couple with signalling partners and does not represent the physiological form of the receptors (Milić *et al.*, 2015)

Mutagenesis approach

An alternative approach employs systematic mutagenesis coupled with functional assays which can capture the GPCR in conformations that preferentially bind either agonist or antagonist (Magnani *et al.*, 2008). In this approach, residues are systematically mutated to alanine and then assessed for binding to ligand (agonist or antagonist) following heat treatment at the apparent T_m of the WT receptor. Thermostabilised mutants exhibit greater levels of activity than the WT receptor and a bias for a certain conformation. Iterative addition of stabilising mutations further increases thermal stability and improves binding of the agonist or antagonist (Robertson *et al.*, 2011). The β_1-adrenergic receptor from turkey in complex with the high-affinity antagonist cyanopindolol was the first structure obtained using this approach

(Warne *et al.*, 2008a), but it has seen been successfully applied to a range of GPCRs (Serrano-Vega *et al.*, 2008; Shibata *et al.*, 2009; Doré *et al.*, 2011; Hollenstein *et al.*, 2013; Robertson *et al.*, 2018). While the mutagenesis approach has been widely used in trapping receptors in certain conformation and facilitated structural studies, it is important to note that it is a resource-intensive process which requires generating hundreds of constructs. Also, the stabilising mutation may not be transferable between distant receptors, and possibly work only between closely related receptors (Milić *et al.*, 2015).

Antibody fragments

Antibody fragments have been used as tools for crystallography for both soluble proteins and membrane proteins (Hunte and Michel, 2002; Griffin and Lawson, 2011; Mujić-Delić *et al.*, 2014). The antibody fragments (Fab or Fv) bind target molecules with high affinity and have the potential to stabilise certain conformation. This approach is especially useful for membrane proteins, which in solution are mostly covered in detergent micelle which limits the formation of crystal contacts to the exposed soluble regions. The presence of the antibody fragment extends the soluble domain of the receptor providing a greater polar surface area for crystal contacts to form (Day *et al.*, 2007; Lim, Fang and Williams, 2011).

The A_{2A} receptor was the first GPCR crystallised in complex with an allosteric inverse-agonist Fab, Fab2838, bound to the intracellular face of the receptor (Hino *et al.*, 2012). The Fab stabilised the inactive conformation of the receptor and mediated the key crystal contacts within the crystal lattice (Hino *et al.*, 2012) (Figure 1-19).

Camelids such as llamas, alpacas and camels contain heavy chain-only functional antibodies (V_{HH}) which lack the light chain, in addition to conventional hetero-tetrameric antibodies (Hamers-Casterman *et al.*, 1993). The recombinant variable domains of these V_{HH} are known as nanobodies and this class of molecules have recently been shown to be an excellent tool for both locking GPCRs in individual conformations and as crystallographic chaperones (Manglik, Kobilka and Steyaert, 2017).

Nanobodies are generally more thermostable and can be produced in larger amounts than IgG- derived fragments such as single chain F_v (scFv) (Dumoulin *et al.*, 2009). They can also be produced in a range of expression systems including *E. coli* (Arbabi-Ghahroudi, Tanha and MacKenzie, 2005), *S. cerevisiae* (Frenken *et al.*, 2000), mammalian cells (Agrawal *et al.*, 2012) and plants (Ismaili *et al.*, 2007).

Nanobody Nb35, was used to stabilise the heterotrimeric G-protein in complex with the β_2- adrenergic receptor. The Nb35 further facilitated the crystallisation of the overall complex leading to a 3.2 Å resolution structure (Rasmussen *et al.*, 2011) (Figure 1-5). The crystal structure of the M2 muscarinic receptor + the agonist Iperoxo was solved in complex with a G-protein mimetic nanobody, Nb9-8 (Kruse *et al.*, 2013) (Figure 1-19).

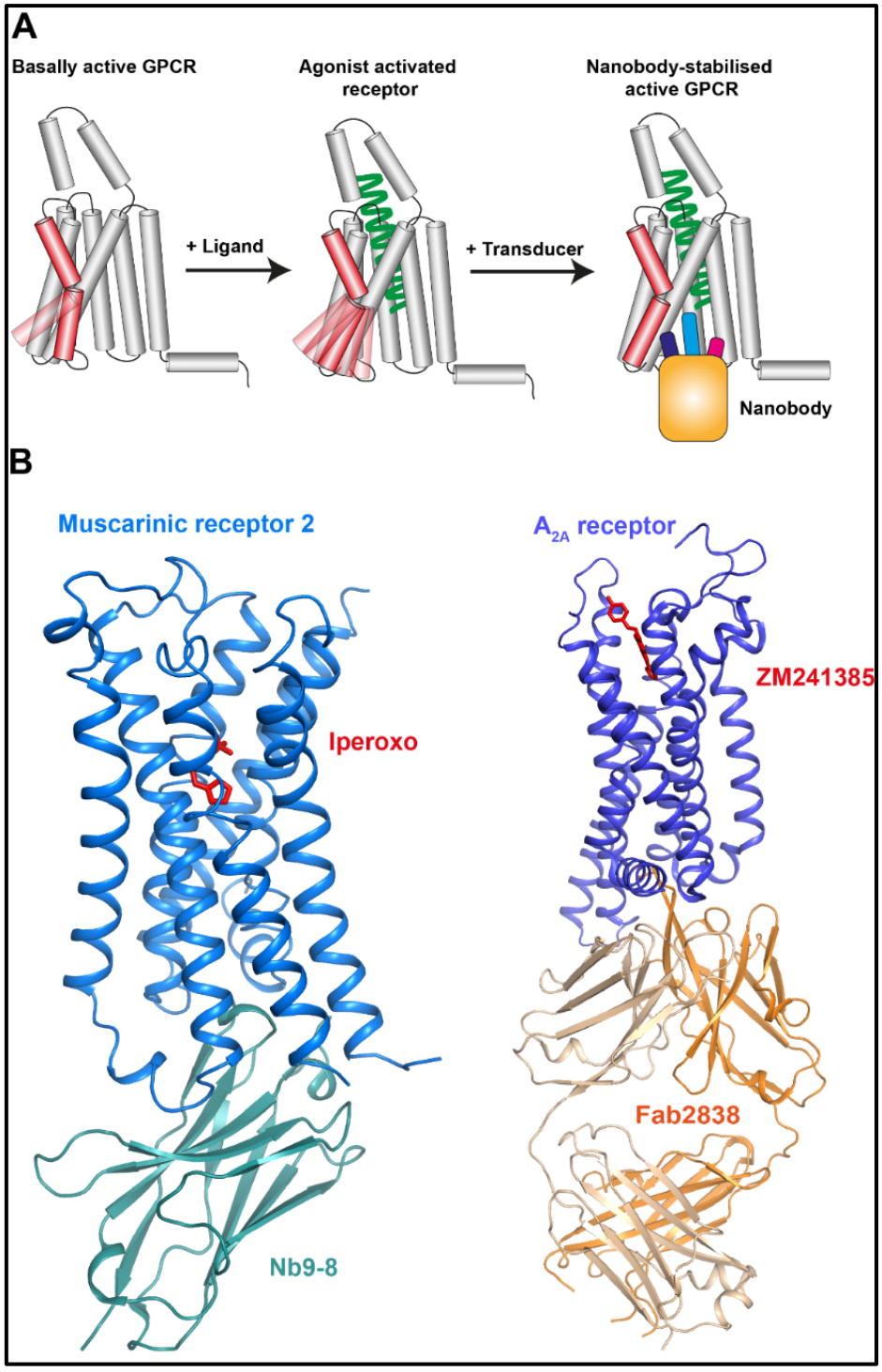


Figure 1-19: Nanobody and Fab as crystallographic chaperones

A) GPCRs exhibit basal activity which contributes to structural flexibility. Ligand binding pushes the equilibrium further towards the active state illustrated by the conformational changes observed in TM helices 6 and 7. This conformational flexibility can prevent the crystallisation process. Binding of transducer molecules such as Fab fragments, nanobodies or G-proteins to GPCRs can stabilise the overall structure and provide additional soluble domains key in the formation of crystal contacts (Manglik, Kobilka and Steyaert, 2017). B) The active structure of the muscarinic receptor (blue) bound to the agonist Iperoxo stabilised by the G-protein mimetic nanobody Nb9-8 (light blue) (left). Structure of inactive A_{2A} receptor (dark blue) bound to the allosteric inverse agonist Fab 2838 (dark and light gold colour) (right).

While antibody fragments and nanobodies are useful as crystallography chaperones, it can be quite difficult to generate appropriate antibody against difficult targets such as GPCRs for structural studies (Hutchings *et al.*, 2017).

Detergents and other agents

Integral membrane proteins (IMP) such as GPCRs exist within the lipid bilayer and are naturally amphipathic with TM regions exhibiting high hydrophobicity (Engel and Gaub, 2008). Detergents are required to both extract the GPCRs from the membrane and maintain the proteins in aqueous solution. At the critical micelle concentration (CMC), specific to individual molecules, detergents self-associate to form micelles and this property has long been exploited in membrane protein extraction from cell lysates (Seddon, Curnow and Booth, 2004). The detergents dodecyl-β-maltoside (DDM) and lauryl maltose neopentyl glycol (LMNG) are widely used for the extraction of membrane proteins as summarised in Table 1-4. More details on detergents can be found in chapter 4.

Table 1-4: A representative table of widely used detergents used for receptor solubilisation and structural studies

Receptor	Detergent	PDB ID	Reference
Rhodopsin Family			
Adenosine A2A receptor	DDM	3EML	(V. P. Jaakola *et al.*, 2008)
Beta-1 Adrenergic Receptor	DM/ OTG	2VT4	(Warne *et al.*, 2008a)
Beta-2 Adrenergic Receptor	DDM	2R4R	(Søren G.F. Rasmussen *et al.*, 2007)
Beta-2 Adrenergic Receptor	DDM/ LMNG	4QKX	(Weichert *et al.*, 2014)
CXCR1	TX-100/ SDS	2LNL	(Park, Bibhuti B. Das, *et al.*, 2012)
M2 Muscarinic Acetylcholine Receptor	Digitonin/ DM/ LMNG	3UON	(Haga, Andrew C. Kruse, *et al.*, 2012)
Neurotensin Receptor	LMNG	4GRV	(White *et al.*, 2012a)
Secretin family			
Glucagon Receptor	DDM	4L6R	(Siu *et al.*, 2013)
Corticotropin-releasing Factor Receptor 1	DM	4K5Y	(Hollenstein *et al.*, 2013)
Glutamate family			
Metabotropic Glutamate Receptor Type 1	DDM	4OR2	(Wu, Wang, Karen J Gregory, *et al.*, 2014)
Metabotropic Glutamate Receptor Type 5	DDM	4OO9	(Doré *et al.*, 2014b)
Frizzled family			
Smoothened Receptor (SMO)	DDM	4JKV	(Wang, Wu, Katritch, Han, X. P. Huang, *et al.*, 2013)

DDM= n-Dodecyl β-D-maltoside; OTG = Octylthioglucoside; TX100 = Triton X 100; LMNG = Lauryl Maltose Neopentyl Glycol; DM = Decyl β-D-maltopyranoside; SDS = Sodium dodecyl sulphate

Amphipols (APols) are milder alternative to conventional detergents and have been shown to induce greater stability in a range of membrane proteins compared to detergents (Mary *et al.*, 2014). These amphipathic molecules keep the integral membrane protein soluble by forming small complexes but interestingly also allow refolding from inclusion bodies (Dahmane *et al.*, 2009; Banères, Popot and Mouillac, 2011; Bazzacco *et al.*, 2012). APols are relatively short polymers (mass is typically 8–20 kDa) that carry a high density of both hydrophobic chains and highly hydrophilic groups (Banères, Popot and Mouillac, 2011). Amphipol has recently been successfully used for stabilising Rhodopsin and used in cryo-EM studies (He *et al.*, 2017). Previously, neutral amphipol (NPol)- stabilised arginine-vasopressin type 2 receptor (V2R) has been used for studying receptor signalling bias using fluorescence spectroscopy (Rahmeh *et al.*, 2012).

Sligar et.al first reported the use of nanodiscs for stabilising IMPs where a membrane scaffolding protein (modified apolipoprotein A) is used to stabilise the IMP in the presence of phospholipids (Bayburt, Grinkova and Sligar, 2002). Previously, detergent solubilised PTH1R was successfully incorporated into nanodiscs. These PTH1R containing particles were shown to be functional and therefore present a very viable option for stabilising functional GPCR from over-expressing cells (Mitra *et al.*, 2013).

Detergents, though useful in membrane protein extraction can cause perturbation to the structure and many membrane proteins exhibit low stability in detergent based solution (Jamshad *et al.*, 2015). Styrene maleic acid co-polymer (SMA) enables detergent-free isolation of membrane proteins and retention, at least to some extent, of their native lipid environment (Jamshad *et al.*, 2011; Postis *et al.*, 2015).

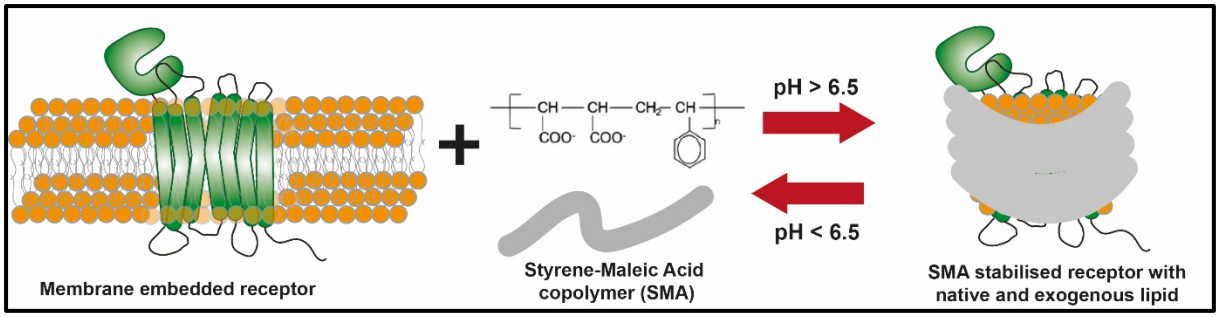


Figure 1-20: A schematic representation of SMALP stabilisation

SMA stabilisation of membrane bound protein and the pH switch which helps the formation and deformation of the nanoparticles. The receptor embedded in its native membrane environment is directly solubilised by the SMA-polymer, which also allows incorporation of native lipids. The solubilisation takes place in the complete absence of any detergent. It is however important to maintain an overall pH > 7 to maintain the SMA particles in solution. Figure adapted from (Jamshad *et al.*, 2011)

The amphipathic property of the SMA is due to the presence of alternating hydrophobic (styrene) and hydrophilic (maleic acid) moieties. In the presence of lamellar membranes, SMA can self-assemble into a disc-like structure along with endogenous lipids. These disc-like nanoparticles range in size from 9-11 Å (Jamshad *et al.*, 2011). The SMA nanoparticles extract small discs of lipid bilayers, containing the IMP encircled by a polymer and termed SMA lipid particles (SMALPs) (Figure 1-20). These particles can then be purified using standard affinity tags (on the IMP) and chromatographic methods. Comparative analysis of the A_{2A} receptor extracted in either SMA or DDM revealed that the SMA-bound A_{2A} was much more stable than DDM-solubilised receptor. In addition, the SMA-solubilised receptor preparation was more resistant to multiple freeze-thaw cycles and demonstrated improved storage stability (Jamshad *et al.*, 2015). SMALPs have also been successfully used for negative stain EM studies using a bacterial secondary transporter, AcrB (Postis *et al.*, 2015). More recently SMA has been used to solve the structure of a bacterial alternative complex III in a super complex with cytochrome oxidase (Sun *et al.*, 2018).

1.5 Antibodies as therapeutics

Over the past decade, there has been an enormous growth in the amount of structural information on GPCRs from almost all relevant classes (Palczewski *et al.*, 2000; Rasmussen *et al.*, 2011; Hollenstein *et al.*, 2013; Wang, Wu, *et al.*, 2013; Doré *et al.*, 2014). This has led

to a much more detailed picture of the structure-function relationships of these receptors. Due to their ubiquitous nature, role in cell signalling cascades and in various diseases, GPCRs are also the targets of many FDA approved drugs. However there remains significant scope in the development of more GPCR therapeutics (Hauser *et al.*, 2017).

1.5.1 Generation of therapeutic antibodies

1.5.1.1 Immunogen

First step in any antibody discovery campaign requires immunogens and it is no different for generating mAbs against GPCRs. However, due to the difficulty associated with generating substantial amounts of highly pure receptor, mAb discovery against membrane bound proteins generally require some novel immunogen formats and a selection of these are summarised in Table 1-5.

Table 1-5: Table summarising immunogen formats commonly used in mAb discovery against membrane-bound proteins. Table adapted from Hutchings *et al.*, 2017.

Immunogen type	Discovery approach	Advantages	Disadvantages
Whole cell and membrane preparations	Immunisation & *In vitro* display	Relatively easy to generate, receptor in native environment, proper conformation of the receptor can be tested easily	Low expression and surface localisation, very high non-specific background, negative panning required, often low immunogenicity
Peptides (Synthetic, constrained etc.)	Immunisation & *In vitro* display	Easy to generate, sometime exhibits native conformation	Can present non-native conformation, low serum availability post immunisation
DNA	Immunisation only	No protein required hence very easy to generate required reagent	Variable expression levels and sera titre
Purified receptor (including thermostabilised receptors)	Immunisation & *In vitro* display	Highly pure and concentrated form of immunogen	Difficult to generate in medium to large scale generally required for immunisation route, purified native receptors are unstable and require stabilising agents such as detergents, which could interfere with immune response
Virus-like particles	Immunisation & *In vitro* display	Easy to generate, receptor generally maintains native conformation	Includes viral antigens, high background and difficult to predict the receptor enrichment

Nano-disc, SMALPs and liposomes	Immunisation & *In vitro* display	Enriched receptor on particles, detergent free, low background	Resource intensive, can require detergent stabilisation in the initial stages, difficult to generate substantial amounts with high purity

1.5.1.2 *In vitro* display techniques

Phage display is a well-established *in vitro* display technology for generating antibodies against a biological target (Nixon, Sexton and Ladner, 2014). This technology was first described almost three decades ago, when bacteriophage particles were used to display a library of peptides (Smith, 1985). The basis of phage display technology is surface presentation of peptides or antibody fragments [Fab or single-chain Fv (scFv) fragments] achieved via fusion with the bacteriophage coat protein. It should be noted that the genetic material coding for the fusion protein resides within the specific phage particle thereby creating a direct link between the genotype and phenotype. This allows enrichment of a specific phage population by selection on immobilised targets (Hoogenboom *et al.*, 1998). Non-lytic filamentous phage strains such as M13, f1 and fd are typically used for generating a phage library though other strains such as T4, T7 and λ have also been used (Smith and Petrenko, 1997). A phage particle consists of an elongated body measuring roughly 1 μm in length and 6 nm in diameter and is covered by ~2700 copies of major coat protein pVIII, a rod shaped alpha helical protein (Marvin *et al.*, 1994). The phage particle body is capped on one end with five copies of minor coat protein; pIII and pVI, while the other end is capped with 3-5 copies of pVII and pIX (Smith and Petrenko, 1997). Very large and diverse libraries displaying either short peptides or antibody fragments are constructed by fusing a large number of sequence variants to either pIII or pVIII coat protein.

To enable antibody discovery, a phage library is incubated with the antigen of interest immobilised in a multi-well plate. The library is allowed to bind to the antigen and the non-binding phage particles are then washed off thereby enriching for antigen-specific binders. This process, also known as panning, is performed iteratively two or more times to enrich for specific binders while removing non-specific binders by increasing selection pressure. The

success of the enrichment process and the selectivity is then assessed using binding assays such as ELISA. Figure 1-21 below summarises a phage display selection or panning against a soluble target immobilised on a solid surface.

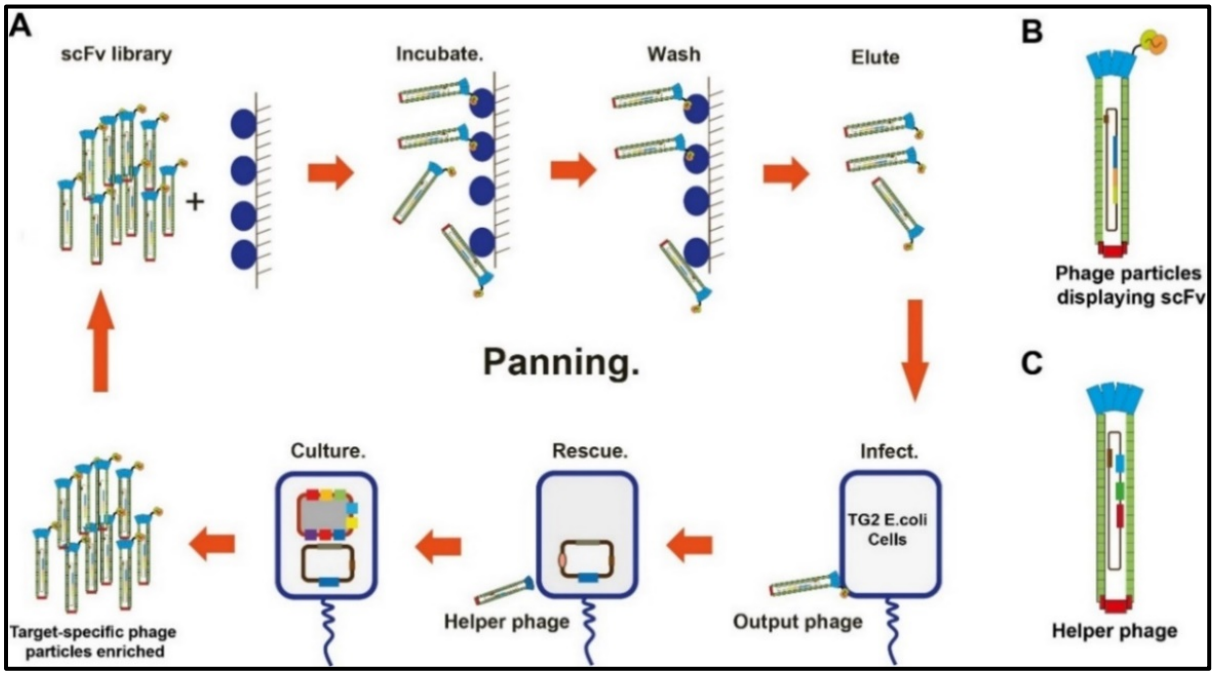


Figure 1-21: Schematic representation of phage library panning

A) The library is incubated with the target antigen (denoted by blue circles) and washed to remove any unbound phage. This enables enrichment of phage particles specific for the target while depleting non-specific phage particles. The bound phage particles are eluted and used to infect bacterial cells. This step amplifies the phagemid, which contains the origin of replication for both M13 phage and *E. coli*, along with gene III, antibiotic resistance marker and multiple cloning sites (Mead and Kemper, 1988). The phagemids however lacks the structural genes required for viral packing, and these are provided, *in trans*, by the helper phage infection in a process known as "phage rescue" (Azzazy and Highsmith, 2002). B) A schematic representation of mature phage displaying the scFv fused to minor coat protein pIII. C) Helper phage used to rescue the phagemids from infected bacterial cells. The various structural genes required for viral packing are shown in blue, green and magenta.

In the past decades, phage display has been extensively used in both academia and industry to generate both research reagents and therapeutic molecules. Adalimumab is a phage-display derived monoclonal antibody (mAb) that binds to human tumour necrosis factor with high affinity and is used for treating a range of autoimmune diseases such as rheumatoid and psoriatic arthritis (Kempeni, 1999). Belimumab is another well-known phage display derived mAb which binds to B lymphocyte stimulator (BLyS), depletes autoantibodies and is approved for treating systemic lupus erythematosus (SLE) (Baker *et al.*, 2003).

1.5.1.3 Hybridoma technology

Hybridoma technology was established by Georges Köhler and César Milstein over 40 years ago and still plays a very important role in generating target specific mAbs (Köhler and Milstein, 1975). Hybridoma technology allows generation of stable cell lines that continuously secrete a defined mAb. The overall process of hybridoma generation is outlined in Figure 1-22.

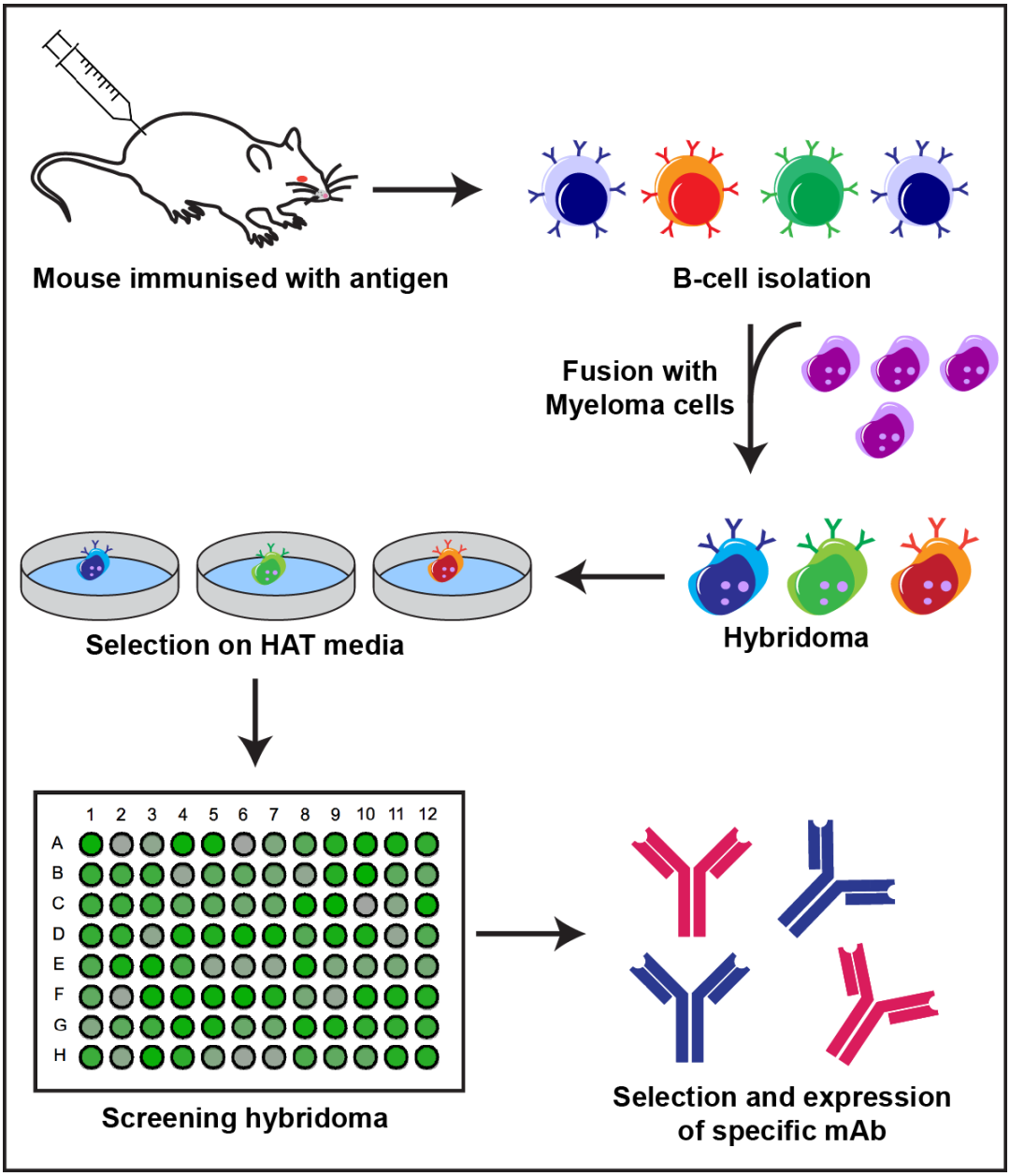


Figure 1-22: Schematic representation of hybridoma technology

Mice are immunised with the antigen of interest and following a specific incubation period, they are euthanised and B-cell containing organs such as the spleen are extracted. The cellular fractions containing the B-cells are fused with mouse myeloma cell line creating the hybridoma. The hybridomas are selected using HAT medium, which only allows the myeloma-fused hybridomas to grow. Following further screening, the specific mAbs are isolated, expressed and purified

In this approach, the antigen-sensitised B-cells (splenocytes) from an immunised mouse are harvested and fused with mouse myeloma cells. Poly-ethylene glycol or electrofusion are routinely used to perform the cell fusion and overall efficiency is low with ~1% of the starting cells successfully fused, and only about 1 x 10^5 forming viable hybrids (Yu *et al.*, 2008). This non-specific fusion generates a mixture of cells composed of unfused splenocytes or myeloma cells along with homokaryotic hybrids (myeloma–myeloma cells or splenocytes–splenocytes) and heterokaryotic hybrids (hybridomas of splenocytes and myelomas). Selection is then performed by growing the mixture in hypoxanthine-aminopterin-thymidine (HAT) medium, allowing selection of only hybridomas (Zhang, 2012). Individual hybridomas are then extensively screened for antibodies that are specific for the target antigen. The selected hybridoma cell-line is then further propagated to produce the monoclonal antibody and stored for future use. Hybridoma technology has revolutionised the mAb discovery and therapeutics area and some FDA-approved hybridoma derived mAbs are listed in Table 1-6

Table 1-6: FDA-approved mAbs derived using hybridoma technology (Arruebo *et al.*, 2011; Zhang, 2012)

mAb Type	Trade name	Generic name	Approval Year	Indication(s)
Murine mAb	ORTHOCLONE OKT3®	Muromonab-CD3	1986	Transplant rejection
(-omab)	ZEVALIN®	Ibritumomab	2002	Non-Hodgkin's lymphoma
	BEXXAR®	Tositumomab	2003	Non-Hodgkin's lymphoma
Chimeric mAb	REOPRO	Abciximab	1994	High risk angioplasty
(-ximab)	RITUXAN®/ MABTHERA®	Rituximab	1997	Non-Hodgkin lymphomas, rheumatoid arthritis
	SIMULECT®	Basiliximab	1998	Transplant rejection
	REMICADE®	Infliximab	1998	Psoriasis, Crohn's disease, ankylosing spondylitis, psoriatic arthritis, rheumatoid arthritis and ulcerative colitis.
	ERBITUX®	Cetuximab	2004	Head and neck cancer; colorectal cancer
Humanised mAb	ZENAPAX®	Daclizumab	1997	Refractory unstable angina. Allograft rejection
(-zumab)	SYNAGIS®	Palivizumab	1998	Respiratory syncitial virus infection
	HERCEPTIN®	Trastuzumab	1998	Non-Hodgkin follicular lymphoma

	CAMPATH®/ MABCAMPAT®	Alemtuzumab	2001	Chronic lymphocytic leukaemia; T cell lymphoma
	XOLAIR®	Omalizumab	2003	Severe asthma
	AVASTIN®	Bevacizumab	2004	Cancer, age related macular degeneration
	TYSABRI®/ ANTEGREN®	Natalizumab	2004	Multiple Sclerosis, Chron's disease
	LUCENTIS®	Ranibizumab	2006	Wet Macular degeneration
	SOLIRIS ®	Eculizumab	2007	paroxysmal nocturnal hemoglobinuria
	CIMZIA®	Certolizumab pegol	2008	Crohns, rheumatoid arthritis
	Actemra®	Tocilizumab	2010	rheumatoid arthritis
Human mAb	VECTIBIX®	Panitumumab	2006	Metastatic colorectal carcinoma
(-umab)	SIMPONI®	Golimumab	2009	Rheumatoid arthritis, psoriatic arthritis and ankylosing spondulitis
	STELARA®	Ustekinumab	2009	Psoriasis, multiple sclerosis
	ARZERRA®	Ofatumumab	2009	Chronic lymphocytic leukemia
	ILARIS®	Canakinumab	2009	Ceryopyrin-associated periodic syndromes
	PROLIA®/ XGEVA®	Denosumab	2010	Postmenopausal osteoporosis
	YERVOY®	Ipilimumab	2011	Activator of the immune system: late stage melanoma and other type of tumors

1.5.1.4 Immunisation and B-cell isolation

While *in vitro* display and hybridoma technology play a key role in the mAb discovery process, some bespoke approaches are also available for high-throughput discovery of mAbs. One such approach is the UCB Core discovery platform, where antigen-specific B-cells from immunised animals are cultured and screened in a high-throughput manner to discover novel and rare antibodies (Tickle *et al.*, 2009). This process is described in Chapter 3.

1.6 Antibodies against GPCR targets

Advantages of mAbs

Out of ~800 known GPCRs only 108 GPCRs are currently targeted by therapeutic agents which means there are no effective therapies targeting the vast majority of this receptor family (Hauser *et al.*, 2018). Currently, ~80 GPCRs are targeted by small-molecules and ~30 receptors are targeted by peptide and peptide-analogues (Hutchings *et al.*, 2017). The lack of

therapeutic agents against a majority of the receptor presents an excellent opportunity for new drug discovery approaches, especially since it well known that GPCRs play a crucial role in various diseased states. Also, as described for the PTH1R, current therapies are far from optimal.

Traditionally, GPCR therapeutics have been dominated by small-molecules (SM) but there is a growing interest in targeting these receptors with mAbs. SM possess a very well-defined chemical structure as opposed to biologics, which makes their characterisation relatively easy. The other major advantage of a SM is the oral delivery route, which in turn helps with patient compliance (Wan, 2016). Most SM can cross cell-membrane and blood-brain barrier with much higher efficiency than large biologic molecules (Smith, 2015).

However, compared to SM, mAbs have certain advantages for instance, mAbs tend to have higher specificity which is especially crucial when targeting receptors which share high sequence similarity (Leader, Baca and Golan, 2008).

Due to their relatively large size mAbs have low central nervous system (CNS) penetration which reduces CNS-related side-effects (Boado *et al.*, 2010). MAbs not only provide high selectivity and affinity for the desired target, they also have a longer serum half-life due to overall size and neonatal Fc receptor (FcRn)-mediated recycling (Liu, 2017).

mAbs can also exhibit other functional effects mediated by the crystallisable fragment (Fc) region such as complement-dependent cytotoxicity (CDC), antibody-dependent cellular cytotoxicity (ADCC), and antibody-dependent cellular phagocytosis (ADCP) (Hansel *et al.*, 2010). These Fc-mediated functional effects have been shown to be particularly important for improving cancer therapeutics (Carter, 2001; Kellner *et al.*, 2017). mAbs and their constituent domains can be further configured to different formats including the Fab domain only (or with modifications such as PEGylation) (Winter *et al.*, 2004; Humphreys *et al.*, 2007), single chain F_v (scFv) containing the variable domains only and finally a combination of two or more V-regions against different targets to generate a multi-specific molecule. The multi-specific molecules such as bi and tri-specifics provide more flexibility to target multiple receptor with a single molecule (Kontermann and Brinkmann, 2015).

Disadvantages of mAbs

Mabs are quite complex molecules when compared to conventional drugs, and therefore requires a complicated and expensive manufacturing process (Chames *et al.*, 2009). Even though the process has come a long way with development of new cell-lines and equipment, mAbs can still cost substantially more to make when compared to small molecules, which in turn makes mAb-based therapy very expensive (Farid, 2007; Samaranayake *et al.*, 2009).

During the early years of mAb-based therapies, immunogenicity against chimeric molecules was a major challenge (Samaranayake *et al.*, 2009). This has been resolved to a large extent using methods such as complementarity-determining region (CDR) grafting (Jones *et al.*, 1986; Carter *et al.*, 1992), specificity-determining residues (SDR) grafting (Kashmiri *et al.*, 2005) and the use of transgenic mouse (Jakobovits, 1995; Kellermann and Green, 2002). However, immunogenicity is still an issue which requires careful monitoring during mAb-mediated treatments.

Membrane penetration and especially cross the blood-brain barrier still remains a massive challenge for most mAb therapeutics (Smith, 2015). Therefore, intracellular targets which are attractive drug targets remain a challenge for mAbs and other large bio-therapeutics.

Current mAbs against GPCRs

Currently there are ~28 mAbs in various stages of clinical development that target GPCRs either as a single entity or in combination with other drugs and these molecules are summarised in Table 1-7.

Table 1-7:mAbs against GPCR targets in clinical development

Target-based Actions	Drug Name	Active Companies	Active Indications	Highest Status
CCR4 chemokine antagonist	Mogamulizumab	Kyowa Hakko Kirin Co Ltd	Cancer	Launched
CXCR4 chemokine antagonist; Stromal cell-derived factor 1 ligand inhibitor	F-50067	Pierre Fabre SA	Cancer	Phase 1
CXCR4 chemokine antagonist	Ulocuplumab	Bristol-Myers Squibb Co	Cancer	Phase 2

G protein coupled receptor 49 antagonist; G protein coupled receptor 49 modulator	BNC-101	Eclipse Therapeutics	Cancer	Phase 1
CD3 modulator; Somatostatin 2 receptor modulator	XmAb-18087	Xencor Inc	Cancer	Phase 1
CXCR2 chemokine antagonist; Programmed cell death ligand 1 inhibitor	Durvalumab + AZD-5069 (SCCHN)	AstraZeneca plc; MedImmune LLC	Cancer	Phase 2
CCR2 chemokine antagonist	Plozalizumab	Takeda Oncology	Melanoma	Phase 1
Glucagon-like peptide 1 receptor agonist; Interleukin 21 ligand inhibitor	Anti-IL-21 + Liraglutide (type 1 diabetes)	Novo Nordisk A/S	Insulin dependent diabetes	Phase 2
CCR3 chemokine antagonist; Eotaxin ligand inhibitor	Bertilimumab	Immune Pharmaceuticals Inc; iCo Therapeutics Inc	Ocular disorder, autoimmune diseases	Phase 2
Glucagon-like peptide 1 receptor agonist	GX-G6	Genexine Co Ltd; I-Mab Biopharma; Il Dong Pharmaceutical Co Ltd	Diabetes mellitus; Obesity	Phase 1
Complement C5a receptor antagonist	Tesidolumab	Novartis AG	Macular degeneration	Phase 2
Glucagon receptor antagonist	REMD-477	REMD Biotherapeutics Inc	Insulin dependent diabetes; Metabolic disorder; Non-insulin dependent diabetes	Phase 2
CCR5 chemokine modulator; Human cytomegalovirus glycoprotein inhibitor	MB-66	Mapp Biopharmaceutical Inc	HIV infection; Herpes simplex virus infection	Phase 1
CCR5 chemokine antagonist	PRO-140 (subcutaneous, HIV infection)	CytoDyn Inc	Graft versus host disease; HIV infection; Inflammatory disease	Phase 3
CGRP receptor antagonist	LY2951742 (Galcanezumab)	Eli Lilly & Co	Cluster headache; Migraine	Pre-registration
Cannabinoid CB1 receptor antagonist	Namacizumab	Bird Rock Bio Inc; Janssen Pharmaceuticals Inc	Fibrosis; Metabolic disorder; Non-alcoholic fatty liver disease; Non-alcoholic steatohepatitis	Phase 1
CGRP receptor antagonist	ALD403 (Eptinezumab)	Alder Biopharmaceuticals Inc	Migraine	Phase 3
CGRP receptor antagonist	Fremanezumab	Otsuka Pharmaceutical Co Ltd; Teva Pharmaceutical Industries Ltd	Cluster headache; Headache; Migraine	Pre-registration

CCR3 chemokine modulator; Eotaxin 2 ligand inhibitor	CM-101 (humanized), ChemomAb	ChemomAb Ltd	Autoimmune disease; Idiopathic pulmonary fibrosis; Inflammatory disease; Non-alcoholic steatohepatitis; Scleroderma	Phase 1
Complement C5a receptor antagonist	REGN-3918	Regeneron Pharmaceuticals Inc	Ocular inflammation; Paroxysmal nocturnal hemoglobinuria; Retinopathy	Phase 1
CGRP receptor antagonist	Erenumab	Amgen Inc; Novartis AG	Migraine	Pre-registration
Complement C5a receptor antagonist; Complement Factor inhibitor	IFX-1	InflaRx GmbH	Hidradenitis suppurativa; Sepsis; Vasculitis	Phase 2
PACAP type I receptor antagonist	AMG-301	Amgen Inc; Novartis AG	Migraine	Phase 2
CXCR5 chemokine modulator	SAR-113244	Sanofi	Systemic lupus erythematosus	Phase 1
Glucagon receptor antagonist	PF-06293620	Pfizer Inc	Non-insulin dependent diabetes	Phase 1
Glucagon-like peptide 1 receptor modulator	GMA-102	Hangzhou Gmax Biopharm Biomedical Engineering Co Ltd	Non-insulin dependent diabetes	Phase 1
Chorionic gonadotropin ligand; Luteinizing hormone receptor agonist	Choriogonadotropin alfa biosimilar, Livzon Pharmaceutical Group	Livzon Pharmaceutical Group Inc	Female infertility	Phase 1
Erbb2 tyrosine kinase receptor modulator; Neurokinin receptor agonist	HER2.taNK	NantKwest Inc	Cancer; Glioblastoma	Phase 1

***The list should not be considered exhaustive**

***Source: Clarivate Analytics (https://clarivate.com/)**

Aims of the project

The central aim of this project is to generate mAbs against PTH1R that are either functional, i.e. modify receptor behaviour, and/or could be used to facilitate PTH1R structural studies.

The overall objectives of this project can be divided into three main parts

1. To discover monoclonal antibodies against PTH1R using *in vitro* display technology and the UCB core discovery approach.
2. Perform functional characterisation of the discovered mAbs to identify those with receptor function-modifying properties using *in vitro* signalling assays.
3. Perform small-scale purification of PTH1R in detergents and SMALPs and use the purified receptor for biophysical analysis of mAbs binding to the receptor.

Parathyroid hormone receptor 1 is a class B GPCR and plays a key role in bone metabolism and calcium homeostasis and therefore it has been studied quite extensively. Forteo®, the N-terminal fragment of PTH (1-84) is an FDA approved drug for treating osteoporosis and there were no reported functional mAbs against this receptor when the project started. This study generated mAbs against the PTH1R extracellular domain (ECD) and extra-cellular loops (ECL) using *in vitro* and immunisation / B-cell isolation approaches respectively. The discovered mAbs were further characterised using *in vitro* signalling assays to determine their ability to potentially modulate intracellular signalling.

A method to over-express PTH1R using a suspension mammalian cell-culture system was also established. Novel solubilisation agents such as Styrene-maleic acid (SMA) copolymer was used to purification and compared against detergents such as DDM and LMNG. The purified receptor and the discovered mAbs were further used to determine the binding kinetics and epitope mapping. The overall workplan is shown in Figure 1-23 & Figure 1-24

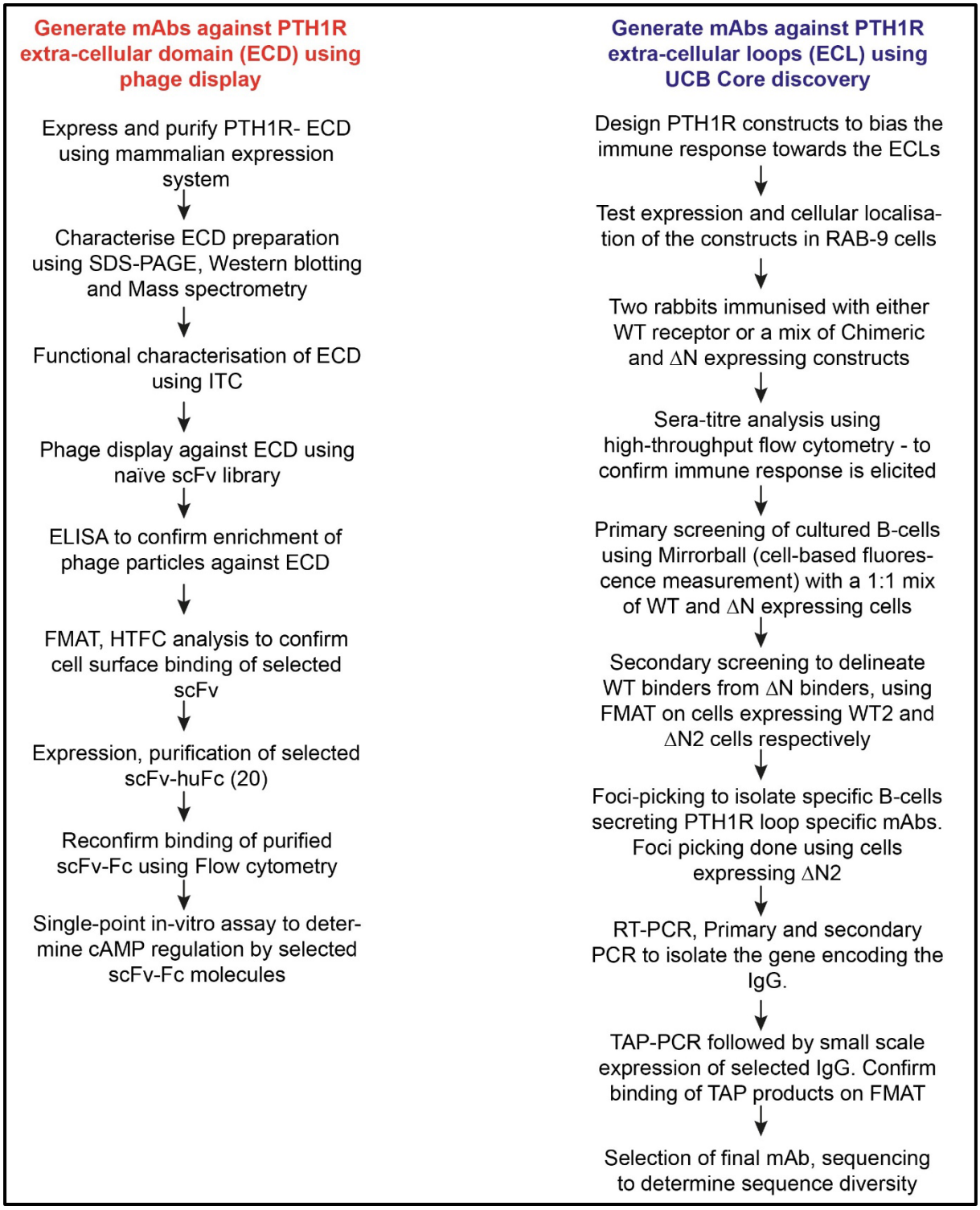


Figure 1-23: mAb discovery workflow

A workflow highlighting the major steps involved in generating mAbs against the PTH1R ECD (left) using phage display technology and PTH1R-ECL using immunisation and UCB core discovery approach (further details in Chapter 2 &3). All steps are further expanded in the relevant chapters.

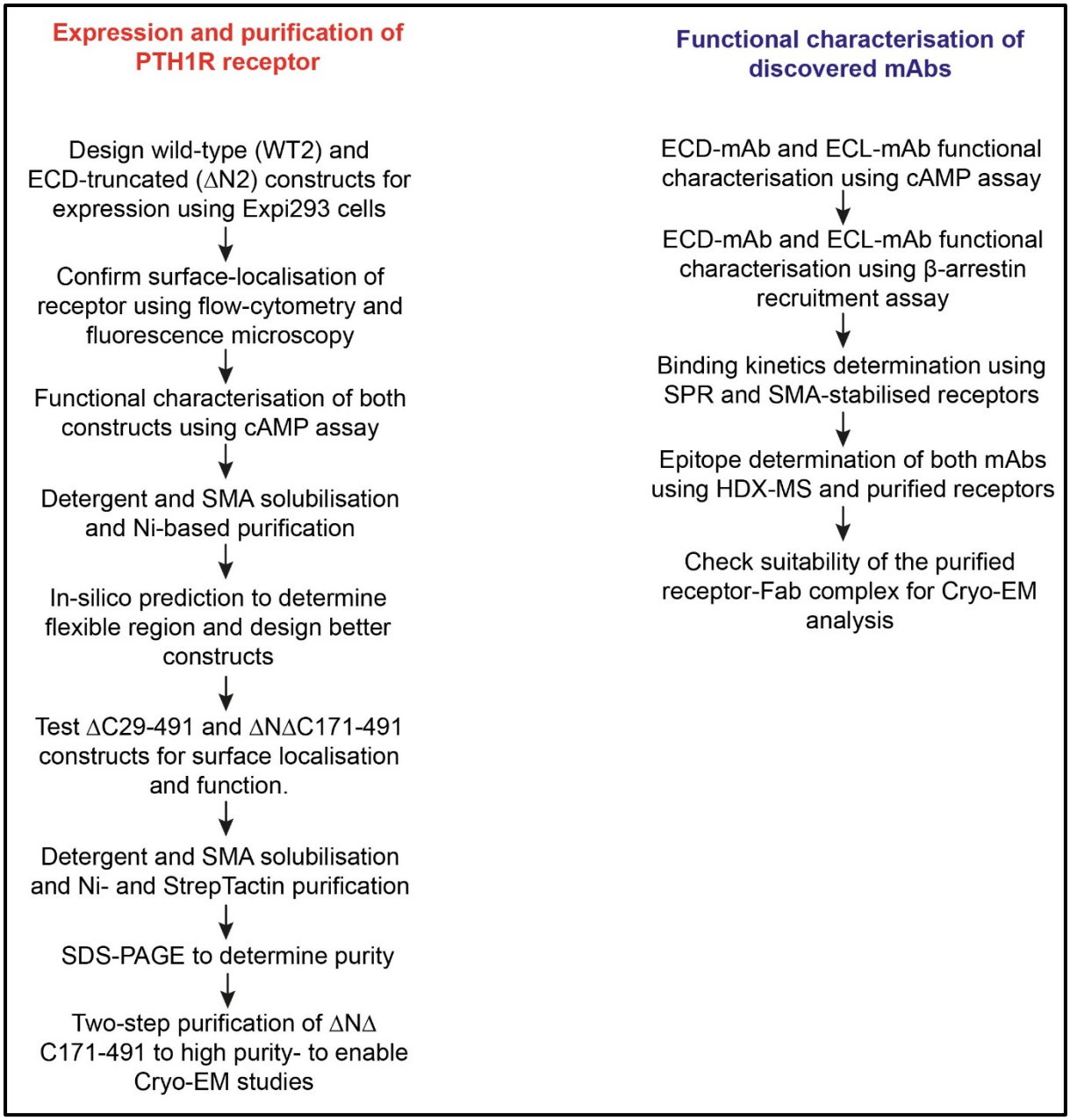


Figure 1-24: Receptor expression, purification and mAb characterisation workflow.

A workflow highlighting the major steps involved in expression and purification of PTH1R constructs (left) and functional and biophysical characterisation of selected mAbs using *in vitro* assays and biophysical techniques (further details in Chapter 4 &5). All steps are further expanded in the relevant chapters.

Chapter 2: Antibody generation against PTH1R extra-cellular domain (ECD) using phage display technology

2. Antibody generation against PTH1R extra-cellular domain (ECD) using phage display technology

2.1 Introduction

As discussed in section 1.5.1.2, antibody discovery using phage display technology is a well-validated method, widely used in both academia and industry to generate research reagents and therapeutics. An example of a therapeutic monoclonal antibody generated using this approach is Adalimumab, which binds with high affinity to the human tumour necrosis factor (TNF) and is used for treating rheumatoid and psoriatic arthritis (Kempeni 1999). Belimumab is another well-known phage display derived monoclonal antibody which binds to the B-cell activating factor (BAFF) also known as B-Lymphocyte stimulator (BLyS), which depletes autoantibodies and is used for treating systemic lupus erythematosus (SLE) (Baker et al. 2003).

While the generation of functional therapeutic antibodies against soluble targets using phage display is well-established, the same is not true for full-length GPCRs and other integral membrane proteins. In most cases, the biggest hurdle in generating therapeutic antibodies against GPCRs includes the inability to reliably produce milligram quantities of the full-length, structurally intact receptor (Hutchings, Koglin and Marshall, 2010). To circumvent the difficulty associated with the full-length protein, efforts have focused on the soluble extra-cellular domain (ECD) of family B GPCRs. Yan et al reported an antibody with antagonist activity towards the glucagon receptor (GCGR), raised using peptides from the ECD (Yan *et al.*, 2009). In addition, an antibody with antagonist activity towards the Calcitonin gene-related peptide receptor (CGRP) was raised by immunising mice with the soluble CGRP ECD (Shi *et al.*, 2015). In this study, we used phage display to generate novel antibodies against the ECD domain of the PTH1R.

The overall aim of this work was to discover novel antibodies binding to the ECD of PTH1R, in the absence of purified full-length receptor. Such antibodies have the potential to facilitate structural studies using X-ray crystallography or Cryo-EM.

The ECD of PTH1R has 5 putative glycosylation sites and three disulphide bonds. It is known that the post-translational modifications of ECDs and loops can play a crucial role in expression, trafficking and activity of a GPCR (Couvineau *et al.*, 1996; Kelley and Kinsella, 2003; Colvin *et al.*, 2006). To preserve the natural glycosylation and the disulphide bonding pattern, we expressed and purified the ECD of PTH1R in mammalian cells. The functionality of the purified ECD was confirmed by PTH-(1-34) endogenous ligand binding using isothermal titration calorimetry (ITC). Three rounds of phage display panning using a naïve single-chain Fv (scFv) library was performed in order to isolate and screen for ECD-specific antibodies. These antibodies were further screened for their ability to bind the full-length receptor transiently expressed on the cell-surface. The overall antibody generation and screening pipeline detailed in this chapter is summarised in Figure 2-1 below:

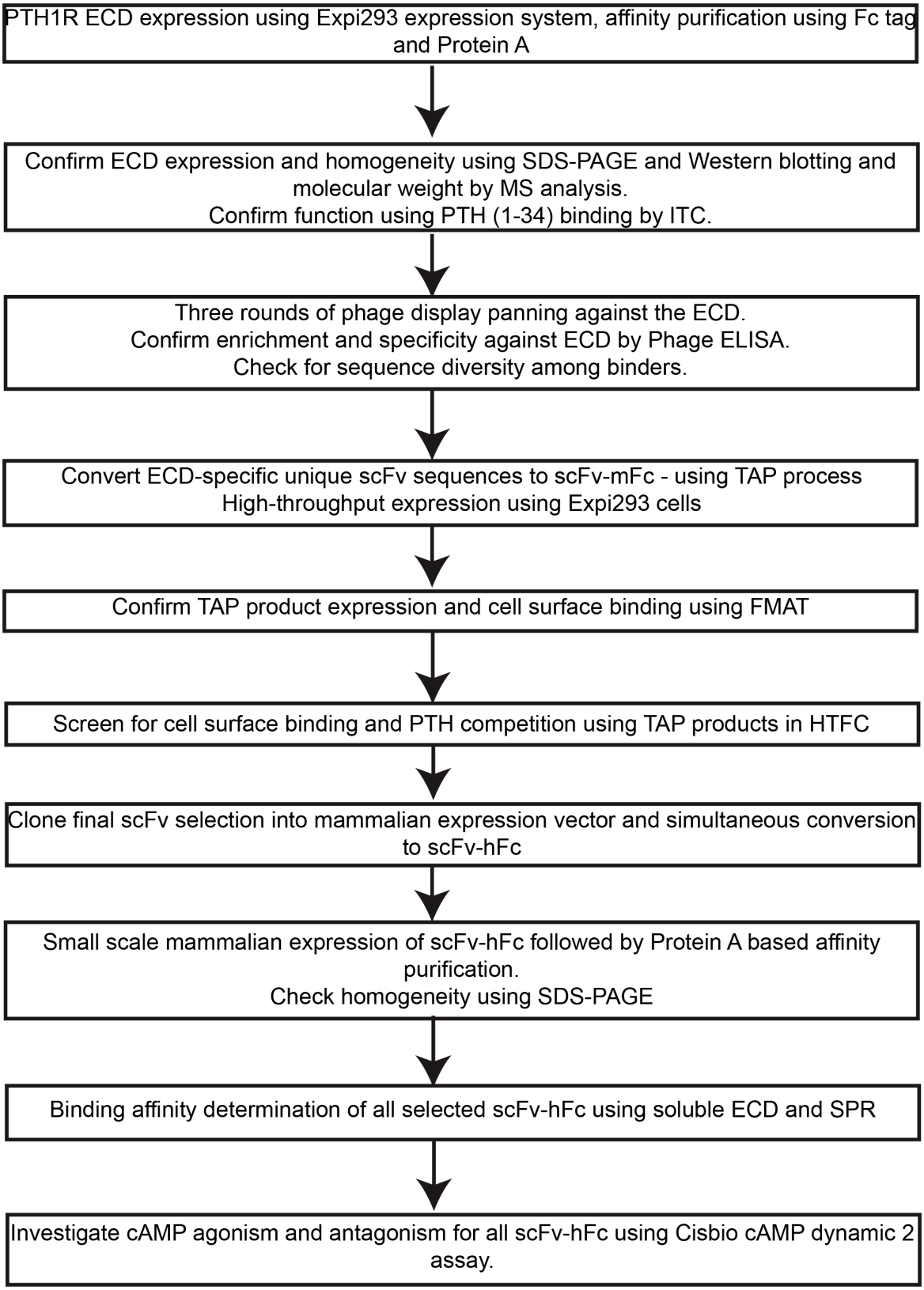


Figure 2-1: A brief overview of discovery and screening pipeline used for the antibody discovery against PTH1R ECD using phage display.
All the steps are further expanded in this chapter.

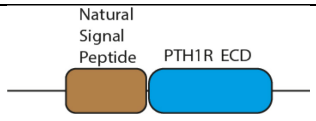
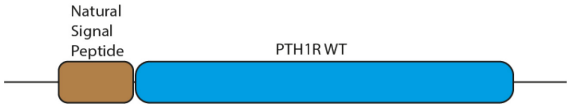
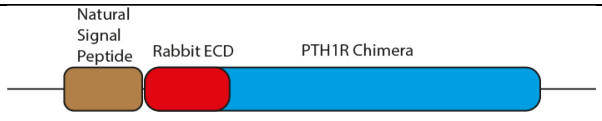
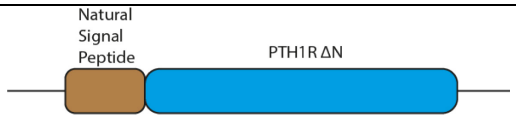
We found 154 unique sequences that bound to the ECD of PTH1R and based on PTH-(1-34) competition and cell-surface binding, 18 antibodies were expressed and purified. The purified antibody molecules successfully bound the full-length receptor expressed on the cell surface. Interestingly, we also found an antibody, PD12, which exhibited nanomolar affinity for the ECD and weak antagonism for the cAMP signalling pathway.

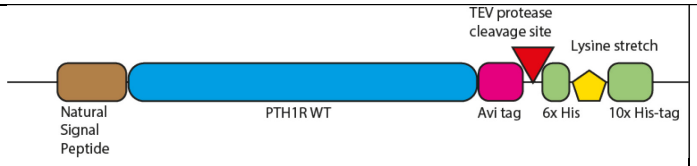
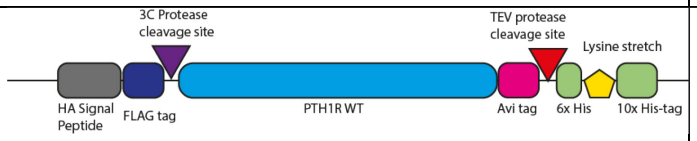
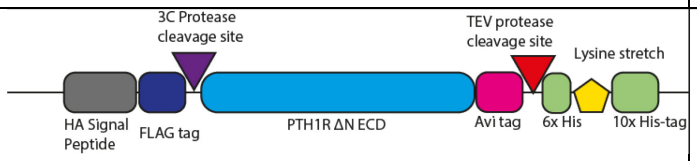
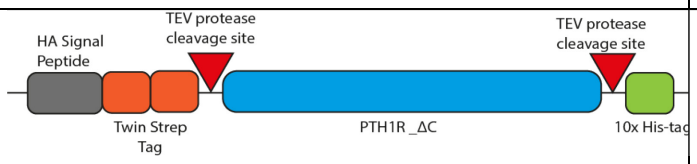
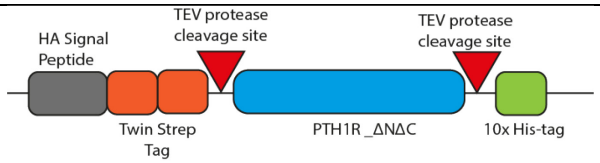
2.2 Material and Methods

2.2.1 Constructs

All the receptor constructs used in this chapter and future chapters are summarised in Table 2-1. The PTH1R amino acid sequence was derived from Uniprot (accession number Q03431) and synthetic genes encoding various versions of the receptor were designed for over-expression, antibody screening and immunisation. All expression constructs were generated using standard molecular biology techniques, unless stated otherwise. All the plasmid variants used in this and future work are derived from the pMH vector backbone, a proprietary UCB mammalian expression vector. Briefly, the vector contains the following elements: a modified human CMV promoter, a Simian virus 40 derived polyadenylation signal sequence, a kanamycin resistance marker, and a pUC origin of replication (see supplementary section for the plasmid map).

Table 2-1: A list of constructs used in this study.

Construct Code[a]	Schematic representation[b]	AA[c]	Plasmid[d]
ECD		M1 - G188	pMH-hFc
WT		M1 - M593	pMH
Chi		M1-N176 E177–M593	pMH
ΔN		T178-M593	pMH

WT1		M1-M593	pMH-Avi-HKH
WT2		D27-M593	pMH-Avi-HKH
ΔN2		T178-M593	pMH-Avi-HKH
ΔC29-491		D29-S491	pMH-Strep-His
ΔNΔC171-491		V171-S491	pMH-Strep-His

[a] The code used for the constructs. This nomenclature is used throughout the document
[b] The schematic representation of the construct cloned into the pre-digested plasmids
[c] The start and stop amino acids for the constructs. The amino acid numbering is based on Uniprot (accession number: Q03431)
[d] The plasmid used for cloning the constructs (further plasmid details can be found in supplementary section)

2.2.2 ECD expression purification and characterisation

2.2.2.1 PTH1R ECD cloning

The synthetic gene encoding the PTH1R ECD (amino acids: M1-G188) was sourced from Atum (California, USA). The insert was sub-cloned into pMH-TEV-hFc vector using *HindIII* and *XhoI,* in order to produce a construct encoding the ECD with a C-terminal Tobacco etch virus (TEV) cleavable human Fc tag. The construct, ECD-huFc, was confirmed by DNA sequence analysis.

2.2.2.2 PTH1R ECD expression using Expi293 expression system

A modified human embryonic kidney (HEK) cell-based expression system (Expi293 expression system, ThermoFisher Scientific) was used for the expression of the ECD-huFc. Lipid based (Expifectamine) transfection was performed at a final cell density of 2.5-3 X 10^6 cells/ml and 1 mg of purified plasmid DNA encoding the ECD-huFc was used/L culture media.

Following transfection, cells were incubated at 37ºC, with shaking at 120 rpm and 8% CO_2 in a humidified atmosphere. Following a 24-hour incubation, 50 µl and 500 ml of Expifectamine transfection enhancer 1 and 2 were added respectively and the culture was incubated for a further 4 days. The supernatant containing the expressed protein was harvested by centrifuging the culture at 3000 x g. The supernatant was then filtered through a 0.22 µm vacuum filtration unit (Millipore) to remove any particulate matter.

The Expi293 expression system was used throughout the study and the above protocol was followed with the volumes of the cells and the reagents scaled according to the final culture volumes. For transient cell surface receptor expression, the incubation period was reduced to 24 h with no enhancer addition.

2.2.2.3 PTH1R ECD purification

The ECD-huFc, was isolated on Protein A resin (MabSelect SuRE, GE Healthcare) was equilibrated with 10 column volumes (CVs) of Tris-buffered saline pH 8.0 (TBS). Sodium chloride was added to the filtered supernatant (section 2.2.2.2) to a final concentration of 100 mM and the ECD-huFc was captured on the protein A column overnight at a flow rate of 1 ml/min at 4°C. The column was washed with 20 CVs of the TBS buffer. The resin was removed from the column and 4 ml of the washed resin slurry, with captured ECD-huFc, was placed in a 50 ml polypropylene tube and incubated overnight with 200 µg of TEV protease-6 His tagged with a C-terminal His-tag, (kind gift from P. Mori, UCB) at 4°C. Following incubation, the resin suspension was centrifuged at 2000 x g and the supernatant containing the cleaved ECD and His-tagged TEV protease was collected. To the collected supernatant, 300 µl of Ni^{2+}-NTA resin (Qiagen) and 20 mM Imidazole were added, the final concentration of NaCl adjusted to 300 mM and the mixture incubated for 1 h at room temperature. The Ni^{2+}-NTA beads with captured TEV-6His protease were separated using filtration columns.

The final eluate containing the purified ECD was buffer exchanged into TBS pH 8.0 using centrifugal filters (Amicon, Millipore), concentrated to 11 mg/ml, flash-frozen in 500 µl aliquots and stored at -80°C for future use.

2.2.2.4 Biophysical characterisation of ECD

2.2.2.4.1 SDS-PAGE and Western blotting

The purified ECD sample was separated on a 4-20% Tris-glycine SDS-PAGE gel under non-reducing and reducing conditions. The SDS-PAGE gel was stained with Coomassie blue stain and destained with deionised (DI) water. For Western blotting, protein bands separated by SDS-PAGE were transferred to a PVDF membrane using a dry-blotting technique. The membrane was blocked with 2% non-fat milk in PBS, 0.1% Tween 20 and then incubated with mouse anti-human PTH1R ECD primary antibody (1:500) followed by goat anti-mouse IgG-HRP conjugated secondary antibody (1: 10,000). Amersham ECL Select (GE Healthcare) reagent and ImageQuant LAS4000 (GE Healthcare) were used to perform the enhanced chemiluminescent detection and imaging.

2.2.2.4.2 Mass spectrometry

The intact molecular mass of the ECD was determined using liquid chromatography-coupled to mass spectrometer (LC/MS) (Acquity UPLC attached to a Xevo G2 Mass spectrometer). All the mass-spectrometry analyses were performed with a deglycosylated ECD sample. Typically, 100 µg of ECD (in TBS pH 8.0) was incubated with 4 µg PNGaseF at 37°C overnight. The digested samples were separated on a C-18 column and the mass to charge ratio (m/z) determined using MS with the m/z range set to 100-5000. The final mass was determined by deconvoluting the m/z data. Dr Rebecca Burnley performed the MS experiment and data analysis.

2.2.2.4.3 Isothermal Calorimetry

The ITC analysis was performed with a MicroCal ITC 200 using PTH-(1-34) (Bachem). In the first experiment, PTH-(1-34) was titrated into the ECD solution placed in the reaction cell. The ECD at 20 µM was added to the sample cell and the syringe was filled with PTH-(1-34) at a final concentration of 200 µM. A total of 19 injections of 2.4 µl were performed with constant stirring set to 750 rpm. In the second experiment, 50 µM PTH-(1-34) was added to the sample cell, while the ECD was injected using the syringe. A total of 16 injections of 2.4 µl

each were performed with the ECD starting concentration set to 500 µM. The binding affinity and the enthalpy of the reactant binding were calculated with the standard one set of independent sites model using Origin 7.0 software (MicroCal).

2.2.3 Phage display against PTH1R ECD

2.2.3.1 Phage panning

A UCB naïve scFv phage library, with a diversity of ~10^{11} colony forming units (cfu), was used for phage display panning on the ECD. 50 µl of the purified ECD at a concentration of 10 µg/ml was added to each well of a 96-well Maxisorp plate (Nunc) and incubated overnight at 4°C. As a negative control, plates with 50 µl of PBS in each well were incubated overnight at 4°C. The plates were washed with PBS / 0.1% Tween 20 and blocked for 1 h at room temperature using 300 µl of the plate blocking buffer (PBS supplemented with 3% BSA). The phage particles were blocked for 1 h at room temperature using the phage blocking solution (3% BSA, 3% fat-free milk in PBS). The plates were washed and 50 µl of phage particles were added to every well in both the ECD coated and the negative control plates and further incubated at room temperature for 1 h. The plates washed twice to remove unbound phage particles and the bound phage were eluted using low pH elution (0.1 M HCl) and immediately neutralised using 0.1 M Tris, pH 8.0. The neutralised phage particles were used to infect TG1 cells (Lucigen Technologies) at an OD_{600} = 0.5-0.8 and plated on a large round petri dish containing Luria Bertani (LB) agar supplemented with 100 µg/ml carbenicillin and 1% glucose prior to incubation overnight at 37°C.

2.2.3.2 Phage rescue and helper phage infection

The phage infected bacterial colonies from section 2.2.3.1 were harvested into 2TY broth and the suspension centrifuged at 3000 *x g* for 10 minutes. The bacterial cell pellet was re-suspended in 2TY broth supplemented with 15% glycerol, and a part of the suspension was stored at -80 °C. The suspension was added to 10 ml of 2TY broth (supplemented with 1% glucose and 100 µg/ml carbenicillin) to give a final OD_{600} = 0.1 to facilitate phagemid rescue. The culture was incubated at 37°C until the OD_{600} = 0.5-0.8, then helper phage was added at

a multiplicity of infection (MOI) of 20. The tubes were incubated at 37°C for 1 h without agitation and the cells collected by centrifugation at 3500 x g for 10 min. To facilitate the release of phage particles, the bacterial cell pellet was re-suspended in 10 ml 2TY broth (supplemented with 100 µg/ml carbenicillin and 50 µg/ml kanamycin) and incubated overnight at 30°C with shaking at 225 rpm.

2.2.3.3 Elution of generated phage particles

The overnight culture, infected with the helper phage, was centrifuged at 3000 x g for 10 minutes to pellet the cells. The supernatant, containing the released phage particles, was transferred to a separate tube and centrifuged at 12,000 x g for 20 min and the resulting supernatant transferred to a fresh 50 ml polypropylene tube. The phage particles were precipitated by adding 2 ml phage precipitation solution (20% w/v Polyethylene Glycol 8000, 2.5 M NaCl) to the supernatant and incubating the solution for 1 h on ice. The phage particles were collected by further centrifuging the tubes at 3500 x g for 10 min and the resulting pellet re-suspended in 1 ml of PBS.

2.2.3.4 Second and third round panning

For the second and the third round of phage panning, a similar protocol as described above was followed except, to further increase the stringency, the starting ECD plating concentration was decreased to 1 µg/ml and the plates were washed 5 times. In addition, for the third panning round, all the bacterial culture steps were performed using the XL1 Blue cells (Agilent Technologies) instead of the TG1 cells. After the third round of panning, single isolated bacterial colonies were consolidated into 48-well culture blocks, referred to as master plates.

2.2.3.5 Phage ELISA

The phage particles were produced as described in section 2.2.3.2 & 2.2.3.3 from the consolidated master plates. The phage particles were blocked using phage blocking solution and added to the plates coated with either the ECD or PBS and incubated at room temperature for 1 h. The plates were washed three times using PBST and the Anti-M13 Phage-HRP

conjugated antibody (GE Healthcare) at a final dilution of 1: 5000 (in PBS + 3% BSA) was added to each well and incubated at room temperature for 1 h. Following the final wash, 50 µl of 3, 3′, 5, 5′-Tetramethylbenzidine (TMB) reagent was added and the absorbance measured at 630 and 490 nm using a plate reader.

2.2.3.6 scFv sequence analysis

For sequencing of the selected binders, 3 ml of 2TY media (supplemented with 100 µg/ml carbenicillin and 0.1% glucose) was inoculated with 20 µl of phage infected culture from the master plate (section 2.2.3.4). The culture was incubated overnight at 37°C with shaking at 225 rpm then the bacterial cell pellet was separated by centrifugation at 3500 x g for 10 min. The bacterial plasmid DNA was extracted using high-throughput DNA purification facility at UCB (G. Smith) and the purified plasmid DNA was sequenced. The resulting DNA sequences were digitally converted to amino acid sequences using Quikseeq (UCB in-house protocol) and aligned using AlignX (Invitrogen). The sequence diversity of the heavy chain variable domain's complementarity determining region 3 (V_H CDR3) was used to screen for the unique sequences.

2.2.4 Screening for phage binders

2.2.4.1 scFv-Fc and Transcriptionally active PCR (TAP) product generation using PCR

A two-stage PCR based approach was used to convert selected scFvs to a transcriptionally active fragment containing a C-terminal mouse gamma 1 Fc fragment (scFv-mFc) (Clargo *et al.*, 2014). The reaction adds a N-terminal human CMV promoter fragment which allows transfection and expression of the final PCR product using a mammalian expression system, without any additional cloning steps.

For the primary PCR, 0.4 µl of the template DNA (purified scFv mini-prep DNA, section 2.2.3.6) was added to a PCR master mix containing 2 µl each of KOD buffer (10x), dNTPs (2 mM each), 18924F primer (at 10 pmol/µl), pHENNotRev primer (at 10 pmol/µl), 1.2 µl of 25 mM $MgSO_4$, 0.4 µl of KOD polymerase and 10 µl of PCR grade water. The samples were

incubated using a thermal cycler using the pre-set program TAP1 (see supplementary section for details).

For the secondary PCR, 50 µl of the reaction mix was prepared as described above with 5 µl each of TAPhCMV3F primer and PolyANestedR primer, both at 10 pmol/µl and 10 ng each of CMV PelB fragment and murine Fc-PolyA fragments. One microliter of the primary PCR product was added and incubated using a thermal cycler with the pre-set program TAP2 (see supplementary section for details).

The final TAP fragments were visualised on 1% agarose gel to determine the fragment size and were used for transfecting the Expi293 cells for expression of scFv-mouse Fc.

Table 2-2: Primers used for performing TAP PCR

Primer Name	Sequence (5'→ 3')
18924(F)	GATGGCCGCGGCCCAGTCGGCCCAGGCC
pHENNotRev	GGTGATGGTGATGGGCGGCCGC
18695 (TAPhCMV3F)	GCCATGTTGACATTGATTATTGACTAG
PolyANestedR	ATACATTGATGAGTTTGGACAAACC

2.2.4.2 High-throughput expression of scFv-mFc TAP products using Expi293 expression system

The Expi293 expression system as described in section 2.2.2.2 was used for high-throughput small-scale (1 ml final volume) expression of scFv-mFc. To harvest the expressed scFv-mFc, the plates were centrifuged at 3500 x g for 10 min to pellet the cells and the supernatant containing expressed scFv-mFc were aseptically removed and consolidated into 96-well plates for further use.

2.2.4.3 Cell-surface binding of scFv-mFc using FMAT

Expi293 cells were transiently transfected with WT and ΔN constructs (see Table 2-1) as described in section 2.2.2.2. The cells were harvested after overnight incubation and washed twice with wash buffer (PBS supplemented with 1% FCS) then diluted to a final cell density of 3 x 10^5 cells/ml in wash buffer. The supernatants containing scFv-mFc (section 2.2.4.2) were tested undiluted and at 10 and 100-fold dilutions prepared in wash buffer. In a black walled 384-well plate (ThermoFisher Scientific), 10 µl of the cell suspension (~3000

cells), 10 µl of the supernatant containing scFv-mFc and 10 µl of goat anti-mouse Fc Alexa Fluor-647 secondary antibody (1: 1666) were added to each well and the plates incubated for 1 h in the dark. The final fluorescence was measured using the FMAT 8100 HTS system (Applied Biosystems) and data analysis performed using the FMAT 8200 HTS system (Applied Biosystems) software. The background signal was set using the fluorescence levels detected from the plate containing cells transfected with the ΔN construct. The final fluorescence signal data from the plate containing WT-transfected cells were exported to Microsoft excel for further analysis.

2.2.4.4 Screening of scFv-mFc using high-throughput flow-cytometry (HTFC)

The Expi293 cells were transiently transfected with ΔN2 and WT2 constructs as described previously in section 2.2.2.2**.** The cells were harvested, washed twice with Flow buffer (PBS pH 7.4, 1% BSA, 0.1% sodium azide and 2 mM EDTA) and re-suspended in Flow buffer at a density of 1 x 10^6 cells/ml. The washed cells expressing WT2 protein were divided into two aliquots. PTH-(1-34) was added to a final concentration of 1.6 µM to one of the aliquots, while the second was left untreated. 45 µl of WT expressing cells (treated and untreated) were added to two separate 96-well v-bottom plates (ThermoFisher Scientific) and 5 µl of scFv-mFc (section 2.2.4.2) added to the respective wells. To determine non-specific binding, ΔN transfected cells were used. All plates were incubated on ice for 1 h and washed twice with Flow buffer. To the washed cells, 35 µl of goat anti-mouse IgG Fc-fragment specific IgG coupled to Alexa Fluor 647 (1: 1000 diluted using flow buffer) was added and further incubated on ice for 1 h. The plates were washed to remove the secondary antibody and re-suspended uniformly in 50 µl of flow buffer and analysed using the IntelliCyt iQue high-throughput flow cytometry (HTFC). An iQue instrument with a 2 laser (blue, red) configuration was used to perform the HTFC. The plates were placed manually and after a 60 second prime, they were agitated for 15 seconds at 1600 rpm and the shake repeated for 4 seconds after every 8 wells. A sip time of 4 second was used and the detector speed was set to medium. The probe was rinsed after every 8 wells. The live cells were gated using a FSC-H vs. SSC-

H dot plot and the data for Alexa Fluor 488 and 647 emissions were recorded using the FL1 and FL4 filters.

2.2.5 Medium-scale expression of selected phage hits as scFv-Fc

2.2.5.1 Conversion of selected scFv to scFv-huFc

The final selected scFv clones were converted to scFv fused to a C-terminal human Fc fragment (scFv-hFc) by sub-cloning the scFv fragments into a pMH vector encoding a human Fc fragment downstream of the multiple cloning site (pMH-hFc). Briefly, the scFv mini-prep purified plasmid DNA (section 2.2.3.6) and the pMH-hFc plasmid were digested simultaneously with the *NcoI* and *NotI* restriction enzymes, gel-purified and ligated with the T4 DNA ligase enzyme. The ligated mixture was used to transform chemically competent *E. coli* cells and positive colonies identified by sub-culturing and DNA sequencing.

2.2.5.2 Expression and high-throughput affinity purification of scFv-hFc

For the scFv-hFc expression, Expi293 cells were transfected with 50 µg scFv-hFc plasmid following the protocol described in section 2.2.4.3. The cells were harvested by centrifuging the culture media at 3500 x g for 1 h and the resulting supernatant was filtered using 0.22 µm filtration units to remove particulate matter (Amicon Steriflips).

An Äkta Pure system (GE Healthcare) capable of multiple tandem purifications was used for the high-throughput affinity purification. The scFv-hFc from the supernatant was captured using a 5 ml HiTrap Protein A HP column (GE Healthcare) at a flow-rate of 3 ml/min. The column was washed with 3 CV of PBS followed by elution using 4 CV of 0.1 M Sodium citrate pH 3.1. A cleaning procedure was included where 1.5 CV of 0.1 M NaOH and 2 CV of PBS were used to clean and equilibrate the column for subsequent purifications. The eluted fractions were collected in a 96-deep well blocks containing 250 µl of 2 M Tris-HCl pH 8.5 to facilitate the immediate neutralisation of the eluted samples. The relevant fractions were pooled and concentrated using Amicon Ultra filtration units with a 10 kDa molecular weight cut-off. The final concentration of all the individual purified scFv-hFc proteins was normalised to ~1mg/ml (or 10µM, assuming an average molecular weight of 100 kDa) with PBS pH 7.4.

2.2.6 Binding of purified scFv-hFc to PTH1R expressing cells using Flow cytometry

Expi293 cells were transiently transfected with the WT2 construct and empty vector as described previously (Section 2.2.2.2**)** and incubated overnight**.** The cells were harvested, washed twice and resuspended in Flow buffer. Typically, 25 µl of the cell suspension containing approximately 10^5 cells were added to each well of a 96 well U-bottom plate and 25 µl of the purified scFv-hFc (at ~10 µM) was added, in triplicate, to give a final scFv-hFc concentration of ~5 µM. The plates were incubated on ice for 1 h and washed twice with Flow buffer. Ten microliter of goat anti-human IgG Fc- Alexa Fluor 488 secondary antibody (1: 10 diluted in Flow buffer) was added to each well and the plates incubated for a further 1 h on ice in the dark. The plates were washed twice, and the cells re-suspended in 200 µl Flow buffer and analysed on a flow-cytometer. A BD FACS Canto HTS equipped with the 3-laser configuration was used to perform the flow- cytometry. The FSC, SSC and FITC voltages were set to 125, 342 and 400 respectively. A total of 10^4 events of the singlet gate were used for the data acquisition, with the flow-rate set to medium. The data was exported in the FCS format and further analysis was performed using FlowJo V10 software (FlowJo LLC). The mean and standard deviation of the geometric mean of the 488 nm fluorescence were calculated using GraphPad Prism 7.0.

2.2.7 Kinetics of ECD binding using Surface Plasmon Resonance (SPR)

A Biacore T200 (GE Healthcare) was used to perform the SPR to measure the binding kinetics of the scFv-hFc binding to the soluble ECD. Using amine coupling, a goat anti-human Fc capture antibody (Jackson Immunoresearch) was immobilised on a CM5 chip. The capture antibody was diluted to 50 µg/ml using acetate buffer, pH 5.0 (GE Healthcare). Flow-cell 1 was blocked without capture antibody while flow-cells 2, 3 and 4 were used to immobilise the capture antibody to give a final capture level of 600-900 RU. The scFv-hFc molecules were diluted to 2 µg/ml (except PD12 which was diluted to 3 µg/ml) using the ECD running buffer (1x HBS-EP+ supplemented with 350mM NaCl) and flowed through flow-cells 2 and 4 at 10 µl/min to give final capture levels of ~100 RU. Six separate dilutions of the ECD were prepared

in ECD running buffer by performing a 3-fold serial dilution starting at the highest concentration of 2 µM. The ECD samples were flowed through all flow-cells at a flow-rate of 30 µl/min and the binding kinetics was determined using the multi-cycle approach. The data analysis was performed using the Biacore T200 evaluation software and a 1:1 binding model was used to fit the binding curves, unless otherwise stated.

2.2.8 Functional characterisation of phage derived antibodies

The scFv-hFc molecules were tested for function using a cell-based functional assay which measured the intracellular cyclic-AMP (cAMP) concentrations. The cAMP dynamic 2 kit (Cisbio) based on the principle of homogenous time-resolved fluorescence (HTRF), was used to determine if the selected molecules exhibited agonism or antagonism. The approach allows time-resolved, ratiometric data analysis while allowing discrimination of the fluorescent signal from other extraneous signals. This technology uses europium-cryptate labelled anti-cAMP antibodies and allophyocyanin labelled cAMP molecules in an immunocompetition format. The labelled cAMP and anti-cAMP mAb produce a FRET signal when in close proximity, whereas competing unlabelled intracellular cAMP causes a decrease in FRET signal (Degorce *et al.*, 2009).

A stable CHOK1 cell-line expressing human PTH1R (DiscoveRx) was used for functional characterisation of the phage derived scFv-hFc molecules. The day before performing the assay, approximately 10,000 cells were plated using the cell-plating reagent 0 (CP0) (DiscoveRx) in a 384-well tissue culture- treated white plate (Corning) and incubated overnight at 37°C with 5% CO_2 and 80% relative humidity. The media was discarded and 5 µl of PBS supplemented with 1 mM 3-isobutyl-1-methylxanthine (IBMX) (PBS/IBMX) was added to every well.

To perform the assay in the agonist mode, 5 µl of the scFv-hFc at stock concentration was added to the cells, giving a final scFv-hFc concentration of 5 µM. The plates were incubated in a 37°C incubator for 30 min, following which 5 µl each of 1x cAMP-d2 and 1x Europium-cryptate labelled Anti-cAMP antibody were added, followed by a further incubation

for 1 h at room temperature. All detection reagents were diluted using the cAMP-GMP buffer (Cisbio). The IBMX at a final concentration of 0.5 mM was required to stop degradation of any accumulated cAMP.

In the antagonist mode, 2.5 µl of the scFv-hFc was added to the cells followed by 30 min incubation at room temperature. The cells were challenged with either an ~EC_{20} or ~EC_{80} concentration of PTH-(1-34) followed by incubation at 37°C for 30 min. The detection reagents were added as described for the agonist mode measurements and following a 1 h incubation room temperature. A schematic representation of the assay in both the modes is shown in Figure 2-2.

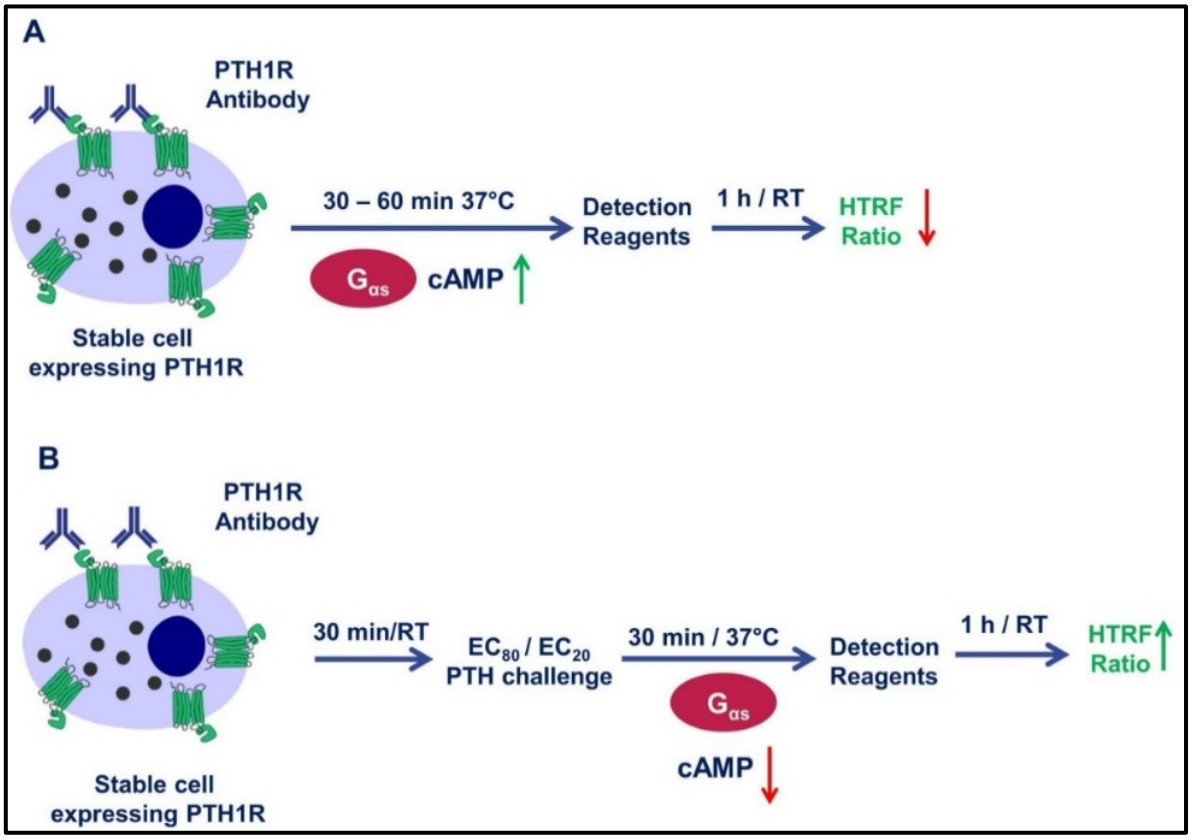


Figure 2-2: A schematic representation of the cAMP assay in agonist and antagonist mode.

A) In agonist mode the cells are incubated with the antibody molecule at 37°C following which detection reagents are added and further incubated for 1 h and the HTRF ratio measured. B) In antagonist mode, the cells are incubated with the antibody following which challenged with EC_{80} or EC_{20} concentration of endogenous ligand (PTH 1-34) and further incubated for 30 min at 37°C. The detection steps after the PTH challenge is similar to the agonist mode.

In both the agonist and antagonist modes the fluorescence of each sample was assessed using a Synergy Neo 2 (BioTek instruments) plate reader with 330 nm excitation and 620/665 nm dual emission filter cubes. The gain was set to auto with a delay of 150 µs

and the data collection time was 500 µs. Equation 2-1 was used to calculate the final HTRF ratio using the absorbance values at 620 and 665 nm.

$$\frac{Absorbance\ at\ 620\ nm}{Absorbance\ at\ 665\ nm}\ X\ 10{,}000$$

Equation 2-1: Formula for calculating the HTRF ratio

2.3 Results

2.3.1 Constructs

The ECD and receptor constructs used in this chapter are shown below in Figure 2-3.

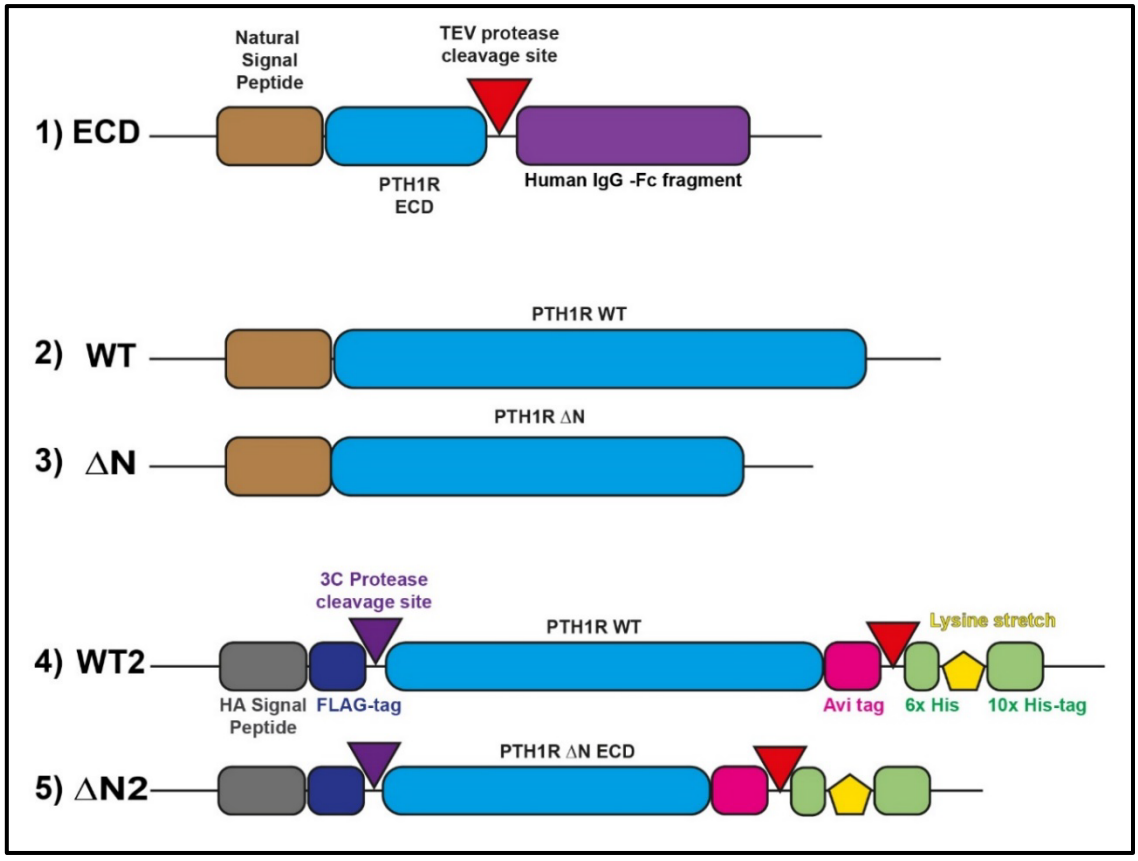


Figure 2-3: PTH1R and PTH1R-ECD constructs used for phage display and selection process. The ECD was cloned upstream of a TEV protease-cleavable human IgG Fc fragment. The signal peptide was left unmodified. Two separate constructs of PTH1R were used for screening phage binders, WT and ΔN. The WT2 and ΔN2 constructs contained same PTH1R fragment as WT and ΔN respectively and in addition had a range of detection and purification tags.

The ECD construct was designed with a human Fc tag at the C-terminus of ECD, which was used for protein A capture during the purification stages. It was also envisaged that the Fc tag could potentially be used for capturing the ECD on a SPR chip for kinetics analysis.

All cell-surface binding studies were carried out using the WT, ΔN, WT2 and ΔN2 versions of PTH1R receptor shown below in Figure 2-3. The ΔN constructs did not contain the N-terminal extra-cellular domain.

2.3.2 PTH1R ECD is pure and functional

The ECD of PTH1R was expressed and then purified to high purity as shown by SDS-PAGE analysis (Figure 2-4). The final protein sample was concentrated to 11 mg/ml in TBS, pH 8.0 with an overall yield of 65 mg/ L cell culture. The protein was aliquoted into 500 µl volumes, flash frozen in liquid nitrogen and stored at -80°C for future use.

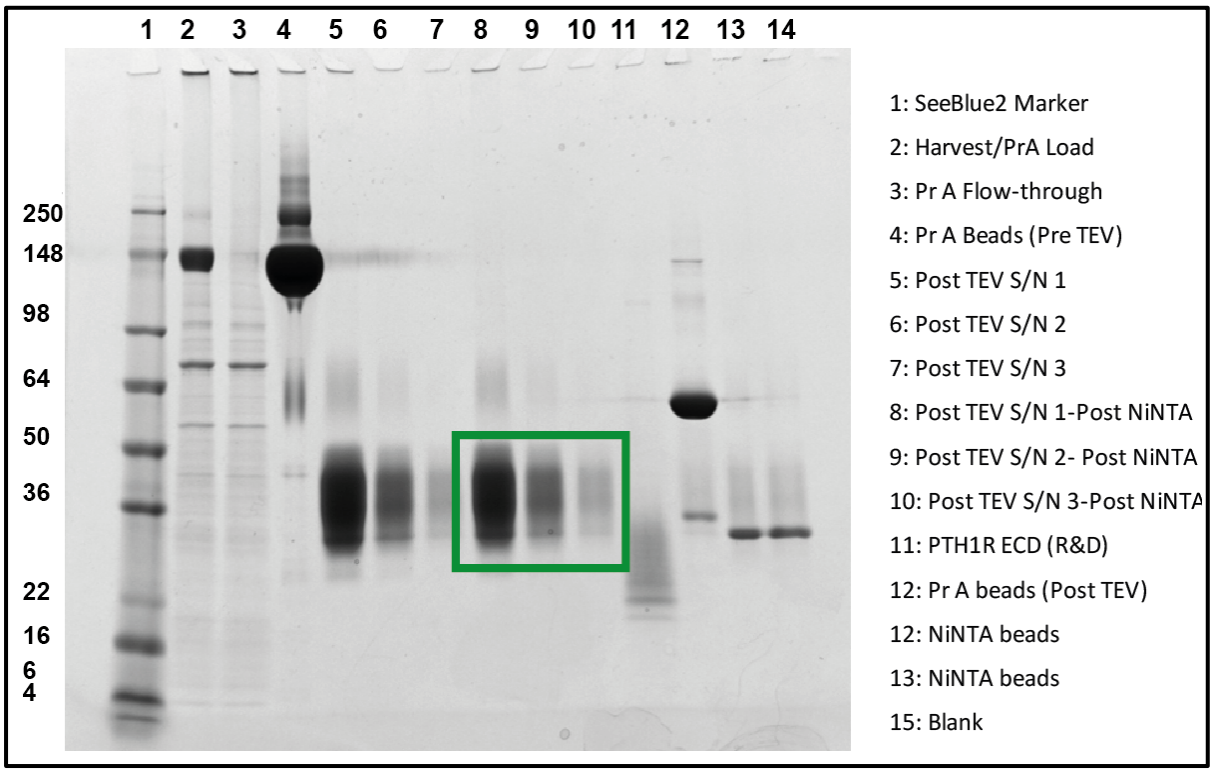


Figure 2-4: SDS-PAGE analysis of fractions from ECD purification

Lane 1 contains SeeBlue molecular weight marker; Lane 2, the filtered supernatant loaded onto the Protein A beads, while lane 3 contains the flow-though. The ECD-hFc was successfully captured on to the beads and this is shown by lane 4. TEV cleavage removes the hFc fragment and three washes containing the eluted ECD and TEV protease are shown in lanes 5-7. Lanes 8-10 contain the final ECD samples following removal of TEV protease. Lane 11 contains ECD from a commercial source while lane 12 contains TEV cleaved Protein A beads and when compared against pre-TEV (Lane 4) confirms successful cleavage of the His tage from the ECD. Lane 13-14 shows TEV-protease captured on Ni^{2+}-NTA beads. The expected molecular weight of the ECD is ~20 kDa but on the SDS-PAGE it appears to migrate between 30-50 kDa (green box) with a diffused banding pattern.

The bands corresponding to the purified ECD sample were diffuse, indicative of glycosylation and migrated at a higher than expected molecular weight. The molecular weight

of the ECD is 20 kDa whereas it appears to migrate between 30-50 kDa (Figure 2-4). Western blot analysis using an ECD-specific antibody confirmed the identity of the ECD while SDS-PAGE analysis using PNGaseF treated ECD samples confirmed the presence of the glycans (Figure 2-5).

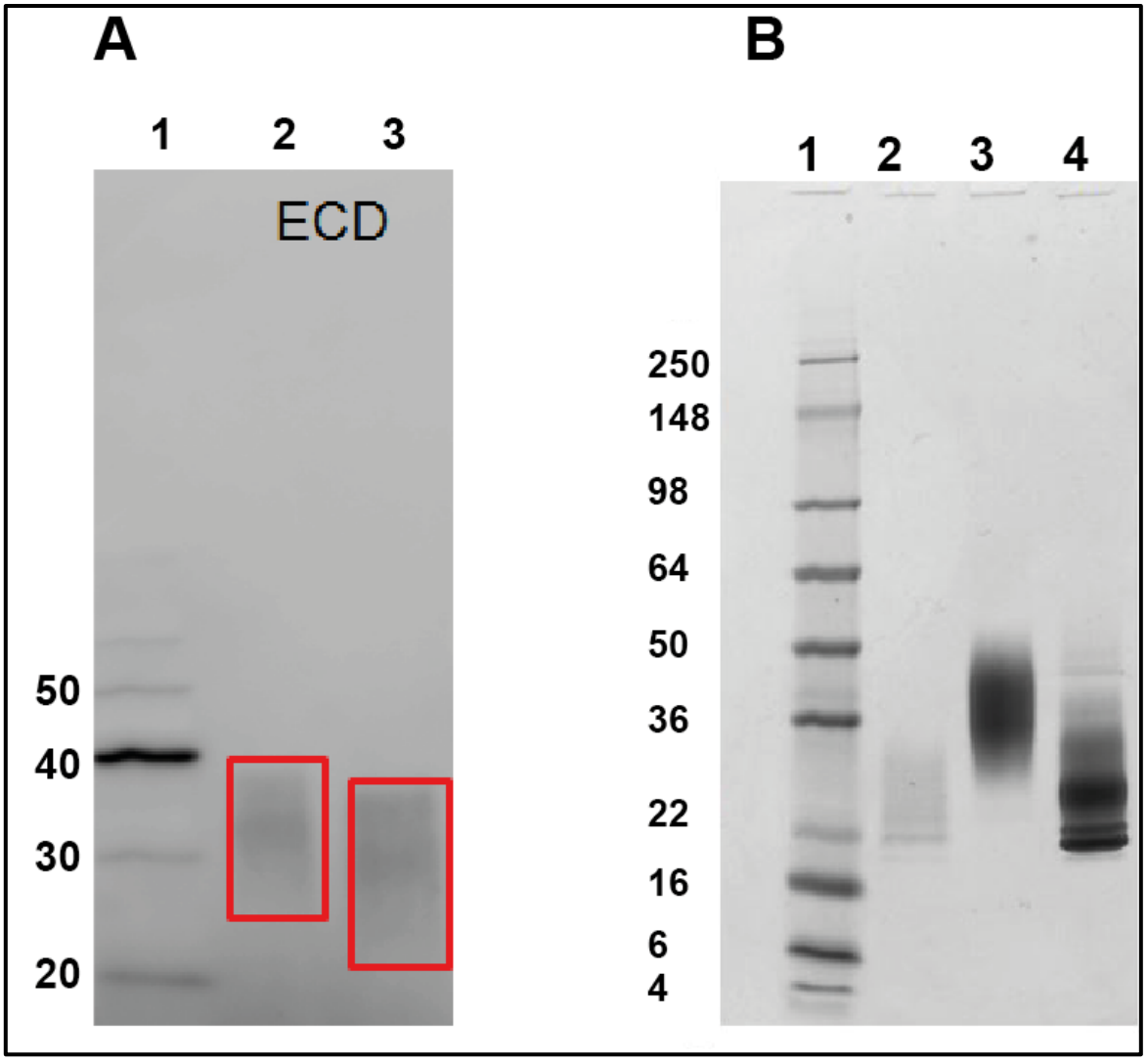


Figure 2-5: Western blot detection and effect of deglycosylation of purified ECD.

A) Western blot analysis of purified ECD. Lane 1, MagicMark Western protein standard, lanes 2 and 3 contain purified ECD under non-reducing (NR) and reducing (R) conditions respectively (bands in red box). (B) SDS-PAGE analysis of ECD following PNGaseF treatment to remove attached glycans. Lane 1, SeeBlue molecular weight marker; Lane 2, commercially available PTH1R ECD (R&D); Lane 3, purified ECD with intact glycosylation and lane 4, PNGaseF treated ECD. PNGaseF enzyme mediated glycan removal confirms successful glycosylation with the protein migrating to the expected region on the gel.

Mass Spectrometry revealed the presence of two major species of 19960 and 20122 Da (Figure 2-6) while the theoretical calculated mass is 20125 Da (ProtParam).

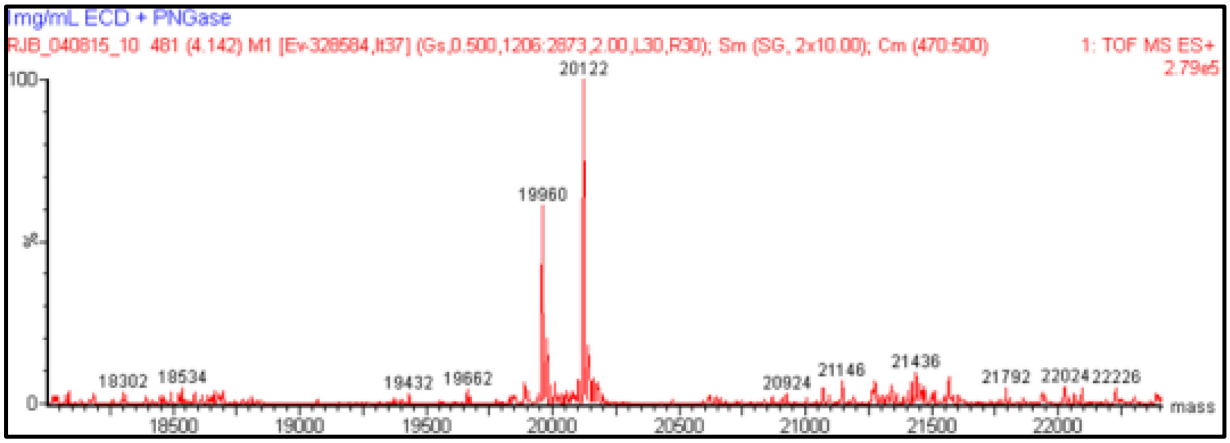


Figure 2-6: LC/MS analysis of ECD sample for molecular weight determination

Following PNGaseF treatment, LC-MS analysis of the ECD confirmed two major species at 19960 and 20122 Da respectively. The expected mass is 20125 Da.

The signal peptide cleavage site for the above sequence is predicted to situated be between A22 and Y23 (http://www.predisi.de). Any incomplete or extra residue cleavage could result in changes in the intact mass and it appears that loss of Y23 could result in a species with a molecular weight of 19962 Da. Therefore, the final ECD sample appeared to be a mixture of two closely-related species. Overall, the intact mass as determined by LC/MS agreed well with the expected mass and confirmed the presence of ECD in the purified sample.

The binding affinity of the ECD for PTH-(1-34) was ~4 μM, as assessed by ITC (Figure 2-7). This is in close agreement with published value of 1 μM using PTH (14-34) (Pioszak and Xu, 2008). Thus, the protein was deemed suitable for phage display mediated antibody discovery.

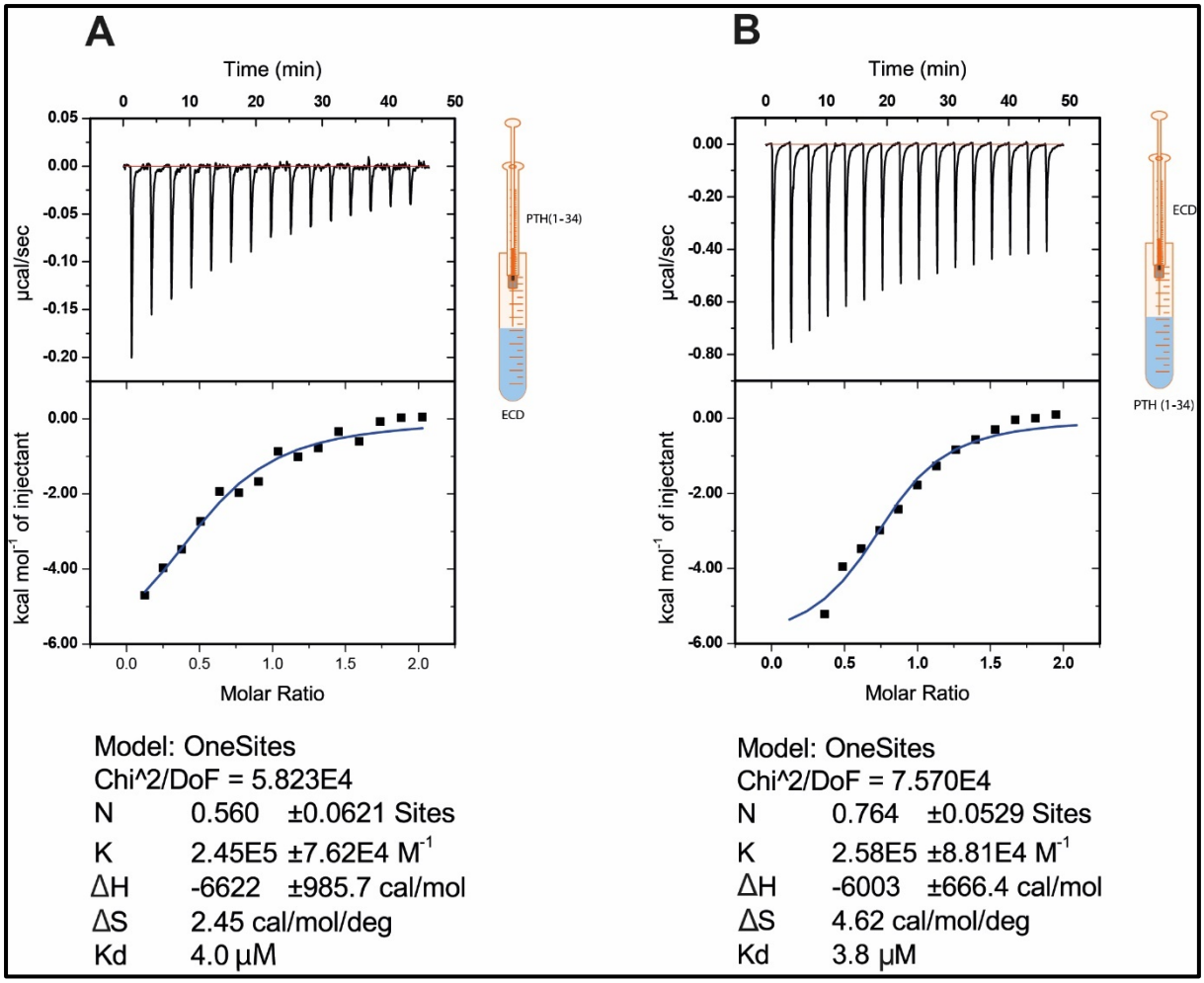


Figure 2-7: Isothermal Titration Calorimetry data showing binding of ECD and PTH (1-34).

A) Binding data for PTH (1-34) titration into purified ECD whereas B) represent the titration of ECD into PTH (1-34) solution, placed in a reaction cell. Both experiments gave similar binding affinity (~4µM). This data matches closely with published data of ~1µM (Pioszak and Xu, 2008) and confirms the functionality of the purified ECD. Each data point represents one injection and the data was fitted using OneSites model with chi-square minimisation (Origin Software).

2.3.3 Phage display outcome and sequence diversity analysis

A naïve scFv phage library, with a diversity of 10^{11} cfu, was used for discovering antibodies against ECD. After three rounds of panning, a total of 480 phage-antibodies specific for the ECD were isolated. The specificity of the selected phage clones was assessed by their ability to bind to the ECD in an ELISA (Figure 2-8).

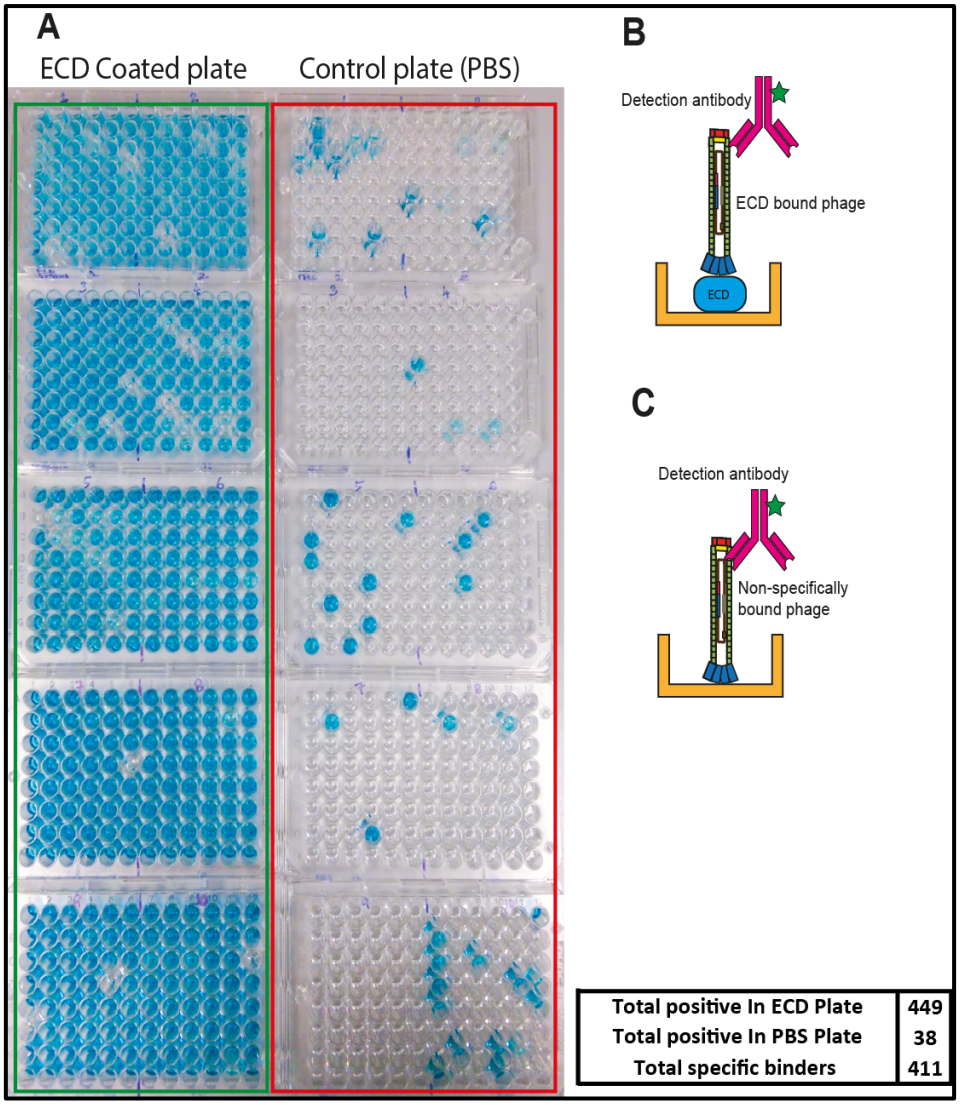


Figure 2-8: Phage ELISA results and a schematic representation of specific and non-specific binding

A) Phage ELISA plates with hits from three rounds of panning. B and C show schematic representations of specific and non-specific phage binding respectively. A total of 411 ECD specific clones were found after three rounds of panning against ECD.

From the ELISA data, it is evident that the majority of the selected phage clones bound specifically to the ECD (positive wells on ECD plate), while 38 clones were non-specific (positive wells on PBS plates). For all subsequent analysis and selection, non-specific phage clones were removed, and 411 ECD-specific clones were taken forward to determine the overall sequence diversity.

The DNA was prepared and sequenced for each ECD-specific clone identified from the phage ELISA. Poorly resolved sequences were discarded and of the remaining sequences

154 were found to be unique at the V_H CDR3 region. Those clones with identical V_H CDR3 regions but different V_L sequences were also taken forward as unique.

2.3.4 A selection of ECD binders also bind to full-length PTH1R on cells.

While the ELISA data using phage particles and the ECD confirmed binding to the isolated ECD, it was important to show that the antibodies also have the ability to bind the full-length PTH1R receptor expressed on the cell surface. Using a two-stage PCR, known as transcriptionally active PCR (Clargo *et al.*, 2014), 154 scFv sequences were converted to scFv-mFc, incorporating an N-terminal human CMV promoter fragment and C-terminal poly-A tail. The overall process of this conversion is presented schematically in Figure 2-9.

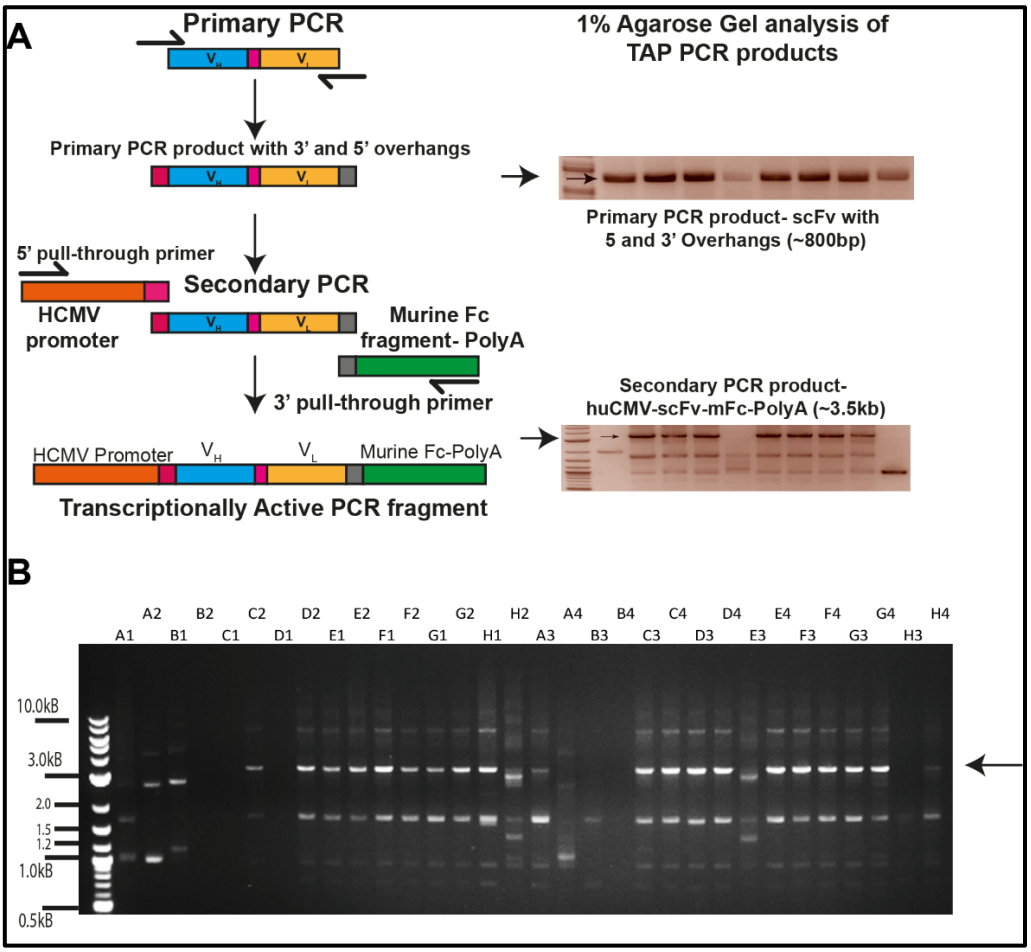


Figure 2-9: A schematic diagram of the TAP method and agarose gel analysis of TAP products.

A) The PCR steps involved in generating a TAP fragment. Primary PCR is used to add 5' and 3' overhangs which are then used for annealing in a secondary PCR. A pull-through primer used in secondary PCR is used to combine the human CMV promoter element, scFv fragment and the Fc fragment with a polyadenylation tail. PCR products were analysed using a 1% Agarose gel after each PCR step to confirm successful generation of fragments. B) 1% agarose gel analysis showing successful generation of TAP fragments for a selection of scFv identified as binding to the ECD. The arrow represents the expected band of the agarose gel.

The agarose gel scan (Figure 2-9, B) confirmed the successful generation of the TAP fragment for a selection of scFv molecules. These expression-ready fragments were used to transfect Expi293 cells and following 5-6-day incubation, the supernatant containing the expressed scFv-mFc tested in further binding assays such as FMAT and HTFC.

Fluorescent Microvolume Assay Technology (FMAT) is a single step, no-wash microvolume assay routinely used in drug-discovery screening (Miraglia *et al.*, 1999; Clargo *et al.*, 2014; Hagemann *et al.*, 2014). In this case, Expi293 cells expressing the WT2 constructs were incubated with the media containing expressed scFv-Fc and a mouse Fc-specific secondary antibody. Following a set incubation period, total fluroescence is measured for each well and compared against control well (which expressed ΔN construct of PTH1R). A higher fluorescence signal would suggest successful cell-surface scFv-Fc binding. FMAT software also allows visual inspection of images of each well to further confirm cell-surface binding.

	1	2	3	4	5	6	7	8	9	10	11	12
A	361.9	285.6	673.5	2444.2	0	1100.1	0	484.6	1702.1	727.5	419.1	411.2
B	0	818.5	2108.1	1572.5	871.8	349.8	0	387.9	854.5	1147	0	1604.1
C	0	0	2611.6	1658.4	1635	0	0	0	996.7	1104.2	972.6	273.9
D	2283.2	1016.7	1490.9	0	511.5	1006.5	486	0	1476.3	1172.5	1753.5	1137.4
E	266.3	2562.2	477.7	1460.2	469.6	0	1769.7	0	1466.4	392.4	1417.7	2051.3
F	793.6	1591.1	1589.2	794.2	429.5	0	0	0	682.5	1517	0	1762.4
G	0	2352.1	2697.7	1058.8	1786.9	1093.3	0	563.4	333.6	841.9	1364.4	416.5
H	0	1061.6	592.7	1139.3	1319.5	0	0	1209	2354.7	1864.1	2867.2	309.5

	1	2	3	4	5	6	7	8
A	1226.5	0	1625.9	559	1536.9	514.7	0	1295
B	0	0	1235.2	1396.7	1570.2	601.3	833	828.5
C	1122	901.7	0	2435.7	1495.6	2861.7	0	
D	0	1655.2	623.2	1037.8	1443.1	1099.9	2233.3	
E	625.9	1393.7	487.7	2796.8	1192.7	1436.7	3847	
F	2210.3	2453	2065.2	3491.7	0	1136.8	1371.8	
G	1189.3	3251	594.1	1087.2	3624.2	0	1390.4	
H	4166.8	873.9	3746.1	3023.7	948	1584.9	0	

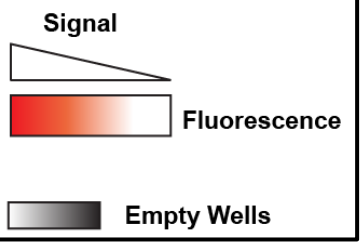


Figure 2-10: FMAT assay to test expression and cell-surface binding of TAP products

The figure above summarises ΔN subtracted total fluorescence from cells expressing WT receptor when stained with scFv-mFc (diluted ten-fold with wash buffer). The shades of red represent the intensity of the fluorescence signal from each well with darker shades representing higher fluorescence. White represents wells with no detectable fluorescence signal over control wells. Grey shaded box represents empty well with no samples.

The FMAT data (Figure 2-10) confirmed that TAP fragments could be successfully expressed in mammalian cells. Importantly, the majority of the ECD specific scFv-mFcs retained binding to the native full-length receptor expressed on the cell-surface as seen by

high fluorescence signals. Interestingly, the FMAT data also highlighted that a small proportion of the scFv-mFc failed to produce any detectable fluorescence signal (Figure 2-10). This would suggest either inability of the scFv-mFc to bind to the full-length receptor or insufficient expression of those individual scFv-mFcs.

FMAT analysis with the supernatant containing scFv-Fc confirmed the validity of TAP approach but the high numbers of positive scFv-Fc hits suggested another means of triaging to a more manageable number which would allow through characterisation.

2.3.5 Final selection based on cell surface binding and PTH competition using HTFC

The scFv-mFc molecules (section 2.2.4.2) were further screened in the presence of a saturating concentration of PTH-(1-34), using high-throughput flow cytometry (iQue). This experiment was used to investigate whether the binding of scFv-Fc to PTH1R was affected by PTH (1-34).

The heat map with the final geometric means (geomean) of fluorescence are shown in Figure 2-11, where panel A represents scFv-Fc binding to cells expressing the WT2 receptor. Any background binding detected with ΔN2-expressing cells were subtracted for the final fluorescence signal.

In panel B, the geomeans represent the effect PTH (1-34) has on scFv-Fc binding. Similar to panel A, this data represents the final fluorescence, after background subtraction, but in presence of 1.6 μM PTH (1-34). It is interesting to note that certain wells for example A1, H9 and E9 (Panel A/B, top plate) show a significant drop in fluorescence signal whereas wells such as H3 (Panel A/B, bottom plate) gains fluorescence signal in presence of PTH (1-34).

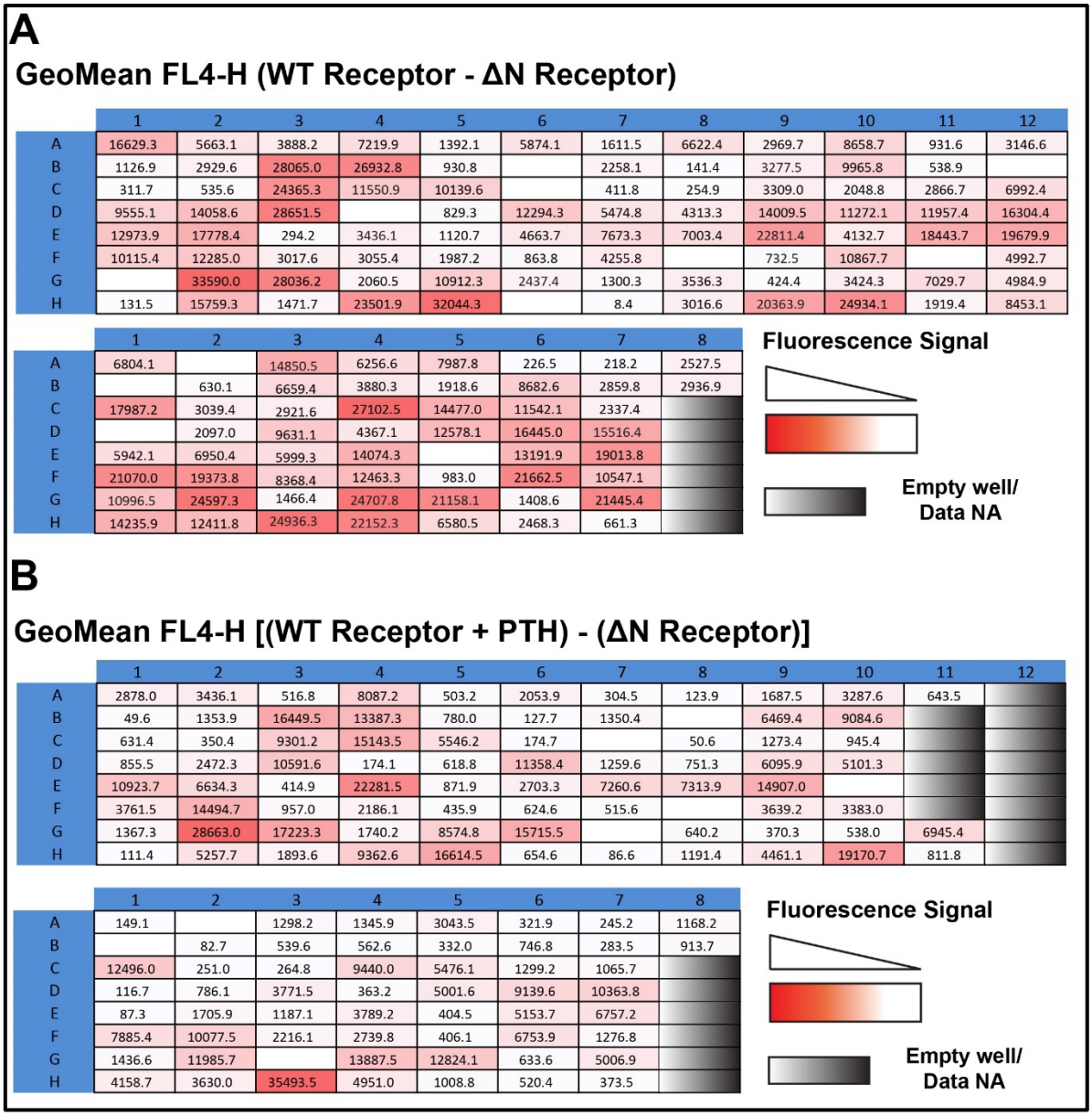


Figure 2-11: iQue analysis of shortlisted ECD binders

A) ΔN-corrected mean fluorescence for scFv-mFc TAP products binding to cells expressing WT receptor B) ΔN-corrected mean fluorescence for scFv-mFc TAP products binding to cells expressing WT receptor in presence of 1.6 µM PTH (1-34). No data was collected for column 12 of plate 3 (WT cells with PTH) due to instrument error. The shades of red represent the intensity of the fluorescence signal from each well with darker shade representing higher fluorescence. Wells with no detectable fluorescence signal (white) suggest complete lack of binding to the full-length receptor.

The HTFC analysis confirmed that the majority of the scFv-mFcs bound to the full-length receptor. Similar to the FMAT assay, some scFv-mFc failed to generate any detectable fluorescence signal suggesting either complete lack of cell-surface binding or insufficient scFv-mFc expression. A final selection was made based on which scFv-mFc exhibited competitive binding to the full-length receptor in the presence of PTH-(1-34) (Figure 2-12).

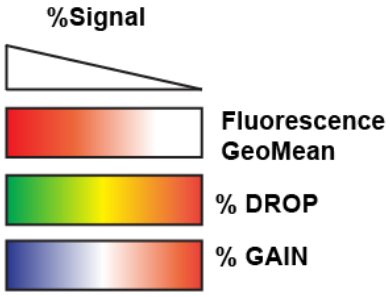
A

CloneID	FL GeoMean	FL GeoMean (1.6µM PTH)	%Signal DROP
PD1	14850.5	1298.2	91.3
PD2	10996.5	1436.6	86.9
PD3	16629.3	2878.0	**82.7**
PD4	14058.6	2472.3	**82.4**
PD5	20363.9	4461.1	**78.1**
PD6	22152.3	4951.0	77.7
PD7	15759.3	5257.7	**66.6**
PD8	27102.5	9440.0	65.2
PD9	32044.3	16614.5	**48.2**
PD10	24707.8	13887.5	43.8
PD11	21158.1	12824.1	39.4
PD12	22811.4	14907.0	**34.7**
PD13	15516.4	10363.8	33.2
PD14	24934.1	19170.7	**23.1**
PD15	33590.0	28663.0	**14.7**
PD16	9965.8	9084.6	**8.8**
PD17	7673.3	7260.6	**5.4**

B

CloneID	FL GeoMean	FL GeoMean (1.6µM PTH)	%Signal GAIN
PG1	3436.1	22281.5	**84.6**
PG2	2437.4	15715.5	**84.5**
PG3	732.5	3639.2	**79.9**
PG4	3277.5	6469.4	**49.3**
PG5	24936.3	35493.5	29.7
PG6	11550.9	15143.5	**23.7**
PG7	7003.4	7313.9	**4.2**

C



D

$$\%\ \text{DROP} = \frac{[\text{Mock corrected WT signal} - \text{Mock corrected (WT + PTH) Signal}]}{\text{Mock corrected WT Signal} \times 100}$$

$$\%\ \text{GAIN} = \frac{[\text{Mock corrected (WT + PTH) Signal} - \text{Mock corrected WT signal}]}{\text{Mock corrected (WT + PTH) Signal} \times 100}$$

Figure 2-12: Selection of final ECD-binding clones based on cell-surface binding and PTH competition

The change in fluorescence signal due to addition of PTH-(1-34) was used a parameter for final selection. A) A list summarising the final clones selected based on PTH competition where a decrease in fluorescence signal was seen upon PTH addition. The CloneID used in the list is used throughout the chapter B) A list summarising the final clones selected based on PTH competition where a gain in fluorescence signal was seen upon PTH addition C) The colouring scheme used to denote the intensity of fluorescence geomean (red to white), percentage drop in signal (green to red) and percentage gain in signal upon PTH addition (blue to red). D) The formulae used for calculating the percentage drop or gain.

A total of 18 scFv sequences (PD1-7, PD9-13, PD16 and PG1-6, from Figure 2-12) were selected for further characterisation and the corresponding scFv genes were sub-cloned into the pMH-huFc vector, re-sequenced to confirm sequence diversity and used for medium scale expression and affinity purification (Figure 2-13). Purified PD1 and PD3 revealed different protein banding pattern on an SDS-PAGE gel compared to other molecules possibly

as a result of post-elution aggregation/degradation. The purified material was used for further binding and functional studies.

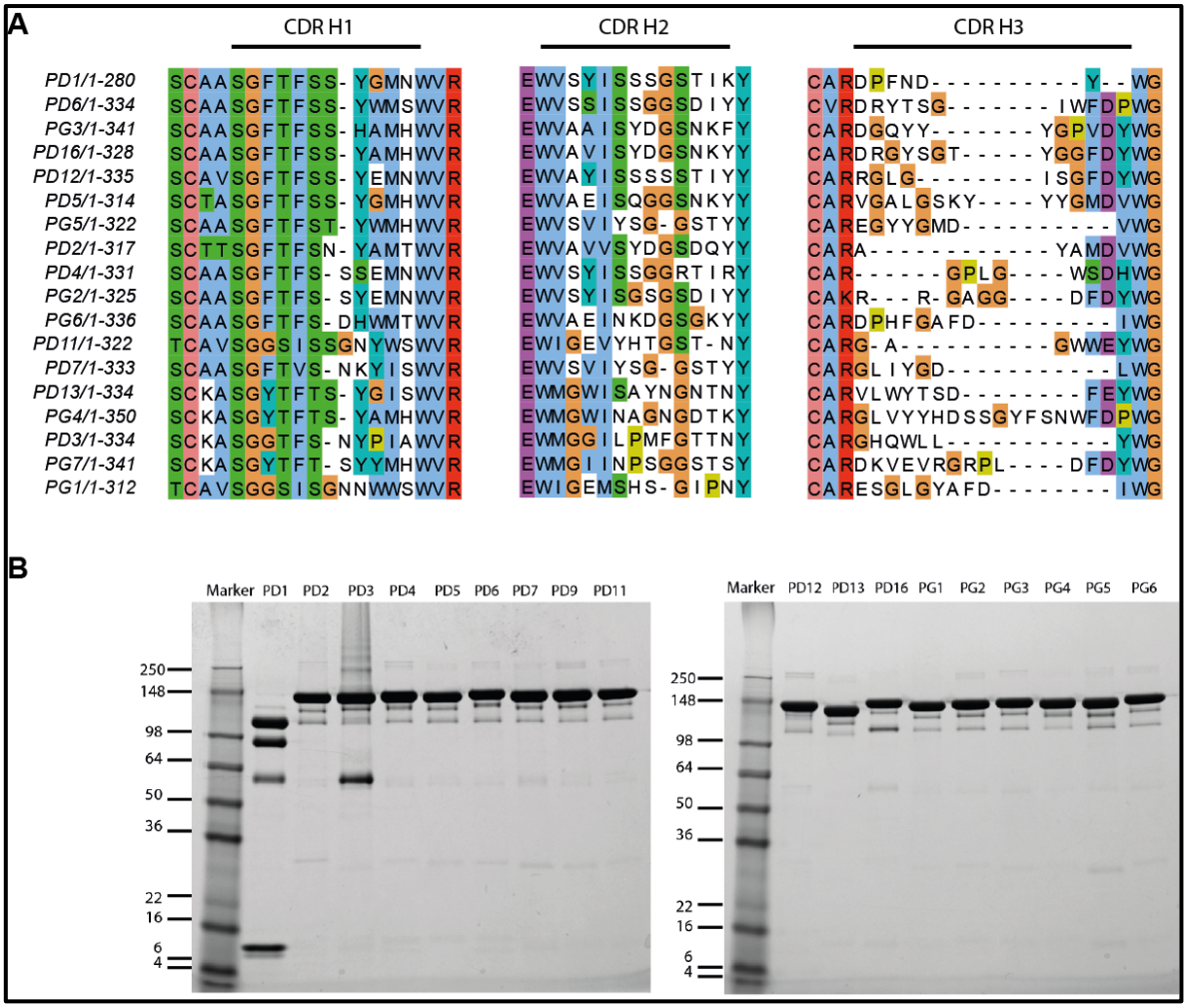


Figure 2-13: Sequence alignment and SDS-PAGE analysis of selected scFv-Fc

A) Alignment of the amino acid sequences of final clones highlighting the CDR regions of the V_H chain. Diversity was maintained in the final clones B) SDS-PAGE analysis was used to determine the purity of affinity (Protein A) purified scFvFc samples.

2.3.6 Binding confirmation of purified scFv-huFc using flow-cytometry

Following purification, all 18 scFv-hFc molecules were tested for cell-surface binding using flow-cytometry on Expi293 cells expressing the WT2 construct. All the purified scFv-hFc molecules successfully bind cell surface expressed full-length PTH1R receptor above the background of mock transfected cells (Figure 2-14).

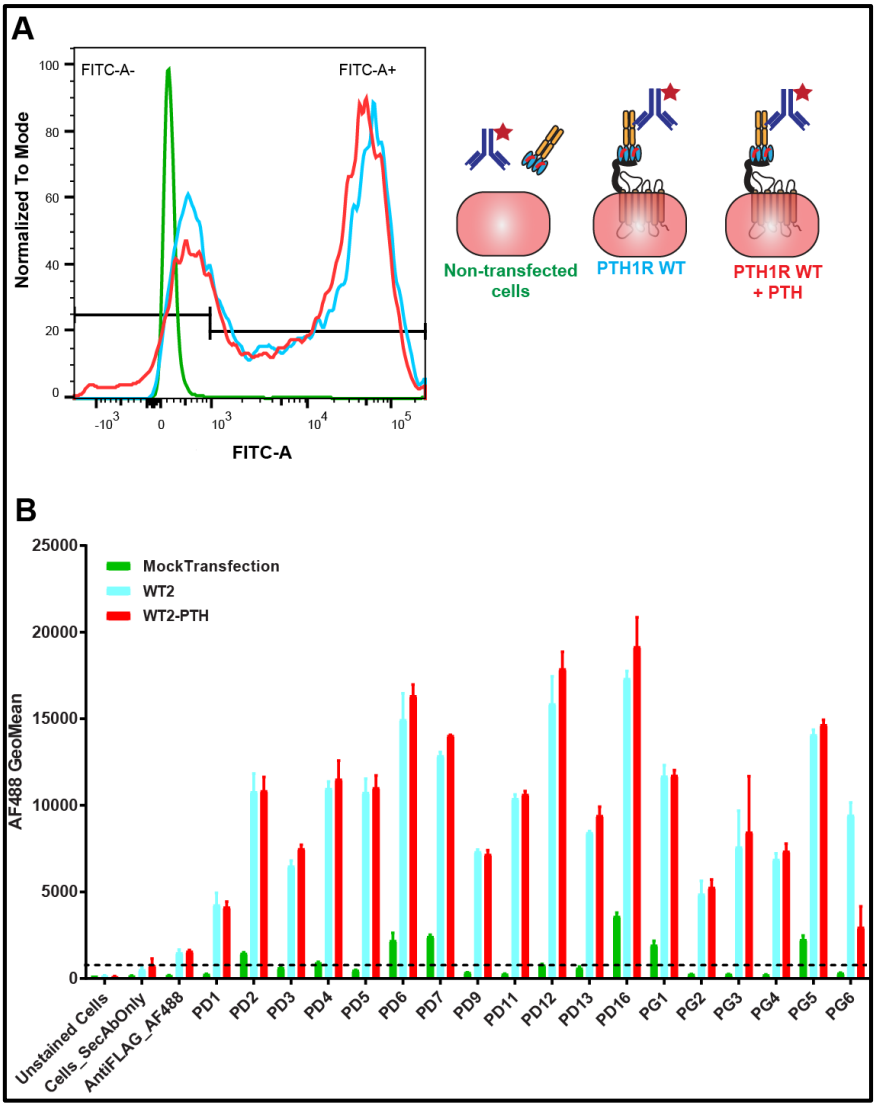


Figure 2-14: Cell-surface binding confirmation of purified scFv-hFc using flow-cytometry

A) A representative overlay of flow cytometry data showing sample data for PD9 scFv-hFc staining of cells transfected with WT2 receptor (cyan) and non-transfected (green) cells. The overlay also shows effect of PTH addition to the WT expressing cells (red trace). B) A plot summarising the geometric mean of fluorescence as shown by all selected ECD binding scFv-hFc molecules. Each data point represents mean and standard deviation of triplicate measurements. The black dashed line represents the fluorescence levels from cells stained with secondary antibody only.

The cell surface expression of the receptor was confirmed using Alexa Fluor 488-labelled Anti-FLAG antibody binding to the N-terminal FLAG tag expressed by the receptor. The secondary antibody exhibited negligible non-specific binding and addition of the PTH did not significantly alter the final fluorescence. Only antibody PG6 exhibited a decreased fluorescence signal in presence of the PTH.

2.3.7 PD12 has low nanomolar affinity for soluble ECD

The binding kinetics of the ECD-specific scFv-hFc, PD12, were determined using surface plasmon resonance (SPR). The purified scFv-hFc was captured using an anti-human Fc antibody, immobilised using amine coupling. A schematic representation of the flow cell capture strategy is shown below in Figure 2-15 along with a representative sensorgram with fitted data for PD12 and PD13.

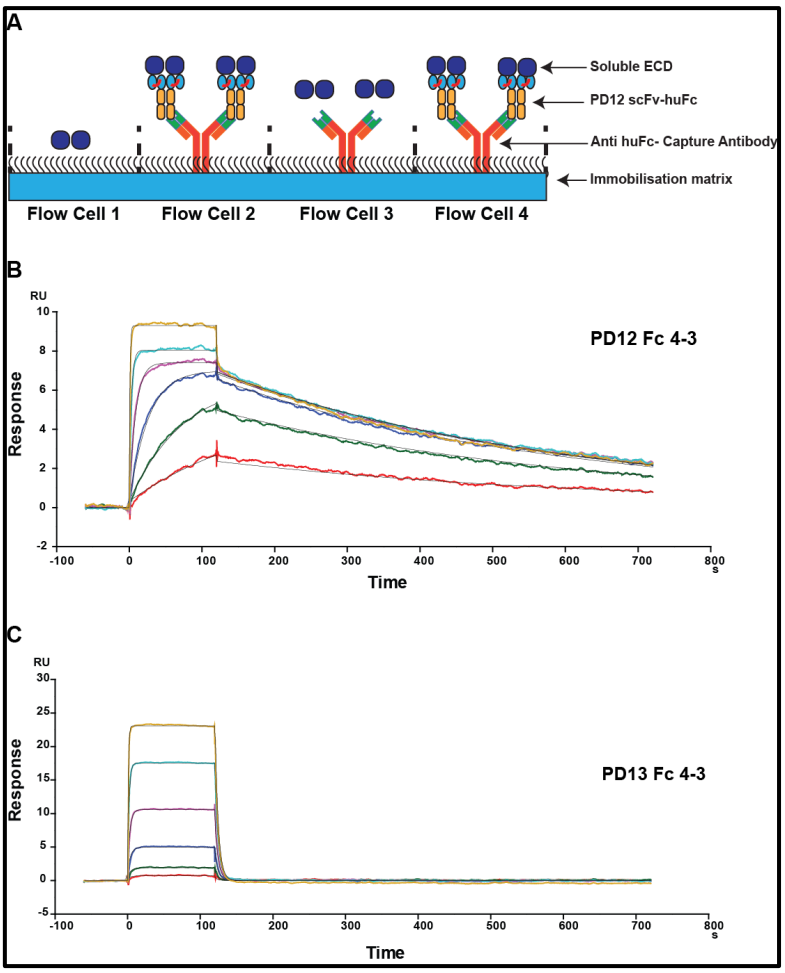


Figure 2-15: Immobilisation strategy for ECD-binding kinetics measurement and representative sensorgrams.

A) The flow-cells capture strategy was designed to detect any non-specific binding exhibited by soluble ECD. Flow cell 1 was blocked, flow cell 3 was used to capture anti-human Fc antibody but not capture scFv-huFc. Flow cells 2 and 4 were used to capture both the capture antibody and scFv-huFc. A representative sensorgram for a high (B) and low (C) affinity binder is also shown.

The majority of the selected scFv-hFc binds to the soluble ECD, and it also interesting to note that the affinity for the ECD ranges from low nanomolar (PD12) to micromolar (Table 2-3). It should also be noted that the affinity data from both sets of flow-cells for each scFv-

hFc closely match indicating that the ECD shows no non-specific binding to the immobilisation matrix or the capture antibody.

It was not possible to fit the kinetic data for PD4 and 7 as the measured affinity value was higher than the highest concentration of ECD tested (2 µM) and barring PD4 and 7, a 1:1 Langmuir model was used to fit the data for all other scFv-hFc molecules. Among the binders tested, PD12 scFv-hFc exhibited the highest affinity for the soluble ECD with a K_D of ~4 nM.

Table 2-3: A table summarising the affinity measurement of scFv-hFc.

	n=1		n=2				
	KD (nM)[b]	KD (nM)[c]	KD (nM)	KD (nM)	Model[d]	Mean	Std.Dev
Molecule[a]	Fc = 2-1	Fc = 3-4	Fc = 2-1	Fc = 3-4			
PD1	253.6	216.7	204.6	188.1	1:1 Langmuir	**215.8**	**27.8**
PD2	1687	1488	1348	1307	1:1 Langmuir	**1457.5**	**171.5**
PD3	1245	1003	1043	929.1	1:1 Langmuir	**1055.0**	**135.2**
PD4	>2000	>2000			Steady-state	**ND[e]**	**ND**
PD5	1076	733.9	959	882.8	1:1 Langmuir	**912.9**	**143.4**
PD6	1319	803.3	966.3	868.6	1:1 Langmuir	**989.3**	**229.8**
PD7	>2000	>2000			Steady-state	**ND**	**ND**
PD9	1230	926.5	1058	920.1	1:1 Langmuir	**1033.7**	**145.5**
PD10	349.5	208.4	270.8	253.7	1:1 Langmuir	**270.6**	**58.8**
PD12	4.551	3.784			1:1 Langmuir	**4.2**	**0.5**
PD13	518.2	519.5	351.7	321.2	1:1 Langmuir	**427.7**	**106.0**
PD16	746	608.2	395	356.7	1:1 Langmuir	**526.5**	**183.5**
PG1	300.3	270.2	183.9	165.6	1:1 Langmuir	**230.0**	**65.4**
PG2	48.46	44.95	41.79	39.03	1:1 Langmuir	**43.6**	**4.1**
PG3	58.78	54.49	63.02	58.66	1:1 Langmuir	**58.7**	**3.5**
PG4	381.2	329.3	310.2	281.1	1:1 Langmuir	**325.5**	**42.1**
PG5	30.37	35.82	29.87	29.36	1:1 Langmuir	**31.4**	**3.0**
PG6	1473	1423	902.7	825.6	1:1 Langmuir	**1156.1**	**339.2**

[a] Molecule ID;
[b]The measured affinity from flow cell 2-1 in nanomolar;
[c]The measured affinity from flow cell 3-4 in nanomolar;
[d]Model used to fit the kinetics data. In most cases 1:1 model gave accurate fitting.
[e] ND represents not-determined

Table 2-3 summarises the final affinity measurements (K_D) for selected scFv-huFc molecules against soluble ECD. The data represents two independent experiments (as shown by N=1 and 2) performed in duplicate using the capture strategy as described above.

2.3.8 PD12 exhibits weak cAMP antagonism

The selected binders were further tested for their ability to modulate intracellular signalling pathways using a functional assay measuring cAMP in the agonist and antagonist modes. The plots shown in Figure 2-16 summarise single point cAMP regulation by the selected scFv-hFc.

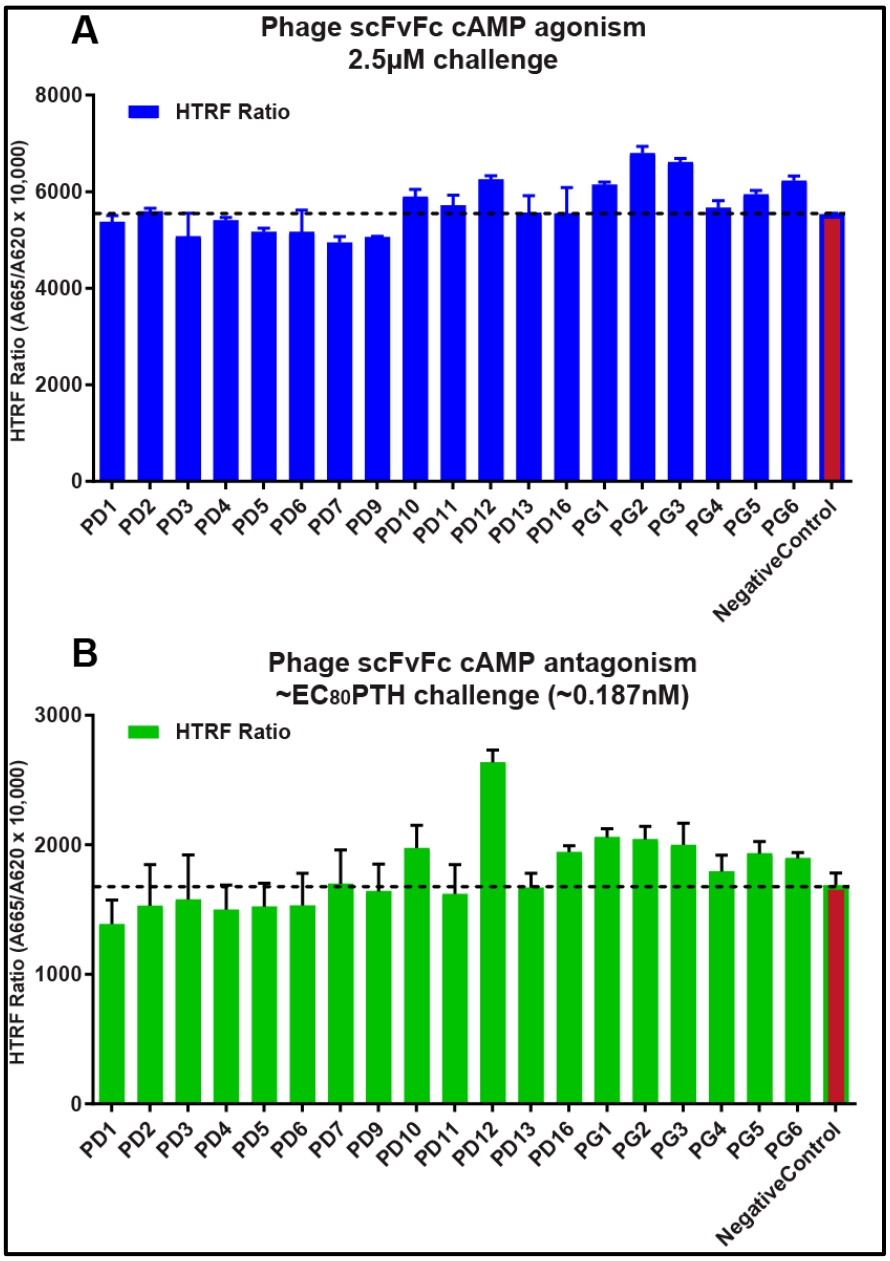


Figure 2-16: Cyclic-AMP (cAMP) regulation by ECD binders on CHOK1 cells stably expressing PTH1R.

A) The final HTRF ratio under agonist mode where the HTRF ratio for all the binders is similar to vehicle control (red bar with blue outline). B) The HTRF ratio in antagonism mode for the selected binders when challenged with ~0.2nM PTH (1-34). The red bar with green border represents vehicle control. The black dashed line represents the signal from vehicle/ negative control. Each bar represents mean and standard deviation of triplicate measurements.

In the agonist mode (Figure 2-16, A), the HTRF ratio for all the molecules matched closely with the vehicle control, whereas in antagonist mode, a slight increase in HTRF ratio was noted for the PD12 scFv-hFc, suggesting weak cAMP antagonism mediated by G_s.

2.4 Discussion

Generating antibodies against GPCRs is challenging mainly due to the difficulty of producing milligram quantities of pure, stable and active full-length receptor (Hutchings *et al.*, 2017). To address this issue, we expressed and purified the N-terminal domain of the PTH1R as a recombinant protein for phage display antibody discovery. Previously, the PTH1R ECD has been successfully expressed using an *E. coli* expression system using the maltose-binding protein tag to improve expression and solubility (Pioszak and Xu, 2008; Pioszak *et al.*, 2009, 2010). However, these ECD preparations lacked glycosylation. The ECD has 4 putative glycosylation sites and to preserve all the post-translational modifications, we used a mammalian expression system to produce milligram quantities of the fully glycosylated ECD. The ECD was expressed with a human Fc tag which gives better yields and higher purity using Protein A affinity purification. The Fc domain has been previously shown to further improve the yield of some difficult to express proteins (J. Zhang *et al.*, 2010). We also envisaged that the Fc tag could also potentially be used for capturing the ECD using an anti-Fc antibody for various assays such as SPR. The purity of the sample was confirmed using SDS-PAGE analysis which also suggested successful glycosylation (Figure 2-4). The binding affinity of the purified ECD to PTH-(1-34) was found to be 4 μM which matched closely with previously published data (Pioszak and Xu, 2008). ITC data further confirmed the applicability of the purified ECD for phage display antibody discovery (Figure 2-7).

Following three rounds of panning with UCB naïve scFv library and purified ECD, 480 phage particles were selected. Among the selected clones, 411 clones were found to be ECD-specific using phage ELISA (Figure 2-8), a routinely-used screening method to screen for specific binders (Kingshury *et al.*, 1995). Further, the sequence diversity among the ECD-specific clones was checked using the V_H CDR3 sequences and 154 unique ECD-binding

sequences were found. Schofield et. al performed phage display on 292 antigen molecules and from primary screening ELISA found on average 25 unique binders per antigen (Schofield et al. 2007). Therefore, in this case the large number of sequences and the diversity suggest a successful phage display panning against the ECD.

Although the primary selection was done using purified ECD and phage particles in an ELISA, we were interested in finding clones that bound to the full-length receptor, when expressed on the cell-surface. To achieve this, all 154 scFv sequences from the phage particles were converted to scFv-mFc using transcriptionally-active PCR (Figure 2-9) (Liang *et al.*, 2002; Regis *et al.*, 2008). The TAP fragments allow expression of scFv-mFc without requiring any cloning and here have been successfully used to enable high throughput screening using flow-cytometry and the FMAT (Clargo *et al.*, 2014; Starkie *et al.*, 2016). From the FMAT data (Figure 2-10), we found that 121 scFv-mFcs retained their binding, with a loss of binding only exhibited by 33 scFv-mFcs, possibly due to unavailability of the original epitope or lack of scFv-mFc expression. HTFC was used as a secondary screening approach to determine the effect of PTH-(1-34) on scFv-mFc binding on cell-surface expressed receptor. A total of 18 molecules were selected from the HTFC data as summarised in Figure 2-12, cloned into mammalian expression vector and sequenced to ensure that sequence diversity was maintained (Figure 2-13).

Using flow-cytometry, it was shown that the purified scFv-hFc could successfully bind to cells expressing PTH1R. It should however be noted that not all scFv-hFc exhibited high specificity as PD2, 6, 7, 16, PG1 and 5 showed higher levels of binding to the untransfected cells compared to the other scFv-hFc molecules (Figure 2-14). To further characterise binding of the purified scFv-hFc to soluble ECD, we used SPR and obtained a range of affinities. PD12 exhibited the highest affinity for ECD at ~4 nM, while the rest of the scFv-hFc molecules showed low nanomolar to micromolar affinities (Table 2-3). Interestingly, PD 2, 6, 7 and 16 showed low affinity for the ECD in SPR assay and also high non-specificity in flow-cytometry but this was not the case for PG1 and 5. Naïve library derived antibodies can exhibit increased cross-reactivity and poor affinities and therefore affinity maturation techniques are employed

to further increase the specificity and affinity (Azzazy and Highsmith, 2002; Bazan *et al.*, 2012). The ECD-specific antibodies were derived after three rounds of panning with no affinity maturation and this might explain the non-specificity and low affinities, although we did not find any correlation between non-specific binding and low affinity.

To date there are no reported function-modifying antibodies against PTH1R and only recently an antagonist antibody targeting the PTH1R ECD with therapeutic benefits has been reported (http://www.xoma.com/assets-available-for-licensure/anti-pth1r/). We were keen to investigate the function-modifying properties among the shortlisted scFv-hFc, and to achieve that, the purified antibody molecules were analysed in a functional assay measuring intracellular cAMP. While in agonist mode, none of the selected molecules showed any measurable activity over buffer control. However, in antagonist mode (with EC_{80} PTH challenge), PD12 showed partial antagonism (Figure 2-16). While this data is encouraging, the antagonist property of PD12 requires further investigation.

Overall, 154 unique ECD-binding antibody sequences were found using phage display panning on soluble ECD. Among the ECD-positive clones, 18 antibody sequences were further selected and tested for function and one antibody, PD12 exhibited weak antagonism with an affinity of ~4 nM. We also believe that a functional assay based screening could be more suitable to discover functional mAbs, but that would require substantial resources at an early stage of mAb discovery and a robust functional assay. It would be interesting to re-visit the remaining ~130 sequences, perform high-throughput mAb expression and test for functionality using the cAMP assay, but this was not possible in this study due to lack of time and resource.

Chapter 3: Antibody generation against PTH1R extracellular loops using UCB core discovery approach

3. Antibody generation against PTH1R extracellular loops using UCB core discovery approach

3.1 Introduction to Core discovery approach

The vast majority of drugs towards GPCRs are small molecules targeting the orthosteric regions of the receptors, which tend to be highly conserved among receptors in the same subfamily (e.g. Histamine H1 and H2 receptors) and thus receptor selectivity is an issue (Jeffrey Conn *et al.*, 2009). Molecules targeting allosteric sites, which show much greater sequence diversity than the orthosteric sites, even among receptor sub-family members, could potentially circumvent this issue (Hutchings, Koglin and Marshall, 2010). The hit rate for small molecule screening is extremely low for the Class B GPCRs (Macarron, 2006). Only a handful of small molecules targeting class-B GPCR such as telcagepant (Ho *et al.*, 2008), ubrogepant (Voss *et al.*, 2016), LY2409021 (Kazda *et al.*, 2016), Verucerfont (Gilligan *et al.*, 2009) and BMS-927711 (Marcus *et al.*, 2013) have entered clinical trials with varying levels of success. Similarly, many class B GPCRs are targeted using their endogenous ligands, their variants and other mimetics. For example, Albiglutide (Matthews *et al.*, 2008), Lixisenatide (Bolli and Owens, 2014) and Liraglutide (Wajcberg and Amarah, 2010) are all mimetics of the Glucagon-like peptide -1 (GLP-1) which binds to the GLP-1 receptor (GLP1R) orthosteric site and used for treating type 2 diabetes mellitus. However, these drugs have a comparatively short serum half-life and are susceptible to proteolytic degradation.

Generating monoclonal antibodies (mAbs) to integral membrane proteins is difficult, mainly due to the inherent instability of these proteins in detergent based solution (Hutchings, Koglin and Marshall, 2010), however this is fast-changing with new and improved methods aiding mAb discovery. Therapeutic mAbs such as AMG334 (against CGRP receptor for treating migraine) (Shi *et al.*, 2016), PRO 140 (against CCR5 for treating HIV infection) (Olson *et al.*, 1999) and Ulocuplumab (against CXCR-4 for treating chronic lymphocytic leukaemia) (Kashyap *et al.*, 2015) are in Phase III clinical trials. Currently, ~57 mAbs are in discovery or

pre-clinical studies and 39 mAbs are in clinical development stages clearly highlighting the potential that mAbs have as biotherapeutics targeting GPCRs (Hutchings *et al.*, 2017).

Most functional mAbs targeting class B GPCR members, bind to the large extra-cellular N-terminal domain (ECD). The extracellular loop regions represent an alternative mAb binding site as there is often marked sequence variability even among closely related receptors (Hutchings, Koglin and Marshall, 2010). Loop-binding antibodies are rare mainly due to the difficulties associated with targeting flexible loop regions. Synthetic peptides of the ECLs present a simple and inexpensive alternative but antibodies raised against synthetic peptides can sometime fail to bind to the native receptor (Hutchings, Koglin and Marshall, 2010). Nevertheless, peptides have been used successfully to generate antibodies which bind to ECL2 of the β_2-adrenergic receptor and exhibit agonist behaviour (Lebesgue *et al.*, 1998).

Currently, all the therapeutic agents targeted against PTH1R are peptide fragments such as Forteo (Neer *et al.*, 2001) and Abaloparatide (Leder *et al.*, 2015) which bind into the orthosteric binding site. No functional antibodies are currently available for PTH1R. Here we describe discovery of antibodies targeting the PTH1R ECL using receptor-expressing syngeneic cell immunisation followed by B-cell isolation and screening using UCB's core discovery automation.

Antibody discovery against difficult targets such as GPCR loops, requires screening a very large number of antigen specific B-cells. While the hybridoma technology (Köhler and Milstein, 1975) revolutionised the mAb discovery process and has been the main workhorse for generating mAbs for several decades, it is limited by low efficiency and a lack of suitable myeloma cell-lines (Liu, 2014). Due to the limitations associated with traditional hybridoma approach, at UCB, high affinity antibodies are generated using a proprietary method known as the "UCB Core antibody discovery", which involves high throughput screening of specific B-cells from immunised animals using state-of-the-art automation without hybridoma generation. This method allows very efficient sampling of the immune repertoire of the immunised animal to discover rare antibodies (Tickle *et al.*, 2015). Figure 3-1, shows the UCB Core antibody discovery platform.

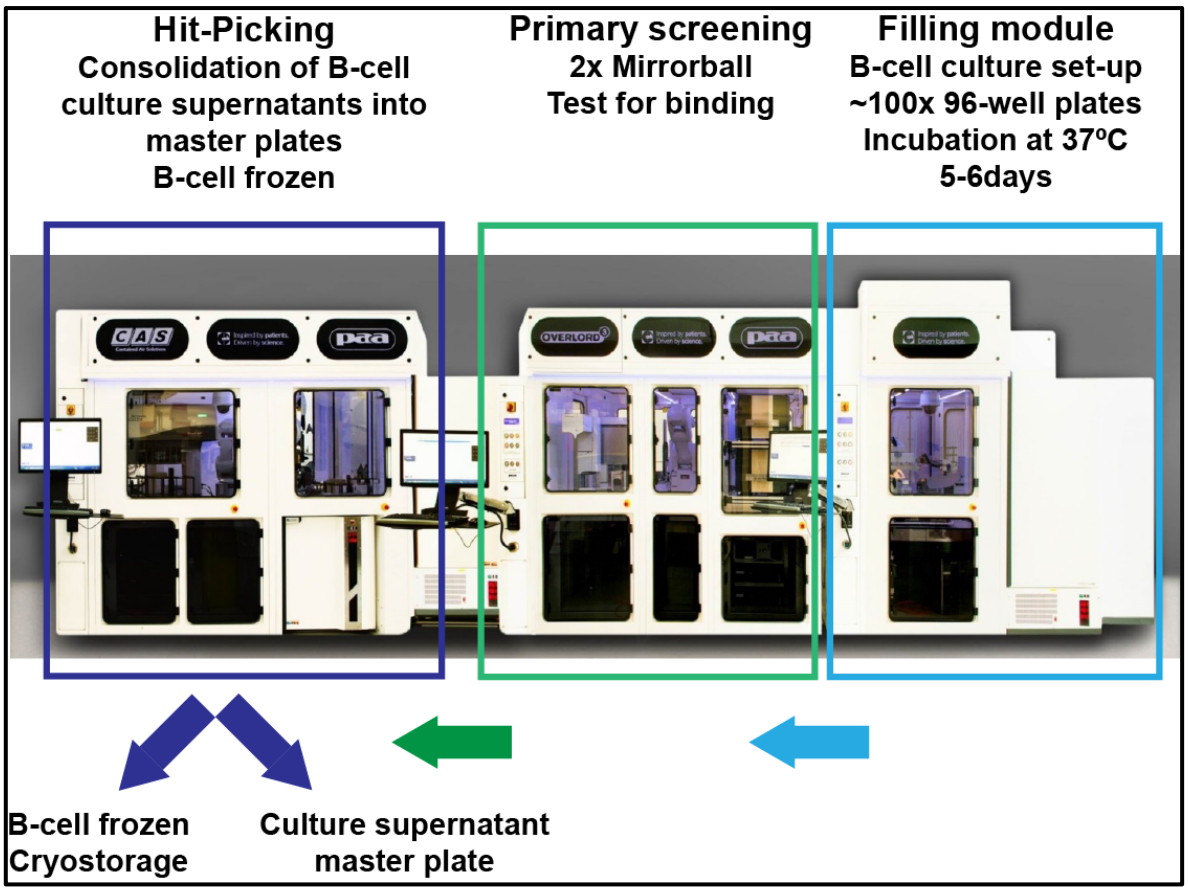


Figure 3-1: UCB Core discovery platform for high-throughput mAb discovery and screening

The UCB core discovery automation is made up of three main modules; the filling, primary screening and hit-picking modules. The filling module is used to set up B-cell cultures in typically hundreds of 96-well plates, and incubated at 37°C for 5-6 days. Primary screening using a no-wash fluorescence-cytometry assay (mirrorball, TTP Labtech) is then performed in order to identify binders in B-cell supernatant from cells expressing receptor or soluble protein. The hit-picking module consolidates the positive supernatant into master plates and also shifts B-cell culture plates into cryo-storage for future screening and B-cell retrieval. The arrows show the direction of plates during the selection and screening phases.

Immunising rabbits (*Oryctolagus cuniculus*) with syngeneic cell-line expressing PTH1R variants and screening for the PTH1R-loop binding antibodies using cells transiently expressing receptor variants circumvents the issue of receptor expression and purification while using an immunogen which presents the receptor in its native form. The overall workflow for the discovery of antibodies that bind to PTH1R ECL is shown in Figure 3-2.

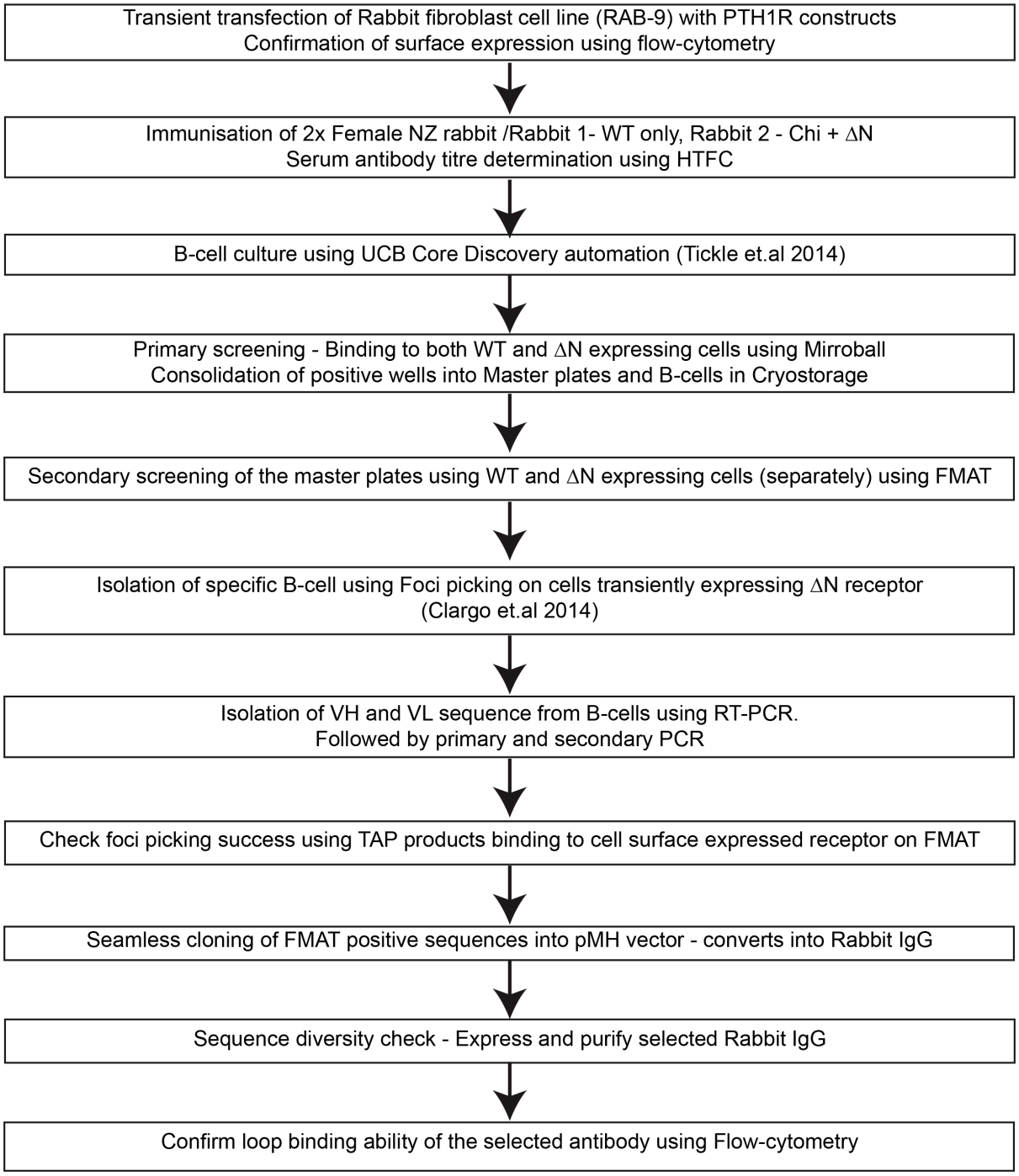


Figure 3-2: A brief overview of the work-flow for discovering loop-binding antibodies against PTH1R post immunisation.
All the steps are further expanded in this chapter.

Following immunisation and screening, we found one predominant family of mAbs, with the same CDR3 sequence. For one selected antibody, ECL-binding was confirmed using flow-cytometry.

3.2 Materials and Methods

3.2.3 Materials

All consumables were purchased from Sigma Aldrich (UK) and ThermoFisher Scientific (UK), unless otherwise stated

3.2.4 PTH1R construct generation

The synthetic gene encoding the full-length wild-type sequence of PTH1R (M1 – M593 referred to as WT hereon) was sourced from Atum (California, USA) with no codon optimisation (see Table 2-1). A silent mutation was introduced at position 534 (ACT → ACC) which introduced an *Xma* I site into the region encoding the junction between the ECD and transmembrane domain 1 (TM1). The insert was sub-cloned into the mammalian expression vector, pMH (see Table 2-1) between *Hind* III and *EcoR* I site using standard molecular biology techniques.

The rabbit-human chimera (Chi) construct encodes a chimeric receptor which contains the N-terminal ECD of rabbit PTH1R (M1 - E177, based on Uniprot accession number G1T397) followed by the human TM domains. The gene encoding the rabbit ECD was sourced from Atum (USA) with 5' *Hind* III and 3' *Xma* I site and ligated into pre-digested pMH-WT vector using T4 DNA ligase.

The ECD-truncated construct (∆N) was generated from the plasmid containing the WT sequence, using a PCR method as described previously (Hansson *et al.*, 2008). Briefly, two primers, Fwd_OE and Rev_OE with complementary overhangs, were used to perform the overlap extension PCR on pMH-WT plasmid. The Fwd_OE primer annealed at the start of TM1 (TRER…) with overhangs complementary to the signal peptide (…SAYALV), whereas the Rev_OE primer (Table 3-1) annealed to the signal peptide with overhangs complementary to the start of TM1 sequence (as shown Figure 3-3). *DpnI* was added to the final PCR product to digest the template plasmid DNA prior to transformation into chemically competent *E. coli* cells. Plasmid DNA from individual clones was sequenced and prepared in large-scale using a Giga-prep kit (Qiagen).

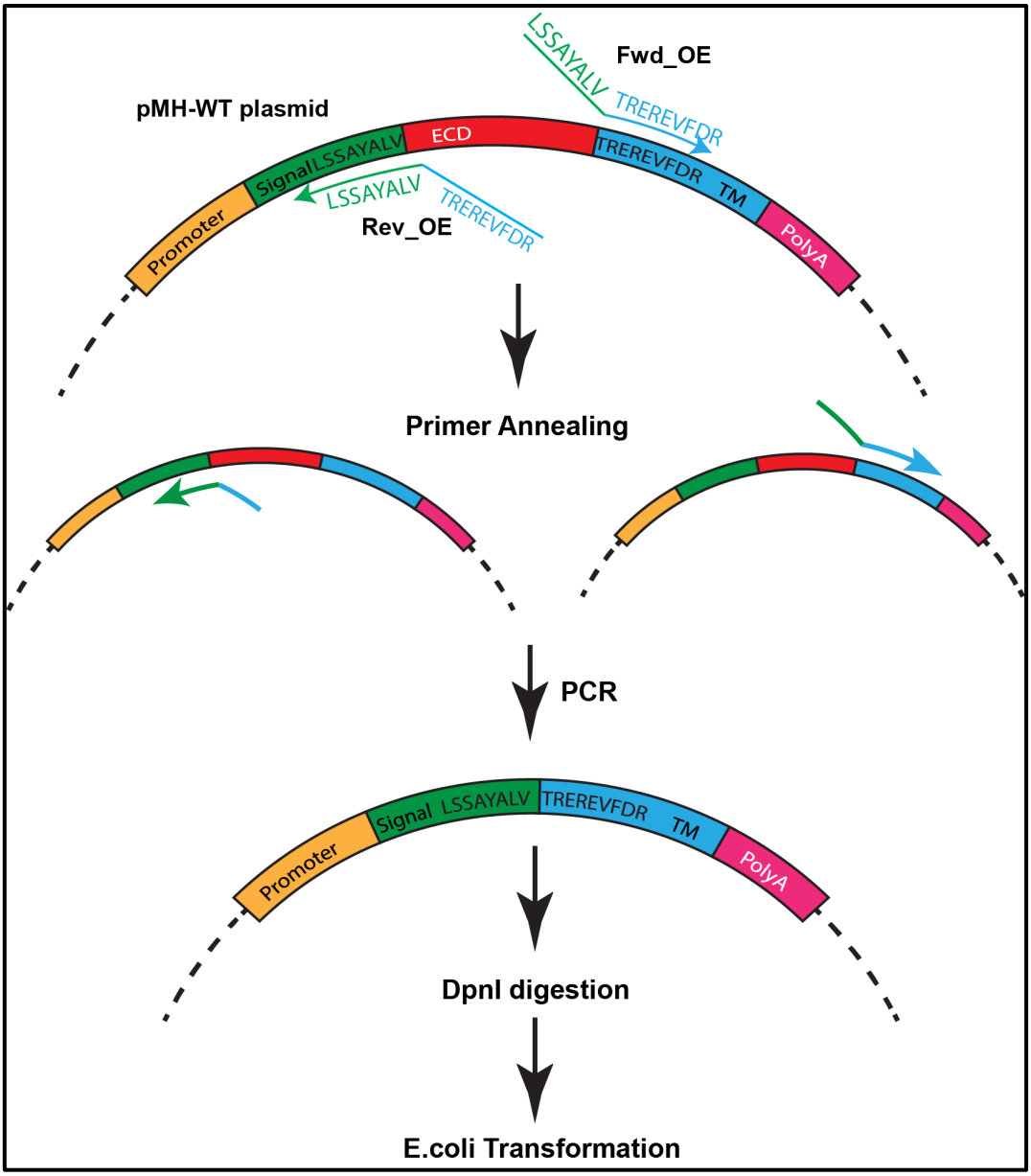


Figure 3-3: PCR-mediated deletion of PTH1R extra-cellular domain (ECD).

The ECD of PTH1R was deleted by performing overlap extension PCR on plasmid encoding the WT receptor (pMH-WT). Two separate primers were designed to bind to the either side of the ECD with complementary overhangs as shown in the figure (Rev_OE and Fwd_OE). The PCR reaction deletes the ECD and the complementary overhangs anneal to form the ΔN version of PTH1R.

Table 3-1: Primer sequences used for ECD deletion.

Primer Name	Sequence (5' → 3')
Rev_OE	GGGGCGGTCAAACACCTCCCGTTCCCGGGTCACCAGCGCGTACGCGGAGCTGAG
Fwd_OE	GGGGCTCAGCTCCGCGTACGCGCTGGTGACCCGGGAACGGGAGGTGTTTGACCG

In all cases, the final plasmid was eluted in EB buffer (0.1 M Tris, pH 8) and the concentration determined using a Nanodrop spectrophotometer (ThermoFisher Scientific). The sequence of the final plasmid preparations was confirmed using DNA sequencing.

3.2.5 Rabbit fibroblast transfection and surface expression analysis using flow cytometry

A Rabbit skin-derived fibroblast cell-line, RAB-9 (ATCC CRL-1414) was transfected with the immunogen constructs (WT, ΔN and Chi) using electroporation. For each transfection, 600 µl of the cell suspension was mixed with the plasmid DNA at a final concentration of 250 µg/ml and placed in a Gene Pulser® Electroporation Cuvette with a 0.4 cm gap (Bio Rad). The cell suspension was pulsed with a current of 5.8-6 mA for 20 mSec. The input current was adjusted to maintain a voltage of 160-180 volts/pulse. The electroporated cells were immediately transferred into 30 ml warm RAB-9 media and transferred to a sterile T175 flask. The stock cells were plated in a CellSTACK-5 chamber tissue culture flask (Corning) with warm RAB-9 media (RPMI media supplemented with 10% Foetal Bovine Serum and 0.5% Glutamine) at a density such that the confluency reached ~70-80% on the day of transfection. The transfected cells were incubated at 37°C with 5% CO_2 in a humidified atmosphere for 24 hours. To harvest the cells, the media was removed and the cells washed with 100 ml of sterile Dulbecco's PBS (ThermoFisher Scientific). The cells were detached using 100 ml of Accutase cell-dissociation reagent (ThermoFisher Scientific) and incubation for ~10-15 min in a 37°C incubator. The detached cells were harvested at 300 x g for 10 min and re-suspended in Earle's balanced salt solution (Sigma) to a final cell density of 5 x 10^7 cells/ml.

For flow-cytometry analysis, a total of 5x10^5 cells were placed in a flow cytometry tube (Corning) and washed twice by centrifugation at 300 x g for 3 minutes with wash buffer (PBS supplemented with 5% FCS). To the washed cells, 1 µg of PTH-(1-34) labelled with Alexa Fluor 488 (referred to as PTH-AF488 hereafter) (Peptide Research) was added and the suspension incubated on ice for 1 h. The cells were washed twice and re-suspended in 300 µl of wash buffer. A BD FACS Canto with a 2-laser configuration was used to generate the

flow cytometry data. PTH-AF488-stained RAB-9 parental cells were used to set the FSC and SSC voltages, while stained PTH1R WT expressing cells were used to set the FITC voltage. The final data was exported in FCS file format and further data analysis was performed using Flow Jo V10 (FlowJo LLC).

For large-scale transfections to aid cell banking for immunisation, the above protocol was modified and each construct was plated in a CellSTACK 5-chamber tissue culture flask at a final cell-density of $1x10^8$ cells per flask. The transfected cells were harvested and an aliquot of $5x10^7$ cells frozen in FBS + 10% DMSO in screw-top cryovials. The cells were stored overnight at -80°C freezer following which they were stored in liquid nitrogen vapour until further use.

3.2.6 Rabbit immunisation

The immunisations were carried out in two Female New Zealand White (NZW) rabbits (>2 kg) using the RAB-9 cells transiently expressing the WT, Chi and ΔN constructs. The first rabbit was immunised with 4 shots of RAB-9 cells expressing the WT receptor, while the second rabbit was immunised with 3 shots of the Chi construct and a final boost with the ΔN construct expressing cells. In each shot, approximately 10^8 cells were administered. In both cases, Complete Freund's adjuvant was used for the first shot only and administered at a site separate to that of the immunogen. Blood samples were taken from the ear 14 days after each dose and termination occurred 14 days after the final dose. The rabbits were anesthetised with isoflurane, terminal bleeds taken and the animals sacrificed using a Schedule 1 method in accordance with the Animals Scientific Procedures Act (ASPA). All animal works were performed by trained special facility unit (SFU) member. The approval for use of the animals for immunisation was provided through the UCB Pharma, UK Animal Welfare and Ethical Review Body (AWERB) and the license was granted by the UK Home Office.

3.2.6.1 Sera titre analysis

The immune response to the specific antigen was determined using a high throughput flow-cytometry assay (HTFC) on cells expressing the PTH1R variants and serum samples taken from the immunised animals at a 14-day time point following each immunisation. Expi293 cells were transiently transfected with the WT2, Chi and ΔN2 variants of PTH1R receptor as described previously (see Table 2-1) and incubated overnight. The transfected cells were harvested and washed twice with Flow buffer (Section 2.2.4.4), re-suspended at a density of 10^6 cells/ml in fresh Flow buffer and 50 µl of cell suspension added to each well of a 96-well plate. The serum samples from the immunised rabbits were diluted 50-fold in Flow buffer and a half-log dilution series then prepared. 35 µl of the diluted sera was added to the wells and the cells incubated on ice for 1 h. The cells were then washed twice with 100 µl of Flow buffer followed by centrifuging at 300 x g for 3 min. 35 µl of a goat anti-rabbit IgG Fc specific Fab_2 fragment conjugated to Alexa Fluor 647 (1: 1000), secondary antibody was added to each well. The plates were further incubated for 1 h on ice under dark conditions, washed twice with Flow buffer and the resulting cell pellet re-suspended in 20 µl of the Flow buffer. The HTFC analysis was done using an iQue (IntelliCyt, USA) with filters for 488 and 647 nm detection. Samples were aspirated for 4 seconds, and the plate was agitated after measuring 8 wells to maintain cell-suspension. The cells were gated according to their FSC and SSC profile. The final fluorescence data were exported and further analysed using Microsoft Excel and GraphPad Prism 6.

3.2.6.2 Spleen, lymph node and PBMC harvest

Single cell suspensions were prepared from the harvested organs (spleen, lymph nodes and PBMCs) of the immunised rabbits. To isolate cells from the spleen, the harvested spleen was transferred into warm RPMI media supplemented with 10% FCS and 1% glutamine. The spleen was chopped into smaller pieces and transferred into gentleMACS C tubes (Miltenyi Biotec) with 5 ml media, and homogenised using the gentleMACS dissociator. The cell suspension was strained through a disposable 70 µm cell strainer (BD Falcon) and

the filtrate centrifuged at 300 x g for 10 min. The cell pellet was then re-suspended in chilled FCS + 10% DMSO. 1 ml aliquots of the cell suspension were placed in each cryogenic tube and stored at -80°C overnight following which the tubes were stored in liquid nitrogen vapour till further use. Cells from the lymph nodes were harvested the same way.

To harvest the bone marrow, bones were excised at both ends following which the marrow was flushed out using a disposable syringe containing 5 ml warm RPMI media supplemented with 10% FCS and 1% glutamine. The cell suspension was then treated as described above for the splenocytes.

To isolate the lymphocytes from blood, blood samples from individual sacrificed animals were diluted 1:1 with sterile PBS and layered onto 15 ml of Lympholyte-Mammal cell separation media (Cedarlane) in 50 ml polypropylene tubes. The solution was centrifuged at 1500 x g for 15 min. The lymphocytes collect as a distinct layer between the Lympholyte-Mammal media and the supernatant. The lymphocyte fraction was carefully aspirated out using a sterile Pasteur pipette and washed with PBS by centrifugation at 300 x g for 10 min. The final cell pellet was frozen as described above for future use.

3.2.7 B-cell culture set up

All the cell culture work and reagent preparation were performed strictly under aseptic condition in a Class II sterile hood. The B-cell populations from each rabbit were cultured in one hundred separate 96-well plates. The plates were further subdivided based on the source of the B-cells. 40 plates were cultured with splenocytes, 30 with lymph node derived cells and 30 plates were seeded with PBMC derived cells. Approximately 4000 B-cells from spleen and 2000 cells from lymph nodes or PBMCs were used for culture set up in each well. The B-cell culture media (referred to as the B-cell media hereon) was prepared by supplementing RPMI 1640 media with 8.7% Foetal bovine serum (FBS) (Sigma), 17.3 mM HEPES (Sigma), 0.86% Penicillin-Streptomycin (Gibco Life Technologies), 3.5 mM L-Glutamine (Gibco Life Technologies), 0.17% Normocin (Invivogen) and 48 µM of 2-mercaptoethanol (ThermoFisher

Scientific). The medium was mixed thoroughly and filtered using a 0.22 µM vacuum filtration device and stored in a 37°C incubator until needed.

Preparation of EL4 cells: EL4 cells are a murine lymphoblast cell line, routinely added to B-cell culture to aid cell growth and antibody production. In this case, 5 x 10^4 EL4 cells (kind gift from Rebecca Munro, UCB) were added to each well of B cells. A total of 1.16 x 10^9 cells was aliquoted from the stock culture and centrifuged at 500 x g for 5 min and the cell pellet re-suspended in 40 ml of warm B-cell media (final cell density adjusted to 2.9 x 10^7 cells/ml). The cells were irradiated with 1.71 Gy/min of X-ray for 10.5 minutes, delivering a dose of ~18 Gy, to arrest any further cell growth and proliferation.

Preparation of B-cells: The frozen aliquots of B-cells were taken out of the liquid nitrogen Dewar flasks and immediately placed on dry ice. The cells were thawed briefly in a 37°C water bath and transferred to a sterile tube containing 10 ml of warm B-cell media. The cells were counted using Trypan blue staining in a haemocytometer. To set up the culture using UCB's core discovery automation (Tickle *et al.*, 2015), the B-cells were mixed with UCB's proprietary B-cell culture supplement (B-cell supplement) and inactivated EL-4 cells as summarised in Table 3-2

Table 3-2: A summary of components added for culturing B-cell using UCB's core discovery automation.

Immunogen[a]	B-cell Source	No. of plates[b]	Culture volume (mls)	Volume of EL4 cells (mls)	Vol. of B-cells (mls)	B-cell Supplement (mls)
RAB9 WT	Spleen	40	900	8	20.7	16
	Lymph Node	30	700	6	3	12
	PBMCs	30	700	6	9	12
RAB9 Chi/ΔN	Spleen	40	900	8	15	16
	Lymph Node	30	700	6	5	12
	PBMCs	30	700	6	10	12

[a] The construct used for immunogen, includes RAB-9 cells expressing WT, Chi or ΔN

[b] Total number of 96-well plates cultured for each immunogen-B-cell source combinations

The B-cell suspensions were added to 6 separate sterile polypropylene bottles and placed in a 37°C water bath with constant stirring. A total of 200 µl cell-suspension was added to each well of a 96-well plate and the plates were incubated in a 37°C incubator for 6 days before proceeding with primary screening. The proprietary automation software and a database system were used to barcode and track the plates during the incubation and screening stages.

3.2.8 Primary screening using fluorescence cytometry (Mirrorball)

The plates containing B-cell culture from the immunised rabbits were screened using fluorescence cytometry (mirrorball, TTP Labtech) (Tickle *et al.*, 2009). Expi293 cells transiently transfected with WT and ΔN constructs (as described previously in Table 2-1) were used to identify wells containing B-cell populations producing PTH1R-specific antibodies. The harvested cells were washed with wash buffer (PBS supplemented with 5% FBS), and re-suspended in wash buffer to give a final cell density of 2 x 10^5 cells/ml. DRAQ5 (Biostatus, UK) was added to the cell suspension to a final concentration of 1 µM and the cell suspensions incubated for 1h in the dark. FITC conjugated goat anti-rabbit Fc secondary antibody (Jackson Immunoresearch) (1: 5000) was then added. 20 µl of the cell suspension was added to each well of a 384-well plate giving a final cell density of ~2000 cells/well. 10 µl of B-cell culture supernatant was added using the UCB core automation, the plates incubated for 2 h at room temperature and then assessed for total fluorescence. The final fluorescence data from each well was uploaded to UCB's internal servers and analysed using Tibco Spotfire 6.5.

Based on the primary screening result, a picking list was prepared and this was used to consolidate the culture supernatant into 12 master plates (referred to as core master plates from hereon). The B-cells from the identified wells were mixed with freezing media (FBS supplemented with 10% DMSO) and stored in a -80°C freezer until further use.

3.2.9 Secondary screening using FMAT

A secondary assay using an FMAT was used to screen for binders that bound to Expi293 cells expressing either the WT or the ΔN construct. Parental Expi293 cells were used

as a control for non-specific binding. The cells were harvested following an overnight incubation and washed twice with FMAT buffer (PBS supplemented with 1% FBS). The cell density was adjusted to 3 x 10^5 cells/ml with FMAT buffer and 10 µl of cell suspension added separately to each well of a 384-well plate. 10 µl each of B-cell supernatant from the master plates and a goat anti-rabbit Fc-specific IgG conjugated to Alexa 647 secondary antibody (1: 1666) were added to each well. The plates were mixed well and briefly centrifuged (100 x g for 1 min), then incubated at room temperature for 1 h in the dark. The plates were read using an FMAT 8100 HTS system (Applied Biosystems) using a stacking robot. The FMAT data was analysed using FMAT software, and the blank-corrected fluorescence data was exported to Microsoft Excel for further analysis. Positive wells were visually checked to confirm cell surface binding of the expressed IgG, before collating the final list for Foci picking.

3.2.10 B-cell foci picking using cell expressing receptor

B-cell foci picking allows separation of the specific antibody producing B-cell from a large non-specific B-cell population (Clargo *et al.*, 2014).

Preparation of Expi293 cells transiently expressing ΔN: The Expi293 cell transfection with the ΔN construct was performed according to the protocol as described in section 2.2.2.. The cells were harvested after overnight incubation, centrifuged to remove the media, and the pellet was re-suspended in PBS supplemented with 5% FCS. The cells were fixed by adding 100 µl of fixative solution A (Fix and Perm permeabilization reagents, ThermoFisher Scientific) per 10^6 cells followed by incubation at room temperature for 15 min. The cells were washed twice and the final cell density was adjusted to 2 x 10^6 cells/ml using PBS/5%FCS.

Recovery of frozen B-cells: The B-cell culture plates were removed from -80°C storage and immediately transferred to dry ice. 200 µl of pre-warmed B-cell media was added to the well to allow rapid defrost of the cell pellet and the resulting suspension transferred into a sterile 1.5 ml microfuge tube. This was repeated 2-3 times until the frozen B-cell pellet was successfully transferred to the microfuge tube following which the cells were washed twice with B-cell media and re-suspended in 60 µl of B-cell media.

Foci droplet preparation: A clean microscope glass slide was siliconised using 25 µl of Sigmacote (Sigma Aldrich). To prepare the foci mix, 60 µl of B-cell suspension, 120 µl of fixed ΔN transfected Expi293 cells and 60 µl of goat anti-rabbit Fc-FITC secondary antibody (1: 300) were added. The suspension was mixed thoroughly and equally spaced droplets were applied to the siliconised glass slide. The droplets were covered with 5 ml of mineral oil (Sigma Aldrich) and the slides were incubated for 1 h at 37°C to allow antibody production and complex formation to occur.

Foci picking: The foci picking was done using a microscope (Olympus IX73) equipped with fluorescence detector and a micromanipulator (Eppendorf TransferMan 4R). The slides were placed under the microscope and the fluorescent foci were detected using the FITC channel and the specific B-cell identified using white light. The micromanipulator was equipped with a glass needle (40 µm internal diameter) (World Precision Instruments) filled with B-cell media and was used to aspirate individual B-cells. The cell was immediately transferred to a fresh sterile PCR tube and frozen by placing on dry-ice. The isolated B-cells were placed in a -80°C freezer till further use.

3.2.11 Primary, secondary and TAP PCR

Following B-cell isolation, three rounds of PCR were used to extract the genetic material encoding for the variable domains.

Reverse Transcription: The cDNA encoding the V_H and V_L fragments were generated by performing Reverse Transcriptase – Polymerase Chain Reaction (RT-PCR) on isolated B-cells. All the RT-PCR work was carried out in a designated laboratory to minimise any mRNA degradation or contamination. The RT-PCR was performed using the SuperScript IV (SSIV) Reverse Transcriptase system (ThermoFisher Scientific). A master mix for 100 reactions was prepared by adding 1 ml of DEPC water, 400 µl of 5x SuperScript IV buffer, 100 µl of DTT (100 mM), 100 µl of Oligo $d(T)_{20}$ (50 µM), 100 µl of 10% NP40, 100 µl of dNTP mix (10 mM each), 100 µl of ribonuclease inhibitor (40 U/µl) and 100 µl of SuperScript IV enzyme. The B-cells were taken out of the -80°C freezer and immediately placed on dry-ice. 20 µl of the

enzyme reagent master mix was added to the PCR tube containing the B-cells and mixed well. Using a PCR thermocycler, the tubes were incubated at 50°C for 10 min followed by 80°C for 10 min. The cDNA generated was immediately used for setting up primary PCR.

For each primary PCR reaction, 1 µl of the RT-PCR product, 10.5 µl of DEPC water, 12.5 µl of KOD Hotstart master mix, and 1 µl of UCB-proprietary primer mix were added to a new PCR tube. “KOD1” PCR program was used for amplifying the primary PCR product (PCR cycle details in supplementary section).

For the secondary PCR reaction, 1 µl of the primary PCR product was mixed with 9 µl of DEPC treated water, 12.5 µl of KOD Hotstart master mix, and 2.5 µl of UCB-proprietary primer mix containing heavy or kappa light chain specific oligonucleotides. “Rb2TAPH” and “Rb2TAPK” PCR program were used to amplify the heavy and kappa light chain secondary PCR products respectively (PCR cycle details in supplementary section).

The TAP fragments from secondary PCR fragments were generated by mixing, 4.5 µl of DEPC treated water, 12.5 µl of KOD Hotstart master mix, 2.5 µl each of UCB-proprietary primer mix (at 2.5 µM), 1 µl of purified CMV fragment (2.5 ng/ul) and 1 µl of purified constant domain fragment (heavy chain or kappa light chain). The secondary PCR product was diluted 10-fold with DEPC-treated water and 1 µl was added as template. “TAPOPT” PCR cycling program was used to generate the TAP product (PCR cycle details in supplementary section).

3.2.12 FMAT analysis of TAP products and selection of binders

The FMAT analysis using TAP fragments expressed in Expi293 cells was performed as described in section 2.2.4.3. Briefly, the TAP fragments generated from the selected B-cells were expressed in 1 ml Expi293 cultures for 5-6 days. The plates were centrifuged to remove the cells and 10 µl of the supernatant (undiluted, 1: 10 and 1: 100) was used to stain 10 µl of cells (~ 3000 cells) transiently expressing WT2 and ΔN2 receptor along with parental cells. 10 µl of a Goat anti-rabbit Fc Fab_2 conjugated to Alexa Fluor 647 secondary antibody (1: 1666) was added to the mix and the plates incubated for 1 h in dark before analysis using FMAT.

3.2.13 Sequencing and cloning of final hits

The V_H and V_L sequences were cloned into a mammalian expression vector using GeneArt seamless cloning (ThermoFisher Scientific). Briefly, the secondary PCR products (section 3.2.11) were separated on a 1% agarose gel and bands specific to V_H and V_L were excised out using the x-tracta gel extraction tool (Sigma Aldrich) and purified using gel purification kit (Qiagen).

For cloning the V_H fragment, 1 µl of a pre-linearized pMRbg1Fc vector (digested with *HindIII* and *XhoI*) was mixed with 1 µl of gel-purified secondary PCR fragment and 2 µl of GeneArt 2x enzyme mix. The mix was incubated at room temperature for 20 min, followed by 2-3 minutes incubation on ice. The ligated mixture was then used for transforming XL-1 Blue competent cells (Agilent Technologies). Similarly, for cloning V_L fragment, similar protocol was followed except pMRbCK vector was digested with Hind III and BsaWI and kappa light chain specific secondary PCR product was used as insert. Both vectors were derived from pMH (see supplementary section). The pMRbg1Fc vector was modified to encode the rabbit IgG heavy chain constant domain (C_{H1}, C_{H2} and C_{H3}) downstream of the XhoI site while pMRbCK was modified to encode for the rabbit (kappa) light chain constant (C_k) domain downstream of the BsaW I site. Isolated colonies were cultured and the plasmid DNA purified using mini-prep kit (Qiagen). The purified DNA was sequenced and aligned using AlignX to determine the sequence diversity among the selected clones.

3.2.14 Expression and purification of a selected rabbit IgG

The CoreAb1 rabbit IgG (referred to as CoreAb1 IgG) was expressed using the Expi293 expression system as described previously in section 2.2.2 and isolated using Protein A affinity purification. Briefly, 30 ml of the Expi293 supernatant was loaded on to a 5 ml HiTrap MabSelect SuRe Protein A column (GE Healthcare) at 1.5 ml/min using an ÄKTAxpress system (GE Healthcare). The column was washed with 3 CVs of the wash buffer (PBS, pH 7.4); following which the bound IgG was step-eluted with 5 CVs of the elution buffer (0.1 M sodium citrate pH 3.4) at a flow rate of 5 ml/min. The relevant fractions were pooled

and concentrated using a centrifugal filter with a 30 kDa molecular weight cut-off (MWCO) and buffer exchanged into PBS pH 7.4. The IgG molecule was tested for purity using SDS-PAGE.

3.2.15 Cell surface expressed PTH1R binding using flow-cytometry

Expi293 cells were transfected with the WT2 and ΔN2 constructs (Table 2-1) as described previously in section 2.2.2. Following transfection, the cells were harvested after overnight incubation and washed twice with Flow buffer (Section 2.2.4.4). The final cell density was adjusted to 10^6 cells/ml with Flow buffer and centrifuged at 300 x g for 2 min to pellet the cells. The Expi293 supernatant containing the CoreAb1 IgG (section 3.2.14) was diluted 10-fold with Flow buffer and 450 µl was added to the cells, mixed well and incubated on ice for 1 h. The cells were washed twice and 200 µl of a goat anti-rabbit IgG Fc-Alexa Fluor 647 secondary antibody (1: 200) (Jackson Immunoresearch) was added and incubated on ice for 1 h in dark conditions. The cells were washed twice and re-suspended in 1 ml of Flow buffer before analysis using a BD FACS canto Carousel equipped with 2-laser configuration. An Anti-FLAG tag antibody conjugated to Alexa Fluor 647 (ThermoFisher Scientific) was used to confirm the receptor surface expression. Both the WT2 and the ΔN2 constructs express an N-terminal FLAG tag as shown in Table 2-1.

The purified CoreAb1 IgG was used to stain a stable CHOK1 cell-line expressing full-length PTH1R receptor (DiscoveRx). Briefly, 10 µg of the purified antibody was added to 10^5 cells in Flow buffer and incubated for 1 h on ice. The cells were washed twice and 40 µl of a goat anti-rabbit IgG Fc - Alexa Fluor 647 secondary antibody (1: 200) was added and incubated on ice for 1 h in dark conditions. After washing the cells twice, the cell pellet was re-suspended in 500 µl of Flow buffer and the flow cytometry analysis was done using a BD FACS Canto carousel.

3.3 Results

3.3.1 Immunisation constructs

Three separate PTH1R constructs were designed to be used for immunising two separate rabbits. One rabbit was immunised with wild-type (WT) version of the receptor, whereas second rabbit was immunised with 3 shots of rabbit-human chimeric PTH1R and a booster shot of ECD-truncated ΔN receptor. The schematic representation of the constructs is shown below:

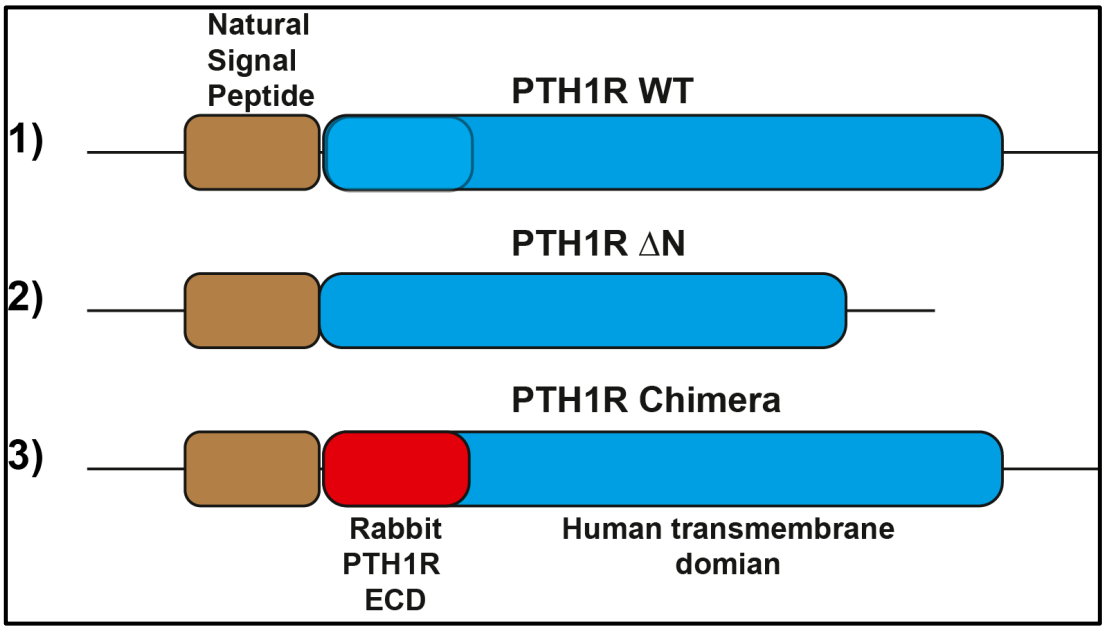


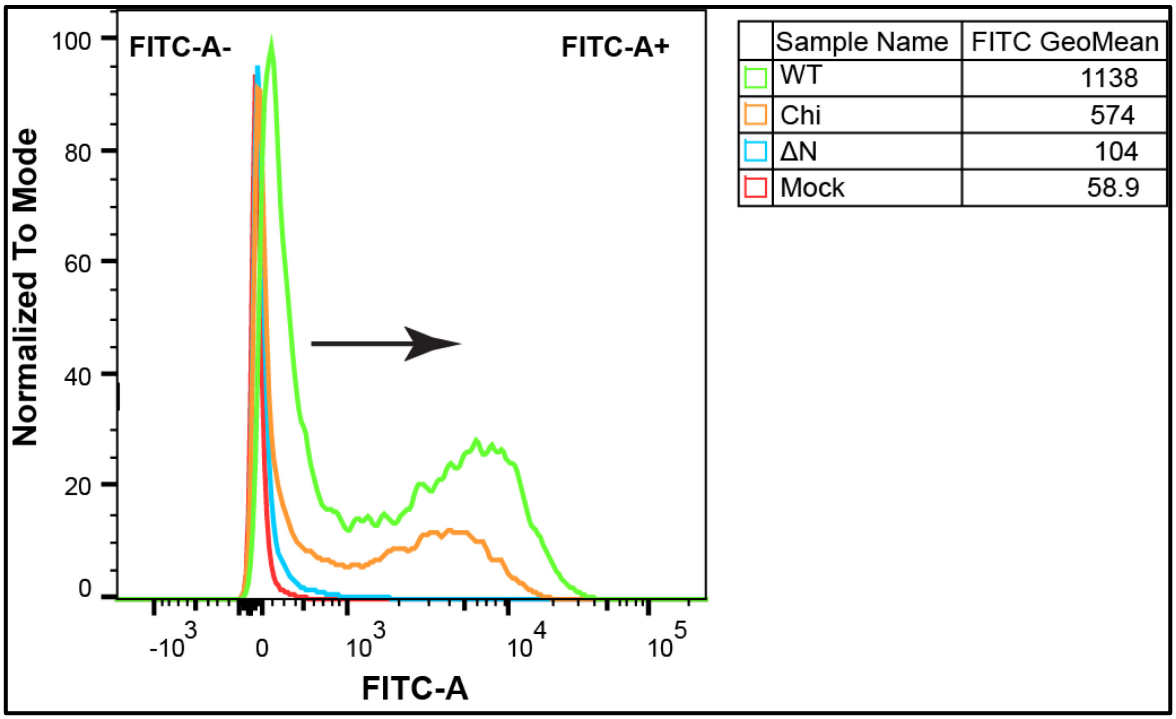
Figure 3-4: Schematic representation of three constructs used for rabbit immunisation

WT construct consisted of wild-type human PTH1R sequence (Uniprot ID: Q03431) without any sequence optimisation and naturally occurring signal peptide. For generating the ΔN construct, the extracellular N-terminal ECD was deleted. The Chi construct was a chimeric construct consisting of rabbit ECD followed by human transmembrane domain sequence.

The overall strategy with these construct and immunisation plan was to bias the rabbit immune response towards the extra-cellular loops. WT construct along with fully human ECD could elicit immune response, however the presence ECD could affect the availability of the ECLs. To further increase the chances of generating loop-binding mAbs, Chi construct was used followed by ΔN construct, where the lack of foreign ECD, could perhaps bias the immune response towards the ECLs.

3.3.2 Immunogen design and surface expression analysis

To aid immunisation, rabbit fibroblast cells (RAB-9) were transiently transfected with the WT, ΔN and Chi constructs of PTH1R and expression of some of the receptor variants was successfully detected using flow-cytometry (Figure 3-5). The WT and Chi construct expressing cells show an increase in fluorescence compared to parental cells confirming receptor expression and successful trafficking to the cell surface. It should be noted that the cells were stained with PTH-(1-34) conjugated to Alexa Fluor 488, which requires the ECD for successful binding (Pal, Melcher and Xu, 2012). The ΔN construct lacks the ECD essential for ligand binding and therefore no shift in fluorescence was detected for this construct (Figure 3-5, light blue trace).



	Sample Name	FITC GeoMean
	WT	1138
	Chi	574
	ΔN	104
	Mock	58.9

Figure 3-5: Flow-cytometry analysis of PTH1R cell surface expression in transiently transfected rabbit fibroblast cells.

The overlay shows the flow-cytometry analysis of Rab9 cells transfected with the WT (Green), Chi (orange), ΔN (light blue) and mock (red) constructs. The shift in overall fluorescence levels is shown by the arrow and the X-axis represents the geometric mean of fluorescence detected in the FITC channel. The table summarises the final geometric mean of the fluorescence detected.

The parental RAB-9 cells did not show any shift in fluorescence when stained with PTH-AF488 confirming specific binding of the detection reagent (Figure 3-5, red trace).

Successful binding of PTH-(1-34) confirmed surface expression of the functional WT and Chi receptor constructs.

3.3.3 Rabbit sera titre analysis confirms immune response to PTH1R

The serum samples from immunised rabbits were tested for PTH1R-specific antibodies using HTFC (Figure 3-6). The sera-titre analysis shows that the cell immunisation had elicited an immune response in both rabbits. The immune response from rabbit-1, immunised with WT receptor only, appears to be directed against the ECD as no significant binding was seen with cells expressing the ΔN receptor, even with bleed number 3 (Figure 3-6, C, bottom left plot). In contrast, the sera titre analysis for rabbit-2, immunised with both Chi and ΔN constructs, suggested the presence of antibodies against the extracellular loops (ECL), as evident from the high fluorescence signal detected with cells expressing the ΔN receptor (Figure 3-6, C, bottom right plot).

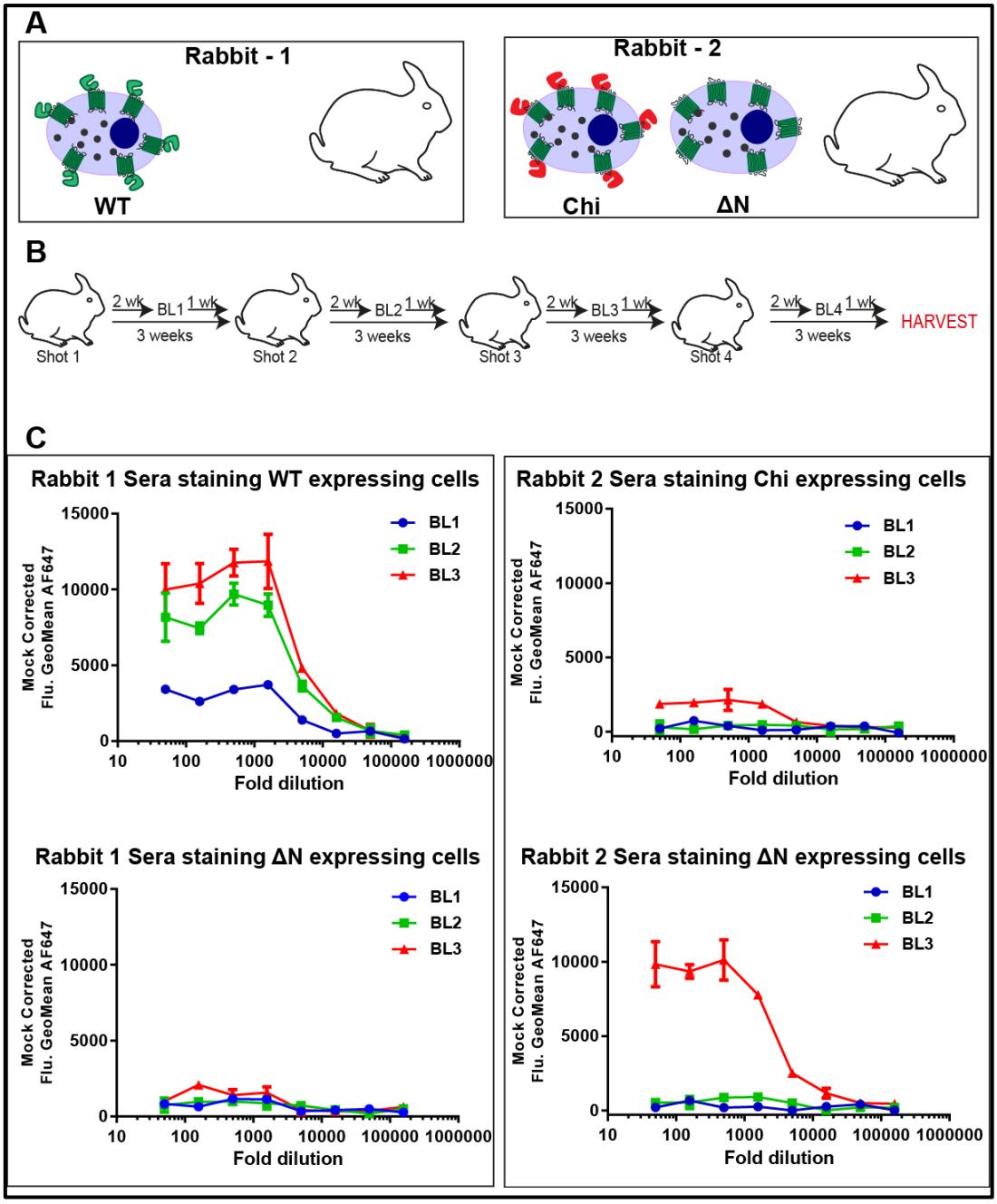


Figure 3-6: Rabbit immunisation with cells expressing PTH1R receptor and sera titre analysis.

A) One female rabbit was immunised with the WT constructs while the second rabbit was immunised with Chi and ΔN constructs. B) The bleed samples were taken two weeks after every shot and in total 4 shots were delivered subcutaneously. C) The sera-titre analysis using HTFC highlights the effect of different constructs. The two graphs on the left represent the sera-titre of rabbit-1 against the WT expressing cells (Top) and ΔN expressing cells (bottom), while the graphs on the right represent the immune response in rabbit 2 and binding to cells expressing Chi (top) and ΔN (bottom). Each data point for bleed 1 (BL1) represents n=1 while BL2 and BL3 represents n=2.

It is interesting to note that in rabbit-2, the immune response against the ECL increased significantly only after the third shot of Chi construct as no significant response was seen following the first two shots.

3.3.4 Primary screening to identify PTH1R-positive wells

Primary screening using the mirrorball® fluorescence cytometer (TTP Labtech) (England *et al.*, 2015; Colley *et al.*, 2018), which measures the cell surface binding using a homogenous no-wash fluorescence assay, shows that both the rabbits generated binders against the PTH1R expressing cells. In this assay, cells expressing antigens were incubated with B-cell culture supernatant, containing receptor-specific antibodies and a species-specific fluorophore-tagged secondary antibody. Upon antibody binding and complex formation, a fluorescence signal over the background is detected which determines the presence of antigen-specific B-cell population (Figure 3-7).

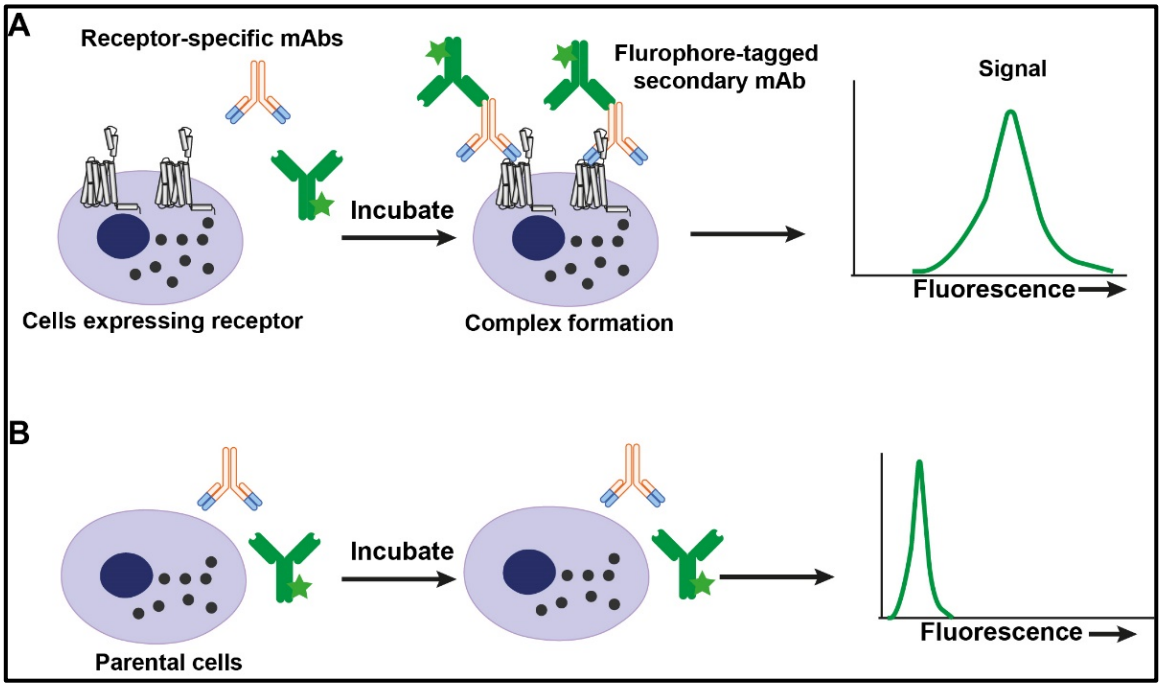


Figure 3-7: A schematic representation of mirroball fluorescence cytometry assay

A: Cells expressing receptor are incubated with receptor-specific mAb and a detection mAb. Following incubation, a higher fluorescence signal is detected due to immune complex formation whereas for control parental cells (B), only background signal is detected.

In this case, the primary screening was done with a mixture of cells expressing the WT and ΔN receptor respectively allowing screening of all PTH1R-sepcific B-cell populations irrespective of ECL or ECD-specificity. The B-cells from rabbit-2 PBMCs appeared to have slightly higher number of binders compared to the PBMC derived B-cells of rabbit 1 (Figure 3-8, A). Interestingly, a large proportion of the positive binders appeared to come from rabbit 2 derived lymph nodes and PBMCs (Figure 3-8, B).

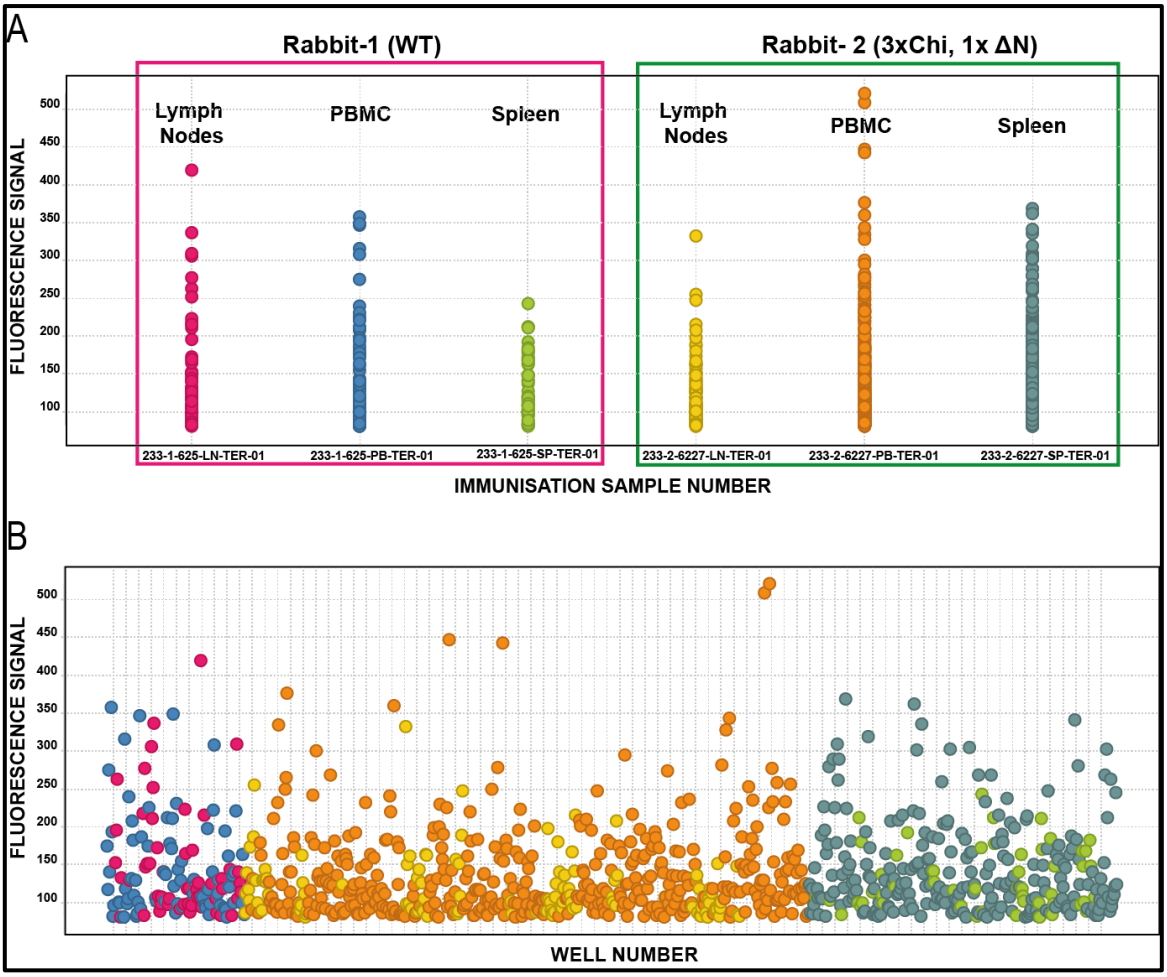


Figure 3-8: Primary screening of the cultured B-cells for cell-surface binding using Mirrorball.

A) Plot summarising the distribution of wells that gave a PTH1R-specific signal among the total culture wells from the two immunised rabbits. The plot also represents the level of signal from culture wells separated according to the B-cell source, where rabbit-1 lymph nodes and rabbit-2 PBMCs show the highest levels of signal. B) The overall distribution of all selected positive wells among the two immunised rabbits with a fluorescence signal cut-off of >81 and cell number cut-off of >1000.

To shortlist the binders and prepare the final 'picking' list, the primary screening data was further analysed by setting the minimum cell number per well to >1000 and a minimum fluorescence signal of >81. Based on the above conditions, 958 wells were found to be positive for PTH1R binding and used for preparing master plates. This gave a final hit rate of 4.98%.

3.3.5 Specific B-cell isolation using FMAT and fluorescent-foci picking

The B-cell culture supernatants for the 958 wells identified from the primary screening (section 3.3.4) were consolidated into master plates and further screened in a secondary assay using FMAT to confirm cell-surface binding (Figure 3-9). Only the B-cell culture supernatant were transferred into master plate wells for the secondary screening, whereas

the cells were frozen and stored for future use (foci picking). Positive wells were identified by both total fluorescence reading and checked visually. These analyses confirmed that a majority of the shortlisted IgGs could successfully bind to both the WT and ΔN constructs while no detectable signal was seen with parental cells (Figure 3-9, A). Unlike the primary screening, the FMAT assay was done separately using either WT or ΔN cells and only IgGs that could successfully bind to both the WT and ΔN cells (as shown in Figure 3-9, A) were taken forward.

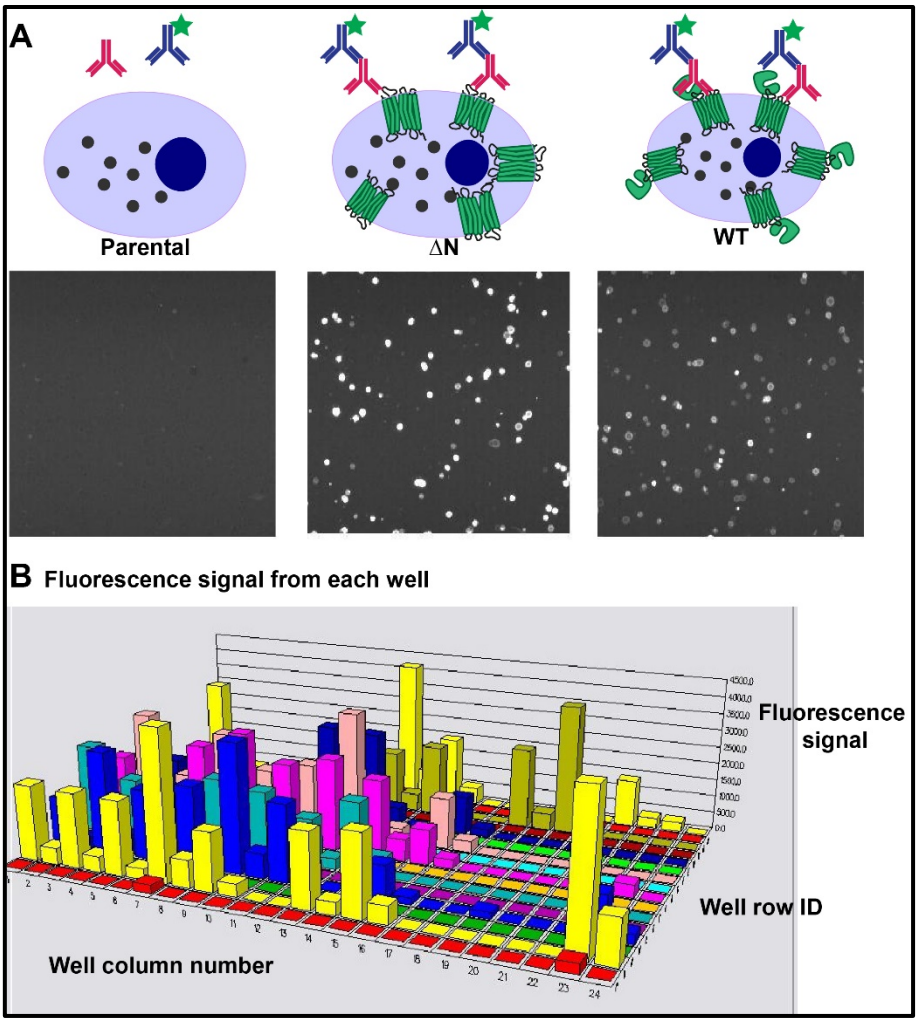


Figure 3-9: FMAT assay set up and final data for a selection of supernatants.

FMAT based binding assay allows screening for binders in a low-volume no wash assay. A) FMAT micrographs showing binding of expressed antibodies to ΔN (centre) and WT (right) constructs expressed on cell surface. While parental cells (left) show no detectable binding, both the WT and ΔN constructs show clear binding of expressed antibody on the cell surface. The binding is confirmed by a halo of fluorescence signal around the cells (white circle) which is not seen with parental cells B) A 3D plot summarising the overall fluorescence signal from each well. The positive wells were always confirmed visually by checking the micrographs (as shown in A)

Based on the well fluorescence measurement (as shown in Figure 3-9, B) and visual analysis of the FMAT data, a total of 30 wells were identified which exhibited binding to both

WT and ΔN cells over parental cells (Table 3-3). The B-cells from the corresponding culture plates were used for foci-picking.

Table 3-3: A table of consolidated positive hits from the FMAT assay.

S.No[1]	Master Plate Well[2]	FMAT Signal[3]		
		Mock	WT	ΔN
1	12F6	0	1346.3	3715.4
2	03H3	0	653.8	3579.7
3	07H4	0	997.7	3538.2
4	04D10	0	917.1	3467.1
5	08G3	0	701	3244.3
6	10C4	0	1079.4	3195.4
7	10D9	0	559.2	3134.1
8	02G3	0	1073.7	3099.1
9	11E8	0	600.5	3063.3
10	03A11	0	611	3052.6
11	07A11	0	536.5	3037.7
12	07G4	0	636.8	2995.1
13	07H3	0	793.6	2944.5
14	02A3	0	700	2915.5
15	12D10	0	609.6	2814.8
16	01C8	0	571.5	2802.5
17	07E4	0	679.7	2765
18	11B9	0	1057.3	2749.1
19	03A5	0	757.4	2711.1
20	05C11	0	650.5	2640.6
21	06C9	0	694.5	2633.1
22	04D9	0	828.7	2621.1
23	08G5	0	643	2565.7
24	03D3	0	618.6	2557.6
25	11A5	0	673.5	2533.8
26	05D12	0	632.7	2505.1
27	06F8	0	536.1	2468.3
28	08C12	0	596.5	2450.2
29	05G11	0	1034.3	2436.5
30	03C3	0	541.4	2431

[1] The sample number for foci-picking
[2] Master plate well identification number. First two digits represent master plate number and the letter and following number represents the well number
[3] Fluorescent data (RFU) from FMAT using parental, WT and ΔN expressing Expi293 cells

The ‘Foci picking’ method is schematically represented in Figure 3-10 and was used to isolate the specific B-cells responsible for PTH1R-specific antibody from a population of non-specific B-cells. The foci picking was performed on all 30 wells summarised in Table 3-3 and multiple clear foci could be detected for all wells (except the well corresponding to 03H3, which did not generate any clear foci) and a representative fluorescent-foci specific to PTH1R ECL is shown in Figure 3-10, B.

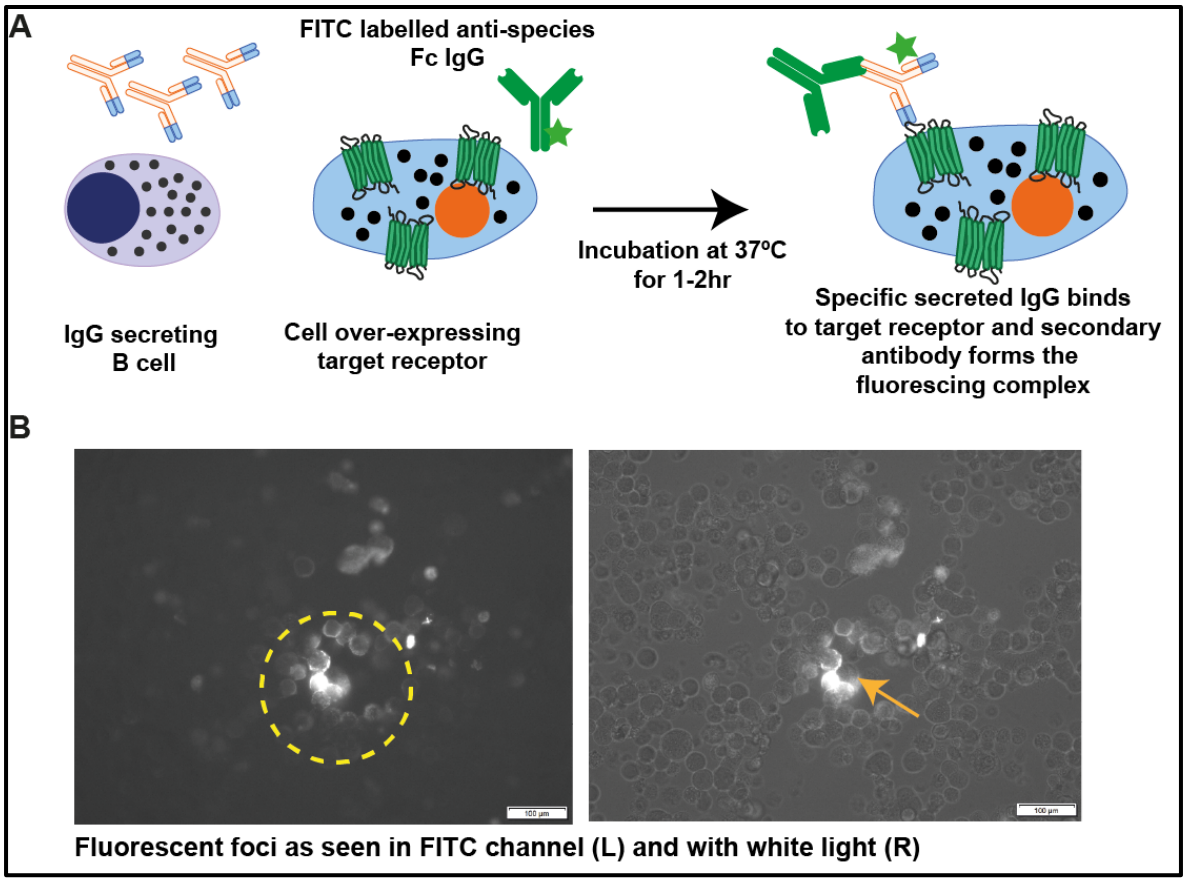


Figure 3-10: Foci picking using Expi293 cells expressing ΔN PTH1R constructs.

A) IgG secreting B-cells are incubated with both Expi293 cells expressing the ΔN construct and a FITC-labelled secondary antibody. The secreted antibody molecules bind to the receptors expressed on the cell, the FITC-labelled secondary antibody then binds to the primary antibody and creates a fluorescent halo around the specific B-cell. This cell is then aspirated using a micromanipulator. B) Representative foci visualised using the fluorescent channel (L) and white light (R). The fluorescent focus is indicated by the dashed yellow circle while the specific B-cell marked for aspiration is shown by the orange arrow. The scale bar in both images represents 100 µm.

At least 8 foci for each culture well (as shown in Figure 3-11, A) were isolated and the individual B-cells used to amplify the genes encoding the antibody heavy and light chains using PCR. Multiple foci are picked to maintain redundancy and account for any losses during B-cell isolation or PCR failures. Following PCR amplification, the PCR products are checked

on 1% agarose gels to confirm the fragment size. The agarose gel analysis confirms successful isolation of the B-cell and subsequent amplification of the antibody gene for majority of the foci picked (Figure 3-11, B). Some PCR reactions did not yield any product, likely due to unsuccessful isolation of B-cell during foci picking or lack of amplification of the genes encoding the light and heavy chains.

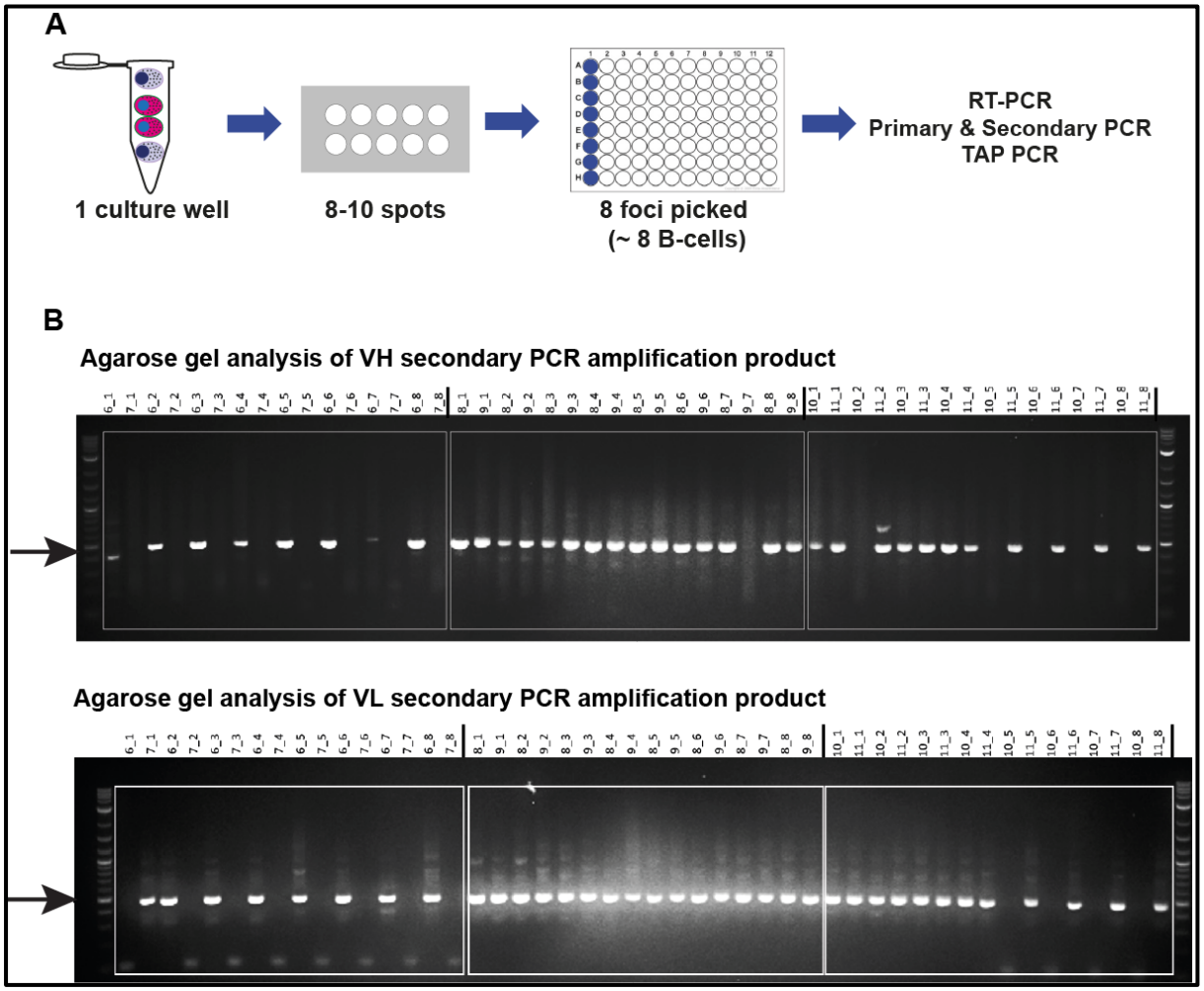


Figure 3-11: Foci picking strategy and agarose gel analysis of secondary PCR products

A) The culture well contains a mixed specific and non-specific B-cell population which was further mixed with ΔN expressing cells and the FITC-labelled secondary antibody. The mixture was placed as multiple drops (8-10) on a siliconised slide and at least 8 separate foci from each slide were picked. The picked B-cells were consolidated into 96-well plates as shown, before amplifying the heavy and light variable sequences using three rounds of PCR. B) Agarose gel analysis of the secondary PCR products shows the successful amplification of the heavy and light chain genes. The black arrow represents the expected size of the two fragments.

The successfully amplified genes were converted to TAP fragments which were used for small scale transient expression of TAP products. The TAP products were tested on FMAT to confirm antibody expression and cell surface binding. As multiple B-cells were picked from

each culture well, only the clone with the highest FMAT signal and a clear secondary PCR product band was taken forward for sequencing. The Figure 3-12 below shows a representative FMAT data analysis on clones from two separate master plates well and outlines the final clone selection strategy.

FMAT signals of TAP products binding to WT and ΔN expressing cells

Cells expressing WT

	12F6		03H3	
	1	2	3	4
A	0	0	0	0
B	0	0	0	0
C	1357	3005	0	0
D	977	0	0	0
E	1489	2644	0	0
F	1005	0	0	0
G	1245	2660	0	0
H	724	0	0	0
I	758	1880	0	0
J	679	0	0	0
K	1212	2979	0	0
L	1289	0	0	0
M	0	0	0	0
N	0	0	0	0
O	1135	3099	0	0
	739	0	0	0

Cells expressing ΔN

	12F6		03H3	
	1	2	3	4
A	0	0	0	0
B	0	0	0	0
C	2218	5333	0	0
D	4944	0	0	0
E	2364	5367	0	0
F	4877	0	0	0
G	2691	6323	0	0
H	3223	0	0	0
I	1814	5589	0	0
J	3372	0	0	0
K	1719	6590	0	0
L	5667	0	0	0
M	0	0	0	0
N	0	0	0	0
O	1927	5794	0	0
P	3618	0	0	0

Undiluted	1:10
1:100	Empty

Figure 3-12: Representative FMAT data using TAP products to confirm successful sequence isolation, antibody expression and cell-surface binding

The data summarises the total fluorescence (in arbitrary units) measured using FMAT from each well. Expi293 cells expressing WT (left) and ΔN (right) receptors were stained with culture supernatant containing antibodies as TAP fragments derived from B-cells picked from each focus. The supernatants were added undiluted, 1:10 and 1:100 diluted for each B-cell in one quadrant along with an unstained control. 12F6 and 03H3 represents the master plate number and well ID (also summarised in Table 3-4). While 6 out of 8 foci picked for 12F6 gave successful antibody sequences, none of the foci for 03H3 yielded an antibody gene. Positive fluorescence signal was detected with at least 1 or more TAP products except well ID: 03H3.

A total of 29 FMAT positive clones were individually cloned into the mammalian expression vector and sequenced to determine the diversity.

3.3.6 Low diversity – one predominant sequence family

Overall, the sequence diversity among the 29 selected clones was low and the isolated sequences appeared to be closely related. For the heavy chain, no diversity was seen in the CDR3 sequence although some amino acid differences were detected in both CDR1 and 2 (Figure 3-13). The kappa light chain, on the other hand, did not show any diversity in any of the CDR regions, although a few amino acid differences were detected in the framework residues (not shown) (Figure 3-13).

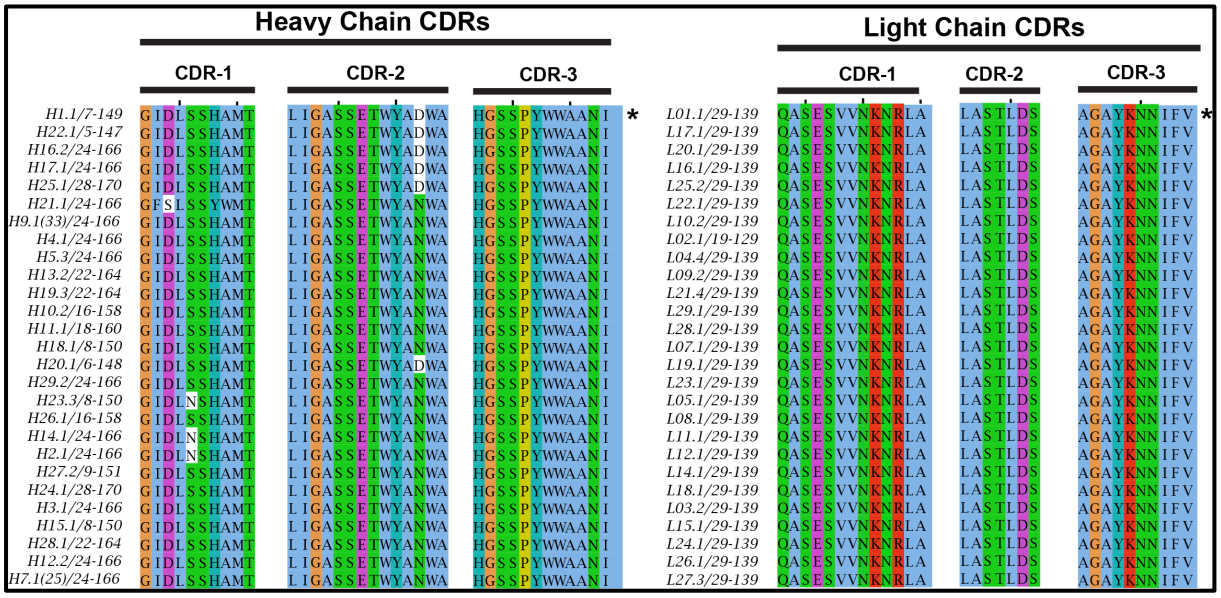


Figure 3-13: CDR sequence diversity among the selected clones

The sequence diversity in the CDR regions of the selected clones is shown. The sequence alignment was performed using T-Coffee (Notredame, Higgins and Heringa, 2000) in JalView (Waterhouse *et al.*, 2009) while the CDR assignment was done using MOE (CCG). The selected heavy and light chain sequence is shown by the asterix.

The V_H and V_L genes from H1.1 and L1.1 respectively were cloned into mammalian expression vectors for expression, cell surface receptor binding and purification.

3.3.7 CoreAb1 IgG was purified to homogeneity

The CoreAb1 IgG, comprised of the V_H and V_L genes from H1.1 and L1.1, was expressed using a mammalian expression system, affinity purified, and analysed using SDS-PAGE. The affinity purification was successfully achieved as summarised in Figure 3-14 and the final purified sample was found to be homogenous on an SDS-PAGE gel.

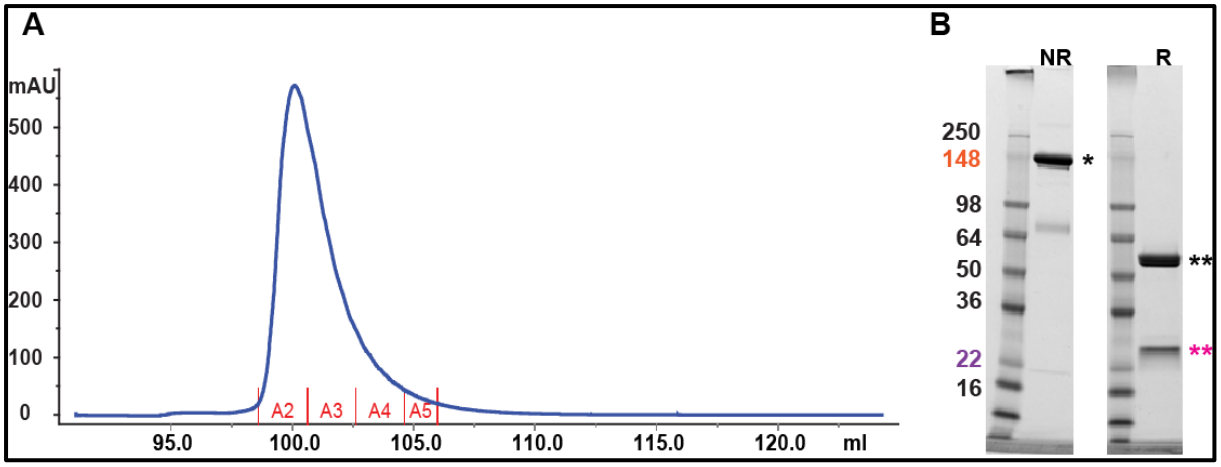


Figure 3-14: Protein A purification and SDS-PAGE gel analysis of CoreAb1 rabbit IgG.

A) Protein A mediated affinity purification of CoreAb1 IgG shows one main peak while the relevant fractions used for final pooling are indicated in red (A3-A5). B) SDS-PAGE analysis of the purified sample in non-reducing (NR) conditions show one major species migrating to ~150 kDa (shown by *) while under reducing (R) condition two separate bands corresponding to the heavy (**) and light chain (**) can be seen.

3.3.8 CoreAb1 IgG binds to the extracellular loop of PTH1R

Flow cytometry analysis using cells expressing PTH1R constructs and CoreAb1 IgG confirmed that the antibody could bind to PTH1R ECL with high specificity. Firstly, the supernatant containing CoreAb1 IgG was used to stain cells expressing WT and ΔN constructs and in both cases a clear shift in fluorescence signal was seen (Figure 3-15, A), indicating that the antibody binds to the ECL, and the presence of the ECD does not hinder binding. Next, the purified antibody was used to stain a CHOK-1 cell-line stably expressing the full-length receptor and this further confirmed the ability of the antibody to bind to the cell-surface expressed full-length PTH1R.

It should also be noted that the selected antibody did not exhibit any non-specific binding to either parental CHOK1 cells or Expi293 cells.

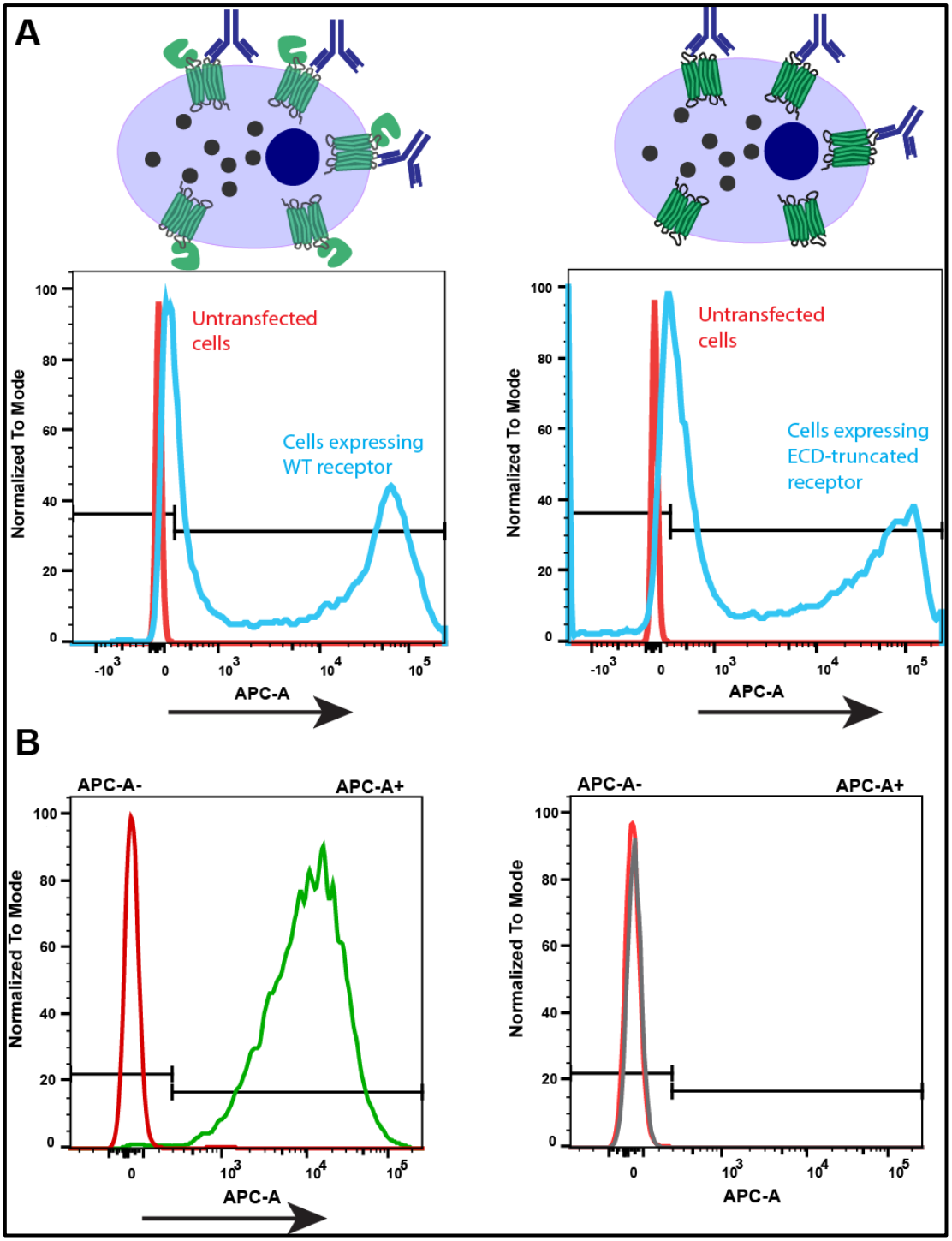


Figure 3-15: Flow cytometry analysis of CoreAb1 IgG

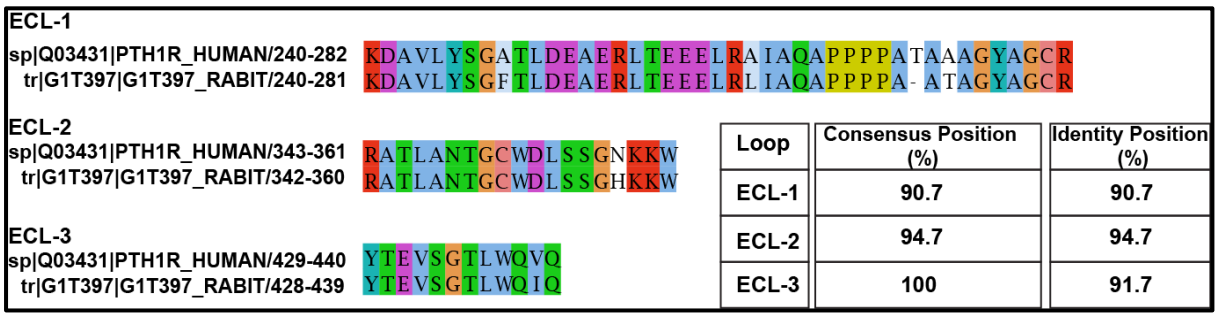
A) Expi293 cells transiently expressing WT (left) and ΔN (right) constructs stained with supernatant containing CoreAb1 IgG show that the antibody successfully binds to both the constructs (cyan trace) with no non-specific binding (shown by red traces). Binding to the ΔN constructs confirms that the antibody binds to the ECL. The shift in fluorescence is shown by the black arrowheads B) The purified antibody successfully binds to the full-length receptor expressed on a stable cell line (green trace) while exhibiting no non-specific binding to parental cells (red trace, left overlay). The secondary antibody exhibits high specificity and shows no non-specific interaction with PTH1R expressing cells (grey trace, right overlay)

3.4 Discussion

The extra-cellular loops (ECLs) of GPCRs are an attractive targets for mAb discovery since the ECLs, even within closely related GPCRs, tend to show high sequence diversity (Unal and Karnik, 2012; Venkatakrishnan *et al.*, 2013). In addition, it was shown that PTH1R ECL-1 plays an important role in ligand binding and function (Piserchio *et al.*, 2000). We were therefore keen to generate antibodies specific for PTH1R ECLs using immunisation and B-cell screening approach. This approach has been shown to be successful in generating functional antibodies against GPCR targets such as the formyl-peptide receptor 1 (FPR-1) (Douthwaite *et al.*, 2015).

While mice, rats or rabbits are widely used for immunisation, here we used rabbits. Rabbits are still a major source of mono and polyclonal antibodies against a large number of targets with broad utility (Weber, Peng and Rader, 2017). It is known that rabbits tend to elicit a stronger immune response to foreign antigens (Feng, Wang and Jin, 2011) and generate a larger panel of diverse antibodies against certain human antigens compared to murine systems (Rief *et al.*, 1998). We immunised rabbits with syngeneic cells, RAB-9, transiently expressing three separate constructs of PTH1R (see section 3.2.6). To improve the probability of generating loop-specific antibodies, we immunised one rabbit with the WT construct, while a second rabbit was immunised with a rabbit-human chimeric construct (Chi), where the ECD of human PTH1R was replaced with that from the rabbit receptor. The second rabbit also received a booster shot of ECD-truncated receptor, ΔN, to bias the immune response to generate ECL-specific antibodies. While the surface expression of the WT and Chi construct was detectable using PTH-(1-34)-AF488, we could not determine the surface expression of ΔN construct. Also, since the constructs were specific for immunisation we did not include any extraneous tags to aid detections and therefore it was not possible to check the surface expression of the ΔN constructs using techniques such as flow-cytometry or immunofluorescence microscopy.

From the sera-titre analysis we found that both rabbits elicited an immune response to the respective antigens, and as expected it appeared that the immune response in rabbit-2 was directed toward the ECLs. Large scale B-cell screening and isolation was performed using the UCB Core discovery platform. This method not only allows screening of a very large number of B-cells, but it also enables discovery of rare antibodies (Tickle *et al.*, 2015). Using the automation, we could culture ~56 million B-cells and screen more than 19,000 wells in under a week. In the absence of UCB Core automation, this process would have been very resource intensive. Inactivated EL4 cells were added to the B-culture acting as feeder cells. Such an approach has been shown to improve antibody expression from B-cells (UCB internal communication). Following primary screening a hit-rate of 5% was achieved. The hit rate represents the total percentage of positive wells for a specific antigen and usually a hit rate of <10% is desired as it has been shown to maintain clonality among the selected B-cell populations (Tickle *et al.*, 2009). Foci-picking is the most labour-intensive and hands-on approach used in the Core-discovery platform, and while at present it is the most appropriate method, other micro-fluidic based methods are being used for mAb screening (Adler *et al.*, 2017; Seah, Hu and Merten, 2018). The sequencing of the final clones revealed low sequence diversity, with one pre-dominant sequence family. One possible explanation for the low sequence diversity in discovered antibodies could be due to the high sequence identity between the human and rabbit PTH1R ECL sequence as shown below (see Figure 3-16).



Loop	Consensus Position (%)	Identity Position (%)
ECL-1	90.7	90.7
ECL-2	94.7	94.7
ECL-3	100	91.7

Figure 3-16: Alignment showing sequence diversity between human and rabbit PTH1R ECL sequence

Overall the sequence diversity between rabbit and human PTH1R ECL is low. ECL-1 appears to be one residue shorter in rabbit when compared to human ECL-1. Sequence alignment performed using T-Coffee in JalView and the percentage identity and consensus was calculated using AlignX (Invitrogen)

UCB Core discovery is routinely used against various soluble proteins and the overall success-rate for antibody discovery is target dependent. Previously, a modified protocol was used to generate mAbs against soluble IL-13, yielding 27 unique sequence families (Lightwood *et al.*, 2013). In contrast, here we could generate only one sequence family against the ECLs of a GPCR. This further highlights the challenges associated with generating mAbs against GPCRs, and particularly the extra-cellular loops. The lack of sequence diversity could be an issue if a series of functional antibodies were required, as in this case we appear to have only one sequence family. One strategy would be test other immunisation strategy, especially in an animal (e.g. mouse) with slightly higher sequence diversity at the loops. Nevertheless, the immunisation and screening process, which allowed us to thoroughly mine the immune repertoire, did deliver antibodies specific to the ECL.

One sequence was selected for characterisation and the rabbit monoclonal IgG, coreAb1, was expressed and purified. The loop binding capability of the purified antibody was further tested using flow-cytometry. The antibody could successfully bind to the ΔN expressing cells which confirmed that the isolated antibody was indeed a loop-specific antibody. It was also interesting to note that binding to the full-length receptor was unaffected which suggests that the presence of the ECD does not affect antibody binding. Previously, using MD simulation, HDX-MS and disulphide crosslinking studies it was shown that the GCGR receptor, a member of the secretin family, can adopt an open conformation when bound to mAb23, an ECD-specific antibody or the endogenous ligand. While in the absence of any ligand it adopts a closed conformation with the ECD making extensive contacts in the ECL (Yang *et al.*, 2015). It is interesting to note that CoreAb1, a loop-specific antibody is able to bind to the full-length PTH1R in the absence of PTH which could suggest that either PTH1R ECD does not make extensive contacts with the ECLs in the absence of PTH and therefore allows CoreAb1 binding to the loops or the overall ECD movement with respect to the TM bundle in PTH1R is different from GCGR.

To the best of our knowledge, this is the first report of a PTH1R antibody specifically targeting the extra-cellular loops. GPCR loop binding antibodies are rare compared to ECD-

binding antibodies mainly due to the fact that these antibodies require extensive screening and careful immunogen design. The only other loop binding antibody targeting a Class B GPCR was reported by Woning et.al in which the authors managed to isolate a loop binding functional antibody against GCGR using DNA immunisation (van der Woning *et al.*, 2016). It would be very interesting to see how CoreAb1 affects the confirmations of the full-length receptor and especially the ECD movement with respect to the TM bundle. This antibody could be a valuable tool for structural elucidation of PTH1R receptor.

In the following chapter we express and purify PTH1R constructs using different approaches and in chapter 5 we use the ECD-mAb (from Chapter 2) and ECL-mAb described here in a range of receptor function assays and in a number of biophysical studies in combination with the receptor.

Chapter 4: PTH1R over-expression, extraction using SMA and detergents

4. PTH1R over-expression, extraction using SMA and detergents

4.1 Introduction

As introduced in Chapter 1 (section1.4), large-scale extraction and purification of membrane proteins remains a challenge, in part due to their inherent flexibility but also due to the instability when extracted from the native membrane environment (McCusker *et al.*, 2008). In the last decade, major efforts by multiple groups have allowed successful over-expression and purification of GPCRs and other integral membrane proteins (Bertheleme, Chae, *et al.*, 2013; He, Wang and Yan, 2014; Lyons *et al.*, 2016). Protein engineering, through mutagenesis to reduce conformational flexibility (Magnani *et al.*, 2008; Serrano-Vega *et al.*, 2008; Shibata *et al.*, 2009), replacement of flexible portions of the receptor such as intracellular loop 3 (ICL3) (Rosenbaum *et al.*, 2007, 2011; V. Cherezov *et al.*, 2007), ICL2 (Hollenstein *et al.*, 2013; Doré *et al.*, 2014c) and the N-terminal domain (Rasmussen *et al.*, 2011; Zou, Weis and Kobilka, 2012) with a soluble, highly stable domain such as T4 lysozyme or BRIL (Thompson *et al.*, 2012; Liu *et al.*, 2012; Siu *et al.*, 2013; Wu *et al.*, 2014; Zhang *et al.*, 2014) has played a major role in the structural studies of GPCRs. While these approaches improve overall thermostability and allow successful expression, isolation and crystallogenesis, they also impact the overall function of the receptor resulting in a construct that does not represent the physiological form of the protein (Bertheleme, Singh, *et al.*, 2013).

With the exception of visual opsins, the endogenous expression levels of GPCRs are quite low and therefore a robust recombinant expression system is required for production. Along with the right construct, the expression system plays a key role in the final quality of the receptor produced. While established and inexpensive expression systems such as *E. coli* have been successfully used to over-express GPCRs for functional studies (Park, Bibhuti B Das, *et al.*, 2012; Egloff *et al.*, 2014), they lack eukaryotic post-translational modification systems (PTMs) such as glycosylation, have markedly different membrane lipid compositions and lack eukaryotic chaperone systems, all of which can affect the overall expression, folding and function of the receptor. GPCR expression using methylotrophic yeast *Pichia pastoris* has

also been successfully used for structural studies of the $A_{2A}R$ and the Histamine H2 receptor (Shimamura *et al.*, 2011; Hino *et al.*, 2012; Byrne, 2015). Yeasts are able to glycosylate proteins however the form of this differs from the native mammalian glycosylation pattern. In addition, the yeast membrane contains the sterol, ergosterol, rather than cholesterol found in mammalian cell membranes and critical for GPCR structure and function (Milić *et al.*, 2015).

Although yeast and *E. coli* represent very cost-effective systems for protein expression, mammalian cell derived expression systems such as Chinese hamster ovary (CHO) (Gamper, Stockand and Shapiro, 2005), Human embryonic kidney (HEK) (Graham *et al.*, 1977) and insect derived cells lines such as Sf9 (derived from *S.frugiperda*) (Vaughn *et al.*, 1977) and High Five (*Trichoplusia ni*) (Davis *et al.*, 1992) are also widely used for expressing mammalian proteins due to their ability to perform native /more native post-translational modifications. For expression of GPCR for structural studies, Sf9 appears to be the most successful expression system (Contreras-Gómez *et al.*, 2013; He, Wang and Yan, 2014) followed by HEK cells (Burg *et al.*, 2015; Hua *et al.*, 2016, 2017).

A key step in the isolation of integral membrane proteins is the process of extraction or solubilisation from the membrane fraction. Solubilisation is generally achieved using detergents which, like polar lipids, have a hydrophobic tail region and a polar head group. At a specific concentration, the critical micelle concentration (CMC) specific to an individual detergent, the detergent molecules self-associate into micelles where the hydrophobic tail region is buried in the core of the micelle and the head group is exposed on the micelle surface able to form interactions with the aqueous environment (Figure 4-1, A).

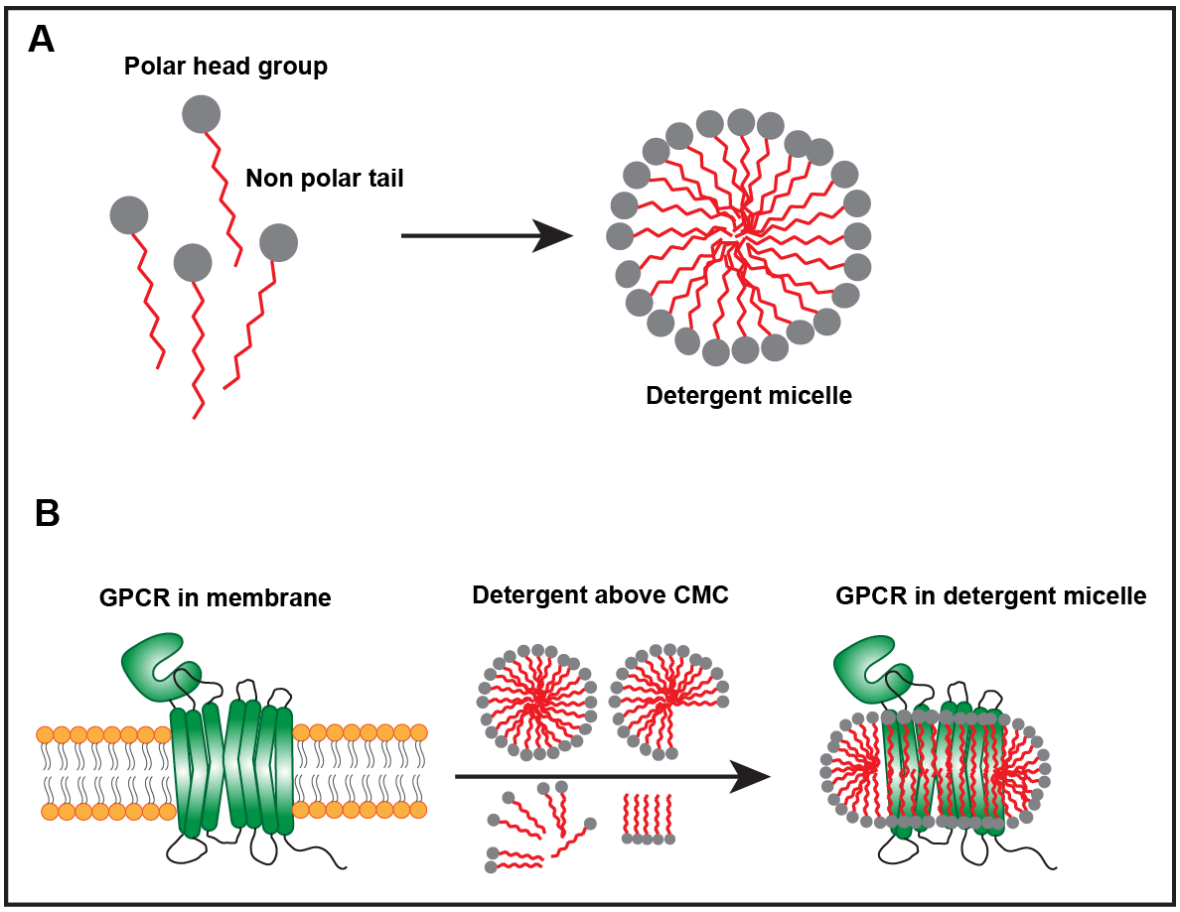


Figure 4-1: Detergent micelle formation and membrane protein solubilisation

A) Detergents consists of polar head group (grey circle) and hydrophobic tails (red lines) and at the critical micellar concentration (CMC) they form micelles. B) The native lipid environment of the GPCR is replaced by detergent micelles during solubilisation using detergents.

In this micellar form, detergents disrupt the interactions between the membrane protein and the membrane, effectively replacing the membrane lipids through the formation of protein-detergent complexes (Figure 4-1, B). If detergent conditions are suitable, the formation of these complexes maintains the structural integrity of the protein. Two of the most widely used detergents for GPCR studies include Dodecyl-β-D-Maltoside (DDM) (Grisshammer, 2009) and Lauryl Maltose Neopentyl Glycol (LMNG) (Chae *et al.*, 2010) generally in combination with Cholesterol Hemisuccinate (CHS). These detergents have enabled not only successful extraction but also promote crystallogenesis and have been used for solving structures of adenosine-2A (A_{2A}) (Jaakola *et al.*, 2008), β_2-adrenergic receptor (β_2AR) (Søren G F Rasmussen *et al.*, 2007), chemokine receptor 5 (CCR5) (Tan *et al.*, 2013), GPR40 (Srivastava *et al.*, 2014), muscarinic M2 (Kruse *et al.*, 2013), muscarinic M3 (Kruse *et al.*, 2012) and

NTSR1 (White *et al.*, 2012b) to name a few. Once solubilised the protein can be studied directly in the detergent micelle or reconstituted into nanodiscs (Denisov and Sligar, 2016) or amphipols (Tribet, Audebert and Popot, 1996). All of these approaches have been successfully applied to the study of GPCRs using techniques such as SPR, HDX-MS as well as functional analysis (Dahmane *et al.*, 2009; Chung *et al.*, 2011; Navratilova, Besnard and Hopkins, 2011; Mitra *et al.*, 2013; Bocquet *et al.*, 2015). Alternatively, membrane proteins can be solubilised using styrene maleic acid copolymer (SMA) which samples small discs of membrane encompassed by a ring of polymer (see Figure 1-20). The key advantage to this method is that the stability and functionality of the membrane protein is not compromised as it is maintained in contact with the membrane lipids at all times (Jamshad *et.al.*, 2011). This approach has been successfully used to purify and characterise the $A_{2A}R$ (Jamshad *et al.*, 2015) but has not been explored extensively for studying other GPCRs. The applicability of SMA in biophysical techniques such as SPR is also not yet well-validated.

This chapter describes efforts to express and purify wild-type (WT2) and truncated versions of PTH1R. The truncations were made at either the N (ΔN2) or C-terminal (ΔC29-491) end of the protein, or a combination of both (ΔNΔC171-491) (see Table 2-1 for construct details). Key aims were 1) to develop a suspension mammalian expression system amenable to easy scale-up or –down, 2) explore approaches such as SMA along with more established methods such as detergent solubilisation for membrane extraction. The overall work-plan is briefly summarised in Figure 4-2:

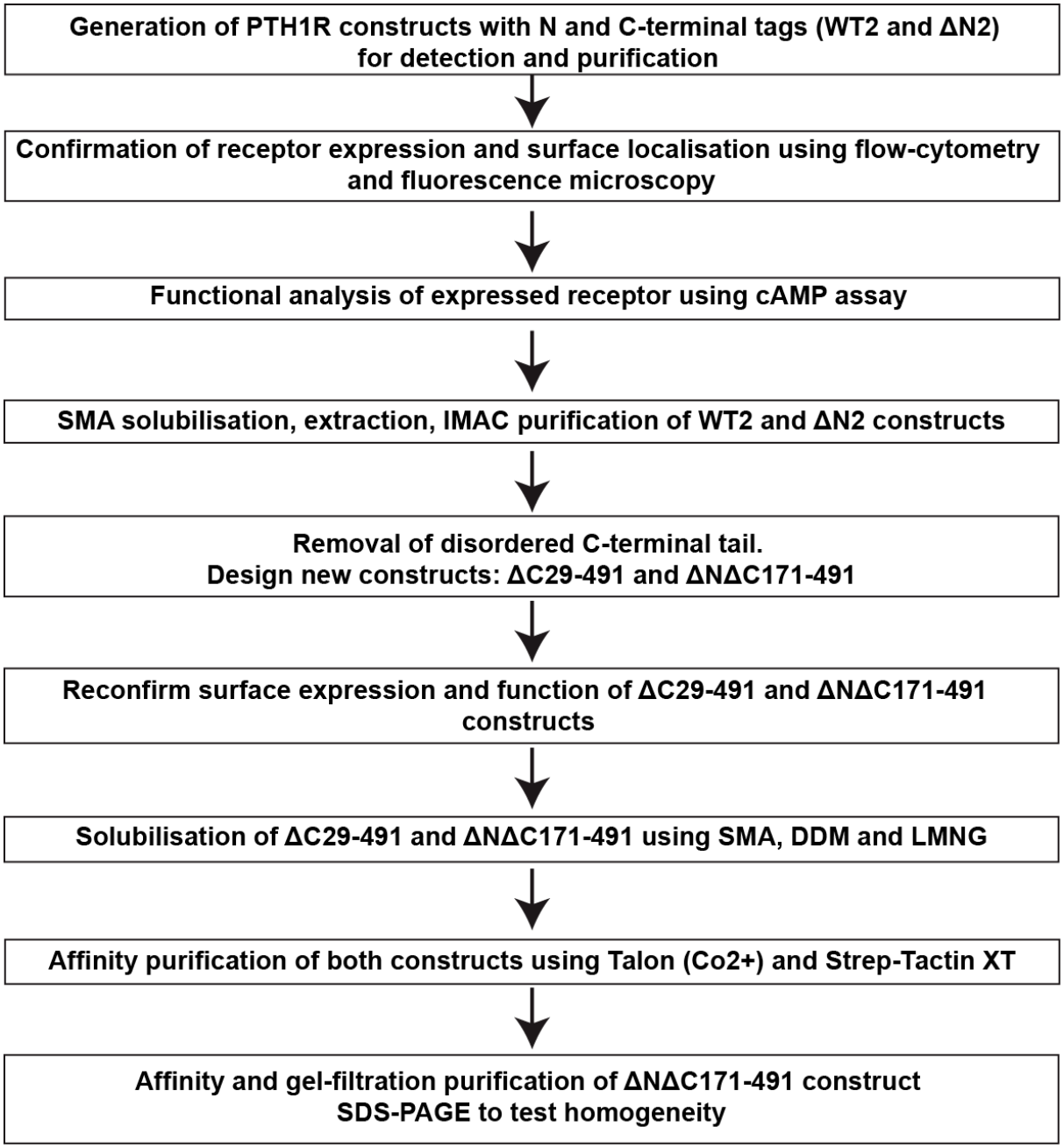


Figure 4-2: PTH1R expression, extraction and purification workflow.

A workflow highlighting the key experiments/ steps involved in PTH1R expression, extraction and purification using SMA and detergents. All the steps are further expanded in this chapter.

In summary, it was found that the WT2 receptor expressed and correctly localised to the cell surface in Expi293 cells but was prone to aggregation when extracted from the membrane environment. The C-terminal truncated constructs appeared to be more amenable to solubilisation using both SMA and detergents and the double truncated receptor (ΔNΔC171-491) construct was purified to high purity.

4.2 Materials and methods

4.2.1 PTH1R constructs for expression and purification

Various full-length and truncated versions of PTH1R were generated to enable over-expression and purification as detailed in Table 2-1. Briefly, the WT2 and ΔN2 constructs of PTH1R were generated using overlap extension PCR which mutated the naturally occurring *XhoI* site encoding L548-E549 (Uniprot accession number Q03431) while adding a 5' *BamHI* site (before nucleotide sequence encoding for D27) and a 3' *XhoI* site (following nucleotide sequence encoding for M593).

In the first PCR step, the DNA sequence encoding the N-terminal fragment (D27-E549) of WT2 was amplified using primers BamHI_Fwd1 and XhoI_mut_R. The DNA sequence encoding the N-terminal fragment of ΔN2 (T178 – E549) was generated using primers BamHI_Fwd2 and XhoI_mut_R. The nucleotide sequence encoding the C-terminal fragment (L548 – M593) for all the constructs was generated using primers XhoI_mut_F and XhoI_Rev using pMH-WT plasmid as the template.

In the second PCR step, 1 µl each of the respective N- and C-terminal fragments from the first step PCRs were combined and amplified using primers, BamHI_Fwd1, XhoI_Rev for WT2 while primers BamHI_Fwd2 and XhoI_Rev were used for ΔN2. The primer sequences are shown in Table 4-1and the overall PCR process is summarised in Figure 4-3 below:

Table 4-1: A summary of PCR primers used for overlap extension PCR

Primer name	Sequence (5' → 3')
BamHI_Fwd1	GCGCGGATCCGATGCAGATGACGTCATGAC
XhoI_mut_R	CAGGTGGTGTGGTCTCCAGGGTCTCCAGGGCTGG
BamHI_Fwd2	GCGCGGATCCACCCGGGAACGGGAGGTGTTTG
XhoI_mut_F	CCAGCCCTGGAGACCCTGGAGACCACACCACCTG
XhoI_Rev	GCGCCTCGAGCATGACTGTCTCCCACTCTTC

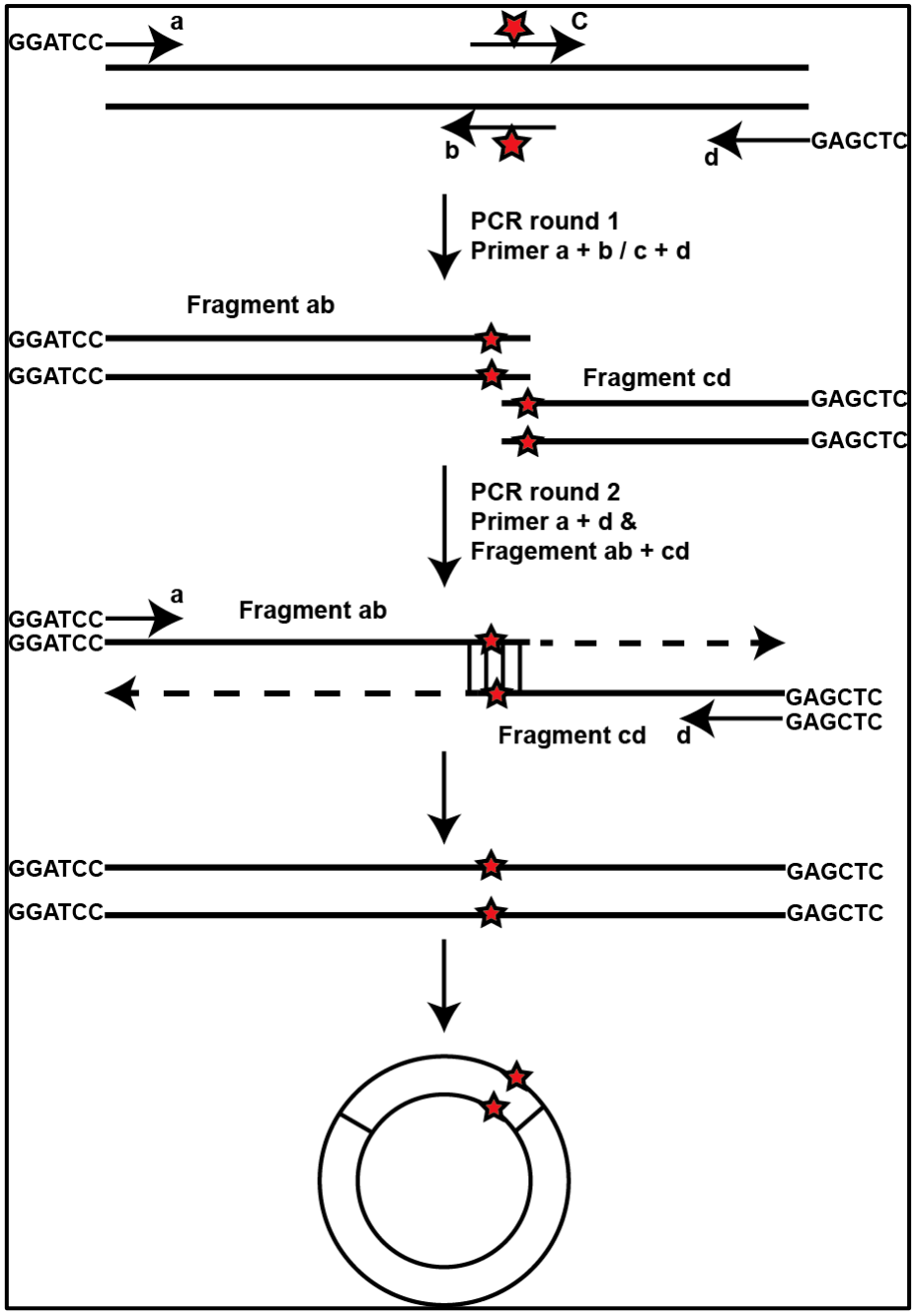


Figure 4-3: Overlap extension PCR coupled with site-directed mutagenesis to generate WT2 and ΔN2 constructs.

A two stage overlap PCR to remove the naturally occurring *XhoI* site (shown by red star), remove the natural signal peptide while adding 5'*BamHI* and 3'*XhoI* sites. In the first PCR reaction, the N-terminal (ab) and C-terminal fragments (cd) were generated and in the second PCR step the fragments were combined using pull-through primers (primer a and d). Figure adapted from (Heckman and Pease, 2007)

All PCR reactions contained 0.6 µl of primers (at 10 µM), 2 µl of template DNA, 10 µl of KOD Hotstart master mix (Millipore) and 6.8 µl of DEPC treated water. The purified PCR products were digested with *BamHI* and *XhoI* and ligated into complementary sites of the pSMA vector between the *BamHI* and *XhoI* site. The pSMA vector is derived from the pMH

vector and adds the Flag epitope tag at the N- terminus followed by the human rhinovirus (HRV) 3C protease site and a TEV cleavage site followed by an Avi-tag and a 10His tag at the C-terminus. The pSMA vector contains the signal sequence of influenza haemagglutinin (MKTIIALSYIFCLVFA) to aid receptor expression and trafficking (Guan, Tong Sun Kobilka and Kobilka, 1992).

To generate the WT1 construct, the WT construct was digested with *HindIII* and *XmaI* and the fragment sub cloned into the pSMA-WT2 plasmid between the *HindIII* and *XmaI* sites. The final expressed receptor contained the same C-terminal tags as WT2 while the N-terminus was untagged and retained the native signal peptide (MGTARIAPGLALLLCCPVLSSAYALV).

To generate the ΔC29-491 and ΔNΔC171-491 constructs, synthetic genes encoding ΔC29-491 (D29 - S491) and ΔNΔC171-491 (V171 - S491) were synthesised (Atum, USA) and sub-cloned into the vector, pStrep using *BamHI* and *XhoI*. The pStrep vector is a pMH derived vector, modified to introduce a TEV-protease cleavable twin-Strep Tag at the N-terminus, and a TEV cleavable 10-His tag at the C-terminus. A schematic representation of all the constructs mentioned above is shown in Table 2-1.

4.2.2 Over-expression using suspension cell line (Expi293)

Expi293 cells were used for all receptor expression work following the protocol described in section 2.2.2.2 with adjustments to reagent volumes based on the overall culture volume. Transfected cells were incubated for either 48 h or 72 h at which point they were harvested for receptor expression analysis or membrane preparation.

4.2.3 Surface expression analysis using flow cytometry and fluorescence microscopy

Expi293 cells transfected with various PTH1R constructs were incubated for 48-72 h at 37°C with 8% CO_2 under humidified atmosphere. The cells were harvested and washed twice with Flow buffer (see section 2.2.4.4) and 10^6 cells were stained with either 1 µg of PTH (1-34) labelled with Alexa Fluor 488 (PTH-488) or 1 µg of anti-FLAG antibody-labelled with DyLight 650. The cells were incubated for 1 h on ice in dark conditions and then washed twice

with Flow buffer. The washed cell pellet was re-suspended in 500 µl of Flow buffer and analysed using a flow-cytometer (BD FACS Canto Carousel), with the flow rate set to medium and 10-20,000 events collected for every sample. The raw data was exported and further analysed using Flow Jo V10.

For immunofluorescence microscopy, cells stained for flow cytometry (as described above) were used without any further treatment. In some cases, Hoechst 33342 (ThermoFisher Scientific) was used to stain the nucleus. 500 µl of the stained cells were placed in a µ-Slide 4 Well (iBidi) and incubated for 30 minutes at room temperature. Cells were imaged using a Leica SP15 microscope equipped with a Helium-Neon laser (power set to 30%) and all data analysis performed using NIH ImageJ software.

4.2.4 Functional characterisation using cAMP assay

Expi293 cells were transiently transfected with WT2, ΔN2, ΔC29-491 and ΔNΔC171-491 constructs as described previously (Table 2-1) and harvested after overnight incubation at 37°C. The cells were centrifuged at 300 x g and the supernatant discarded. The pellet was re-suspended in cAMP assay buffer (PBS supplemented with 1 mM IBMX) and the cell density was adjusted to 2 x 10^6 cells/ml. To perform the PTH-dose response analysis, 5 µl of the cell suspension was placed in each well of a 384-well white plate in quadruplicate. The PTH-(1-34) was re-suspended in PBS supplemented with 0.1% BSA to a final concentration of 2 µM and an 11 point, 5-fold serial dilution was prepared in a separate 96-well plate. 5 µl of each dilution was then added to the plated cells and incubated for 30 min at 37°C, followed by addition of 5 µl each of 1x cAMP-d2 and 1x Cryptate labelled-Anti-cAMP antibody to each well to allow immuno-competition to occur. The data analysis and the HTRF approach is described in detail in section 2.2.8.

4.2.5 Large scale PTH1R construct expression and membrane preparation

For preparing membranes, large scale (1-2 litre) Expi293 cell transfection was carried out using the protocols detailed previously (section 2.2.2.2). The transfected cells were harvested following 48 h incubation by centrifugation at 3000 x g for 10 min and the

supernatant discarded. The cell pellet was flash frozen in liquid nitrogen and stored at -80°C for future use.

To prepare the membrane fraction, the cell pellet was defrosted on ice and 40 ml of lysis buffer was added (25 mM HEPES pH7.2, 1 mM EDTA, 10 mM iodoacetamide and protease inhibitor cocktail (Roche)). The cell pellet was then re-suspended thoroughly in the lysis buffer and cells were homogenised by passing the slurry twice through a chilled cell-disrupter with the pressure set to 8 kpsi. The extent of homogenisation was checked using a light microscope. Unbroken cells and larger debris were removed by centrifuging the slurry at 9000 x g for 10 min at 4°C. To isolate membranes the supernatant was centrifuged at 190,000 x g for 90 min at 4°C in a Sorvall WX+ ultracentrifuge using a T865 rotor. The membrane pellet was collected and homogenised using a Potter-Elvehjem PTFE pestle and glass tube (45 ml, Sigma Aldrich) in high-salt wash buffer (25 mM HEPES pH 7.2, 10 mM iodoacetamide, 500 mM NaCl, protease inhibitor cocktail (Roche)). Following the high salt wash, the membrane suspension was again centrifuged at 190,000 x g for 1 h at 4°C. Pelleted membranes were then re-suspended using homogenisation in membrane storage buffer (MSB) (50 mM Tris pH 8.0, 150 mM NaCl, and 10% glycerol) at a final concentration of 80 mg/ml (by wet weight). The total protein concentration was determined using BCA assay (Pierce) and 5 ml aliquots of raw membrane were flash-frozen in liquid nitrogen and stored at -80°C for future use.

4.2.6 SMA extraction of PTH1R constructs from Expi293 membranes

Typically, 0.8-1 g of membrane was re-suspended in SMA solubilisation solution (50 mM Tris, pH 8.0, 150 mM NaCl, 10 % glycerol, and 2.5% w/v SMA polymer) to give a final membrane concentration of 30-40 mg/ml (by wet weight). To solubilise the membrane, the suspension was incubated for 1-2 h at room-temperature with slow-shaking. Insoluble material was removed by centrifuging the suspension at 190,000 x g for 1 h at 4°C, and the supernatant containing the solubilised receptor was collected and used immediately for purification. For these experiments two sources of SMA polymer were used: UCB-SMA, sourced from Cray

Valley UK and hydrolysed by chemists at UCB following published conditions (Lee *et al.*, 2016) and pre-hydrolysed SMA from University of Birmingham (kind gift from Prof. Mark Wheatley).

4.2.7 Detergent extraction of PTH1R constructs from Expi293 membranes

Lauryl-maltose neopentyl glycol (LMNG) (Anatrace) and n-dodecyl-β-D-maltopyranoside (DDM) (Anatrace) were used to solubilise the PTH1R constructs from Expi293 membranes. Membrane containing PTH1R protein, prepared as described in section 4.2.5, was solubilised by re-suspending in LMNG solubilisation buffer (50 mM Tris pH 8.0, 150 mM NaCl, 10% glycerol, 0.5% LMNG and 0.03% cholesterol hemisuccinate (CHS)) or DDM solubilisation buffer (50 mM Tris pH 8.0, 150 mM NaCl, 10% Glycerol, 1% DDM and 0.2% CHS) to give a final total protein concentration of 3-4 mg/ml (by BCA assay). In both cases, the suspension was incubated at 4°C for 3-4 h with gentle shaking. Insoluble material was removed by centrifugation at 190,000 x g for 1 h at 4°C and the resulting supernatant containing solubilised receptor was collected and immediately used for purification.

4.2.8 Affinity purification of solubilised receptor

4.2.8.1 IMAC purification using Ni-NTA and Talon

Typically, 0.8-1 gram of raw membrane was used for solubilisation and small-scale purification. The SMA or detergent solubilised receptor was purified using IMAC purification in batch mode. Briefly, 1 ml of Ni^{2+}-NTA resin (Qiagen) was washed with 20 column volumes (CVs) of MSB, added to the solubilised membrane preparation and incubated at 4°C overnight with gentle shaking. All further purification steps for the SMA solubilised receptor were performed at room temperature while detergent mediated purifications were carried out at 4°C or on ice. After overnight incubation, the Ni^{2+}-NTA beads were collected in an empty PD10 column and washed with 20 CVs of MSB and bound receptor was eluted using 4 CVs each of MSB supplemented with 10, 20, 40, 80 and 500 mM imidazole.

For Talon purification, the solubilised receptor was captured on 1 ml Talon resin (Clontech) as described above. The resin was filtered using an empty PD10 column and the

flow-through was collected. The resin was washed with 10 CVs of MSB supplemented with 150 mM NaCl (high-salt wash), 10 CVs of MSB supplemented with 5 mM imidazole (low-imidazole wash) and eluted with 10 CVs of MSB supplemented with 50 mM imidazole. The eluted fractions were analysed using SDS-PAGE and relevant fractions were pooled and concentrated using centrifugal-filtration devices with a 100 kDa MWCO filter (Millipore).

4.2.8.2 Strep-Tactin XT purification

The ΔC29-491 and ΔNΔC171-491 constructs were expressed with an N-terminal Twin-Strep tag® and purified using Strep-Tactin XT® resin (IBA). Typically, 1-2 grams of membrane was solubilised using DDM, LMNG or SMA as described above. The solubilised suspension was transferred to a 50 ml polypropylene tube and 1 ml of Strep-Tactin XT resin, washed with MSB, was added. The final NaCl concentration was adjusted to 300 mM and 1 mM EDTA was added to the suspension and incubated at 4°C overnight with gentle shaking. The resin was collected using an empty PD10 column and washed with 20 CVs of Strep Wash buffer (Table 4-2). To elute the protein, the resin was re-suspended in 5 CVs Strep elution buffer (Table 4-2) and incubated at 4°C with gentle shaking for 30-40 min. The eluate was collected and concentrated using filtration devices with a 100 kDa MWCO filter.

Table 4-2: Composition for wash and elution buffer used for Strep-Tactin XT purification

Solubilisation agent [a]	Step [b]	Buffer composition
SMA	Wash	50 mM Tris pH8.0, 300 mM NaCl, 1 mM EDTA and 10% glycerol
	Elution	50 mM Tris pH8.0, 150 mM NaCl, 1 mM EDTA, 50 mM Biotin and 10% glycerol
DDM	Wash	50 mM Tris pH8.0, 300 mM NaCl, 1 mM EDTA, 10% glycerol, 0.05% DDM and 0.02% CHS
	Elution	50 mM Tris pH8.0, 150 mM NaCl, 1 mM EDTA, 50 mM Biotin, 10% glycerol, 0.01% DDM and 0.02% CHS
LNMG	Wash	50 mM Tris pH8.0, 300 mM NaCl, 1 mM EDTA, 10% glycerol, 0.01% LMNG and 0.0006% CHS
	Elution	50 mM Tris pH8.0, 150 mM NaCl, 1 mM EDTA, 50 mM Biotin, 10% glycerol, 0.01% LMNG and 0.0006% CHS

[a] The reagent used for solubilisation of the membrane
[b] Denotes the purification step

4.2.9 Size exclusion chromatography (SEC) purification of Strep-Tactin XT® purified receptor

Using a HPLC (Agilent 1100, Agilent), affinity purified receptor (typically 100-300 µg) was injected onto a Superose 6 10/300 GL column (GE Healthcare), prequilibrated with 1.5 CVs of DDM running buffer (50 mM Tris pH 8.0, 150 mM NaCl, 0.05% DDM and 0.01% CHS) and eluted using 1.5 CV of DDM running buffer at a flow-rate of 0.3 ml/min. Fractions (500 µl) were collected based on absorbance at 280 nm and appropriate fractions were pooled and concentrated using an Amicon Ultra-0.5 (Millipore) with a 100 kDa MWCO filter. All purification and fraction collection steps were performed at 4°C, while the column was maintained at 8°C.

4.2.10 Characterisation using SDS-PAGE and analytical SEC chromatography

Purified receptor samples were analysed using SDS-PAGE and analytical SEC to determine homogeneity. For SDS-PAGE analysis, typically 3 µg of purified samples were mixed 1:1 with LDS sample loading buffer and separated on 4-20% Tris-glycine gels with a constant voltage of 225 V for 55 minutes. Samples were analysed under non-reducing (in presence of 10 mM N-ethyl maleimide (NEM)) and reducing (50 mM dithiothreitol (DTT)) conditions. Samples were also de-glycosylated under native conditions using PNGaseF (NEB, UK) following the manufacturer's protocol. For analytical SEC, ~25 µg of purified receptor was injected onto a Superose 6 16/300 GL column and separated as described in section 4.2.9.

4.3 Results

4.3.1 Full-length and ECD-truncated PTH1R shows successful surface expression and trafficking

Expression of WT2 and ΔN2 PTH1R constructs in Expi293 cells was analysed using flow-cytometry. The WT2 version of PTH1R has equivalent sequence as wild-type PTH1R (Uniprot accession number: Q03431) but includes extra detection and purification tags as shown in Figure 4-4 . The overall aim with the WT2 construct was to investigate if it was

possible to extract and purify wild-type PTH1R without any major modifications (insertion, deletion and mutations).

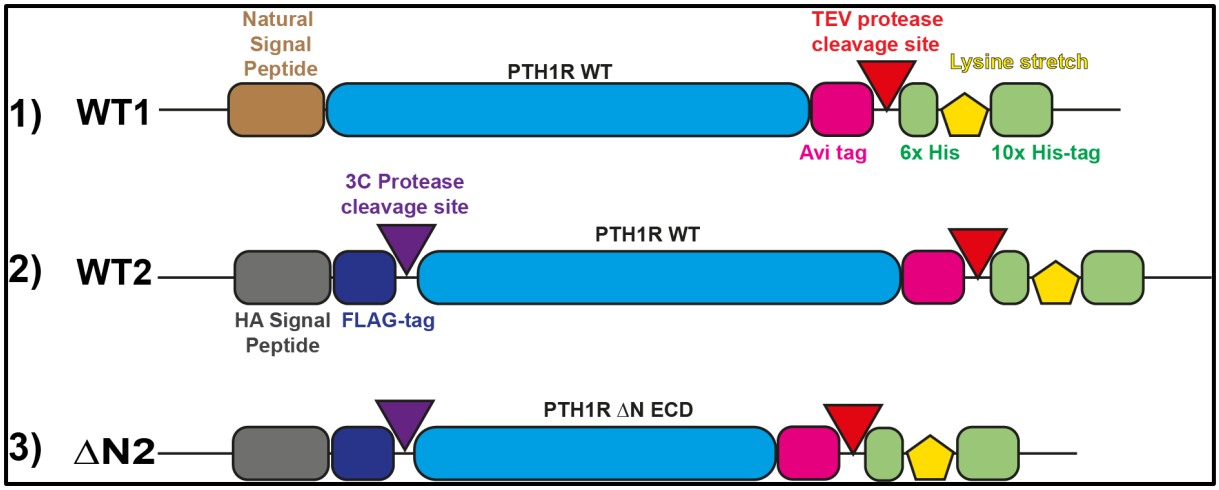


Figure 4-4: Schematic representation of WT1, 2 and ΔN2 constructs

The different signal peptide is highlighted in the figure above. The WT1 construct has same C-terminal tags but consisted of non-cleavable natural signal peptide. Whereas, both WT2 and ΔN2 contained HA signal peptide. The PTH1R sequence was unmodified in both WT1 and 2, while the ΔN2 construct did not contain the ECD.

It is also known that the presence of large flexible ECD can be detrimental for receptor extraction and purification, and therefore some of the x-ray crystallography derived structures of class B receptor were solved without of the ECD (Hollenstein *et al.*, 2013; Siu *et al.*, 2013). To address the issue of instability caused by ECD during PTH1R extraction and purification, the ΔN2 constructs was used in parallel to WT2 construct. The ΔN2 construct also contained only one glycosylation site and no disulphide bond, as opposed to 4 glycosylation sites and 3 disulphide bonds in WT2 construct.

Cells were stained with an anti-FLAG tag antibody and successful expression was confirmed by an increase in fluorescence (Figure 4-5). As expected, when staining with PTH-AF488, an increase in fluorescence was observed for cells transfected with WT2 PTH1R. The ΔN2 construct, which lacks the ECD, exhibited a very minor shift in fluorescence signal (Figure 4-5, B, left, orange trace), suggesting weak binding of PTH (1-34).

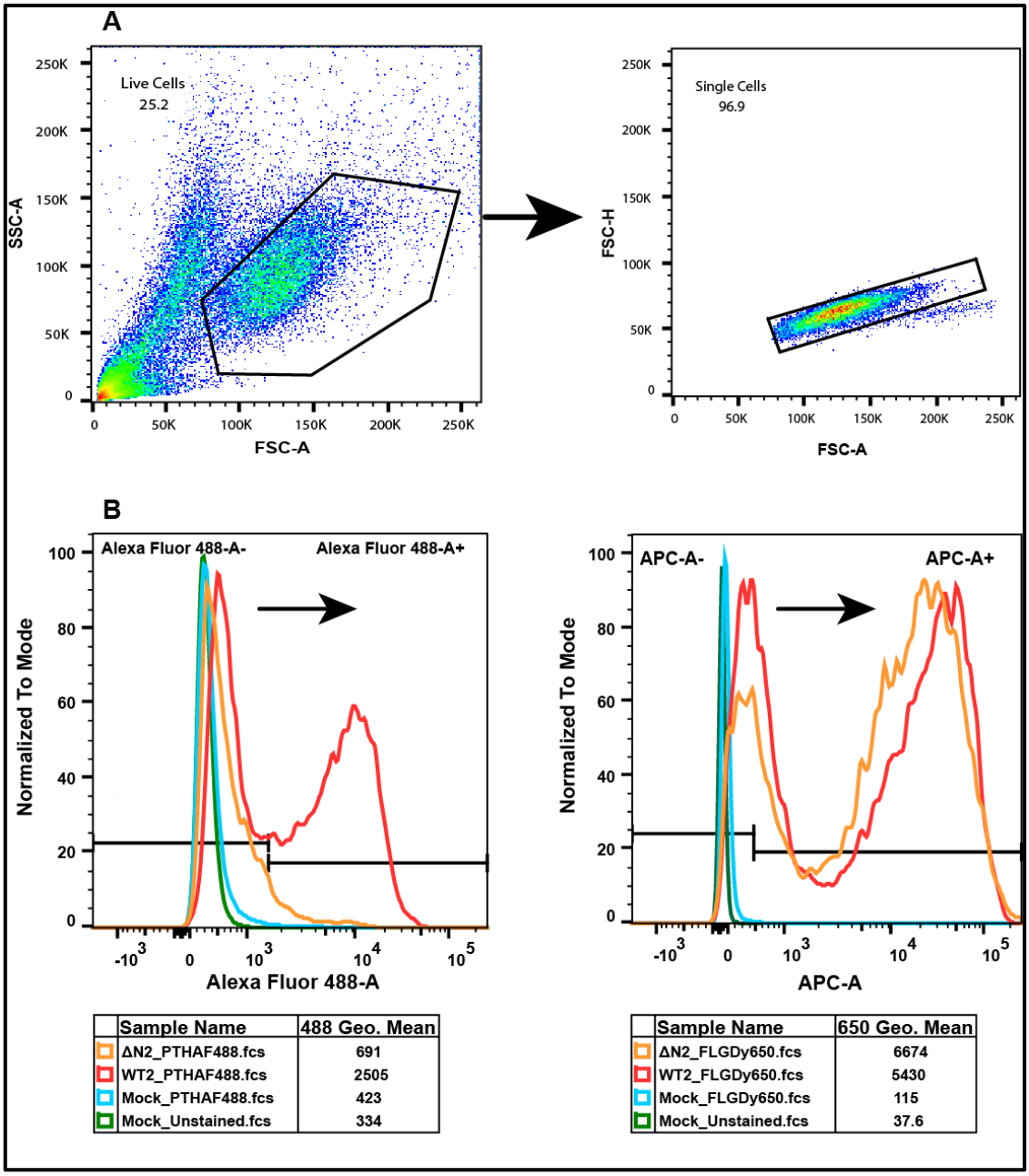


Figure 4-5: PTH1R WT2 and ΔN2 construct expression by flow-cytometry

A) Overview of the gating strategy for determination of total fluorescence by flow-cytometry. Initially, Expi293 cells transiently expressing PTH1R constructs were gated by FSC-A and SSC-A (L) to isolate the living cells following which single cells were gated using FSC-A and FSC-H (R). All fluorescence analysis was performed on singlet population only. B) Left, overlay showing the total fluorescence, normalised to mode, measured in cells expressing the WT2 (Red) and ΔN2 (Orange) stained with PTH-AF488. Right, overlay showing the total fluorescence from cells expressing the WT2 (Red) and ΔN2 (Orange) stained with Anti-FLAG tag antibody conjugated to DyLight 650. In both cases the parental cells (Green) stained with either detection reagents showed no shift in total fluorescence confirming lack of any non-specific binding. The black arrows show the shift in fluorescence in cells expressing the receptor.

The receptor expression and localisation were further confirmed using fluorescence microscopy. Similar to the flow-cytometry data, receptor expression and trafficking to the surface was evident for both constructs, while un-transfected parental cells showed no non-

specific binding (Figure 4-6). The ΔN2 receptor localisation was confirmed using the anti-FLAG antibody as this construct is unable to bind the PTH-AF488 due to the lack of the ECD.

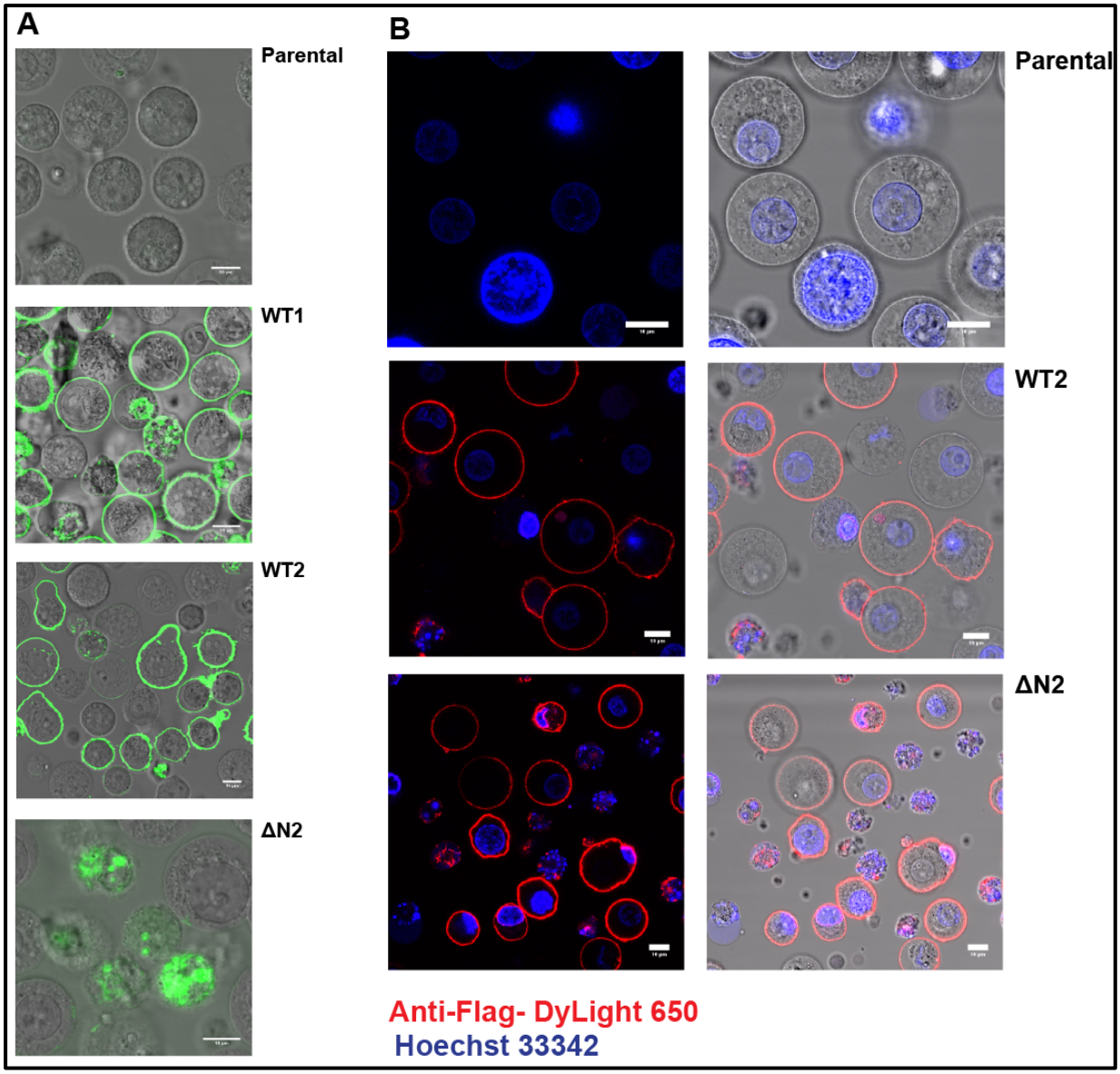


Figure 4-6: Fluorescence microscopy to determine receptor localisation

A) Fluorescence microscopy analysis of Expi293 cells transiently transfected with WT1 and WT2 constructs and stained with PTH-AF488 confirm receptor expression and surface localisation. Parental cells show no PTH-AF488 binding while ΔN2 expressing cells show some intracellular staining. B) Fluorescence micrographs of cells expressing the WT2 and ΔN2 receptor stained with anti-FLAG tag antibody conjugated to DyLight 650 confirms receptor expression and surface localisation for both constructs. Parental cells show no non-specific binding. The nucleus (shown in blue) was stained with Hoechst 33342, a cell-permeant nuclear counterstain. All size bars represent 10 µm.

Using a combination of flow-cytometry and fluorescence microscopy, the expression and localisation of the expressed receptor was confirmed. Utilising PTH-AF488 to follow

expression of PTH1R not only revealed successful expression and localisation but also confirmed the receptor was correctly folded and able to bind its natural ligand.

WT1 and 2 are similar constructs with minor modifications at the N-terminus (Figure 4-4). The expression levels of both WT1 and WT2 constructs as assessed by fluorescence microscopy were similar (Figure 4-6), illustrating that the change of signal peptide and addition of the FLAG tag did not hinder receptor expression, trafficking or ligand binding.

4.3.2 Expression constructs are functional and modulate cAMP

While PTH binding as assessed by flow-cytometry and fluorescence microscopy confirmed the native ligand binding conformation of the receptor, it did not yield any information on the signalling capabilities of the constructs. *In vitro* functional assay measuring intracellular cyclic AMP was used to confirm intracellular signalling activity of the surface expressed receptor. The concentration-response curves shown in Figure 4-7, shows that the full-length WT2 receptor is fully functional, signals through the G_s-protein and exhibits a PTH concentration-dependent increase in intracellular cAMP. In contrast, the ECD-truncated ΔN2 receptor shows an extremely limited ability to mediate ligand dependent increases in intracellular cAMP, due to its markedly reduced binding affinity for PTH (1-34).

The assay is based on immunocompetition between intracellularly generated cAMP and added d2-labelled cAMP. In the absence of intracellular cAMP, the labelled cAMP and anti-cAMP mAb bind to give a HTRF signal, and therefore a high HTRF value indicates low intracellular cAMP. In the presence of intracellular cAMP e.g. following downstream signalling through the PTH-R, the binding of anti-cAMP mAb to labelled cAMP is hindered which in turn causes a drop in HTRF ratio. A drop in HTRF therefore indicates an increase in receptor signalling.

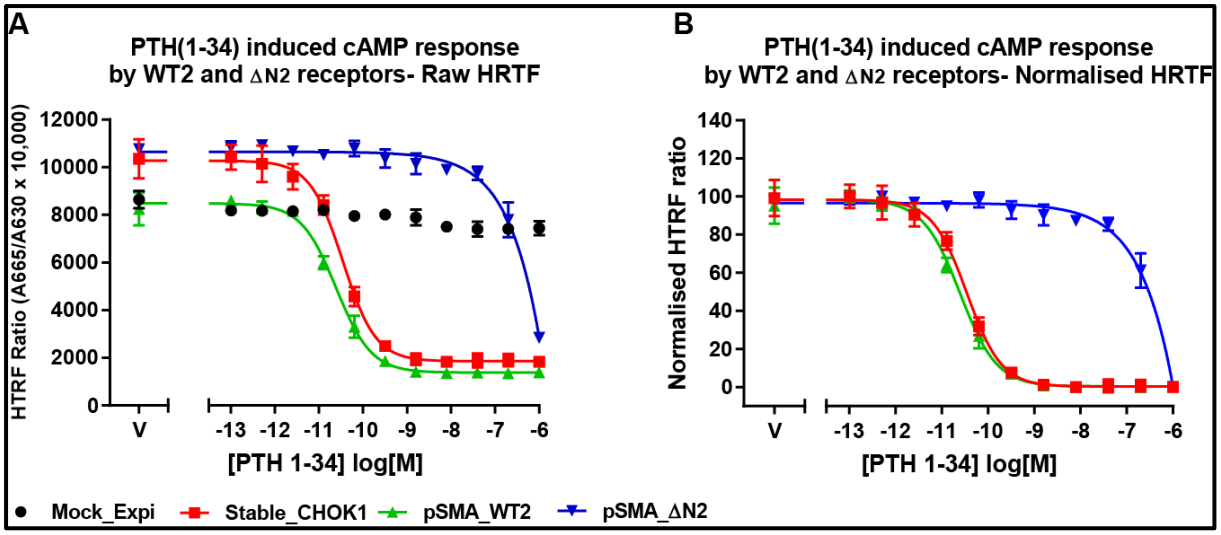


Figure 4-7: Functional characterisation of PTH1R WT2 and ΔN2 constructs using cAMP assay

A) Concentration-response curves showing cAMP regulation by Expi293 cells transiently-expressing receptor variants along with parental cells. A CHOK-1 cell line stably expressing PTH1R was used as a positive control. The CHOK-1 cells expressing the full-length PTH1R (Red) and Expi293 cells transiently expressing the WT2 constructs (green) show a concentration-dependent up-regulation of cAMP levels with increasing PTH (1-34) concentration. The ΔN2 construct shows impaired cAMP up-regulation due to the lack of the ECD, while the parental Expi293 cells (Blue) show no response at any PTH concentration. B) The raw HTRF ratio shown in A is replotted after normalising the HTRF ratio. Each data point represents quadruplicate measurements and the mean and the standard deviation is plotted.

The WT2 construct expressed on Expi293 cells exhibited a similar pEC_{50} (-10.6) when compared to a CHOK-1 cell line stably expressing the WT receptor (-10.4). However, it should be noted that for Expi293 cells transiently expressing PTH1R constructs, some variability in the basal cAMP levels and the overall EC_{50} was seen between experiments (Figure 4-8, A). This is likely to be due to variations in expression level as a result of the receptor being transiently expressed. The basal cAMP levels and the EC_{50} values for the stable cell-line, challenged with PTH (1-34) was found to be more robust and repeatable between different experiments (Figure 4-8, B).

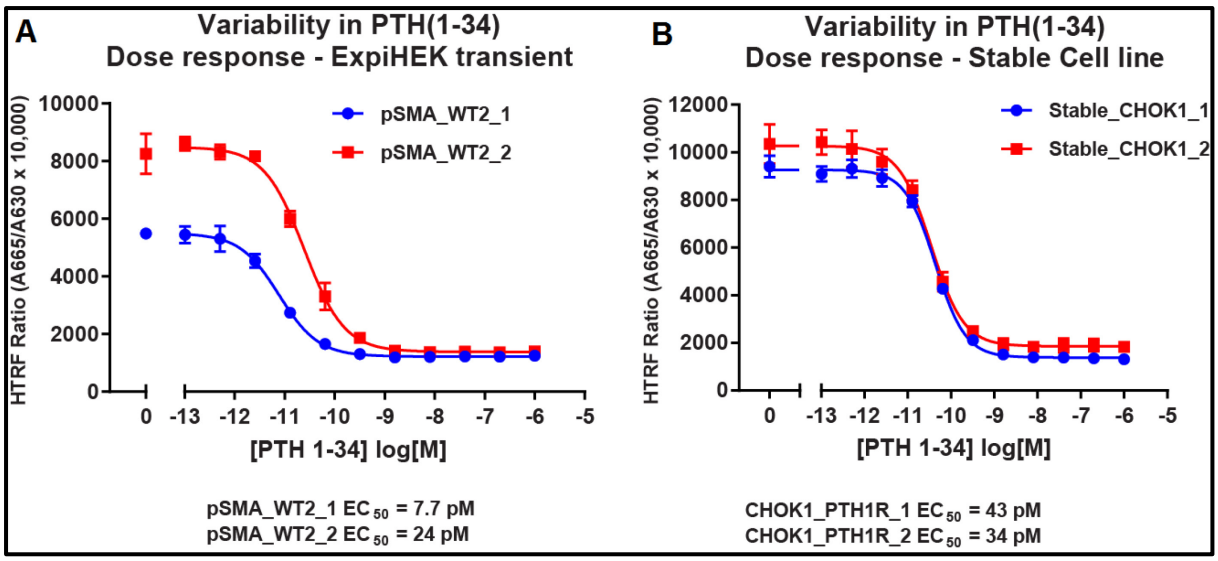


Figure 4-8: Variability in the PTH concentration-dependent responses between stable and transiently transfected cells

A) The basal cAMP levels in transiently transfected Expi293 cells differed between different transfection batches (red vs blue trace), which in turn caused a slight shift in calculated EC_{50}. B) The basal cAMP levels and overall EC_{50} response was much more robust in CHOK-1 cells stably expressing full-length PTH1R

4.3.3 WT2 and ΔN2 expression constructs are unstable and exhibit poor SMA solubilisation

The WT2 and ΔN2 constructs were expressed in Expi293 cells solubilised with SMA and purified using IMAC purification (Ni^{2+}-sepharose). Overall, the recovery of SMA-solubilised protein was poor for both receptor constructs (Figure 4-9 C). The WT2 construct was batch purified using Ni^{2+}-sepharose and low and high-imidazole eluted fractions were pooled and further purified using gel-filtration (Figure 4-9 B). Most of the protein appeared to elute with high imidazole and the gel-filtered protein was detectable as a weak band on Western blot (Figure 4-9 C, shown by arrow). A number of high molecular weight bands were visible for several of the samples tested indicating that significant amounts of the protein may have been lost due to aggregation. By visually inspecting the SDS-PAGE and Western blot, it appeared that the final yield was poor and a major fraction of the receptor was aggregating.

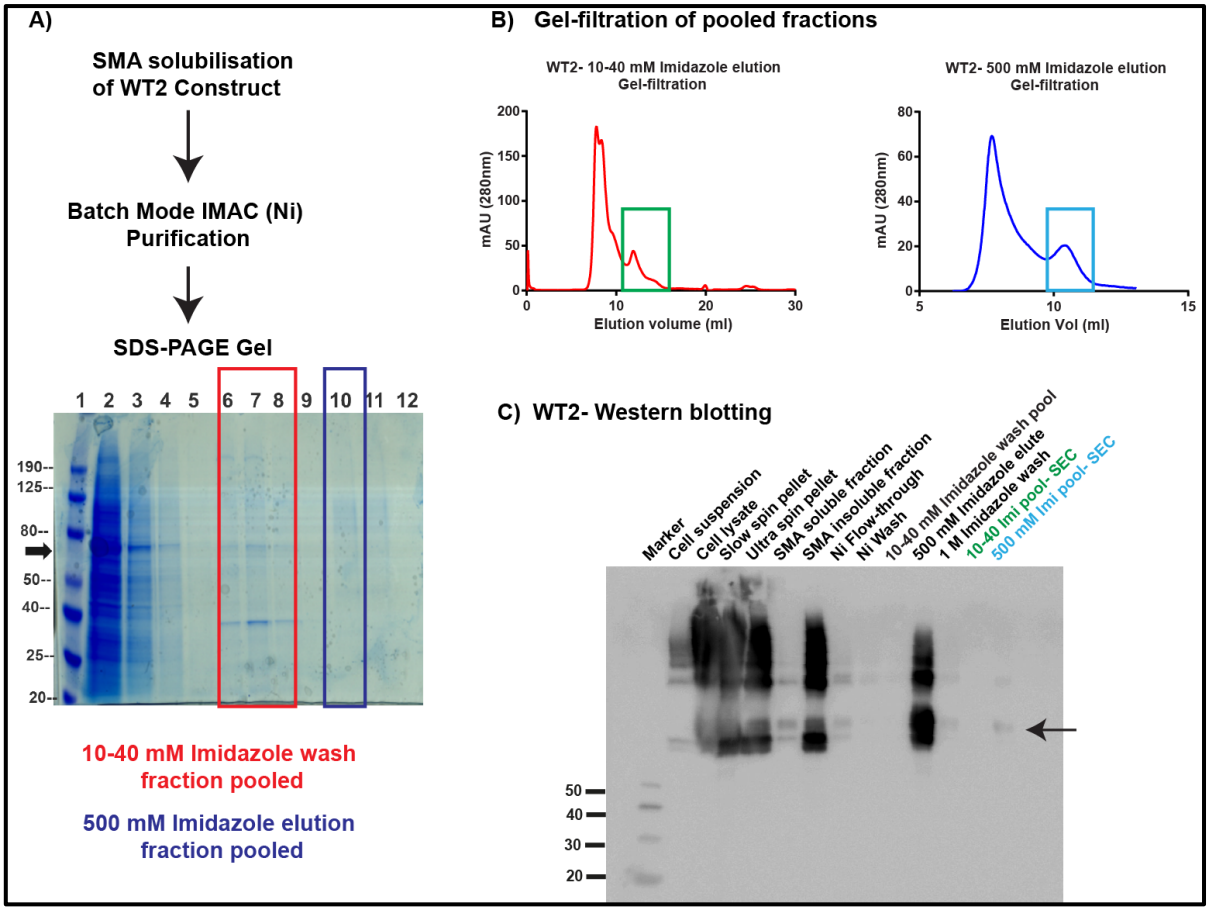


Figure 4-9: SMA solubilisation and IMAC purification of WT2 construct.

A) A work-flow summarising the solubilisation and isolation of the WT2 construct using SMA. The samples eluted from the Ni^{2+} resin were analysed using SDS-PAGE and fractions from the low imidazole elution (shown by red bounding box) and 500 mM imidazole wash (blue bounding box) were further purified using S200 gel-filtration. B) The gel-filtration traces of the low-imidazole elution (red trace) and 500 mM imidazole elution (blue trace) are shown. The relevant factions indicated by the green and light blue boxes were collected and pooled for further analysis by Western blot analysis. C) The pooled fractions from the gel-filtration along with samples from the various stages of extraction and purification were analysed by Western blotting. The lanes are labelled with the names of the respective fractions. A large amount of receptor was aggregated (Lane, SMA insoluble fraction). No band specific for WT2 was detected from the pooled gel-filtration fraction from the low imidazole elution (labelled in green) while a faint band was detected for the high imidazole elution (labelled light blue). The black arrow points to the expected WT2 band on the Western blot.

High molecular weight bands were seen with the ΔN2 construct as well indicating aggregated receptor, but the final IMAC eluate for the ΔN2 construct appeared to be of higher purity when compared to the WT2 construct. The 250 and 500 mM imidazole eluate samples gave a specific band on the Western blot analysis (Figure 4-10, lanes labelled as '250 mM Imidazole wash' and '500 mM Imi eluate).

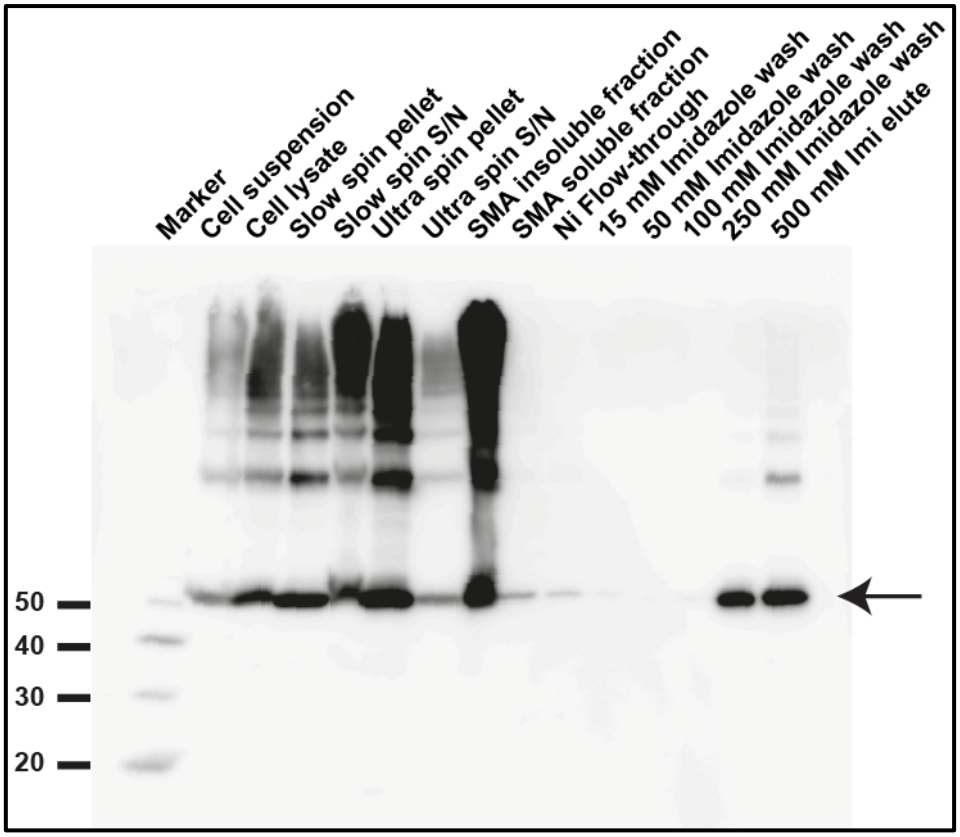


Figure 4-10: SMA extraction and IMAC purification of ΔN2 construct

Western blot analysis of the fractions from various stages of the ΔN2 extraction and purification. A large proportion of the receptor was aggregated during membrane preparation stages and SMA solubilisation. The large majority of the solubilised receptor eluted with 250 mM or 500 mM imidazole buffers. Some extra bands were also detected with the high (500 mM) imidazole wash. The black arrow shows the expected position of the correct protein.

It was clear that a large proportion of the receptor was aggregating during extraction from the native membrane environment. Also, the final yield of purified WT2 construct after gel-filtration was barely detectable with western blotting.

In silico analysis of the full-length PTH1R receptor using DISOPRED 3 (Jones and Cozzetto, 2014) suggested that the C-terminal domain, following the putative helix 8, was highly disordered along with ECL1 (Figure 4-11, A). Based on the disorder prediction result, two C-terminally truncated constructs were designed. The ΔC29-491 construct was generated by removing amino acids Ser492 to Met593 from the full-length receptor, while the double truncated, ΔNΔC171-491 construct was made by removing the N-terminal ECD (Asp29-Cys170) and the C-terminal domain (Ser492-Met593) (Figure 4-11, B).

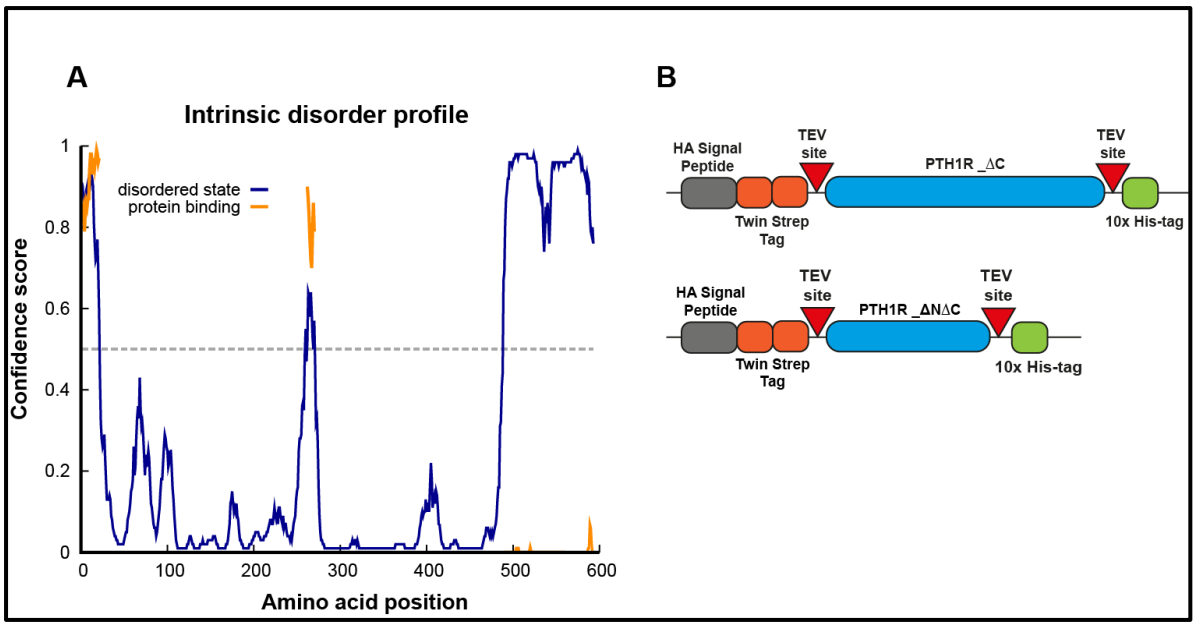


Figure 4-11: DISOPRED 3 analysis of PTH1R and C-terminal tail truncated construct schematic.

A) Disorder analysis of PTH1R using DISOPRED 3 suggested that the C-terminal tail following helix 8 exhibited high disorder along with ECL1 and a portion of the N-terminal ECD. The grey dotted line represents a confidence score cut-off of 0.5 and residues with a higher score than this are expected to exhibit more disorder. B) Schematic representation of two constructs designed to remove the disordered C-terminal tail. The ΔC29-491 construct consisted for the N-terminal ECD and all seven TMs along with the putative helix 8, while the ΔNΔC171-491 construct had both the N-terminal ECD and C-terminal tail removed. Both the constructs also incorporated N-terminal HA signal peptides, a twin strep tag and a TEV protease cleavage site and a C-terminal TEV cleavage site and 10x-His tag to aid purification, detection or surface immobilisation.

4.3.4 Surface expression and *in vitro* function of C-terminal truncated constructs remain unaffected

The expression and surface localisation of the C-terminal tail truncated PTH1R constructs were confirmed using flow-cytometry and fluorescence microscopy as described for the WT2 and ΔN2 constructs. It should however be noted that the detection antibody in this case was the loop binding antibody, ECL-mAb, described in chapter 2 as opposed to PTH (1-34)-AF488 and anti-Flag antibody which were used for staining cells expressing the WT2 and ΔN2 construct. Cells expressing the truncated constructs demonstrated good surface expression when compared to parental cells as shown in Figure 4-12 A.

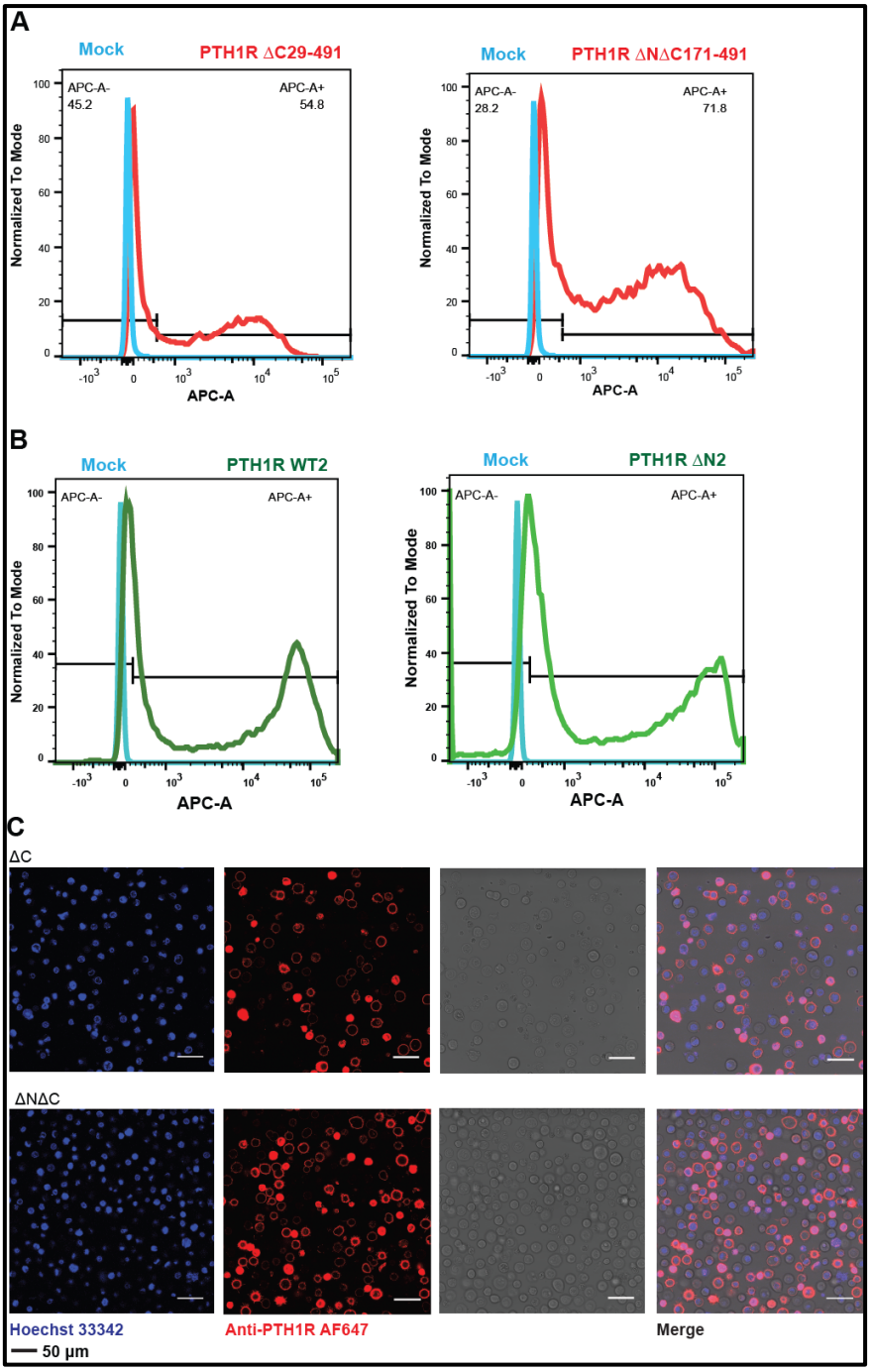


Figure 4-12: Expression and cell-surface localisation of the C-terminal tail truncated receptor using flow-cytometry and fluorescence microscopy.

A) Flow cytometry analysis of receptor expression in Expi293 cells transiently expressing ΔC29-491 (left) and ΔNΔC171-491 (right) constructs. The cells were stained with PTH1R loop binding antibody, ECL-mAb labelled with Alexa Fluor 647 (section 3.3.7) and in both cases a clear shift in overall fluorescence was noted. Non-transfected parental cells (cyan) did not show any measurable shift in fluorescence. B) Transient expression of WT2 and ΔN2 constructs using Expi293 cells was checked using Expi293 conditioned media containing ECL-mAb, followed by an anti-rabbit Fc IgG labelled with Alex Fluor 647 secondary antibody C) Fluorescence microscopy confirmed surface localisation of the expressed receptor constructs. The white scale bar represents 50 µm.

When compared to WT2 and ΔN2 receptors transiently expressed on Expi293 cells, the C-terminal truncated constructs showed similar levels of receptor expression (Figure 4-12, B). The fluorescence microscopy data confirmed the successful trafficking of the receptor and its localisation on the cell-surface (Figure 4-12, C). Truncation of the C-terminal tail did not appear to reduce receptor expression or trafficking when compared to WT2 and ΔN2 constructs, both of which contain intact C-terminal tails. The ΔC29-491 construct also exhibited a similar PTH-induced cAMP response (pEC_{50} = 10.75) when compared to the WT receptor expressed in a stable cell-line (pEC_{50} = 10.46). In contrast, the ΔNΔC171-491 construct was unable to elicit a measurable cAMP response almost certainly due to the reduced PTH-(1-34) binding affinity of this construct.

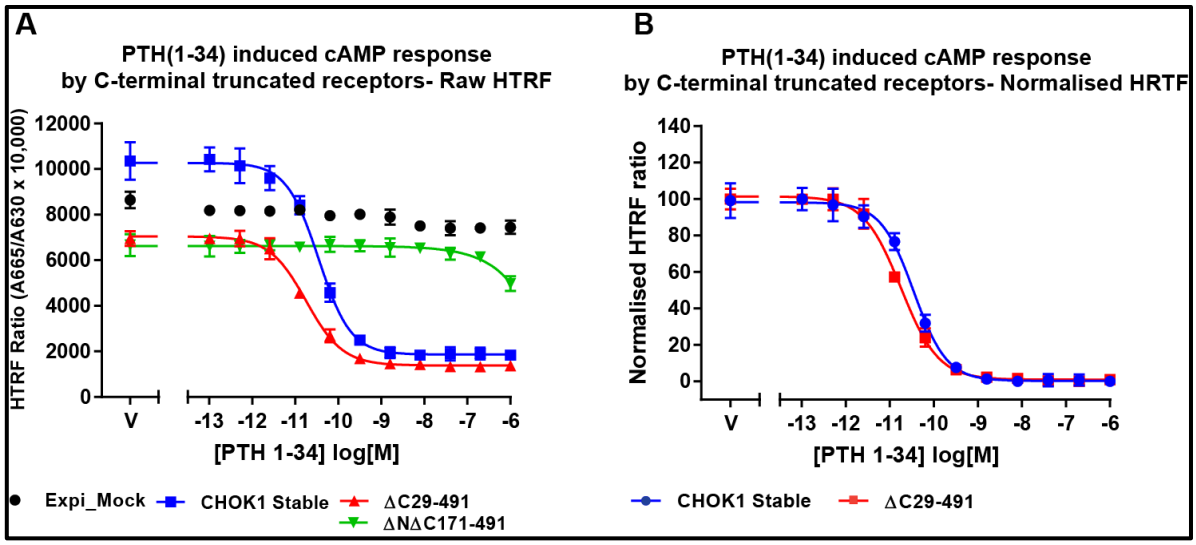


Figure 4-13: Functional characterisation of PTH1R ΔC29-491 and ΔNΔC171-491 constructs using cAMP assay

A) Concentration-response curves showing PTH (1-34) induced cAMP responses in Expi293 cells transiently expressing C-terminal truncated receptor variants ΔC29-491 (red), ΔNΔC171-491 (green) and CHOK-1 stable cell-line expressing the full-length PTH1R (blue) along with parental Expi293 cells (black). ΔC29-491 shows comparable cAMP response to the stable cell line upon challenged with PTH (1-34) concentration-range. The ΔNΔC171-491 construct shows a severely impaired cAMP up-regulation due to the lack of the ECD, while the parental Expi293 cells show no response at any PTH concentration. The raw HTRF data is plotted. B) Normalised HTRF data for stable cells and ΔC29-491 show very similar concentration-response curves and therefore EC_{50}. Each data point represents quadruplicate measurements and mean and standard deviation is plotted.

Overall, it was established that the C-terminal truncation did not have any negative impact on the receptor expression, membrane localisation and function. These constructs

were used for over expression using Expi293 cells followed by small-scale extraction and batch purification.

4.3.5 Strep-Tactin XT improves purification of both SMA and detergent solubilised ΔC29-491 and ΔNΔC171-491 constructs

The ΔC29-491 and ΔNΔC171-491versions of PTH1R receptor were solubilised using either SMA or detergent to investigate the suitability of these constructs for large scale isolation. The receptor variants solubilised using SMA were batch purified using either Strep-Tactin XT or Co^{2+} IMAC (Talon). A similar recovery of enriched receptor was obtained in the final eluate from the two different capture resins as assessed by SDS-PAGE analysis. SDS-PAGE analysis of ΔC29-491 and ΔNΔC171-491 constructs enriched using Talon resin shows successful enrichment of receptor variants in the final eluate (Figure 4-14, A). The samples were analysed under non-reducing (NR) and reducing (R) conditions (shown by pink brackets for ΔC29-491 and orange brackets for ΔNΔC171-491). Upon reduction, the sample appears to resolve better which suggests either SDS-PAGE gel running artefacts or disulphide-mediated heterogeneity under NR conditions. The Talon purified samples were further analysed following de-glycosylation under native conditions (Figure 4-14, A; lane labelled Degly). The heterogeneity appears to increase for ΔC29-491 when treated with PNGaseF, possibly due to partial glycan removal, and a smeared banding pattern is seen (Figure 4-14, A, black bracket). The ΔNΔC171-491 construct appears to behave very similarly to the ΔC29-491 construct, but unlike ΔC29-491 a well-defined band is seen after PNGaseF treatment (Figure 4-14, A, indicated by the green asterisk). It should be noted that ΔC29-491 has 5 glycosylation sites as opposed to one in ΔNΔC171-491. In both cases, the PNGaseF band is shown by red asterisk.

Upon visual inspection of the SDS-PAGE gel, the Strep-Tactin XT enriched fraction for both ΔC29-491 and ΔNΔC171-491 constructs appears to be slightly purer from those obtained using Talon resin (Figure 4-14, B). Also, the level of heterogeneity under non-reducing

condition for both construct appeared to be lower than Talon purified receptor (green and cyan bracket vs. pink and orange brackets).

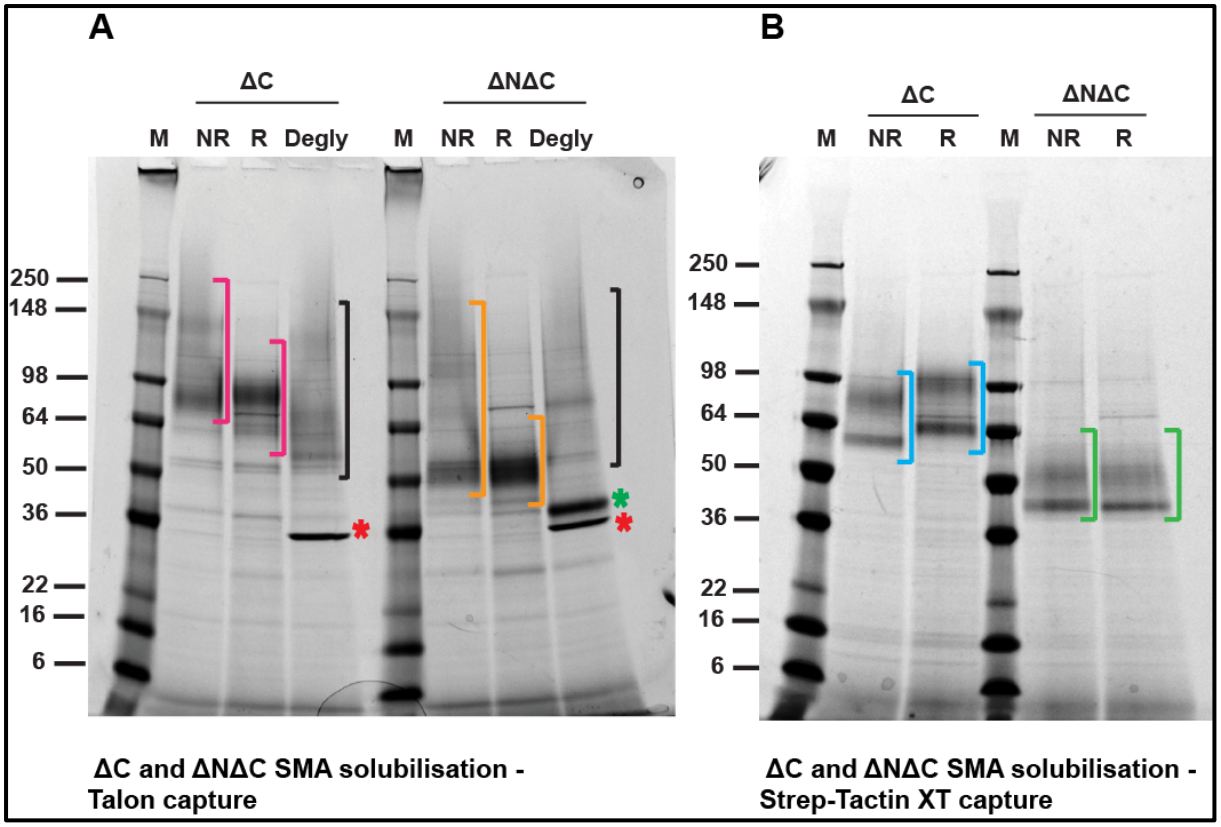


Figure 4-14: SDS-PAGE analysis of Talon (Co^{2+}) and Strep-Tactin XT enriched ΔC29-491 and ΔNΔC171-491 PTH1R constructs.

A) SDS-PAGE analysis of Talon purified ΔC29-491 and ΔNΔC171-491 constructs under non-reduced (NR), reduced (R) and native-de-glycosylated (Degly) conditions shows enrichment of the receptor (pink and orange brackets). Upon de-glycosylation, the heterogeneity appears to increase as shown by the black brackets. The band specific for PNGaseF is shown with the red asterisk (*). The band corresponding to de-glycosylated ΔNΔC171-491 is indicated by the green asterisk (*). B) SDS-PAGE analysis of Strep-Tactin XT purified ΔC29-491 and ΔNΔC171-491 constructs under non-reduced (NR) and reduced (R) conditions shows enrichment of the receptor as indicated by cyan and green brackets.

Next, the receptor variants were solubilised using either DDM or LMNG following which the solubilised receptor was purified using Strep-Tactin XT resin in batch mode. The Strep-Tactin eluate was enriched with the receptor variants although other co-eluting species could also be seen (Figure 4-15).

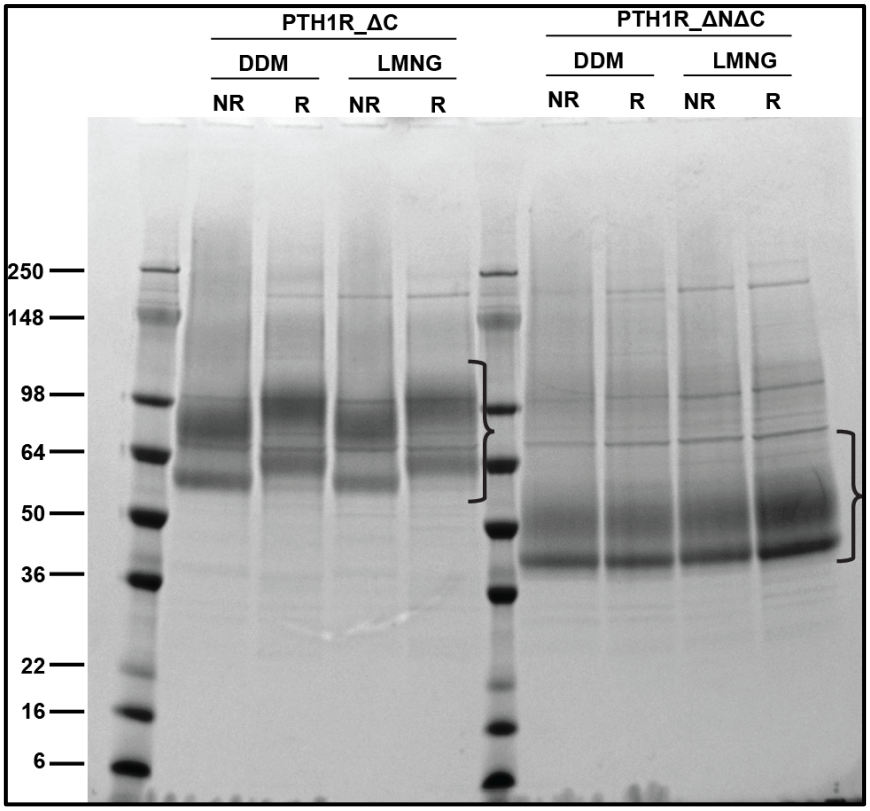


Figure 4-15: SDS-PAGE analysis of Strep-Tactin XT purified DDM and LMNG solubilised ΔC29-491 and ΔNΔC171-491 constructs.

SDS-PAGE analysis confirms enrichment of the ΔC29-491 and ΔNΔC171-491 construct solubilised using either DDM or LMNG and affinity purified using Strep-Tactin XT resin. All samples were analysed in non-reduced (NR) and reducing condition (R). The expected bands for both the constructs are shown by black brackets. The diffuse banding pattern is likely to be the result of glycosylation.

Overall, the final yield after Strep-Tactin XT capture was variable but in general 100-200 µg of partially purified receptor could be purified from ~ 500 ml Expi293 culture volume. Visual inspection of SDS-PAGE gels revealed that Strep-Tactin XT was consistent in purifying the C-terminal truncated constructs, with comparatively better yields and purity compared to IMAC.

4.3.6 Generation of pure ΔNΔC171-491 PTH1R construct

One step-affinity capture was able to enrich the receptor constructs but required further purification steps to improve the purity. To further increase the purity of the receptor sample, the Strep-Tactin XT eluate containing enriched ΔNΔC171-491 was concentrated using a 100 kDa MWCO filter and then 100 µl of the sample was applied to a Superose 6 column. The concentrated sample contained a large proportion of co-eluting species and high molecular

weight species as demonstrated by the SDS-PAGE analysis of the sample (Figure 4-16, A). Fractions specific for monomeric receptor were collected from the preparative gel-filtration as shown in Figure 4-16, B.

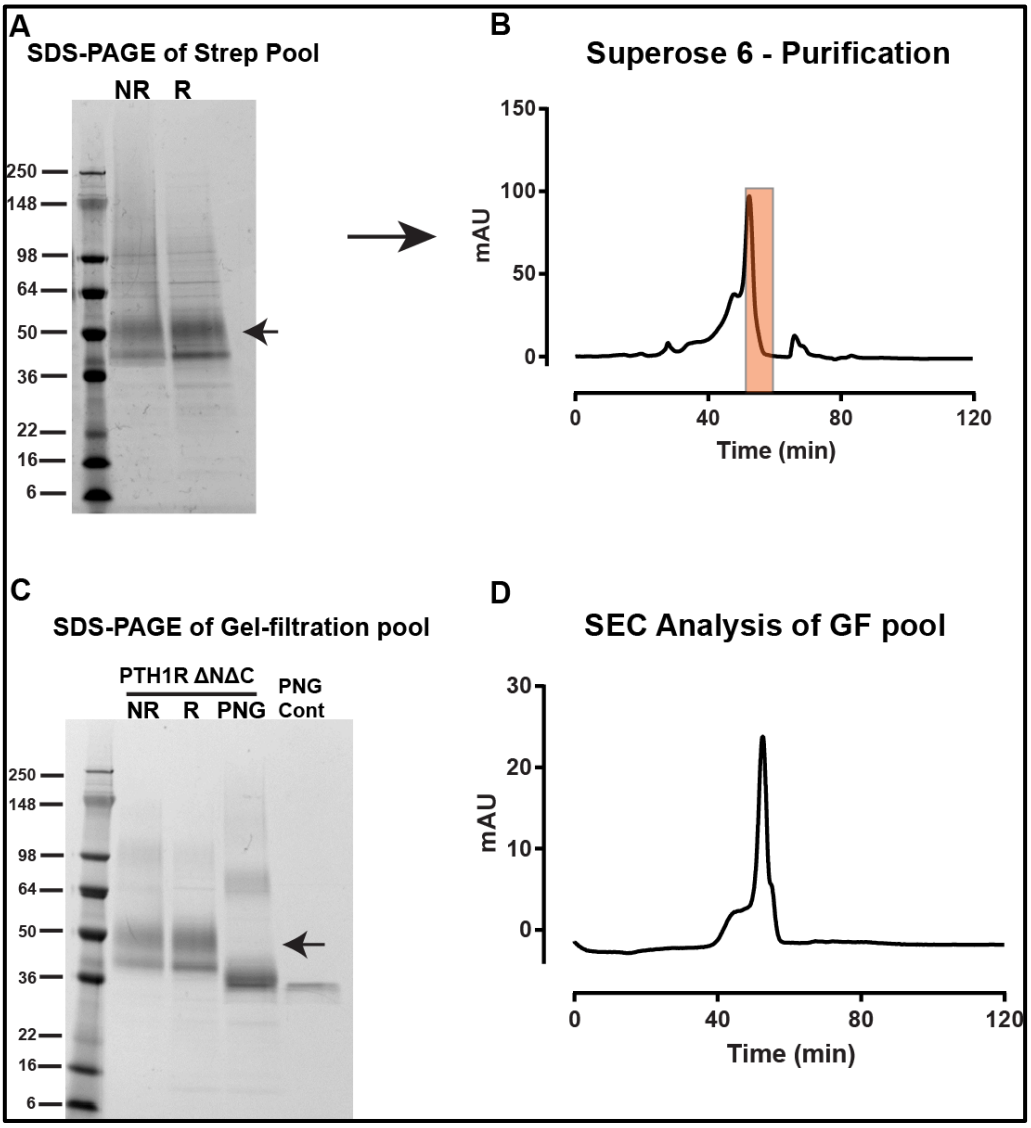


Figure 4-16: Affinity and gel-filtration purification of ΔNΔC171-491 construct

A) SDS-PAGE gel analysis of Strep-Tactin XT purified ΔNΔC171-491 construct under non-reducing (NR) and reducing (R) conditions. The expected band for ΔNΔC171-491 is indicated by the black arrow. B) The gel-filtration purification trace for ΔNΔC171-491 construct shows the overall profile of the pooled sample and the monomeric fraction is indicated by the orange box. C) SDS-PAGE analysis of the monomeric fraction under non-reduced (NR), reduced (R) and PNGaseF treated (PNG) conditions confirms sample purity and the expected band is shown by black arrow. PNGaseF control (PNG Cont) samples indicated the position of PNGaseF on the gel. D) The pooled fraction was analysed using analytical gel-filtration (Superose 6 column) which further confirmed the overall purity of the final sample.

The monomeric fraction was further concentrated and the final yield was found to be ~33 µg. The gel-filtered sample was tested for purity using SDS-PAGE (Figure 4-16, C) and

size-exclusion chromatography (Figure 4-16, D). Both analyses indicated that ΔNΔC171-491 construct purified to high purity. The analytical gel-filtration trace also showed some co-eluting peaks on either side of the main peak. Overall, it was found that 30-40 µg of ΔNΔC171-491 construct could be generated with high purity from a starting culture volume of 300-500 ml.

4.4 Discussion

The majority of GPCR structures have been obtained using protein produced using either a baculovirus-insect cell system or a mammalian expression system. HEK cells have been successfully used for generating purified GPCR for structural work. Burg et.al successfully overexpressed the human cytomegalovirus US28 GPCR in HEK293 cells (Burg *et al.*, 2015). The CB_1 cannabinoid and smoothened receptor structures were also solved using protein produced with HEK293 cells (Byrne *et al.*, 2016; Hua *et al.*, 2017). Here, we used Expi293, a modified HEK293 cell line, that is widely used for over-expressing soluble proteins such as antibodies and antibody fragments (Fang *et al.*, 2017). Our choice was driven by the existing expertise with this expression system at UCB and ease of use. These cells are adapted for suspension culture, making scale up straightforward, however, this expression system can be expensive compared to other commonly used expression approaches.

We used the full-length construct (WT2) without any modifications to the either the ECD or the TMD regions, because this construct represents the physiologically relevant form. However, it is also known that the flexible ECD can be detrimental for receptor extraction and purification and both the GCGR and CRF1R structure were solved with a construct devoid of the ECD (Hollenstein *et al.*, 2013; Siu *et al.*, 2013), hence an ECD-truncated, ΔN2 construct was also used for extraction and purification work. Using Expi293 expression system, we successfully expressed the full-length receptor constructs, and demonstrated correct membrane localisation (Figure 4-6). These constructs could bind the endogenous ligand and regulate cAMP by coupling to G-protein (Figure 4-7), but the full-length constructs were not amenable to extraction and purification as they were prone to high losses of material through aggregation (Figure 4-9, Figure 4-10). It is possible that the receptor aggregation was caused

by disordered regions in the PTH1R sequence, particularly the C-terminal end. Aggregation could also be caused due to disulphide scrambling since PTH1R ECD has 3 disulphide bonds (Pioszak and Xu, 2008; Parthier *et al.*, 2009).

Within the class B family, the truncation of C-terminal residues is routinely used to improve receptor stability and aid purification. Recently Zhang et.al reported a high resolution cryo-EM structure of a C-terminally truncated construct of GLP1R (Y. Zhang *et al.*, 2017). Similarly the thermostability of GCGR was improved by truncating 45 residues from the C-terminus; this also facilitated high resolution structure determination using X-ray crystallography (H. H. Zhang *et al.*, 2017). Indeed, *in silico* analysis of the PTH1R sequence suggested that the C-terminal tail of the receptor, following the putative helix 8, is disordered. Removal of C-terminal disordered residues did not have any negative impact on the receptor expression and membrane trafficking (Figure 4-12). We also confirmed that the truncated constructs were fully functional and could up-regulate intracellular cAMP when challenged with PTH (1-34).

The C-terminal truncated receptor variants, ΔC29-491 and ΔNΔC171-491, were more amenable to detergent and SMA solubilisation showing a much lower degree of aggregation compared to the other constructs assessed. Using a single-step affinity purification, it was possible to obtain 100-300 µg of protein fraction enriched with ΔC29-491 or ΔNΔC171-491 from ~500 ml of Expi293 culture. The protein sample is not completely homogeneous at this stage so further optimisation of the purification protocol is required, through for example inclusion of a SEC step.

Next, we wanted to investigate the applicability of styrene-maleic acid copolymer (SMA) as a solubilisation agent and compare against detergents such as DDM and LMNG. SMA is an amphiphilic copolymer which has been successfully used to solubilise multi-pass transmembrane protein in the complete absence of detergents (Jamshad *et al.*, 2015). In our hands, the overall solubilisation using SMA was poor and we found that a large fraction of the receptor ended up in the insoluble fractions (Figure 4-9). This could be due to various reasons such as batch to batch variation in SMA quality, source of polymer and choice of expression

platform. We believe that this work was one of the early attempts to solubilise membranes from a suspension mammalian cell culture as the majority of the published data have used *E. coli* (Morrison *et al.*, 2016), yeast or membrane fractions from adherent mammalian cells (Jamshad *et al.*, 2015). It remains to be seen if the overall solubilisation of PTH1R from Expi293 membranes could be further improved using SMA. We also found that IMAC-based purification of SMA-stabilised receptor was challenging as binding of the solubilised receptor to IMAC resin was very weak. This could be due to the anionic nature of SMA which has been shown to impair His-tag binding to Ni^{2+}-NTA (Dörr *et al.*, 2015). Nevertheless, it was possible to solubilise PTH1R variants (full-length and C-terminal truncated) using SMA and perform small scale purification using IMAC (Figure 4-10, Figure 4-9, Figure 4-14: left). We explored different affinity tags and resins such as Strep-Tag II and Strep-Tactin XT® as this approach has been successfully used for the CB_2 receptor (Yeliseev, Zoubak and Schmidt, 2017). In our hands, we successfully purified DDM, LMNG or SMA solubilised ΔC29-491 and ΔNΔC171-491 constructs, using Strep-Tactin XT. The overall quality of Strep-Tactin XT purified protein as assessed by SDS-PAGE was higher when compared to other affinity resins such as Talon (Figure 4-14).

Single step affinity purification using Strep-tag allowed us to use both SMA and detergents (DDM and LMNG) for solubilisation but the final eluate consisted of impurities and high molecular weight species. While semi-pure sample could be useful for some techniques, we were keen to purify the receptor to high purity. Using the double-truncated receptor ΔNΔC171-491, solubilised in DDM and adding a second gel-filtration step, we purified the receptor to high-purity with a final yield of ~33 µg from a 500-ml volume of suspension culture (or 60-70 µg per 1 litre of Expi293 culture). Previous attempts at PTH1R purification have shown a range of final protein yields. Mitra et.al purified PTH1R in nanodiscs and reported a final protein yield ranging roughly from 0.05 to 0.2 µg of PTH1R per 10-cm plate of HEK293S cells (Mitra *et al.*, 2013). Using COS -cells, n-DM solubilisation and single-step affinity chromatography approximately 18 µg of hPTH1R was purified per mg of crude membranes (Shimada *et al.*, 2002). More recently, structures of GLP-1R and CT, both in complex with

heterotrimeric G-protein, were published where authors managed to purify 200 and 500 µg respectively of the receptor-G-protein complex from 1 litre culture of insect cells (Liang *et al.*, 2017, 2018). Overall, we feel that our final receptor yield is similar to that achieved for GPCRs by other laboratories but could certainly be improved further. For techniques, such as X-ray crystallography, which require large amounts of pure protein our current system would not be suitable. Expression level, purification and final yield would require further optimisation. To facilitate large scale production of functional PTH1R, a stable cell line expressing the C-terminal truncated construct would be best suited, as the expression levels and receptor function would be much more robust than we obtain using transient transfections.

The overall aim of the work outlined in this chapter was to develop a solubilisation and purification method to generate a few hundred micrograms of PTH1R receptor which we achieved. The amounts of purified receptor generated using the approaches described above have allowed various biophysical analysis such as SPR, HDX-MS and Cryo-EM (see chapter 5).

Chapter 5: Biophysical and functional analysis of phage and core antibodies binding to full-length PTH1R

5. Biophysical and functional analysis of phage and core antibodies binding to full-length PTH1R

5.1 Introduction

As described in Chapter 2, it was possible to generate PTH1R specific antibodies using both phage display, raised against the ECD only, and the UCB core antibody production approach, raised against the full receptor. Chapter 4 outlines the successful production of pure PTH1R. This chapter describes attempts to characterise the binding between the antibodies and the receptor and assess whether antibody binding influences receptor function using a range of techniques as outlined below.

5.1.1 PTH1R signalling

PTH1R binds to parathyroid hormone (PTH) and parathyroid hormone-related peptide (PTHrP) and both peptide hormones can activate the receptor (Datta and Abou-Samra, 2009). The first 34 N-terminal residues of PTH, termed PTH (1-34), can fully activate PTH1R and is an FDA approved drug for treating osteoporosis (Neer *et al.*, 2001). Upon activation, PTH1R couples principally to G_s which in turn activates the adenylyl cyclase - cAMP - protein kinase A (PKA) intracellular signalling pathway. However, PTH1R is also known to signal through the $G\alpha_q$- phospholipase C (PLC) – β-inositol triphosphate – cytoplasmic Ca^{2+} - protein kinase C (PKC) pathway (Abou-Samra *et al.*, 1992) and the $G\alpha_{12/13}$ – phospholipase D – transforming protein RhoA pathway (Singh *et al.*, 2005). More recently, it has been shown that PTH1R can couple to β-arrestin and additionally signal through the extracellular signal-regulated kinase1/2 (ERK1/2) pathways (Syme, Friedman and Bisello, 2005; Gesty-Palmer *et al.*, 2006).

In terms of cell-based assays we explored the effects of the antibodies on receptor coupling to both the cAMP and β-arrestin pathways. The levels of intracellular cAMP are tightly regulated and production is controlled by the adenylyl cyclase family of enzymes which converts adenosine tri-phosphate (ATP) to cAMP and inorganic phosphate (Williams, 2004). Most high-throughput cell-based assays measuring intracellular cAMP regulation follow a

general principle, where the levels of cellular cAMP are detected using competition with either a fluorophore or radiolabelled cAMP (Williams, 2004). Homogeneous time-resolved fluorescence (HTRF) has been successfully applied to the measurement of intracellular cAMP levels (Cisbio, FRANCE). The HTRF approach is described in detail in section 2.2.8.

PTH1R is also known to signal through β-arrestin and currently there is a lot of interest in this pathway as it has a role in anabolic bone formation. A β-arrestin biased agonist, PTH-βarr, which causes anabolic bone formation in *in vivo* studies has been reported (Gesty-Palmer and Luttrell, 2011). The recruitment of β-arrestin to the cell surface is controlled by phosphorylation of activated GPCRs by GRKs, which in turn generates a binding site for β-arrestin (Pitcher, Freedman and Lefkowitz, 1998). β-arrestin binding prevents further G-protein coupling to the activated receptor and initiates receptor internalisation (Luttrell and Lefkowitz, 2002). Enzyme-fragment complementation (EFC) technology (Eglen, 2002) is one approach used successfully to study β-arrestin recruitment (DiscoveRx, USA). Other approaches include Bioluminescence Resonance Energy Transfer (BRET) and Fluorescence resonance energy transfer (FRET). Here we used the EFC approach to explore the effect of the mAbs on receptor- β-arrestin coupling.

5.1.2 Hydrogen-Deuterium Exchange – Mass spectrometry (HDX-MS) as a tool for epitope mapping

Hydrogen-deuterium exchange of amides is widely used to study protein dynamics and can complement structural data derived from X-ray crystallography (Katta, Chait and Carr, 1991; Englander, 2006). HDX allows researchers to study fine structural changes in large proteins with exceptional accuracy (Chalmers *et al.*, 2006; Bruning *et al.*, 2007). The basis of HDX is the exchange of amide hydrogens for deuterium. Exchange at any particular site of a protein is influenced by factors such as surface exposure, and the overall secondary and tertiary structure of the protein surrounding a given amide (Katta, Chait and Carr, 1991). HDX measurement is generally achieved using either NMR or MS (Czerski, Vinogradova and Sanders, 2000; Engen and Smith, 2001). While NMR can provide single amide resolution,

protein size can be a limiting factor. HDX coupled to a mass spectrometer on the other hand can handle protein of any size and the overall protein requirement is much lower compared to NMR (X. Zhang *et al.*, 2010). A schematic representation of HDX-MS and its use in epitope mapping is shown in Figure 5-1.

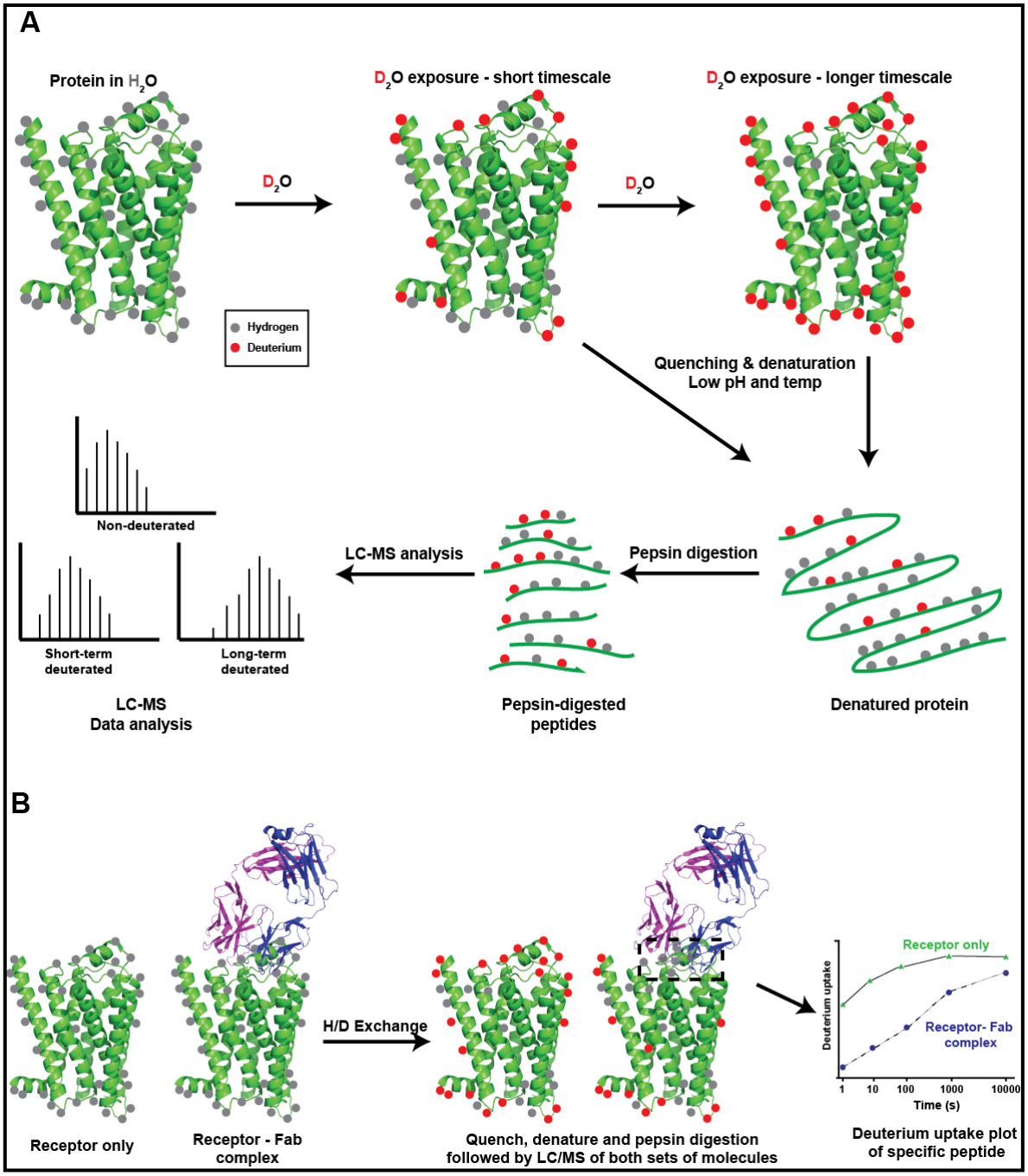


Figure 5-1: Schematic representation of HDX-MS analysis and its use in epitope mapping.

A) Workflow involved in HDX-MS analysis of proteins. Solvent-accessible hydrogens (grey circles) exchange for deuterium (red circles) when the protein is exposed to deuterated buffer. This exchange is reversible and to avoid back-exchange for hydrogen, low temperature is maintained throughout the analysis. The exchange is also time-dependent and therefore a time-course is always performed. Following incubation, the protein is denatured and digested with

pepsin, followed by an LC-MS separation and analysis of the peptides. The deuterated peptides show a shift in overall mass of the peptide which can be used to further identify the peptides undergoing exchange. B) Differential exchange is used to determine epitopes using HDX-MS. The deuterium uptake of protected hydrogen (indicated by black dotted line box) is slower in receptor- Fab complex when compared to receptor alone and this allows determination of peptides which play a role in protein-protein interactions. The deuterium uptake plots of protected peptides in complex (blue) show slower deuterium uptake when compared to apo receptor (green). Fig adapted from (Vadas and Burke, 2015).

In recent years, the HDX-MS analysis of GPCRs has allowed a better understanding of receptor dynamic involved in activation and deactivation. HDX-MS was used to study the structural dynamics of G-protein binding the β_2-adrenergic receptor solubilised in detergent (Chung *et al.*, 2011). Similarly, HDX-MS analysis of β-arrestin 1 binding to the β_2-adrenergic receptor gave a useful insight into molecular interactions critical for receptor desensitisation (Shukla *et al.*, 2014).

While improvements in methodology have made HDX-MS more accessible to the GPCR field, successful application of this technique still remains relatively challenging. Short digestion times, required to prevent back-exchange of incorporated deuterium, post-translational modifications such as glycosylation, palmitoylation and the presence of detergents (X. Zhang *et al.*, 2010) which interfere with enzymatic digestion of the receptor and the downstream MS analysis (Rabilloud, 2009) can all cause problems. Nevertheless, HDX-MS is fast becoming method of choice for studying receptor activation, structural dynamics and epitope determination. We used this technique to characterise the antibody/GPCR interaction sites.

5.1.3 Emerging role of CryoEM in GPCR structural biology

For decades, X-ray crystallography has played a key role in three-dimensional structure determination of proteins but there are a few major bottlenecks associated with X-ray based structural studies. As a starting point, X-ray crystallography requires well-formed three dimensional crystals, which can be a big hurdle for flexible and difficult to express proteins such as GPCRs (Seddon, Curnow and Booth, 2004). The presence of the detergent micelle can hinder crystal lattice formation by reducing the surface area available to form crystal contacts (Moraes *et al.*, 2014). X-ray crystallography also requires screening hundreds

of conditions to derive the optimal condition for reproducible crystal growth, which turn requires a large amount of highly pure protein (Bill *et al.*, 2011). Nevertheless, various groups have solved high resolution structures of GPCRs using X-ray crystallography, but this approach requires a lot of optimisation and receptor engineering (Jazayeri, Dias and Marshall, 2015). More recently, cryo-EM has emerged as a powerful technique for three-dimensional structure determination of biological samples (Vinothkumar and Henderson, 2016). Several reasons are responsible for cryo-EM's popularity in the membrane protein field and one of the most important is markedly reduced sample consumption when compared to crystallographic approaches (Rawson *et al.*, 2016). Cryo-EM also does not require crystals and is more amenable to post-translational modifications than crystallography (Fernandez-Leiro and Scheres, 2016). It also has the potential to capture dynamic information as the protein molecules in a single sample can be in different conformations.

In this technique, the protein of interest is placed on a metal grid, usually copper, coated with amorphous carbon with holes. The excess sample is blotted and the grid is flash frozen in liquid ethane (Dubochet *et al.*, 1982). The freezing of protein solution on grids causes formation of a thin-layer of vitreous ice which also contains the protein molecules frozen in various orientations and potentially different conformations. Numerous images are captured which contain the two-dimensional projections of individual protein complexes which are known as particles. Using various computer programs, these 2D projections are combined to provide a single 3D reconstruction (Fernandez-Leiro and Scheres, 2016).

Recently, structures of the class B GPCRs, CTR and GLP1R in complex with heterotrimeric G-proteins, were solved using cryo-EM which further emphasises the important role cryo-EM is playing in GPCR structural biology (Liang *et al.*, 2017; Zhang *et al.*, 2017; Liang *et al.*, 2018). We attempted preliminary single particle cryo-EM on the receptor-antibody complexes.

In this chapter, we performed a series of functional and biophysical analyses as described above, as well as SPR in order to characterise receptor-mAb binding using the ECD- binding PD12 scFv-Fc (referred to as ECD-mAb from hereon) and ECL-binding CoreAb1

mAb (referred to as ECL-mAb from hereon). Interestingly, we found that the ECD-mAb affected β-arrestin recruitment while the ECL-mAb acted as a neutral allosteric ligand. We also found that both mAbs bind PTH1R with high affinity and we were able to successfully map the binding epitopes using HDX-MS.

5.2 Material and methods

5.2.1 Functional characterisation of ECD binding (ECD-mAb) and core-derived loop binding (ECL-mAb) antibody

5.2.1.1 Cyclic AMP (cAMP) assay using stable cell-line

Measurement of cAMP changes in response to addition of ligand was performed as described in chapter 2 (Section 2.2.8). Typically, 5000-10,000 CHOK-1 cells stably expressing PTH1R (DiscoveRx) were plated overnight in a white tissue culture treated 384-well plate using CP0 plating media and incubated at 37°C in a humidified atmosphere. The Following day, the media was discarded and the cells were re-suspended in 5 µl of PBS + 1 mM IBMX.

To perform the PTH (1-34) concentration-response experiments, lyophilised PTH (1-34) was dissolved in PBS + 0.1% BSA to a stock concentration of 50 µM. A 12 point, 5-fold serial dilution of PTH was performed at a starting concentration of 2 µM using PBS + 0.1% BSA including a buffer blank. Similarly, a 12-point, 3-fold serial dilution of ECD-mAb and ECL-mAb was performed using PBS at a starting concentration of 2.5 µM. The concentration-response curves for the antibodies in agonist and antagonist mode were generated as described previously in section 4.2.4. For antibody concentration-response curves in agonist mode all dilutions were prepared at 2x the working concentration while for antagonist mode the dilutions were prepared at 4x the working concentration. For determining antagonism, cells were incubated with antibodies for 30 min at room-temperature followed by a PTH (1-34) challenge at either ~EC_{20} or ~EC_{80} concentration. Each sample was measured in quadruplicate and the experiment was repeated twice. The mean calculated HTRF ratio and standard deviation for each data point was plotted using GraphPad Prism 7. Non-linear

regression data fitting was performed using a log (inhibitor) vs. response (three parameter) model to calculate the EC_{50}.

5.2.1.2 β-arrestin recruitment assay

The β-arrestin recruitment assay was performed using a PathHunter β-arrestin eXpress kit based on enzyme fragment complementation (EFC) technology. The assay ready cells were thawed in a 37°C water bath and immediately transferred to warm cell plating reagent to give a final cell density of 10^5 cells/ml. A total of 100 µl of cell suspension was added to each well of a sterile, white 96-well plate (DiscoveRx) and incubated for 48 hr in a 37°C incubator with 5% CO_2 and in a humidified environment. Following incubation, the cells were used for assay in either agonist or antagonist mode. For agonist mode,10 µl of 3-fold serially diluted PTH, ECD-mAb or ECL-mAb, prepared at 11x the working concentration was added and the mixture was incubated for a further 90 mins in a 37°C incubator. For antagonist mode, 5 µl of antibody sample prepared at 22x the working concentration was added followed by a 30-min incubation and then cells were challenged with 5 µl of PTH (1-34) prepared at 22X the working EC_{80} concentration. All antibody dilutions were performed using PBS while PTH (1-34) dilution was done in PBS + 0.1% BSA. After incubation, 55 µl of the working detection reagent (prepared by mixing 4.75 ml of cell assay buffer, 1.25 ml of substrate reagent 1 and 0.25 ml of substrate reagent 2, and kept in the dark) was added and the cells further incubated for 1 h in the dark at room temperature. The final luminescence from each well was read using a Synergy Neo 2 plate reader. The luminescence readings were plotted using GraphPad Prism 7 and non-linear regression data fitting was performed using a log (inhibitor) vs. response (three parameter) model to calculate the EC_{50}.

5.2.2 Binding kinetics of ECD-mAb and ECL-mAb using surface plasmon resonance (SPR)

ΔC29-491 and ΔNΔC171-491 constructs were solubilised in styrene-maleic acid co-polymer and purified using either Strep-Tactin XT or Talon affinity purification as described previously in (Chapter 4, section 4.2.8). The protein was eluted in 50 mM Tris, 150 mM NaCl,

10% glycerol, pH 8.0. SPR measurement was used to determine the affinity of ECD-mAb and ECL-mAb for PTH1R constructs. Binding assays were carried out using a Biacore T200 instrument (GE Healthcare Bio-Sciences AB). Anti-His antibody (GE Healthcare Bio-Sciences AB) was diluted to 50 µg/ml in 10 mM sodium acetate, pH 4.5 buffer and immobilised on a CM5 Sensor Chip (GE Healthcare Bio-Sciences AB) via amine coupling chemistry to a level of ~5000 response units (RU). All binding assay steps were performed using a running buffer comprised of 50 mM Tris, 500 mM NaCl, 0.005% (v/v) P20, pH 8.1. Single step affinity purified ΔC29-491 and ΔNΔC171-491 constructs at concentrations of 0.2-0.3 mg/mL were used to achieve 200-300 RU capture using the C-terminal His_{10}-tags and immobilised anti-His antibody. Due to the limited yield of ΔC29-491 and ΔNΔC171-491 proteins, the kinetic profiles of ECD-mAb and ECL-mAb binding to both receptor constructs were determined using a single cycle kinetics method. Each antibody was titrated over the captured ΔC29-491 or ΔNΔC171-491, respectively, at concentrations ranging from 2 to 200 µM (1:4 dilution, total 5 concentrations tested). In the single cycle kinetics method, five concentrations of the antibody tested were injected one after another, each for 180 s, starting from the lowest to the highest, and a single dissociation phase was recorded for 20 min following injection of the highest concentration of the antibody. The flow rate used for the binding assay was set to 30 µL/min. The chip surface was regenerated by flowing 50 mM HCl twice at a flow-rate of 10 µL/min for 90s each. A blank run with the same condition was performed prior to the antibody sample injection. Background subtracted binding curves were analysed using the T200 evaluation software (version 3.0) following standard procedures and kinetic parameters were determined using the 1:1 binding model as outlined in the GE Healthcare guidelines.

The SPR experimental work and the final data analysis was performed by Dr Marta Westwood, UCB.

5.2.3 Reformatting ECD-mAb and ECL-mAb to Fab format

The ECD-mAb was reformatted to the Fab fragment using cloning services provided by ATUM (USA). Briefly, a synthetic gene encoding the V_H region of ECD-mAb was cloned

into pMH-Fabnh vector using Type II cloning. The vector is derived from the pMH vector (see supplementary section) and encodes a CH_1 fragment downstream of the V_H sequence. The final protein product encoded by the plasmid is a mature Fab heavy chain. The V_L sequence was ordered as described above and cloned into the pMhCK vector. This vector is also derived from the pMH vector and encodes a kappa constant domain following the V_L sequence (Figure 5-2, A).

ECL-mAb IgG was reformatted to Fab using standard molecular biology techniques. The DNA sequence encoding the V_H domain (Section 3.2.13) was digested using *HindIII* and *XhoI* and ligated into the pMRbFabnh plasmid. The pMRbFabnh plasmid is based on the pMH vector and encodes for a rabbit C_{H1} domain downstream of the V_H domain. The final protein product from the plasmid is a mature Fab heavy chain fragment of rabbit origin (Figure 5-2, B). The plasmid DNA encoding the V_L domain was used from previously prepared stock (Section 3.2.13).

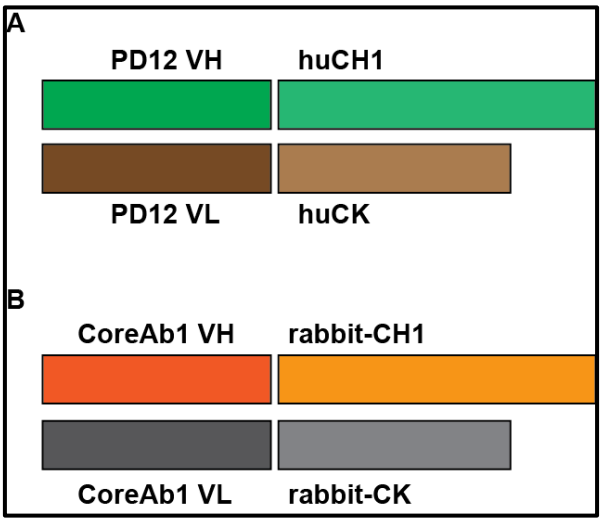


Figure 5-2: The variable and constant domains of ECD-mAb (A) and ECL-mAb (B) Fab fragment

5.2.4 ECD-mAb and ECL-mAb Fab expression and purification

Fab expressions were performed using the Expi293 expression system as described previously (section 2.2.2). Briefly, 500 ml of Expi293 cell suspension at a density of 2 x 10^6 cells/ml were transfected with 250 µg of plasmid encoding for the heavy and light chains respectively using Expifectamine (ThermoFisher Scientific). The cells were incubated for 5

days in a 37°C incubator with 8% CO_2 and constant stirring. The cells were harvested and the supernatant was filtered using a 0.22 µm filter device (Millipore) prior to protein purification.

Both Fab samples were purified using an Akta Pure system (GE Healthcare) capable of performing tandem purifications. Samples were loaded onto a 50 ml Protein G column (GE Healthcare) at a flow-rate of 5 ml/min followed by 2 CV equilibration with PBS, pH 7.4. The column was washed with 2 CV of PBS followed by a 3 CV elution using 0.1 M glycine buffer, pH 2.7 and 8 ml fractions were collected. A column cleaning step was included between isolation of the two Fab samples which included sequential addition of of 1 CV PBS, 2 CV 10% methanol, 2 CV PBS and 2 CV of 6 M GuHCl at a follow-rate of 5 ml/min. Relevant fractions were pooled and checked for homogeneity using analytical size exclusion chromatography.

Affinity purified ECD-mAb Fab was further purified using gel-filtration chromatography. Pooled Fab sample was loaded onto a S200 Sepharose column (HiLoad 16/60) using the Akta system. The sample was purified isocratically using PBS pH 7.0 at a flow-rate of 1 ml/min. Relevant fractions were pooled and checked for homogeneity using analytical SEC. All analytical SEC steps were performed using a TSK Gel 3000 column attached to an Agilent 1100 HPLC system.

5.2.5 Hydrogen-Deuterium Exchange- Mass spectrometry (HDX-MS) analysis of ECD-mAb and ECL-mAb antibody

HDX-MS was used to determine protection in the deuterium uptake of the PTH1R-ECD or ΔNΔC171-491 upon Fab binding. ΔNΔC171-491 was purified using affinity purification as described previously (Section 4.2.8) and eluted in 50 mM Tris, 150 mM NaCl, 0.01% LMNG and 0.002% CHS, pH8.0.

20 µM ECD was analysed with/without 20 µM ECD-mAb Fab, and 13.8 µM ΔNΔC171-491 was analysed with/without 20.7 µM Fab. Liquid handling was accomplished using the LEAP PAL robotic system. 3 µl of the protein solution was mixed with 57 µl of the H_2O equilibration buffer (time 0) or the D_2O labelling buffer (incubated at 20°C for 30 s, 2 min, 15 min, 1 hr or 4 hr). The equilibration and labelling buffers were 10 mM potassium phosphate in

H_2O (pH 7.0) or D_2O (pD 7.0), respectively, and included 0.01% LMNG for ΔNΔC171-491. 50 µl of each reaction mixture was added to 50 µl of quench solution cooled to 1°C, before immediate injection into the Waters HDX module and Acquity M-Class UPLC system (50 µl sample loop). Quench solution was prepared by mixing 4 M guanidinium-HCl (Gu-HCl), 62.5 mM TCEP, 100 mM phosphate in H_2O, pH 2.4 for ECD and 100 mM potassium phosphate in H_2O, pH 2.4 for ΔNΔC171-491. Upon injection, the sample was washed over a Waters Enzymate pepsin column using 0.02% HCOOH in H_2O at a flow rate of 100 µl/min with a pressure of approximately 6500 psi. Resulting peptides were trapped on a Waters Acquity UPLC BEH C18 VanGuard trapping column (2.1 x 5 mm, 1.7 µM particle) over 3 minutes. Peptides were then washed off the trap column onto an analytical Waters Acquity UPLC BEH C18 column (100 x 1.0 mm, 1.7 µM particle), and the following gradient used for elution: 0 mins: 5% B; 6 mins: 35% B; 7 mins: 40% B; 8 mins 95% B; flow rate 40 µl/min (Solvent A = 0.02% HCOOH in H_2O; Solvent B = 0.02% HCOOH in MeCN) followed by 2 wash steps. Mass spectrometry data were collected on a Waters Synapt G2si instrument, over the m/z range 50-2000 Th, with a scan rate of 0.3 s. MSe data were acquired using a trap collision energy ramp of 18 to 40 V for the high-energy function. Mass calibration was performed using the MS/MS spectrum of doubly charged [Glu-1]-fibrinopeptide B, and lockmass data on the same peptide were acquired for mass correction during data processing. Data were collected in triplicate, with a blank run performed between each set of 3.

Data were processed using PLGS v3.0.2 and DynamX v3.0 software packages from Waters. PLGS processing parameters included: Low Energy Threshold: 100 counts; Elevated Energy Threshold: 50 counts; Elution Start Time: 1 minute; Elution End Time: 9 minutes; Intensity Threshold: 500 counts. PLGS Workflow search parameters included: Minimum fragment ions matched: 3; Primary digest reagent: non-specific; Variable glycosylation modification: N-linked; False discovery rate: 4. Data were exported into DynamX and peptide assignments filtered further as follows: Minimum intensity: 1000; Maximum sequence length: 25; Minimum products per amino acid: 0.2; Maximum MH+ error: 10 ppm. After processing, all assignments were interrogated manually, and only peptides with a suitable signal to noise

ratio and unambiguous peak-picking were taken forward. Final data representing mean and standard deviation of the triplicate measurement were plotted using GraphPad Prism 7.

The HDX-MS experimental work and the final data analysis was performed by Dr Rebecca Burnley, UCB.

5.2.6 ECL-mAb Fab and DDM stabilised ΔNΔC171-491 complexing and purification

ΔNΔC171-491 was solubilised using DDM and affinity purified using Strep-Tactin XT as described previously (Chapter 4, Section 4.2.8.2). Affinity purified receptor, at a final concentration of 28 μM was mixed with loop-binding ECL-mAb Fab (final concentration of Fab: 33 μM) and incubated overnight at 4°C. The complex was gel-filtered using a Superose 6 column (16 x 300 mm) attached to a HPLC system. The complex was purified isocratically using running buffer (50 mM Tris, 150 mM NaCl, 0.05% DDM and 0.01% CHS) with a constant flow-rate of 0.3 ml/min at 4°C. 500 μL fractions were collected and relevant fractions were pooled and concentrated using a centrifugal filtration device with a 100 kDa molecular weight cut-off.

Western-blotting and SDS-PAGE were used to confirm successful complexation of Fab and the receptor. Fractions from the gel-filtration separation were loaded onto 4-20% Tris-glycine gel and separated using a constant voltage of 225 V for 55 minutes. Coomassie blue staining was used to visualise the separated protein bands on the SDS-PAGE gel. For Western blotting, the protein bands were transferred onto a PVDF membrane using a semi-dry blotting technique (iBlot). To detect ΔNΔC171-491, the membrane was stained with HRP-conjugated anti-Strep II tag antibody (1: 4000) (Novagen). For Fab detection, HRP-conjugated goat anti-rabbit $F(ab)_2$ specific IgG (Jackson Immunoresearch) was used. The stained blots were developed with Amersham ECL select (GE Healthcare) and imaged using an ImageQuant LAS4000 (GE Healthcare).

5.2.7 Cryo-EM analysis of ECL-mAb Fab binding to DDM stabilised ΔNΔC171-491

5.2.7.1 Sample freezing on grid

The ECL-mAb Fab: ΔNΔC171-49 complex (referred to as Fab-receptor complex from hereon) was frozen on to a Quantifoil Copper 300 mesh grid with hole size of 1.2/1.3 µm. The grid was glow-discharged for 60 seconds at 25 mA using a PELCO easiGlow™ Glow Discharge Cleaning System (Ted Pella). A total of 2.5 µl of the prepared complex was applied to the grid. The grid was then blotted to remove excess liquid using a FEI Vitrobot Mark IV (ThermoFisher Scientific) at 4°C with 100% humidity. The grid was blotted with a blotting force set at +7 and blotting time of 2.5 seconds. The blotted grid was immediately plunge-frozen into liquid ethane that was pre-cooled to -196°C using liquid nitrogen. The frozen grid was carefully transferred into a storage box and kept at -196°C.

5.2.7.2 Data collection

Micrographs of the prepared grid were collected on a FEI Titan Krios microscope (ThermoFisher Scientific) operated at 300 keV. Images were recorded at a nominal magnification of x 56,000 on a Falcon III 4k x 4k direct electron detector (FEI, Thermo Fisher), resulting in a 1.07 Å/pixel sampling rate on the specimen level. Micrographs were collected with a 3.5 µm defocus value in linear mode, with 3 seconds' exposure and an electron dose of 0.5 $e^-/Å^2$. The recorded micrographs were displayed and annotated by Digital Micrograph 3 package (FEI, Thermo Fisher).

Cryo-EM data collection and analysis was performed by Dr Jun He, UCB.

5.3 Results

5.3.1 ECD-mAb is a weak cAMP antagonist

The ECD-mAb was tested using an *in vitro* cAMP assay to determine its role in cAMP regulation through G_s. Using a single point assay, no agonist activity was detected but it appeared to be a weak antagonist (Section 2.3.8, Figure 2-16). ECD-mAb was further tested

for antagonism using a concentration-response experiment where CHOK1 cells stably expressing PTH1R were incubated with a concentration range of ECD-mAb, following which the cells were challenged with either ~EC_{80} or EC_{20} concentration of PTH (1-34). The concentration-response curves are shown in Figure 5-3 below:

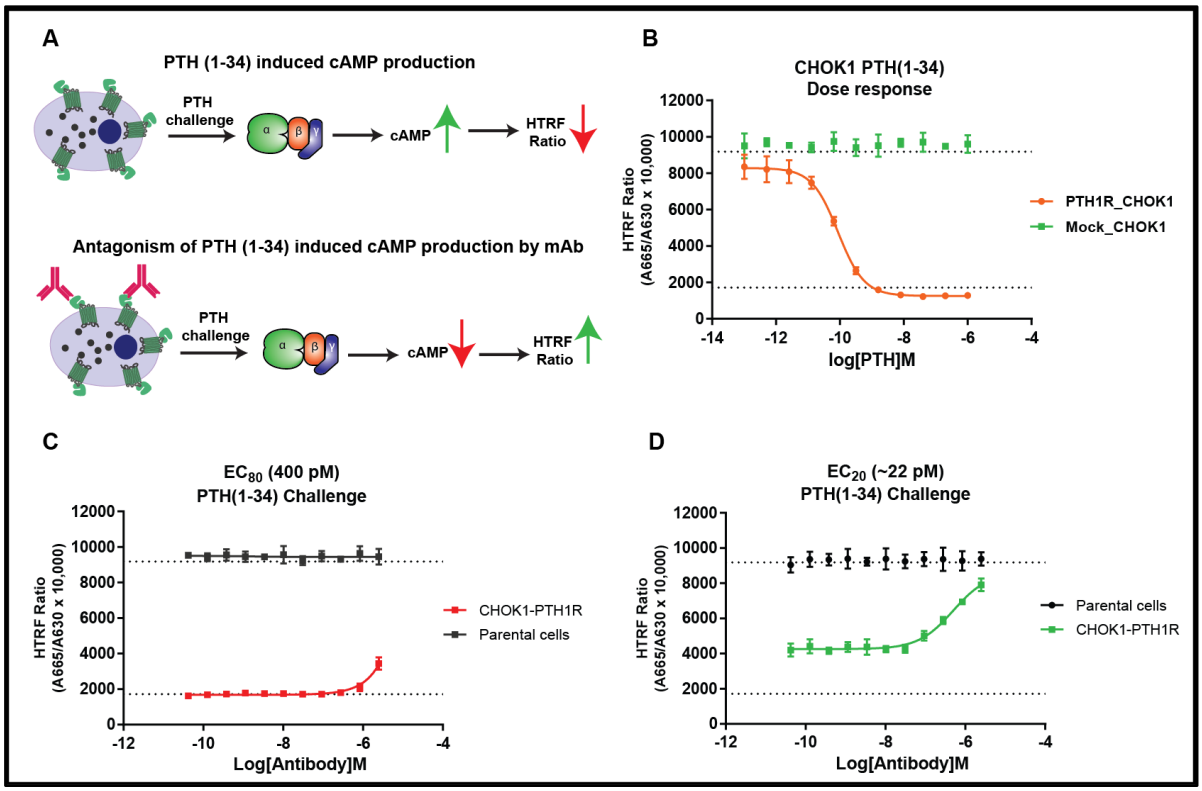


Figure 5-3: cAMP antagonism by ECD-mAb scFvFc

A) Schematic representation of PTH (1-34) induced G_s agonism leading to an increase in intracellular cAMP levels which in turn reduces the HRTF ratio. In mAb mediated antagonism, cells are incubated with a concentration-range of mAb followed by either the EC_{20} or EC_{80} concentration of PTH (1-34) challenge. A decrease in intracellular cAMP production would result in an increase in HTRF ratio. B) Concentration-response curves for PTH (1-34) challenge on CHOK-1 cells stably expressing PTH1R (orange) and parental CHOK1 cells (green). The concentration-response curve was used to calculate the EC_{50}. C) cAMP antagonism using parental (black) and stable CHOK-1 cells shows weak antagonism at high concentrations of ECD-mAb when cells are challenged with ~EC_{80} concentration (400 pM) of PTH (1-34). Similarly, antagonism at EC_{20} (22 pM) challenge of PTH (1-34) was tested (D).

The assay is based on immunocompetition, a decrease in intracellular cAMP would cause an increase in HTRF ratio. It is clear from the above data that ECD-mAb exhibits weak antagonism when challenged with high concentration (EC_{80}) of PTH (1-34) while mAb mediated antagonism increases at lower concentration of PTH (1-34). The parental cell did not show any effect on cAMP modulation with PTH (1-34) or ECD-mAb.

5.3.2 ECD-mAb antagonises β-arrestin recruitment

The ability of ECD-mAb to modulate PTH1R coupling to the β-arrestin pathway was tested using an *in vitro* assay based on enzyme fragment complementation technology (EFC) from DiscoveRx. Briefly, the cell-surface expressed PTH1R was tagged with a ProLink tag (enzyme donor), and the β-arrestin was co-expressed with a β-galactosidase enzyme fragment (enzyme acceptor). Upon receptor activation, β-arrestin is recruited to the surface and the enzyme acceptor and donor combines to form a fully functional β-galactosidase enzyme. The fully-functional enzyme acts on the substrate to produce luminescence, measured using a luminometer (Figure 5-4, A). ECD-mAb in scFvFc and Fab formats were tested in the agonist format of the assay along with PTH (1-34).

Non-linear fitting of the PTH (1-34) concentration-response curve generated an EC_{50} value of 10 ± 4.3 nM, whereas no agonism for β-arrestin recruitment was seen with ECD-mAb scFvFc alone (Figure 5-4, B). However, ECD-mAb appeared to antagonise β-arrestin recruitment with low nanomolar IC_{50} in both the scFvFc and Fab format (Figure 5-4, C, D). The calculated IC_{50} values for antagonism by scFv-Fc and Fab were found to be ~104 ± 14.1 nM (n=2) and ~182.6 ± 1.5 nM (n=2) (raw RLU fitted without any constrains) and 62.6 ± 6.5 nM and 143.5 ± 0.7 nM (normalised RLU values fitted with bottom values constrained to 0) respectively.

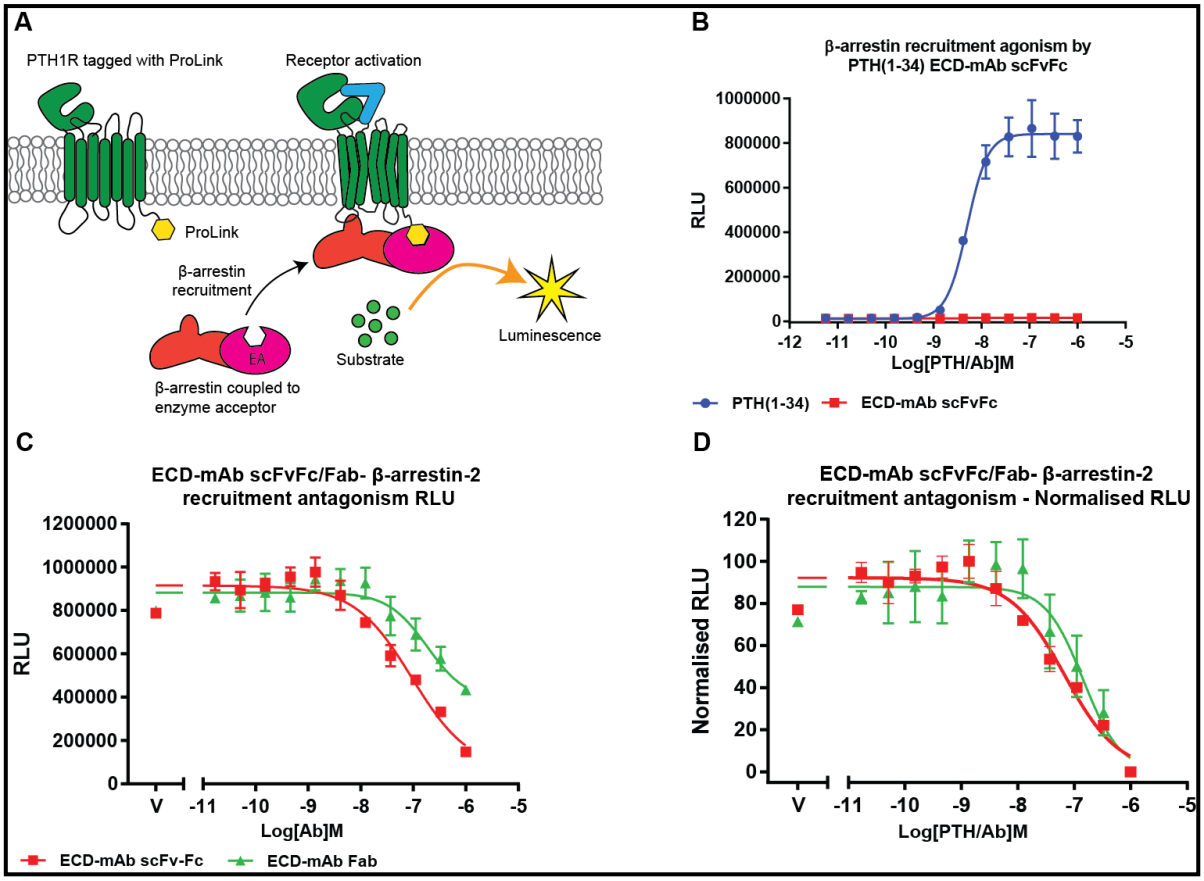


Figure 5-4: β-arrestin recruitment agonism and antagonism by ECD-mAb scFvFc and Fab.

A) Schematic representation of β-arrestin recruitment assay. B) PTH (1-34) (blue) and ECD-mAb scFvFc (red) concentration-response curve for β-arrestin recruitment agonism gave an IC_{50} of 10 nM for PTH (1-34) while no agonism was seen for the ECD-mAb alone. C) Effect of ECD-mAb on PTH (1-34)-mediated β-arrestin recruitment shows a concentration dependent antagonism by both the scFv-Fc (red) and Fab (green) versions of ECD-mAb. The data was fitted without constraints using a Sigmoidal equation. D) Normalised RLU plot where the lowest measured value was constrained to 0 and the data fitted with a sigmoidal equation.

5.3.3 ECL-mAb is a neutral allosteric ligand (NAL)

The ability of ECL-mAb to modulate receptor coupling to the cAMP and β-arrestin signalling pathways was also assessed. To determine agonist activity, PTH1R expressing stable cells were challenged with different concentrations of ECL-mAb and to determine the antagonistic activity, cells were pre-incubated with different concentrations of the IgG, followed by a PTH (1-34) challenge at either ~EC_{20} or EC_{80} concentrations. It was found that ECL-mAb IgG and Fab were unable to modulate cAMP signalling in either agonist or antagonist format of the assay as shown in (Figure 5-5).

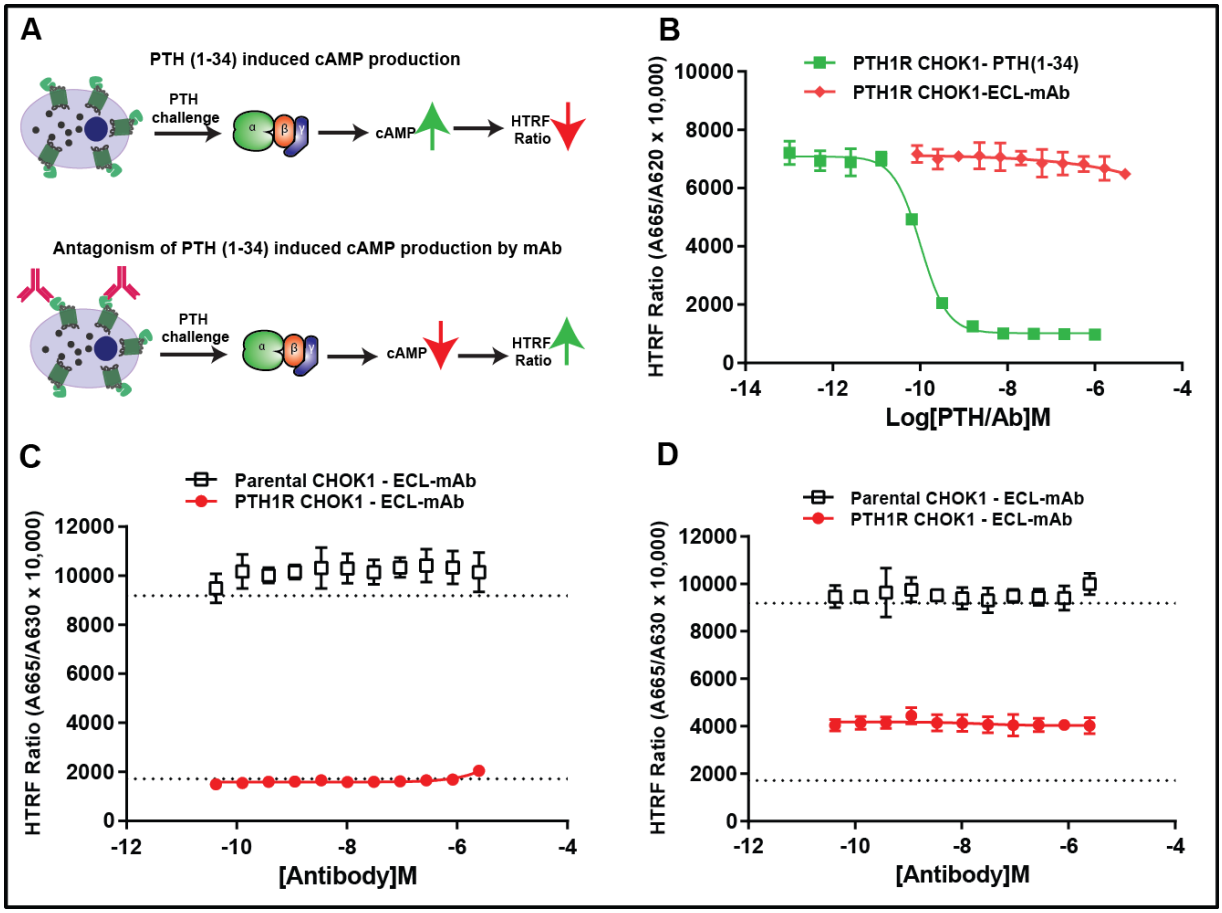


Figure 5-5: cAMP agonism and antagonism by loop binding ECL-mAb IgG

A) Schematic representation of PTH (1-34) induced G_s agonism leading to an increase in intracellular cAMP levels which in turn reduces the HRTF ratio. In mAb mediated antagonism, cells are incubated with a concentration-range of mAb followed by EC_{20} or EC_{80} PTH (1-34) challenge. A decrease in intracellular cAMP production would result in an increase in HTRF ratio. B) Concentration-response curves of PTH (1-34) and ECL-mAb IgG to determine cAMP agonism by PTH1R activation. The PTH (1-34) challenge gave an EC_{50} of ~87 pM, while ECL-mAb failed to show any up-regulation of intracellular cAMP. C, D) ECL-mAb did not exhibit any antagonism of PTH (1-34)-mediated cAMP up-regulation. The antagonism was tested in presence of 400 pM (C) and 25 pM (D), equivalent to EC_{20} and EC_{80} respectively. The antagonism assay was performed using parental cells (black open symbol) and CHOK-1 cells stably expressing PTH1R (red closed circles).

ECL-mAb IgG was also unable to modulate β-arrestin recruitment as shown in Figure 5-6.

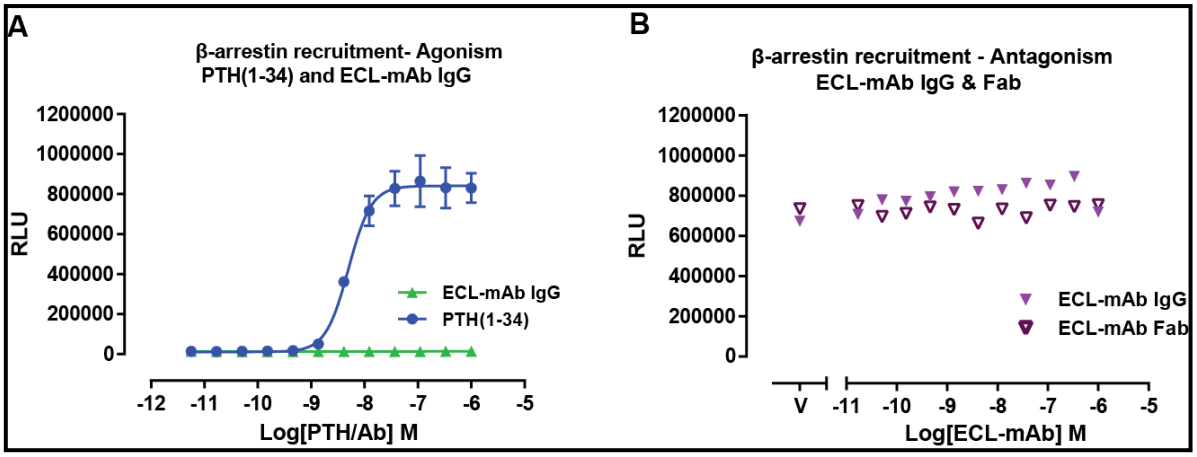


Figure 5-6: β-arrestin recruitment agonism and antagonism by ECL-mAb IgG

A) PTH (1-34) and ECL-mAb IgG concentration-response experiment to determine agonism of β-arrestin recruitment shows no agonism by ECL-mAb IgG (green) while a concentration-dependent agonism was exhibited by PTH (1-34) (blue). The EC_{50} of β-arrestin recruitment by PTH (1-34) was found to be 10 nM. B) A concentration-response curve highlighting lack of antagonism of PTH-mediated β-arrestin recruitment by ECL-mAb IgG (solid triangle) or ECL-mAb Fab (open triangle) formats. Antibody incubated cells were challenged with EC_{80} concentration (40 nM) of PTH (1-34).

The ECL-mAb IgG binding to PTH1R did not affect PTH (1-34) binding or function which suggests that it is an allosteric binder. It was unable to modulate either G-protein dependent signalling or β-arrestin recruitment and based on the above data the ECL-mAb appeared to be a neutral allosteric ligand (NAL).

5.3.4 ECD-mAb and ECL-mAb binds the full-length receptor with high affinity

SMA-stabilised receptor variants were used to determine the binding kinetics of ECD-mAb and ECL-mAb IgG using surface plasmon resonance (Biacore T200). The solubilised receptor was enriched using affinity capture (Talon or Strep Tactin XT ®) and used for SPR analysis. The receptor variants contained C-terminal 10-His tags used for capture to the Biacore chip immobilised with His-tag specific polyclonal antibody. ECD-mAb bound to the ΔC29-491 construct with an affinity of ~4 nM and no binding was seen with ΔNΔC171-491 due to the lack of the ECD (Figure 5-7, A & B). ECL-mAb on the other hand, bound to ΔC29-491 and ΔNΔC171-491 with equal affinities (~0.5-1 nM) (Figure 5-7, C & D). Both the antibodies were tested using SMA-stabilised ΔC29-491 and ΔNΔC171-491 (Figure 5-7, E) constructs using single cycle kinetics. The kinetics data for both the mAb is summarised in Table 5-1

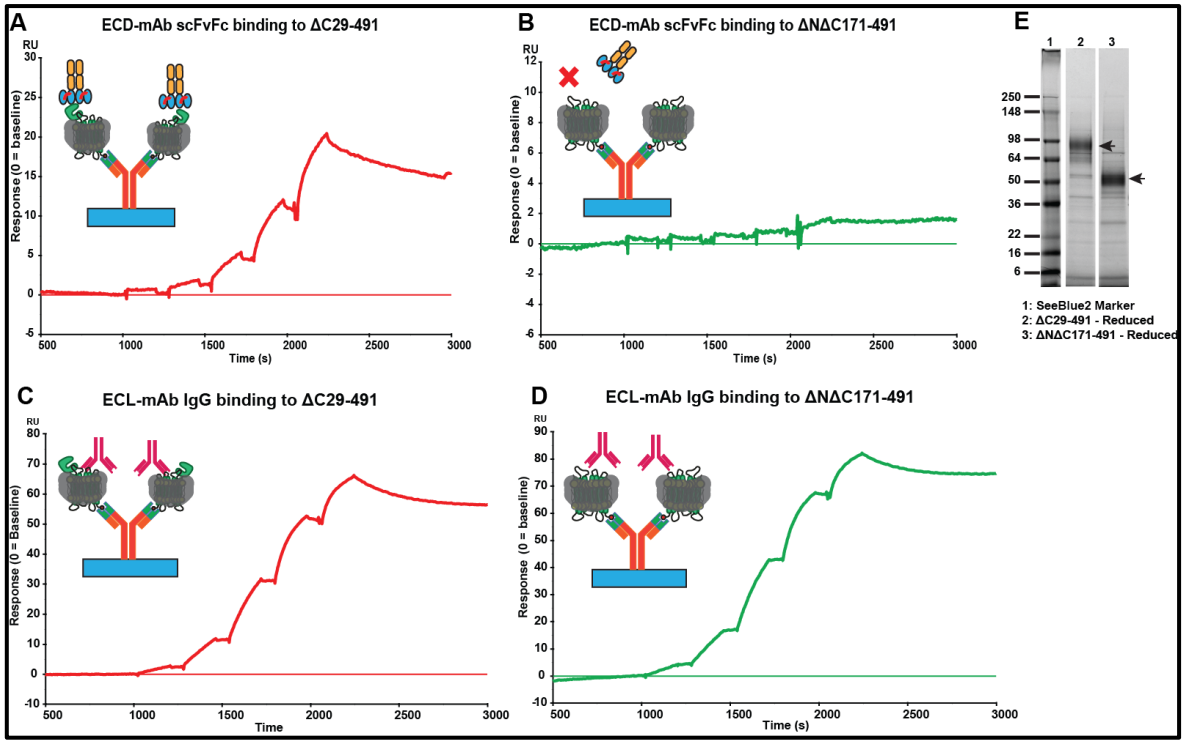


Figure 5-7: Binding kinetics analysis of ECD and ECL-mAb binding to purified PTH1R receptor constructs.

Single kinetics analysis of ECD-mAb binding to the SMA-solubilised ΔC29-491 (A) and ΔNΔC171-491 (B) constructs. While the mAb exhibits concentration-dependent binding to the ΔC29-491 construct, in the absence of ECD, the mAb shows no binding as seen with the ΔNΔC171-491 construct (B). Single kinetics analysis of ECL-mAb binding to the SMA-solubilised ΔC29-491 (C) and ΔNΔC171-491 (D) constructs. A similar ECL-mAb binding profile is obtained for both receptor constructs. E) SDS-PAGE analysis confirming enrichment of receptor variants. The expected position on the gel is shown by the arrows. Lane 1: molecular weight marker, 2: ΔC29-491 and 3: ΔNΔC171-491.

Table 5-1: Table summarising the affinity measurement of ECD-mAb and ECL-mAb IgG binding to SMA-stabilised PTH1R constructs.

Run-1					
Sample[1]	**Construct[2]**	**ka (1/Ms)[3]**	**kd (1/s)[4]**	**KD (M)[5]**	**$t_{1/2}$ (min)[6]**
ECD-mAb scFvFc	ΔC29-491	8.78E+04	2.81E-04	3.20E-09	40.93
ECD-mAb scFvFc	ΔNΔC171-491	N/A	N/A	N/A	N/A
ECL-mAb IgG	ΔC29-491	1.29E+05	1.35E-04	1.05E-09	85.19
ECL-mAb IgG	ΔNΔC171-491	1.16E+05	1.07E-04	9.17E-10	107.48
Run-2					
Sample	**Construct**	**ka (1/Ms)**	**kd (1/s)**	**KD (M)**	**$t_{1/2}$ (min)**
ECD-mAb scFvFc	ΔC29-491	1.13E+05	4.54E-04	4.04E-09	25.33
ECD-mAb scFvFc	ΔNΔC171-491	N/A	N/A	NA	N/A
ECL-mAb IgG	ΔC29-491	1.52E+05	1.35E-04	8.84E-10	85.19
ECL-mAb IgG	ΔNΔC171-491	1.74E+05	1.02E-04	5.90E-10	112.75

[1] ECD-mAb was raised against the ECD only and ECL-mAb IgG was raised against the extracellular loops (ECL) of the protein
[2] SMA stabilised PTH1R construct immobilised and used for mAb binding
[3] ka = on-rate
[4] kd = off-rate
[5] KD represents the measured affinity in M
[6] $t_{1/2}$ represents the complex half-life values, ($t_{1/2} = \ln(2)/k_{off}$)

The ECL-mAb binds to both versions of the receptor with sub-nanomolar affinities indicating that presence of the ECD does not affect mAb binding. It is also interesting to note that the complex half-life measurements for ECD-mAb are lower than those for the ECL-mAb. This, taken with the higher off-rate exhibited by the ECD-mAb, indicates that this antibody forms less stable receptor complexes. It is possible that the format of the ECD-mAb, an scFv-Fc construct as opposed to the ECL-mAb IgG construct, might influence both the off-rate and complex half-life.

5.3.5 ECD-mAb binds to the N-terminal region of PTH1R ECD

Identification of the binding site for the ECD-mAb was determined using hydrogen-deuterium exchange-mass spectrometry (HDX-MS). This was achieved using soluble ECD domain and ECD-mAb, complexed and incubated in a deuterated buffer. The deuterium uptake by various peptides was checked and the peptides specific for the N-terminus of ECD found to be protected when bound to the ECD-mAb. Figure 5-8 below shows the difference in deuterium uptake between the apo-ECD and ECD-mAb scFvFc complex for the peptides which exhibited the highest difference in deuterium uptake. The overall epitope was found to be ^{31}VMTKEEQIFL^{40}—^{49}EKRLKEVLQRPA^{60}. It should however be noted that peptide corresponding to ^{41}LHRAQAQC^{48} was not detected in the MS analysis (Figure 5-8, C) and may or may not be part of the epitope. Also, from the HDX-MS data it is not possible to identify the key residues which form the epitope and only peptide level details could be discerned.

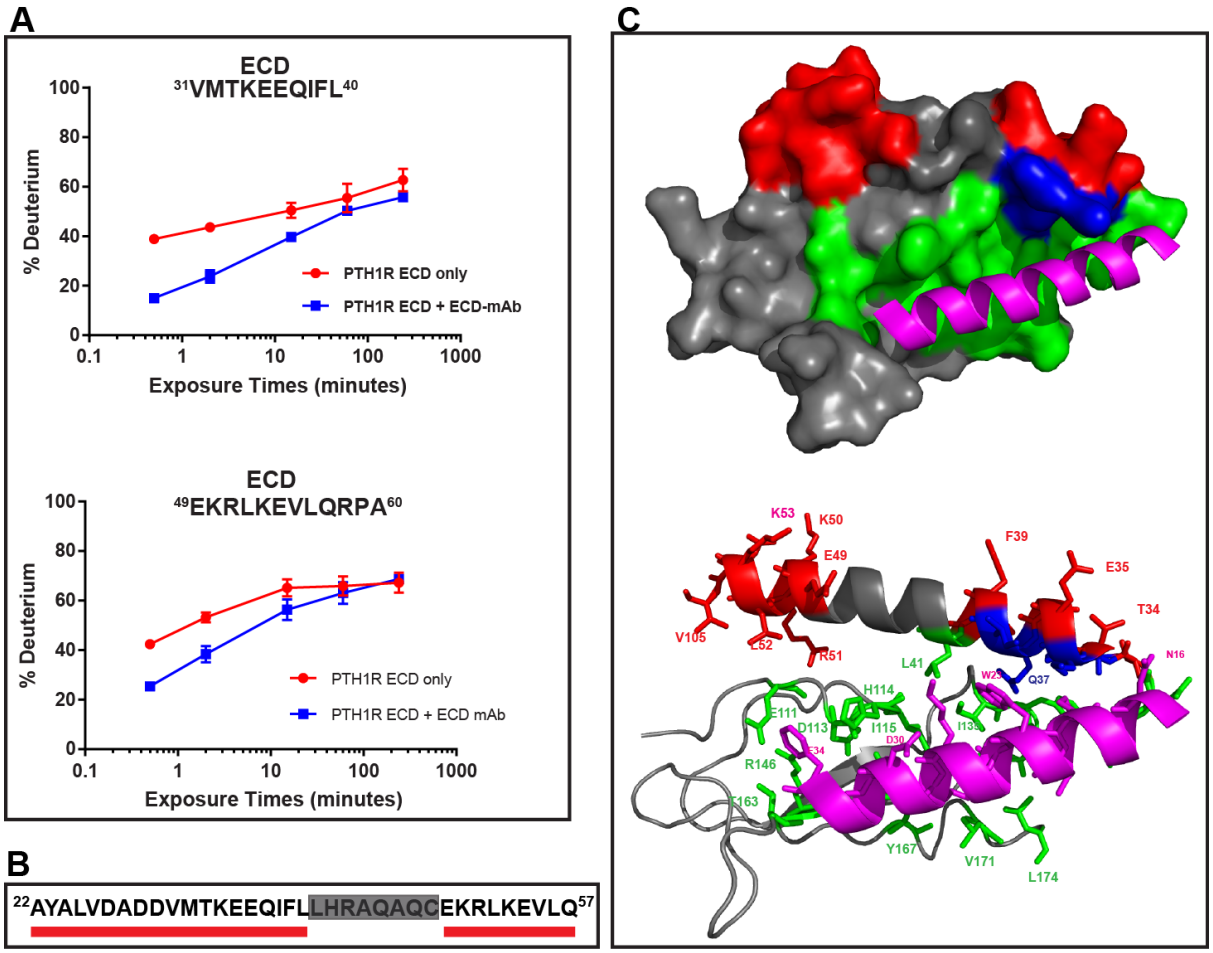


Figure 5-8: HDX-MS analysis of PTH1R ECD bound to ECD-mAb scFvFc

A) Deuterium uptake plot showing the difference in apo (red) and mAb bound PTH1R-ECD (blue). Peptides corresponding to the sequence ^{31}VMTKEEQ----EVLQRPA^{60} exhibited slow exchange rates when bound to ECD-mAb scFvFc. B) The coverage map (shown by red bar) shows incomplete sequence coverage and peptide covering the region ^{41}LHRAQAQC^{48} (shown with grey box) was not detected in the MS analysis. C) Top: Surface representation of the ECD-PTH crystal structure (PDB ID 3C4M) showing binding of PTH into the hydrophobic groove of the ECD. Bottom: The HDX-MS derived epitope and the PTH binding residues are shown with stick representation while the overall structure is shown in cartoon representation. Residues which form the ECD-mAb epitope are represented as red sticks while residues involved in PTH (1-34) binding (within 8Å cut-off) are shown as green sticks. Some ECD-mAb epitope residues also overlapped with PTH binding residues and these are shown in blue stick representation. PTH is shown in magenta cartoon representation and the important PTH residues interacting with ECD are shown as magenta sticks.

The residues determined by HDX-MS were mapped onto the crystal structure of PTH1R ECD (PDB ID: 3C4M) (Figure 5-8, B). While the overall epitope of the mAb appears to be largely separate from the PTH (1-34) binding site (Figure 5-8, C, residues shown in green stick representation), some overlap could be seen as demonstrated by the blue coloured residues (in stick representation) in Figure 5-8, C.

5.3.6 ECL-mAb binds to the extra-cellular loop -1 of PTH1R

The epitope of loop-binding, ECL-mAb IgG, was determined using LMNG-solubilised double-truncated PTH1R construct (ΔNΔC171-491). HDX-MS was carried out on ECL-mAb IgG pre-incubated with receptor and the receptor-only control. The deuterium uptake plots for all three loops are shown in Figure 5-9. Overall, it appears that ECL 2 and 3 play no role in antibody binding and the binding site is located solely within ECL-1.

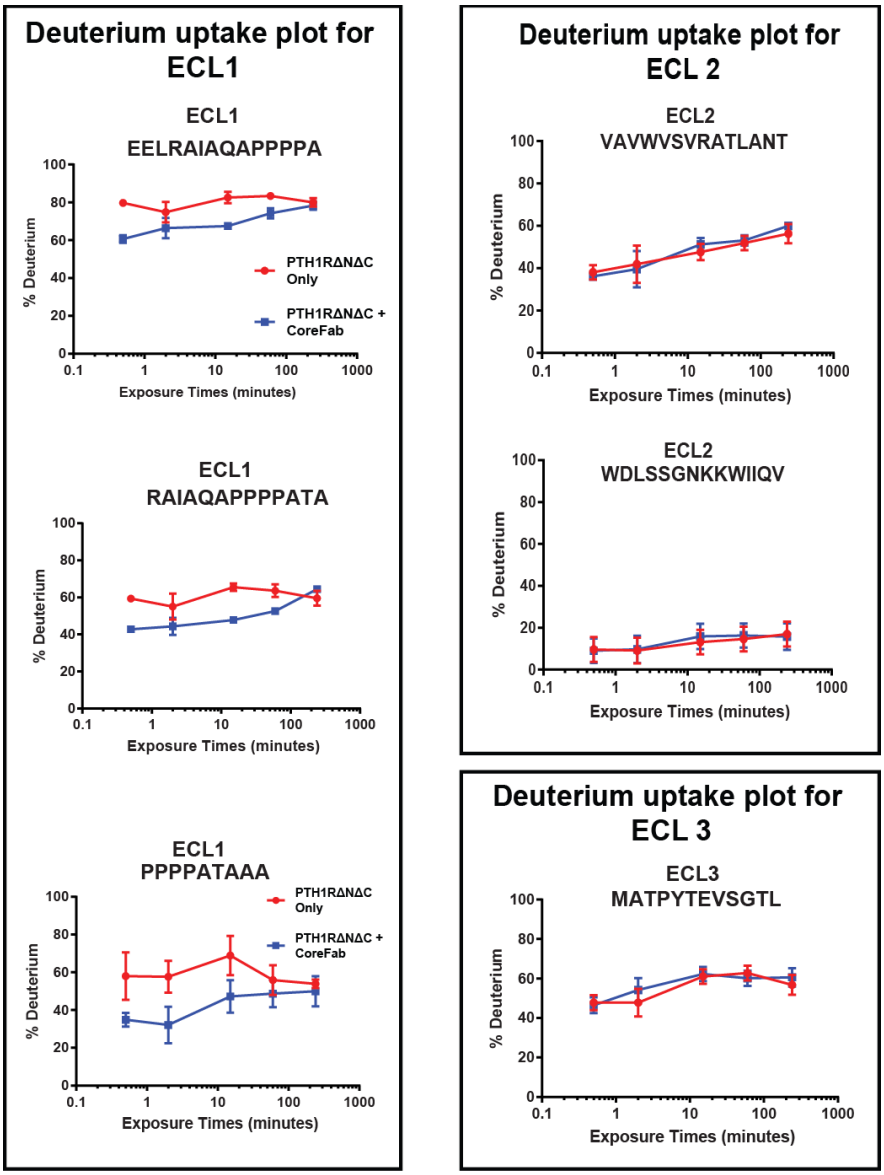
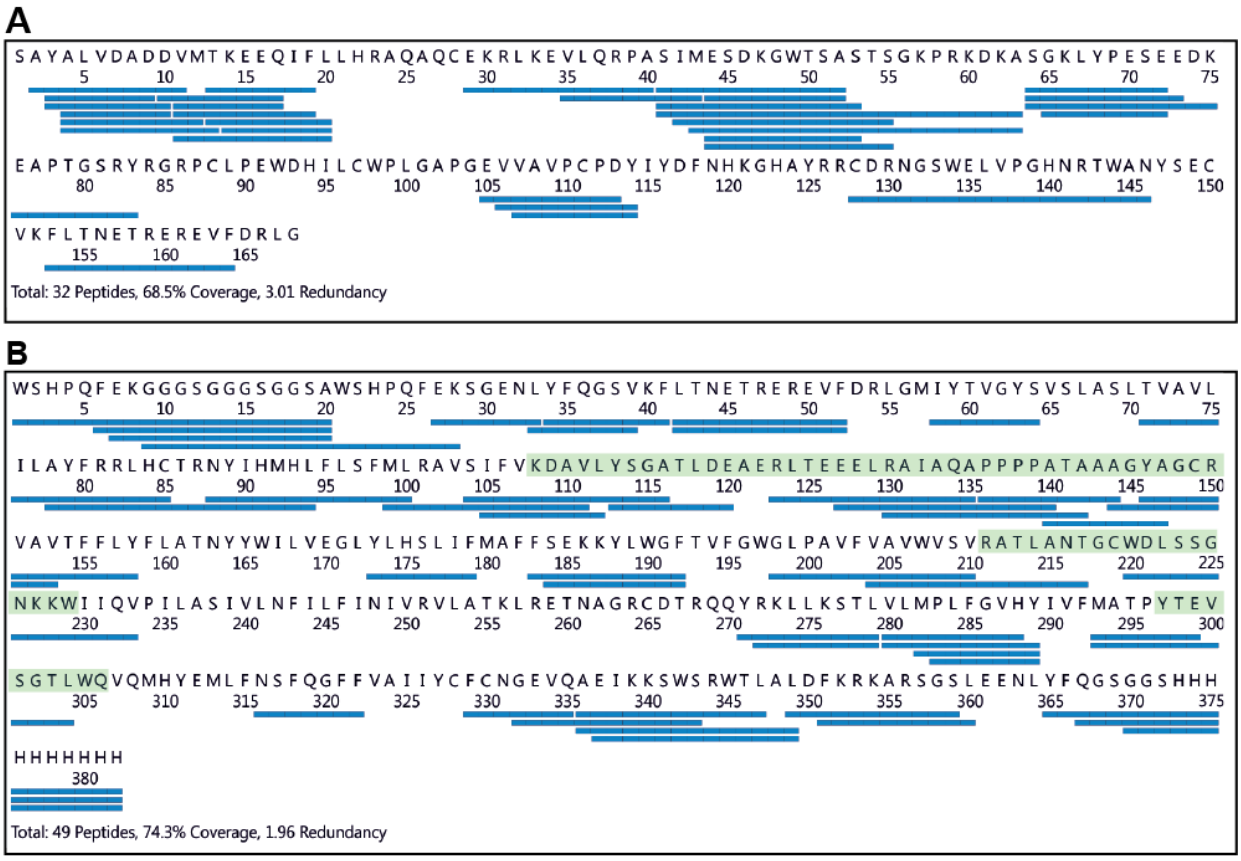


Figure 5-9: HDX-MS analysis of ECL-mAb binding to ΔNΔC171-491

Deuterium uptake plots for three extracellular loops are shown. Only ECL-1 peptides appear to show a difference in uptake when in complex with the ECL-mAb whereas peptides of ECL2 and 3 remain unchanged. The deuterium uptake by the receptor-mAb complex and the receptor only control is shown in blue and red respectively. The plot shows the change in uptake with respect to time (in sec).

The overall sequence coverage for ECD-mAb: PTH1R ECD and ECL-mAb: ΔNΔC171-491 were found to be 68.5% and 74.3% respectively similar to other HDX-MS studies in the literature (Figure 5-10, A & B). A difference chart is routinely used to rapidly determine the qualitative and quantitative differences in deuterium uptake which also shows the location of such differences (Houde, Berkowitz and Engen, 2011). With ECD-mAb, the difference chart suggested one epitope at the N--terminal end of the ECD (Figure 5-10, C), while for the ECL-mAb, the greatest difference in deuterium uptake was seen with peptides close to the ECL1 region (Figure 5-10, D).



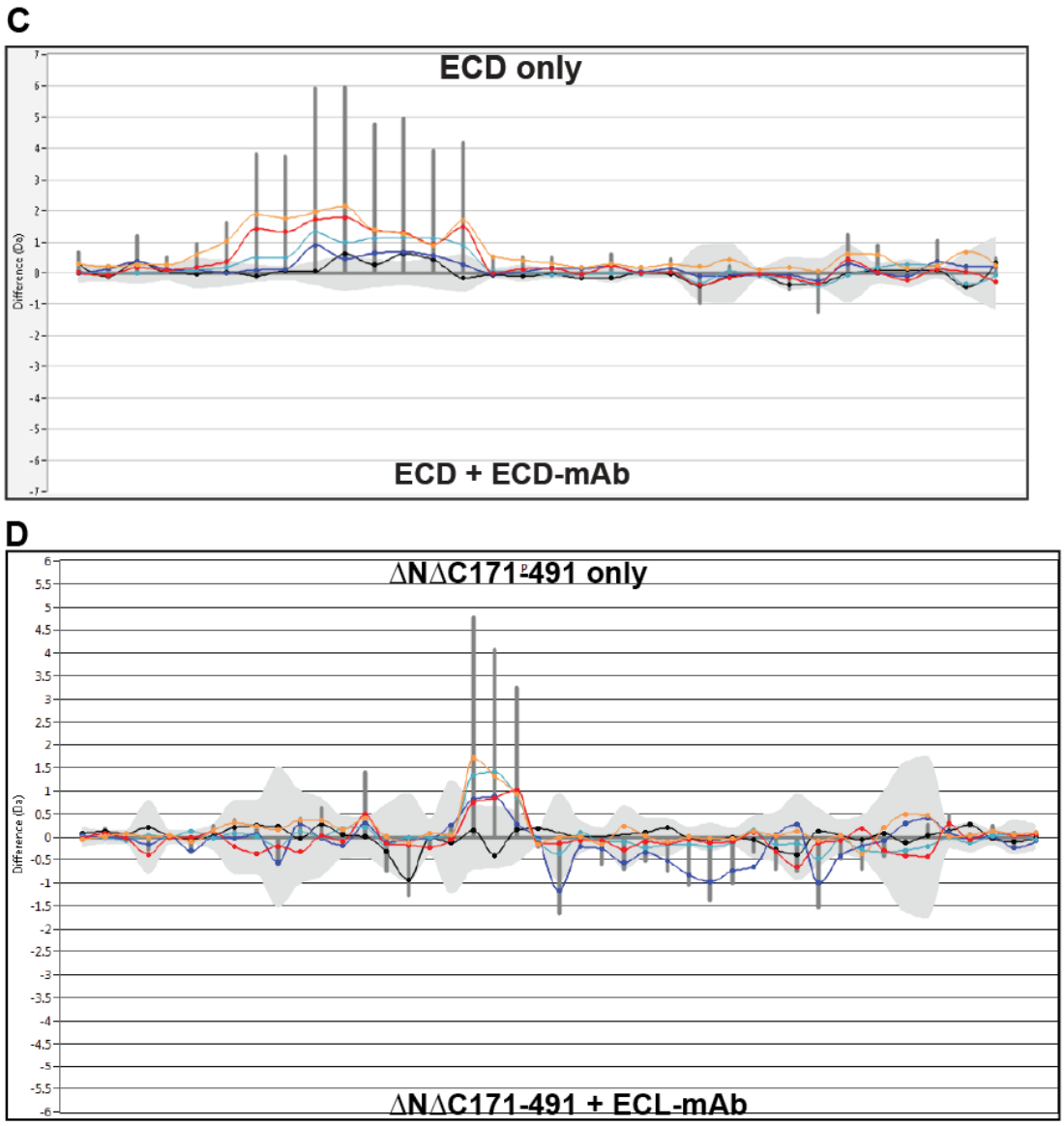


Figure 5-10: Sequence coverage map and difference chart for ECD-mAb and ECL-mAb epitope mapping by HDX-MS

A & B) Sequence coverage map of ECD-mAb and ECL-mAb binding to the ECD and ΔNΔC171-491 respectively. The ECD-mAb: ECD complex shows relatively poor sequence coverage when compared to ECL-mAb binding to ΔNΔC171-491. C & D) Shows the difference chart for ECD-mAb and ECL-mAb respectively. The region with most protection is shown by vertical bars in upward direction

5.3.7 Cryo-EM allows visualisation of ECL-mAb: ΔNΔC171-491 complex

Recently, Cryo-EM has proven to be a very useful technique for full-length structure determination and its applicability was tested with the double-truncated receptor complexed with the ECL-mAb. Affinity purified ΔNΔC171-491 was complexed with the Fab format of ECL-mAb (ECL-Fab) and purified using gel-filtration as shown in Figure 5-11. Three separate

fractions were individually collected containing the high-molecular weight (HMW) (black box), receptor-Fab complex (green box) and excess Fab (blue box) protein populations. SDS-PAGE analysis revealed a single band for the receptor-Fab complex (Figure 5-11, C, lane marked: Complex Frac). Visual analysis of the SDS-PAGE bands indicated that the HMW fraction was very similar to the complex fraction, however this might represent aggregated protein given the fact that it elutes earlier than the complex fraction on a gel-filtration column (Figure 5-11, A & B). This HMW fraction contained both Fab and receptor indicating presence of aggregated receptor-Fab complex or some conformational or glycosylation variants of the receptor in complex with the Fab.

Excess Fab was added during complex formation in order to ensure receptor saturation. It was possible to largely separate the complex from the free Fab by gel filtration. The Fab only sample migrates as a single homogenous band of the expected molecular weight (~50 kDa) on the SDS-PAGE gel (Figure 5-11, C, lane marked: Fab Frac). A band specific for receptor was also detected in the excess Fab fraction indicating co-elution or spill-over of complex fraction to the Fab fraction.

Since the receptor and Fab have similar molecular weights (~50 kDa), they co-migrate on the gel and therefore Western blotting was used to confirm the presence of both the receptor and the Fab in the complex fraction. Western blotting with an anti-Strep II tag antibody confirmed the presence of the receptor (Figure 5-11, E) while Western blotting with an anti-rabbit Fab fragment-specific antibody confirmed the presence of the ECL-Fab (Figure 5-11, D).

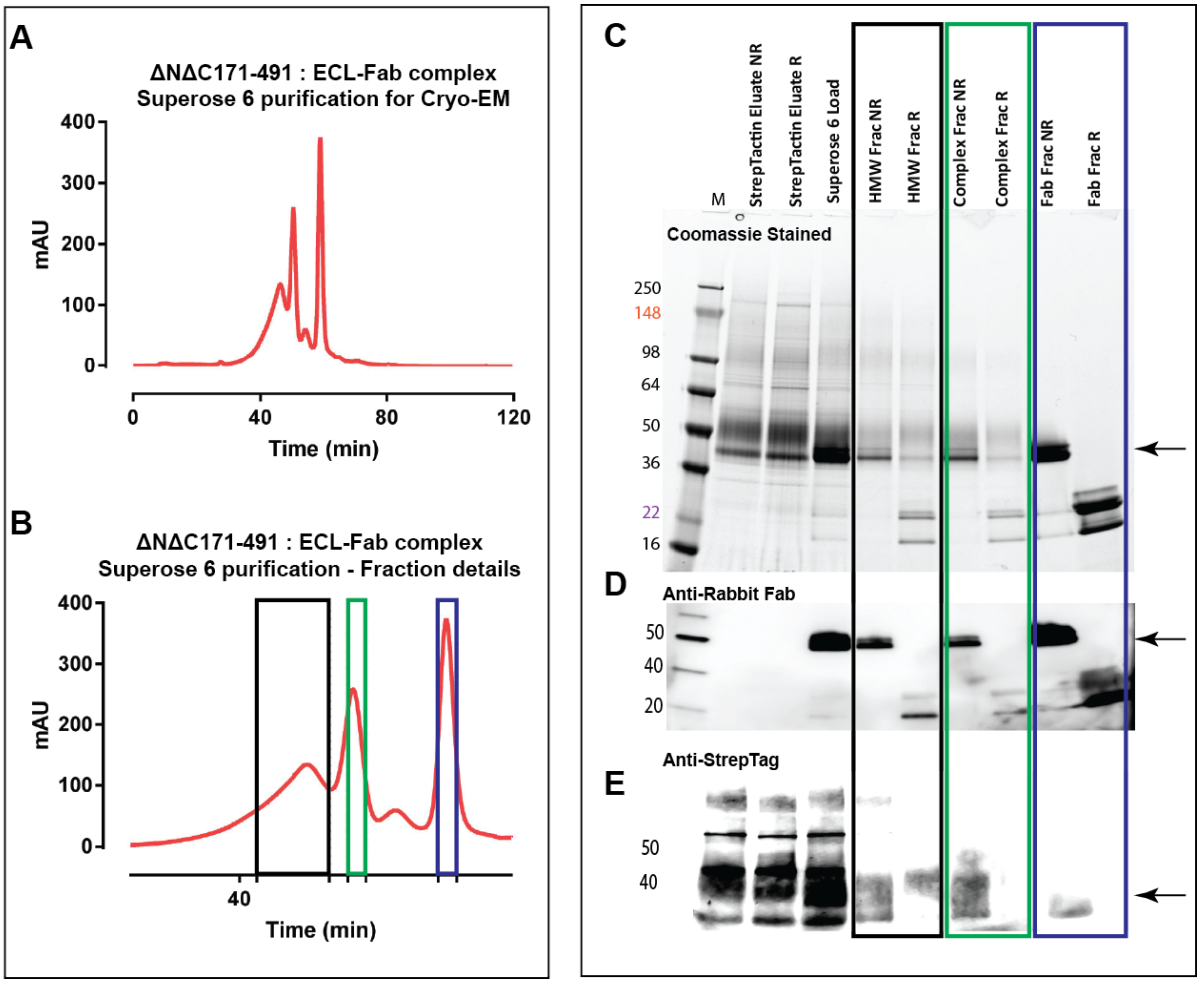


Figure 5-11: ΔNΔC171-491 – ECL-mAb complex purification using gel-filtration and fraction analysis using SDS-PAGE and Western blotting.

A) Superose 6 purification of ΔNΔC171-491 complexed with ECL-mAb. The complex was purified using an Agilent 1100 HPLC system and 0.5 ml fractions were collected. B) An enlarged version of the chromatogram shown in A, where the different peaks corresponding to HMW, complex and excess Fab are indicated with the black, green and blue boxes respectively. C) SDS-PAGE analysis of the gel-filtration fractions with each lane labelled with sample name. R: reduced and NR: non-reduced. D) Anti-Fab Western blotting shows the presence of the ECL- Fab in load, HMW, complex and excess Fab fractions. The band corresponding to the non-reduced Fab is indicated by the black arrow. E) Anti-PTH1R Western blotting using Anti-Strep Tag antibody indicates the presence of receptor in all collected fractions as shown by black arrow.

The purified receptor-Fab complex was frozen on a Cryo-EM grid to determine the overall topology of the complex (Figure 5-12, A). Buffer blank with 0.01% LMNG is also shown in (Figure 5-12, C) for comparison.

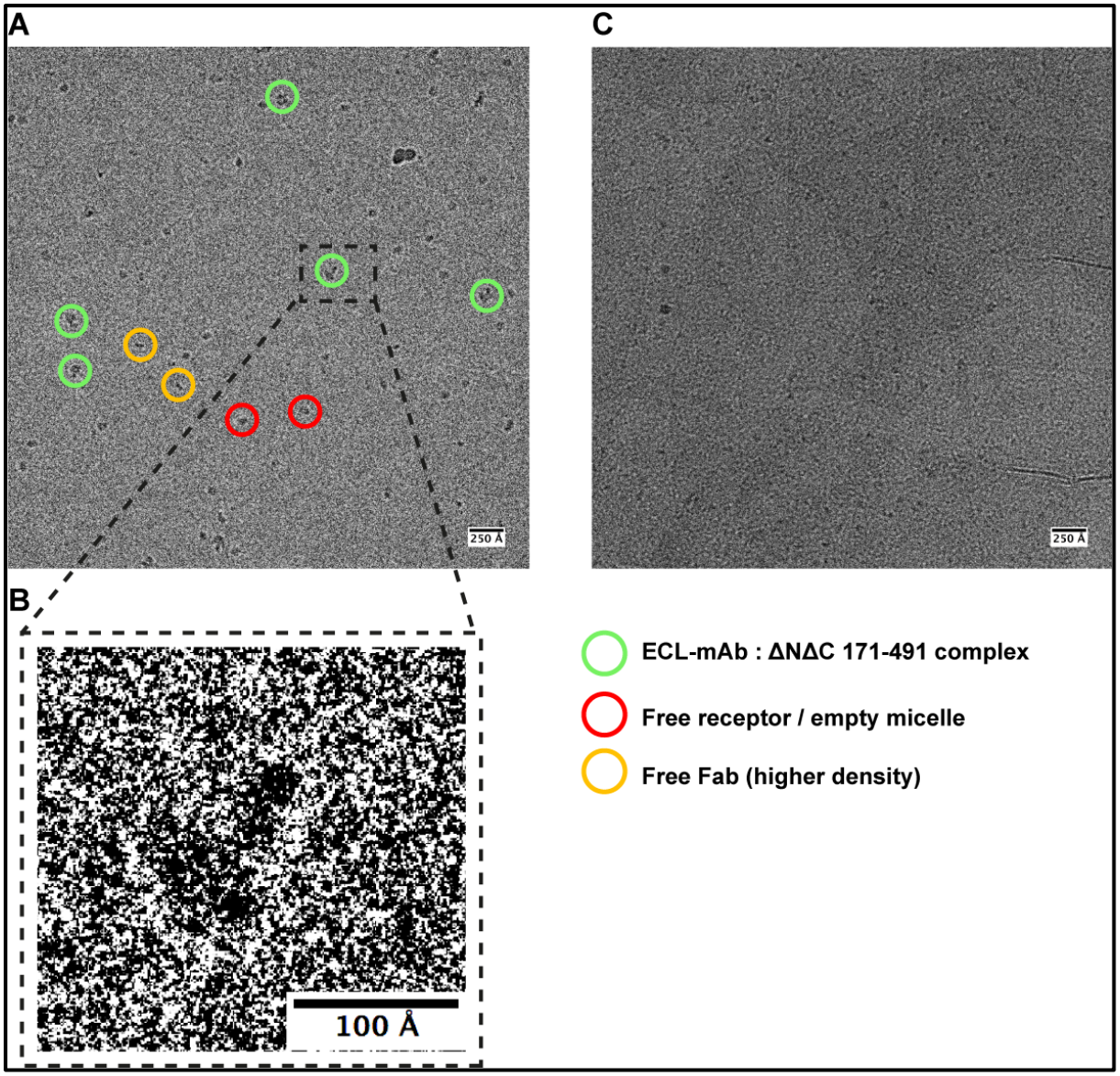


Figure 5-12: Cryo-EM micrographs showing receptor-Fab complex

A) Representative micrograph of a cryo-EM grid containing ΔNΔC171-491-ECLmAb Fab complex. B) A zoomed view of a selected particle highlights the complex formation. C) A micrograph of a buffer blank containing 0.01% LMNG is shown for comparison. The scale bar for A and C is 250 Å, while the scale bar for C is 100 Å

The image indicates successful formation of receptor-Fab complex and some free Fab and receptor/empty detergent micelles were also detected. The particles putatively representing the complex (Figure 5-12, B) were found to be approximately 8-10 nm in size consistent with published data (see Figure 5-13). A mushroom-shaped structure was visible which is potentially composed of the receptor encased in detergent micelle and a Fab molecule protruding from the micelle.

5.4 Discussion

The ability of the ECD- and ECL-mAb to modulate PTH1R mediated intracellular signalling was investigated using *in vitro* functional assays measuring intracellular cAMP levels and β-arrestin recruitment. PTH1R is also known to affect intracellular Ca^{+2} levels via $G_{\alpha q}$, however we were unable to establish a reliable assay to assess this activity.

ECD-mAb is functional

A key aim of the research outlined in the thesis was to raise functional antibodies against the ECD and ECL of PTH1R as when the project started no functional mAbs had been reported against PTH1R. Recently the Xoma corporation reported a PTH1R antagonist mAb demonstrating the suitability of the receptor as a functional mAb target (http://www.xoma.com/assets-available-for-licensure/anti-pth1r/). Here, we found that ECD-mAb was a weak antagonist for cAMP production but this effect was only detected at very high concentrations of mAb (~1 μM). This weak antagonism could be caused due to either direct competition with PTH (1-34) or steric hindrance caused by ECD-mAb binding. In any case the antagonism only at such high concentrations of the mAb is not physiologically relevant.

Interestingly, the ECD-mAb appeared to be a potent inhibitor of β-arrestin recruitment, with a nanomolar IC_{50}. It is possible that mAb binding causes conformational changes in the TMDs of the receptor which either directly hinders β-arrestin binding or alternatively prevents phosphorylation of the C-terminal tail by the GRKs which indirectly inhibits β-arrestin recruitment. The exact mechanism of the antagonism is still not clear and would require further investigation using techniques such as bioluminescence resonance energy transfer (BRET). We are not aware of any mAbs against PTH1R with a similar activity and thus the ECD-mAb is the first reported negative-allosteric modulator of β-arrestin recruitment in PTH1R. β-arrestin biased PTH1R agonists are known to have a positive pharmacological effect (Gesty-Palmer and Luttrell, 2011) but further *in vivo* studies would be required to explore the physiological effect of β-arrestin recruitment antagonism in PTH1R.

ECL-mAb is a tool mAb for studying PTH1R

The extracellular loop binding, ECL-mAb appeared to be a non-functional antibody with no effect on either PTH (1-34) mediated cAMP signalling or β-arrestin recruitment. Its effect on $G_{\alpha q}$ mediated signalling remains unknown. Loop-binding mAbs against GPCRs are quite rare and to the best of our knowledge, there are no existing loop binding mAb against PTH1R, generated using the native form of the receptor. ECLs play a key role in ligand binding and receptor activation in class B GPCR (Barwell, Conner and Poyner, 2011; Koth *et al.*, 2012; Wheatley *et al.*, 2012; Woolley *et al.*, 2017; Dal Maso *et al.*, 2018) and in PTH1R it is known that ECL-1 makes direct contact with PTH (1-34) through L^{261} (Piserchio *et al.*, 2000). The preliminary HDX-MS data for ECL-mAb appears to suggest that the mAb binding site is in ECL-1 close to the 'PPPP' motif. It is therefore quite surprising that the ECL-mAb is unable to modulate PTH (1-34) binding or signalling.

Flow cytometry (Figure 3-15) and SPR (Table 5-1) data revealed that the presence or absence of the ECD does not hinder ECL-mAb binding. This is interesting since it is known that in some members of Class B family, such as GCGR, the ECD interacts with the ECLs acting as an intrinsic negative regulator of receptor activity in the absence of substrate (Koth *et al.*, 2012). Since the binding of ECL-mAb to the full-length receptor is unhindered, it would suggest that the ECD of PTH1R interacts differently with the ECL, but this requires further investigation as the ECD-ECL interaction can differ between closely related receptors. Even though the ECL-mAb is not functional it has the potential to be a useful tool for structural elucidation of PTH1R.

SMA simplifies mAb-receptor SPR work

Next, we wanted to investigate the binding profile of both the antibodies and we used SMA-stabilised receptor to achieve this. Previously, detergents (Navratilova, Besnard and Hopkins, 2011) and nanodisc-stabilised receptor (Bocquet *et al.*, 2015) have been used for SPR analysis but in both cases the receptor was initially solubilised in detergents. Detergents replace the natural protein-protein and protein-lipid interactions with protein-detergent interaction, often leading to destabilisation of detergent solubilised membrane proteins (Popot,

2010). We wanted to develop a method where we could perform SPR measurements using purified receptor, in complete absence of detergents. We developed a reproducible method for determining on-rate, off-rate and affinity using SMA-stabilised receptor, this is one of the early attempts at using SMA-stabilised receptor for SPR assays. Overall, we found both mAbs bound to their respective binding site with low nanomolar affinities with the ECD-mAb exhibiting slightly faster off-rate compared to ECL-mAb.

HDX-MS allows successful epitope mapping

While SPR data further confirmed the specific binding of ECL and ECD-mAb to PTH1R, it did not provide any information regarding the actual binding sites of the mAbs. X-ray crystallography is routinely used for accurately mapping epitopes and paratopes, but this remains very challenging for GPCRs. To circumvent the issues associated with X-ray crystallography, we used HDX-MS to determine the epitope of ECD-mAb and ECL-mAb. Some aspects of HDX-MS analysis of GPCR can be challenging, particularly obtaining high sequence coverage and redundancy, both of which are crucial for obtaining robust HDX-MS data. Some groups, with extensive optimisation, have managed to get sequence coverage of 89%, using DDM-stabilised β_2-adrenergic receptor and an extensive liquid-chromatography (LC) gradient, improving the resolution of the chromatography step and allowing more peptides to be identified (X. Zhang *et al.*, 2010), but this still remains a challenge. Previously, poor sequence coverage was seen with receptors solubilised in LMNG (Chung *et al.*, 2011) (Shukla *et al.*, 2014). However here, we successfully used LMNG-stabilised ΔNΔC171-491 to determine the epitope of ECL-mAb and found that the mAb binds to the ECL-1 of PTH1R. We also managed to get sequence coverage of 74.3%, with no major optimisation efforts, and the extracellular loops had good coverage even though peptide redundancy, was comparatively low. We believe, with further optimisation by screening for other detergents, reducing agents and quenching conditions we could further improve the sequence coverage. Recently, bicelles have been shown to be amenable to HDX-MS and could be adopted to improve the overall sequence coverage of PTH1R (Duc *et al.*, 2015).

The HDX-MS data for the ECD-mAb suggested an overlap with the PTH (1-34) binding site which could explain the weak cAMP antagonism seen with ECD-mAb. We hypothesize that at high concentrations of mAb, it either sterically hinders or competes PTH (1-34) out of the orthosteric binding site. A definitive explanation would require more accurate epitope determination of the ECD-mAb:ECD co-complex, using X-ray crystallography.

Early CryoEM data suggests successful complex formation

X-ray crystallography of GPCRs requires a considerable amount of pure protein and while we were able to express and isolate high quality PTH1R this was only in small amounts (~200-300 µg). However, we were keen to determine the suitability of our constructs and the discovered mAbs for structural studies using Cryo-EM. We attempted to complex both ECD-mAb and ECL-mAb with ΔC29-491, but we were only successful in purifying the ECL-mAb-ΔNΔC171-491 complex. Cryo-EM has recently proved to be a key player in GPCR structure determination and full-length structures of class B GPCR such as calcitonin (Liang *et al.*, 2017) and GLP-1 (Y. Zhang *et al.*, 2017) receptors were solved using cryo-EM. We therefore attempted cryo-EM with double-truncated PTH1R (ΔNΔC171-491) in complex with ECL-mAb purified to high purity. From the micrographs, we could identify particles which we believe represent the complex as shown in Figure 5-12.

The overall particle size was found to be ~10 nm. This matches closely with some of the existing data where particles ranging from 4 nm to 20 nm were reported (Figure 5-13). It should however be noted that we were unable to successfully perform 2D-averaging due to low particle numbers. The micrographs of ΔNΔC171-491: ECL mAb complex is compared to CT and GLP-1 micrographs in Figure 5-13. The data presented in this chapter represents an excellent start for further structural studies of the PTH1R-ECL-mAb complex using cryo-EM

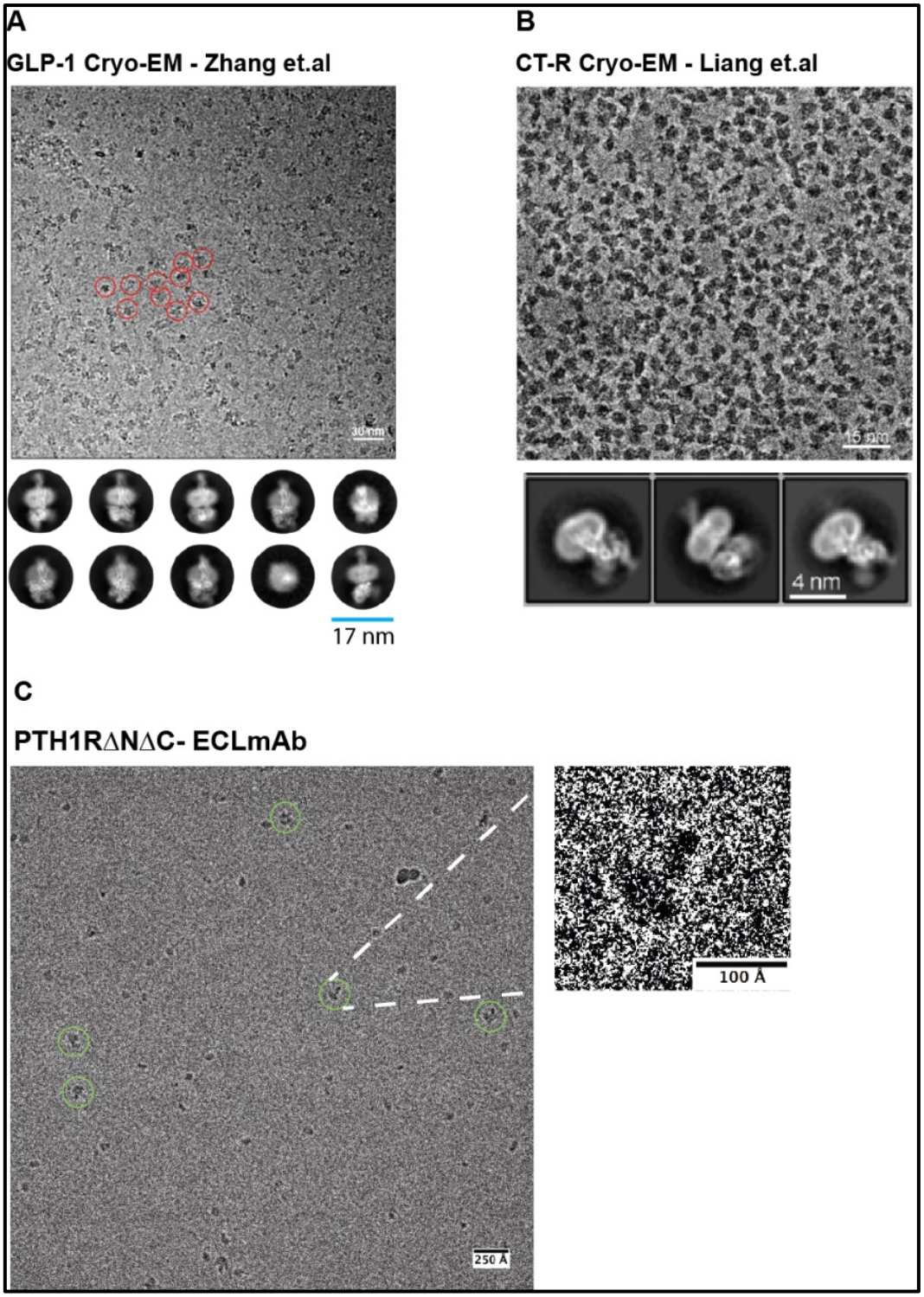


Figure 5-13: Comparison of ΔNΔC171-491: ECL mAb particle size on cryo-EM grid with published structures.

CryoEM micrographs showing GLP-1 in complex with heterotrimeric G-protein (A) (Y. Zhang *et al.*, 2017) and Calcitonin receptor in complex with heterotrimeric G-protein (B) (Liang *et al.*, 2017). C) Micrograph representing ΔNΔC171-491: ECL mAb particles.

Discussion and future work

6. Discussion and future work

mAbs against PTH1R – advantages of mAbs

Monoclonal antibodies are widely used for treating a range of diseases, mainly cancers and autoimmune disorders (Carter and Lazar, 2017). As of 2016 over 60 mAbs had received regulatory agency approval with a worldwide revenue of ~US$89 billion (Carter and Lazar, 2017). It is estimated that by 2020, the combined world sales of mAbs would be close to US$125 billion (Ecker, Jones and Levine, 2014). It is therefore clear that mAbs will play a key therapeutic role for the foreseeable future. mAbs provide certain advantages over small molecule and peptide-based therapeutics such as longer serum half-life, higher affinity and specificity for the target molecule (Hutchings *et al.*, 2017).

Due to their ubiquitous nature and the significant role they play in various cellular process, GPCRs are targeted by ~30% of all FDA-approved drugs (Hauser *et al.*, 2017). Yet out of ~800 GPCRs only about 108 are known drug-targets (Hauser *et al.*, 2017). Therefore, this receptor superfamily presents extensive opportunities for therapeutic intervention and novel drug discovery. However, the discovery and development of therapeutic mAbs targeting GPCRs has been more challenging, with significantly fewer molecules at all stages of clinical development when compared to soluble protein targets. Recent advances in the field including better purification of the target receptor molecule and more nuanced antibody discovery methodologies however have led to a resurgence in development of GPCR specific mAbs (Hutchings *et al.*, 2017).

Here we attempted to generate monoclonal antibodies against the extracellular regions of PTH1R using UCB's core antibody discovery technology to target the loops and phage display to target the ECD. The overall aim was to discover antibodies that could modulate receptor function. Functional mAb binding to the ECD has been reported for the GCGR and GLP1R (Mukund *et al.*, 2013; Biggs *et al.*, 2017) showing that targeting the ECD is a feasible approach to generating function-modifying mAbs. Purified PTH1R ECD was used for phage display panning, which yielded ~150 unique scFv sequences that exhibited binding to PTH1R

ECD by ELISA and FACS. Due to time constraints and resource limitations, it was not possible to perform a functional characterisation of all 150 scFvs and therefore a flow-cytometry based PTH-competition assay was used to triage the identified scFvs. Based on the PTH-competition data (Section 2.3.5) 18 molecules were taken further for functional characterisation to determine their role in G_s mediated cAMP regulation (section 2.3.5).

Clone PD12, one of the phage derived mAbs was shown to inhibit cAMP regulation, but only at concentrations above 1 μM (Figure 5-3). It is yet to be determined if this inhibition is due to either I) direct mAb-induced conformational change of the ECD or II) a non-specific mAb concentration effect. We can rule out the effect being due to inhibition of PTH binding as a cause since the substrate can still bind the ECD in the presence of the mAb. Future work could include revisiting all the identified scFvs from the phage panning and testing them for functionality. It is possible that there could be more mAbs with 'functional' ECD-binding.

The ideal approach would be to functionally screen all the identified phage scFv sequences using *in vitro* assays measuring G_s, G_q and β-arrestin activity. This could be achieved using high-throughput expression of all the identified scFv molecules, followed by a single-point cAMP, IP-1 and β-arrestin recruitment assay. The assay could be performed using culture media containing the expressed scFv molecules, without any purification steps and compared against PTH (1-34) response. This should allow rapid identification of functional mAbs (if any), which could then be further tested using concentration-response experiments as shown in Figure 5-5.

ECD-mAb affects β-arrestin recruitment while ECL-mAb is a neutral allosteric ligand

The only functional mAb available against PTH1R, reported by Xoma Corp., antagonises PTH-mediated cAMP accumulation (http://www.xoma.com/assets-available-for-licensure/anti-pth1r/). Using an *in vitro* assay, we found that the PD12 ECD binding mAb inhibits PTH1R β-arrestin recruitment with a nanomolar IC_{50} (Figure 5-4). To date, no other mAbs have been described that affect β-arrestin recruitment by PTH1R. The physiological implication of this effect remains to be seen and as a first step the mAb should be further

tested in immortalised bone cell lines such as Ros 17/2.8, MG63 and U2OS. This mAb additionally represents a very useful tool to study the function of β-arrestin recruitment by this receptor.

Functional mAbs binding to the extracellular loops of class B GPCRs are rare with only one reported to date (van der Woning *et al.*, 2016). In an attempt to discover anti-PTH1R loop binding mAbs we used the UCB 'Core' antibody discovery technology (Tickle *et al.*, 2015) targeting the full-length and ECD-truncated receptor expressed on the cell surface (Chapter 3). Various PTH1R receptor constructs were generated to produce both the immunogens and as tools for antibody screening. We identified a family of closely related mAb sequences which bound specifically to PTH1R ECL but the overall sequence diversity was low, likely representing a single clonotype family derived from a single B-cell somatic hypermutation cascade. Overall, the mAb discovery campaign was successful considering the fact that the sequence similarity between human and rabbit PTH1R ECLs is greater than 90% (Figure 3-16). The ECL-mAb was found to be non-functional as it did not affect G_s or β-arrestin signalling (Figure 5-5 & Figure 5-6).

Whilst it appears that this antibody is a neutral allosteric ligand, we can't rule out that it might affect coupling to the G_q, since this pathway was not investigated as part of this study. Interestingly, the binding of this mAb is not hindered by the presence of ECD, which potentially makes this mAb an important 'tool antibody' to elucidate PTH1R structure.

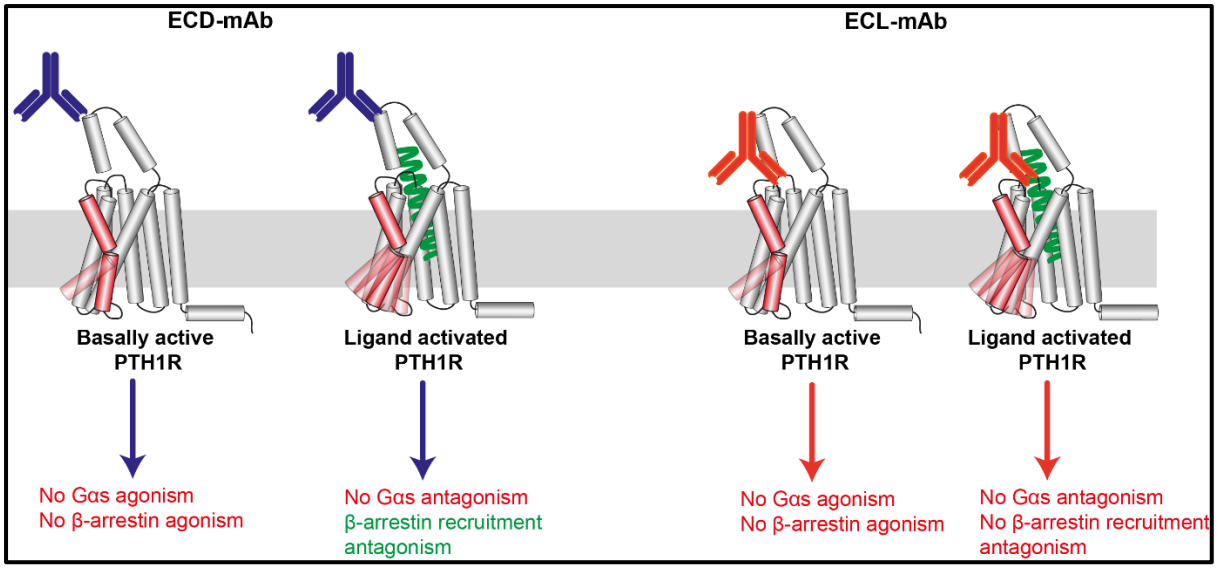


Figure 6-1: A schematic summarising the function of ECD and ECL-mAb

The figure highlights the overall functionality of the discovered mAbs. The ECD mAbs does not affect the binding of cognate ligand and has no effect on Gαs mediated cAMP signalling. The ECD-mAb inhibits β-arrestin recruitment with nanomolar IC_{50}. The loop-binding ECL-mAb is a neutral allosteric ligand, it allows binding of cognate ligand with no effect on cAMP signalling or β-arrestin recruitment.

Since we have discovered a large panel of mAbs against the ECD, and one high-affinity mAb against the ECL, it would be interesting to generate and test bispecific antibodies (potentially bi-paratopic) and determine whether cross-linking of two epitopes or indeed an overall higher affinity targeting might lead to novel functional effects, such as cAMP antagonism, not seen with either mAbs alone. The bi-paratopic mAb could potentially lock the ECD with the TMD thereby preventing PTH (1-34) binding.

Biophysical analysis of mAb binding to PTH1R

SMA-solubilisation and SPR

Purifying GPCRs and other membrane bound proteins can be challenging due to their propensity to aggregate when removed from the native membrane environment (Suzuki *et al.*, 2018). Recently, development of novel solubilising agents such as LMNG (Chae *et al.*, 2010) and SMA (Knowles *et al.*, 2009) has enabled structural and biophysical studies on various membrane bound proteins. While MNG-derivates have been very successful in structural studies, SMA has allowed biophysical characterisation of receptors in the absence of any detergents (Lee *et al.*, 2016). Here we used both detergents (DDM and LMNG) and SMA to

solubilise PTH1R (and its truncated variants). We found that all three reagents could successfully solubilise the receptor from membrane preparations but the overall solubility varied considerably (see Chapter 4). SMA reportedly allows detergent-free extraction of receptors embedded in cognate lipids, and relatively straight-forward purification using IMAC approaches (Jamshad *et al.*, 2015), but in our hands, we found that IMAC purification was challenging and the overall purity of the IMAC purified PTH1R was poor (Figure 4-9 & Figure 4-10). Resin-bound samples eluted at very low concentrations of imidazole, suggesting poor affinity of SMA-solubilised receptor for the Ni^{2+} resin and this in turn increased sample heterogeneity. One possible reason for this could be due to the charged nature of SMA, which hinders the charge mediated binding to Ni^{2+} beads (Dörr *et al.*, 2015). In our case, SMA was not suitable for generating a homogenous receptor preparation although we were able to use the enriched receptor preparation for analysis by SPR. The SPR assay was performed in the absence of any detergent. SPR revealed that both ECD and ECL-mAb bound to PTH1R with high affinity. Interestingly the ECL-mAb bound to both the ΔC29-491 and ΔNΔC171-491 construct with similar affinities, further supporting the fact that the presence of the ECD does not affect ECL-mAb binding.

LMNG-solubilisation and HDX

Hydrogen-deuterium exchange- mass spectrometry has been used extensively to study soluble protein interactions but has been used far less for membrane proteins. With recent advances in receptor stabilisation however, and improved HDX protocols, this technique is gaining popularity in the GPCR field (Chung *et al.*, 2011; Shukla *et al.*, 2014; Duc *et al.*, 2015; Vadas and Burke, 2015; H. H. Zhang *et al.*, 2017). We used HDX for epitope determination and obtained an acceptable level of sequence coverage (~79%) giving us confidence in the epitope. The results revealed a binding site for the ECD antibody which overlapped with the PTH binding site, while the ECL-mAb's epitope was found to be in ECL1 of PTH1R (Figure 5-8 & Figure 5-9). For the HDX work, we solubilised and purified the receptor

in LMNG as opposed to SMA, to allow incorporation of a low pH quenching step. SMA discs are unstable at low pH which would hinder the quenching step essential for HDX analysis.

We believe that with further optimisation of the LC gradient, quenching step and receptor preparation, we could further improve the sequence coverage obtained by HDX. It should also be noted that for the ECD-mAb, the sequence coverage was relatively poor around the determined epitope (Figure 5-8). This could be due to inefficient disulphide bond reduction and further optimisation of reduction condition could improve the sequence coverage which would allow a more accurate determination of ECD-mAb epitope.

Ideally, it would have been preferable to perform both the SPR and HDX analysis with either SMA or LMNG solubilised receptor. But in this case, this was not possible and the choice of solubilisation reagent was dictated by downstream applications. Due to pH-sensitivity, the SMA-solubilised receptor was not suitable for HDX analysis as mentioned before and therefore LNMG was preferred. We believe that the solubilisation approach should have minimal impact on the final data. For instance, we found that both mAbs bound to cell-surface expressed receptor using flow-cytometry (Figure 2-14 & Figure 3-15) and the binding is not hindered in either SMA solubilised receptor (Table 5-1) or LMNG solubilised receptor (Figure 5-9). This gives us the confidence that neither SMA or detergent had any detrimental effect on mAb binding.

Further uses of discovered mAbs

The approach used in this study showed that it is possible to generate mAbs against difficult targets such as GPCRs. It also highlights the importance of pursuing mAb discovery using multiple approaches, phage display and immunisation based mAb discovery methods. We also showed that generating mAbs against extracellular loops can be challenging and in this case while we were successful in generating a high-affinity mAb against PTH1R ECL-1, this mAb lacked function and came from a single clonotype group. We propose that this mAb could be used as a tool for structural elucidation of PTH1R, whose full-length structure is yet to be determined. We did make some progress in that direction and managing to purify a

complex of ECL-mAb with the double truncated PTH1R construct. This complex could also be detected on a cryo-EM grid, though at this stage 2D averaging was not possible. With further improvement in Cryo-EM sample preparation it might be possible to elucidate the full-length structure of PTH1R.

In summary, from two large antibody discovery campaigns using both phage display and immunization, we obtained multiple hits with two novel mAbs worthy of further characterisation. The ECD-mAb appears to affect the β-arrestin recruitment in an *in vitro* assay using CHOK-1 cell-line. This requires further investigation using physiologically relevant cell-lines and probe the relevance of this in a therapeutic setting. This mAb would be useful to further understand the mechanism of β-arrestin recruitment and its inhibition in PTH1R. We also isolated a rare loop binding mAb binding to the ECL-1 of PTH1R, using the immunisation approach. The ECL-mAb binds to the PTH1R ECL1 which high specificity and affinity but does not affect either G_s or β-arrestin mediated down-stream signalling. The ECL-mAb could be used as a tool mAb for structural elucidation of PTH1R using cryo-EM or X-ray crystallography.

We feel that some of the learnings from this work could be directly used for other members of Class B GPCRs, such as mAb discovery using phage display and the ECD. All members of the sub-family contain a large, soluble ECD which could be used for antibody discovery. However, it would be recommended to have a robust functional screening assay to help with better selection of 'functional' mAbs at an early stage of discovery. Similarly, some of the methodology we have used for SPR and HDX, could be translated directly to other GPCRs, provided they can be purified successfully using either detergent or SMA.

Bibliography

Abou-Samra, A. B. *et al.* (1992) 'Expression cloning of a common receptor for parathyroid hormone and parathyroid hormone-related peptide from rat osteoblast-like cells: a single receptor stimulates intracellular accumulation of both cAMP and inositol trisphosphates and increases intracel', *Proceedings of the National Academy of Sciences*. Proceedings of the National Academy of Sciences, 89(7), pp. 2732–2736. doi: 10.1073/pnas.89.7.2732.

Adler, A. S. *et al.* (2017) 'Rare, high-affinity anti-pathogen antibodies from human repertoires, discovered using microfluidics and molecular genomics', *mAbs*. Taylor & Francis, 9(8), pp. 1282–1296. doi: 10.1080/19420862.2017.1371383.

Agrawal, V. *et al.* (2012) 'Stable expression of chimeric heavy chain antibodies in CHO cells', *Methods in Molecular Biology*, 911, pp. 287–303. doi: 10.1007/978-1-61779-968-6_18.

Allen, J. A. and Roth, B. L. (2011) 'Strategies to Discover Unexpected Targets for Drugs Active at G Protein–Coupled Receptors', *Annual Review of Pharmacology and Toxicology*. Annual Reviews, 51(1), pp. 117–144. doi: 10.1146/annurev-pharmtox-010510-100553.

Anastas, J. N. and Moon, R. T. (2013) 'WNT signalling pathways as therapeutic targets in cancer', *Nature Reviews Cancer*. Springer Nature, 13(1), pp. 11–26. doi: 10.1038/nrc3419.

Arbabi-Ghahroudi, M., Tanha, J. and MacKenzie, R. (2005) 'Prokaryotic expression of antibodies', *Cancer and Metastasis Reviews*, 24(4), pp. 501–519. doi: 10.1007/s10555-005-6193-1.

Arruebo, M. *et al.* (2011) 'Assessment of the evolution of cancer treatment therapies', *Cancers*. Multidisciplinary Digital Publishing Institute (MDPI), pp. 3279–3330. doi: 10.3390/cancers3033279.

Assil, I. Q. *et al.* (2001) 'Juxtamembrane region of the amino terminus of the corticotropin releasing factor receptor type 1 is important for ligand interaction', *Biochemistry*, 40(5), pp. 1187–1195.

Attramadal, H. *et al.* (1992) 'Beta-arrestin2, a novel member of the arrestin/beta-arrestin gene family', *J Biol Chem*, 267(25), pp. 17882–17890. Available at: http://www.ncbi.nlm.nih.gov/pubmed/1517224 (Accessed: 4 May 2018).

Azzazy, H. M. E. and Highsmith, W. E. E. (2002) 'Phage display technology: Clinical applications and recent innovations', *Clinical Biochemistry*. Elsevier BV, 35(6), pp. 425–445. doi: 10.1016/S0009-9120(02)00343-0.

Baker, K. P. *et al.* (2003) 'Generation and Characterization of LymphoStat-B, a Human Monoclonal Antibody That Antagonizes the Bioactivities of B Lymphocyte Stimulator', *Arthritis and Rheumatism*, 48(11), pp. 3253–3265. doi: 10.1002/art.11299.

Ballesteros, J. *et al.* (1998) 'Functional microdomains in G-protein-coupled receptors: The conserved arginine-cage motif in the gonadotropin-releasing hormone receptor', *Journal of Biological Chemistry*, 273(17), pp. 10445–10453. doi: 10.1074/jbc.273.17.10445.

Ballesteros, J. A. *et al.* (2001) 'Activation of the beta 2-adrenergic receptor involves disruption of an ionic lock between the cytoplasmic ends of transmembrane segments 3 and 6.', *Journal of Biological Chemistry*, 276(31), pp. 29171–29177. doi: 10.1074/jbc.M103747200.

Banères, J.-L. L., Popot, J.-L. L. and Mouillac, B. (2011) 'New advances in production and functional folding of G-protein-coupled receptors', *Trends in Biotechnology*. Elsevier BV, 29(7), pp. 314–322. doi: 10.1016/j.tibtech.2011.03.002.

Baron, R. and Kneissel, M. (2013) 'WNT signaling in bone homeostasis and disease: from human mutations to treatments', *Nature Medicine*. Springer Nature, 19(2), pp. 179–192. doi: 10.1038/nm.3074.

Barwell, J., Conner, A. and Poyner, D. R. (2011) 'Extracellular loops 1 and 3 and their associated transmembrane regions of the calcitonin receptor-like receptor are needed for CGRP receptor function', *Biochimica et Biophysica Acta (BBA) - Molecular Cell Research*. Elsevier BV, 1813(10), pp. 1906–1916. doi: 10.1016/j.bbamcr.2011.06.005.

Bayburt, T. H. H., Grinkova, Y. V. V. and Sligar, S. G. G. (2002) 'Self-Assembly of Discoidal Phospholipid Bilayer Nanoparticles with Membrane Scaffold Proteins', *Nano Letters*. American Chemical Society, 2(8), pp. 853–856. doi: 10.1021/nl025623k.

Bazan, J. *et al.* (2012) 'Phage displaya powerful technique for immunotherapy: 1. Introduction and potential of therapeutic applications', *Human Vaccines and Immunotherapeutics*. Taylor & Francis, 8(12), pp. 1817–1828. doi: 10.4161/hv.21703.

Bazarsuren, A. *et al.* (2002) 'In vitro folding, functional characterization, and disulfide pattern of the extracellular domain of human GLP-1 receptor', *Biophysical Chemistry*. Elsevier BV, 96(2–3), pp. 305–318. doi: 10.1016/s0301-4622(02)00023-6.

Bazzacco, P. *et al.* (2012) 'Nonionic homopolymeric amphipols: Application to membrane protein folding, cell-free synthesis, and solution nuclear magnetic resonance', *Biochemistry*, 51(7), pp. 1416–1430. doi: 10.1021/bi201862v.

Benovic, J. L. *et al.* (1987) 'Functional desensitization of the isolated beta-adrenergic receptor by the beta-adrenergic receptor kinase: potential role of an analog of the retinal protein arrestin (48-kDa protein).', *Proceedings of the National Academy of Sciences of the United States of America*, 84(24), pp. 8879–82. Available at: http://www.ncbi.nlm.nih.gov/pubmed/2827157 (Accessed: 4 May 2018).

Bertheleme, N., Singh, S., *et al.* (2013) 'Loss of constitutive activity is correlated with increased thermostability of the human adenosine A2Areceptor', *British Journal of Pharmacology*. Wiley, 169(5), pp. 988–998. doi: 10.1111/bph.12165.

Bertheleme, N., Chae, P. S., *et al.* (2013) 'Unlocking the secrets of the gatekeeper: methods for stabilizing and crystallizing GPCRs.', *Biochimica et biophysica acta*. Elsevier B.V., 1828(11), pp. 2583–91. doi: 10.1016/j.bbamem.2013.07.013.

Bessette, P. H. *et al.* (1999) 'Efficient folding of proteins with multiple disulfide bonds in the Escherichia coli cytoplasm', *Proceedings of the National Academy of Sciences*, 96(24), pp. 13703–13708. doi: 10.1073/pnas.96.24.13703.

Biggs, E. K. *et al.* (2017) 'Development and characterisation of a novel glucagon like peptide-1 receptor antibody', *Diabetologia*. Springer Nature, 61(3), pp. 711–721. doi: 10.1007/s00125-017-4491-0.

Bill, R. M. *et al.* (2011) 'Overcoming barriers to membrane protein structure determination.', *Nature biotechnology*. Nature Publishing Group, 29(4), pp. 335–40. doi: 10.1038/nbt.1833.

Bjarnadóttir, T. K., Fredriksson, R. and Schiöth, H. B. (2007) 'The Adhesion GPCRs: A unique family of G protein-coupled receptors with important roles in both central and

peripheral tissues', *Cellular and Molecular Life Sciences*. Springer Nature, 64(16), pp. 2104–2119. doi: 10.1007/s00018-007-7067-1.

Boado, R. J. *et al.* (2010) 'Pharmacokinetics and brain uptake of a genetically engineered bifunctional fusion antibody targeting the mouse transferrin receptor', *Molecular Pharmaceutics*, 7(1), pp. 237–244. doi: 10.1021/mp900235k.

Bockaert, J. *et al.* (2004) 'GPCR interacting proteins (GIP)', *Pharmacology & Therapeutics*. Elsevier BV, 103(3), pp. 203–221. doi: 10.1016/j.pharmthera.2004.06.004.

Bocquet, N. *et al.* (2015) 'Real-time monitoring of binding events on a thermostabilized human A2A receptor embedded in a lipid bilayer by surface plasmon resonance', *Biochimica et Biophysica Acta (BBA) - Biomembranes*. Elsevier BV, 1848(5), pp. 1224–1233. doi: 10.1016/j.bbamem.2015.02.014.

Bolli, G. B. and Owens, D. R. (2014) 'Lixisenatide, a novel GLP-1 receptor agonist: Efficacy, safety and clinical implications for type 2 diabetes mellitus', *Diabetes, Obesity and Metabolism*, pp. 588–601. doi: 10.1111/dom.12253.

Bortolato, A. *et al.* (2014) 'Structure of Class B GPCRs: new horizons for drug discovery.', *British journal of pharmacology*. Wiley, 171(13), pp. 3132–45. doi: 10.1111/bph.12689.

Bruning, J. B. *et al.* (2007) 'Partial Agonists Activate PPARγ Using a Helix 12 Independent Mechanism', *Structure*, 15(10), pp. 1258–1271. doi: 10.1016/j.str.2007.07.014.

Burg, J. S. *et al.* (2015) 'Structural basis for chemokine recognition and activation of a viral G protein-coupled receptor', *Science*. American Association for the Advancement of Science (AAAS), 347(6226), pp. 1113–1117. doi: 10.1126/science.aaa5026.

Byrne, B. (2015) 'Pichia pastoris as an expression host for membrane protein structural biology', *Current Opinion in Structural Biology*. Elsevier Ltd, 32, pp. 9–17. doi: 10.1016/j.sbi.2015.01.005.

Byrne, E. F. X. *et al.* (2016) 'Structural basis of Smoothened regulation by its extracellular domains', *Nature*. Springer Nature, 535(7613), pp. 517–522. doi: 10.1038/nature18934.

Cabrera-Vera, T. M. *et al.* (2003) 'Insights into G Protein Structure, Function, and Regulation', *Endocrine Reviews*. The Endocrine Society, 24(6), pp. 765–781. doi: 10.1210/er.2000-0026.

Carter, P. *et al.* (1992) 'Humanization of an anti-p185HER2 antibody for human cancer therapy.', *Proceedings of the National Academy of Sciences*. National Academy of Sciences, 89(10), pp. 4285–4289. doi: 10.1073/pnas.89.10.4285.

Carter, P. (2001) 'Improving the efficacy of antibody-based cancer therapies', *Nature Reviews Cancer*. Springer Nature, 1(2), pp. 118–129. doi: 10.1038/35101072.

Carter, P. J. and Lazar, G. A. (2017) 'Next generation antibody drugs: pursuit of the "high-hanging fruit"', *Nature Reviews Drug Discovery*. Springer Nature, 17(3), pp. 197–223. doi: 10.1038/nrd.2017.227.

Chae, P. S. *et al.* (2010) 'Maltose–neopentyl glycol (MNG) amphiphiles for solubilization, stabilization and crystallization of membrane proteins', *Nature Methods*. Springer Nature, 7(12), pp. 1003–1008. doi: 10.1038/nmeth.1526.

Chalmers, M. J. *et al.* (2006) 'Probing protein ligand interactions by automated

hydrogen/deuterium exchange mass spectrometry', *Analytical Chemistry*, 78(4), pp. 1005–1014. doi: 10.1021/ac051294f.

Chames, P. *et al.* (2009) 'Therapeutic antibodies: Successes, limitations and hopes for the future', *British Journal of Pharmacology*, 157(2), pp. 220–233. doi: 10.1111/j.1476-5381.2009.00190.x.

Cherezov, V. *et al.* (2007) 'High-Resolution Crystal Structure of an Engineered Human 2-Adrenergic G Protein-Coupled Receptor', *Science*, 318(5854), pp. 1258–1265. doi: 10.1126/science.1150577.

Cherezov, V., Rosenbaum, D. M., Hanson, M. A., *et al.* (2007) 'High-Resolution Crystal Structure of an Engineered Human b 2 -Adrenergic', *Science*, 318(November), pp. 1258–1266. doi: 10.1126/science.1150577.

Cherezov, V., Rosenbaum, D. M., Hanson, M. a, *et al.* (2007) 'High-resolution crystal structure of an engineered human beta2-adrenergic G protein-coupled receptor.', *Science (New York, N.Y.)*, 318(5854), pp. 1258–65. doi: 10.1126/science.1150577.

Chien, E. Y. T. *et al.* (2010) 'Structure of the human dopamine D3 receptor in complex with a D2/D3 selective antagonist', *Science*, 330(6007), pp. 1091–1095. doi: 10.1126/science.1197410.

Chien, E. Y. T. *et al.* (2010) 'Structure of the Human Dopamine D3 Receptor in Complex with a D2/D3 Selective Antagonist', *Science (New York, N.Y.)*, 330(6007), pp. 1091–1095. doi: 10.1126/science.1197410.

Christopoulos, A. *et al.* (2014) 'International Union of Basic and Clinical Pharmacology. XC. Multisite Pharmacology: Recommendations for the Nomenclature of Receptor Allosterism and Allosteric Ligands', *Pharmacological Reviews*. American Society for Pharmacology & Experimental Therapeutics (ASPET), 66(4), pp. 918–947. doi: 10.1124/pr.114.008862.

Chun, E. *et al.* (2012) 'Fusion Partner Toolchest for the Stabilization and Crystallization of G Protein-Coupled Receptors', *Structure*. Elsevier BV, 20(6), pp. 967–976. doi: 10.1016/j.str.2012.04.010.

Chung, K. Y. *et al.* (2011) 'Conformational changes in the G protein Gs induced by the β2 adrenergic receptor.', *Nature*. Nature Publishing Group, 477(7366), pp. 611–5. doi: 10.1038/nature10488.

Clargo, A. M. *et al.* (2014) 'The rapid generation of recombinant functional monoclonal antibodies from individual, antigenspecific bone marrow-derived plasma cells isolated using a novel fluorescence-based method', *mAbs*. Informa UK Limited, 6(1), pp. 143–159. doi: 10.4161/mabs.27044.

Colley, C. S. *et al.* (2018) 'Screening Strategies for the Discovery of Ion Channel Monoclonal Antibodies', *Current Protocols in Pharmacology*. Wiley-Blackwell, 82(1), p. e44. doi: 10.1002/cpph.44.

Colvin, R. A. *et al.* (2006) 'CXCR3 Requires Tyrosine Sulfation for Ligand Binding and a Second Extracellular Loop Arginine Residue for Ligand-Induced Chemotaxis', *Molecular and Cellular Biology*, 26, pp. 5838–5849. doi: 10.1128/MCB.00556-06.

Contreras-Gómez, A. *et al.* (2013) 'Protein production using the baculovirus-insect cell expression system', *Biotechnology Progress*. Wiley, 30(1), pp. 1–18. doi: 10.1002/btpr.1842.

Couvineau, A. *et al.* (1996) 'Mutagenesis of N-glycosylation sites in the human vasoactive intestinal peptide 1 receptor. Evidence that asparagine 58 or 69 is crucial for

correct delivery of the receptor to plasma membrane', *Biochemistry*, 35(6), pp. 1745–1752. doi: 10.1021/bi952022h.

Culhane, K. J. *et al.* (2015) 'Transmembrane signal transduction by peptide hormones via family B G protein-coupled receptors', *Frontiers in Pharmacology*. Frontiers Media SA, 6(November), pp. 1–23. doi: 10.3389/fphar.2015.00264.

Czerski, L., Vinogradova, O. and Sanders, C. R. (2000) 'NMR-Based Amide Hydrogen–Deuterium Exchange Measurements for Complex Membrane Proteins: Development and Critical Evaluation', *Journal of Magnetic Resonance*. Elsevier BV, 142(1), pp. 111–119. doi: 10.1006/jmre.1999.1920.

Dahmane, T. *et al.* (2009) 'Amphipol-Assisted in Vitro Folding of G Protein-Coupled Receptors', *Biochemistry*. American Chemical Society (ACS), 48(27), pp. 6516–6521. doi: 10.1021/bi801729z.

Dal Maso, E. *et al.* (2018) 'Extracellular loops 2 and 3 of the calcitonin receptor selectively modify agonist binding and efficacy', *Biochemical Pharmacology*. Elsevier BV, 150(February), pp. 214–244. doi: 10.1016/j.bcp.2018.02.005.

Dann, C. E. *et al.* (2001) 'Insights into Wnt binding and signalling from the structures of two Frizzled cysteine-rich domains.', *Nature*, 412(6842), pp. 86–90. doi: 10.1038/35083601.

Datta, N. S. and Abou-Samra, A. B. (2009) 'PTH and PTHrP signaling in osteoblasts.', *Cellular signalling*. Elsevier Inc., 21(8), pp. 1245–54. doi: 10.1016/j.cellsig.2009.02.012.

Davis, T. R. *et al.* (1992) 'Baculovirus Expression of Alkaline Phosphatase as a Reporter Gene for Evaluation of Production, Glycosylation and Secretion', *Nature Biotechnology*. Springer Nature, 10(10), pp. 1148–1150. doi: 10.1038/nbt1092-1148.

Day, P. W. *et al.* (2007) 'A monoclonal antibody for G protein–coupled receptor crystallography', *Nature Methods*. Springer Nature, 4(11), pp. 927–929. doi: 10.1038/nmeth1112.

DeAlmeida, V. I. and Mayo, K. E. (1998) 'Identification of binding domains of the growth hormone-releasing hormone receptor by analysis of mutant and chimeric receptor proteins.', *Molecular endocrinology (Baltimore, Md.)*, 12(5), pp. 750–65. doi: 10.1210/mend.12.5.0102.

Degorce, F. F. *et al.* (2009) 'HTRF: A Technology Tailored for Drug Discovery - A Review of Theoretical Aspects and Recent Applications', *Current Chemical Genomics*. Bentham Science Publishers Ltd., 3(1), pp. 22–32. doi: 10.2174/1875397300903010022.

Denisov, I. G. and Sligar, S. G. (2016) 'Nanodiscs for structural and functional studies of membrane proteins', *Nature Structural & Molecular Biology*. Springer Nature, 23(6), pp. 481–486. doi: 10.1038/nsmb.3195.

DeWire, S. M. *et al.* (2007) 'β-Arrestins and Cell Signaling', *Annual Review of Physiology*. Annual Reviews, 69(1), pp. 483–510. doi: 10.1146/annurev.physiol.69.022405.154749.

DeWire, S. M. and Violin, J. D. (2011) 'Biased ligands for better cardiovascular drugs: dissecting G-protein-coupled receptor pharmacology.', *Circulation research*, 109(2), pp. 205–16. doi: 10.1161/CIRCRESAHA.110.231308.

Doré, A. S. *et al.* (2014a) 'Structure of class C GPCR metabotropic glutamate receptor 5 transmembrane domain', *Nature*, 511(7511), pp. 557–562. doi: 10.1038/nature13396.

Doré, A. S. *et al.* (2014b) 'Structure of class C GPCR metabotropic glutamate receptor

5 transmembrane domain', *Nature*. Nature Publishing Group, 511(7511), pp. 557–562. doi: 10.1038/nature13396.

Doré, A. S. *et al.* (2014c) 'Structure of class C GPCR metabotropic glutamate receptor 5 transmembrane domain.', *Nature*, 511(7511), pp. 557–62. doi: 10.1038/nature13396.

Doré, A. S. S. *et al.* (2011) 'Structure of the Adenosine A2A Receptor in Complex with ZM241385 and the Xanthines XAC and Caffeine', *Structure*. Elsevier BV, 19(9), pp. 1283–1293. doi: 10.1016/j.str.2011.06.014.

Dörr, J. M. *et al.* (2015) 'The styrene–maleic acid copolymer: a versatile tool in membrane research', *European Biophysics Journal*. Springer Nature, 45(1), pp. 3–21. doi: 10.1007/s00249-015-1093-y.

Dorsam, R. T. and Gutkind, J. S. (2007) 'G-protein-coupled receptors and cancer', *Nature Reviews Cancer*. Springer Nature, 7(2), pp. 79–94. doi: 10.1038/nrc2069.

Douthwaite, J. A. *et al.* (2015) 'Affinity maturation of a novel antagonistic human monoclonal antibody with a long V<inf>H</inf> CDR3 targeting the Class a GPCR formyl-peptide receptor 1', *mAbs*, 7(1), pp. 152–166. doi: 10.4161/19420862.2014.985158.

Doyle, N. *et al.* (2017) 'Abaloparatide, a novel PTH receptor agonist, increased bone mass and strength in ovariectomized cynomolgus monkeys by increasing bone formation without increasing bone resorption', *Osteoporosis International*. Springer Nature, 29(3), pp. 685–697. doi: 10.1007/s00198-017-4323-6.

Dubochet, J. *et al.* (1982) 'Frozen aqueous suspensions', *Ultramicroscopy*, 10(1–2), pp. 55–61. doi: 10.1016/0304-3991(82)90187-5.

Duc, N. M. *et al.* (2015) 'Effective Application of Bicelles for Conformational Analysis of G Protein-Coupled Receptors by Hydrogen/Deuterium Exchange Mass Spectrometry', *Journal of The American Society for Mass Spectrometry*. Springer Nature, 26(5), pp. 808–817. doi: 10.1007/s13361-015-1083-4.

Duc, N. M., Kim, H. R. and Chung, K. Y. (2015) 'Structural mechanism of G protein activation by G protein-coupled receptor', *European Journal of Pharmacology*. Elsevier, 763, pp. 1–9. doi: 10.1016/j.ejphar.2015.05.016.

Dumoulin, M. *et al.* (2009) 'Single-domain antibody fragments with high conformational stability', *Protein Science*, 11(3), pp. 500–515. doi: 10.1110/ps.34602.

Eason, M. G., Jacinto, M. T. and Liggett, S. B. (1994) 'Contribution of ligand structure to activation of alpha 2-adrenergic receptor subtype coupling to Gs.', *Molecular pharmacology*, 45(4), pp. 696–702. Available at: http://molpharm.aspetjournals.org/content/45/4/696.abstract?ijkey=2f950d3b24ed0d890461cf78b8e963507feac014&keytype2=tf_ipsecsha (Accessed: 18 June 2015).

Ecker, D. M., Jones, S. D. and Levine, H. L. (2014) 'The therapeutic monoclonal antibody market', *mAbs*. Informa UK Limited, 7(1), pp. 9–14. doi: 10.4161/19420862.2015.989042.

Eglen, R. M. (2002) 'Enzyme Fragment Complementation: A Flexible High Throughput Screening Assay Technology', *ASSAY and Drug Development Technologies*, 1(1), pp. 1–1. doi: 10.1089/154065802761001356.

Egloff, P. *et al.* (2014) 'Structure of signaling-competent neurotensin receptor 1 obtained by directed evolution inEscherichia coli', *Proceedings of the National Academy of Sciences*. Proceedings of the National Academy of Sciences, 111(6), pp. E655–E662. doi:

10.1073/pnas.1317903111.

Engel, A. and Gaub, H. E. (2008) ‘Structure and Mechanics of Membrane Proteins’, *Annual Review of Biochemistry*, 77(1), pp. 127–148. doi: 10.1146/annurev.biochem.77.062706.154450.

Engen, J. R. and Smith, D. L. (2001) ‘Investigating protein structure and dynamics by hydrogen exchange MS.’, *Analytical chemistry*, 73(9), p. 256A–265A. Available at: http://www.ncbi.nlm.nih.gov/pubmed/11354508 (Accessed: 14 March 2018).

England, E. *et al.* (2015) ‘Application of the mirrorball high-sensitivity cytometer to multiplexed assays for antibody drug discovery’, *Journal of Biomolecular Screening*. SAGE PublicationsSage CA: Los Angeles, CA, 20(4), pp. 536–544. doi: 10.1177/1087057114557776.

Englander, S. W. (2006) ‘Hydrogen exchange and mass spectrometry: A historical perspective’, *J Am Soc Mass Spectrom*, 17(11), pp. 1481–1489. doi: S1044-0305(06)00551-4 [pii]\r10.1016/j.jasms.2006.06.006 [doi].

Fang, X. T. *et al.* (2017) ‘Efficient and inexpensive transient expression of multispecific multivalent antibodies in Expi293 cells’, *Biological Procedures Online*. Springer Nature, 19(1), p. 11. doi: 10.1186/s12575-017-0060-7.

Farid, S. S. (2007) ‘Process economics of industrial monoclonal antibody manufacture’, *Journal of Chromatography B: Analytical Technologies in the Biomedical and Life Sciences*, pp. 8–18. doi: 10.1016/j.jchromb.2006.07.037.

Fenalti, G. *et al.* (2014) ‘Molecular control of δ-opioid receptor signalling’, *Nature*. Springer Nature, 506(7487), pp. 191–196. doi: 10.1038/nature12944.

Feng, L., Wang, X. and Jin, H. (2011) ‘Rabbit monoclonal antibody: Potential application in cancer therapy’, *American Journal of Translational Research*. e-Century Publishing Corporation, pp. 269–274. Available at: http://www.ncbi.nlm.nih.gov/pubmed/21633632 (Accessed: 16 November 2017).

Fernandez-Leiro, R. and Scheres, S. H. W. W. (2016) ‘Unravelling biological macromolecules with cryo-electron microscopy’, *Nature*. Nature Publishing Group, 537(7620), pp. 339–346. doi: 10.1038/nature19948.

Fredriksson, R. *et al.* (2003) ‘The G-protein-coupled receptors in the human genome form five main families. Phylogenetic analysis, paralogon groups, and fingerprints.’, *Molecular pharmacology*, 63(6), pp. 1256–1272. doi: 10.1124/mol.63.6.1256.

Frenken, L. G. J. *et al.* (2000) ‘Isolation of antigen specific Llama V(HH) antibody fragments and their high level secretion by Saccharomyces cerevisiae’, *Journal of Biotechnology*, 78(1), pp. 11–21. doi: 10.1016/S0168-1656(99)00228-X.

Gamper, N., Stockand, J. D. and Shapiro, M. S. (2005) ‘The use of Chinese hamster ovary (CHO) cells in the study of ion channels’, *Journal of Pharmacological and Toxicological Methods*. Elsevier BV, 51(3), pp. 177–185. doi: 10.1016/j.vascn.2004.08.008.

Gao, C. and Chen, Y.-G. (2010) ‘Dishevelled: The hub of Wnt signaling’, *Cellular Signalling*. Elsevier BV, 22(5), pp. 717–727. doi: 10.1016/j.cellsig.2009.11.021.

Gardella, T. J. *et al.* (1996) ‘Inverse agonism of amino-terminally truncated parathyroid hormone (PTH) and PTH-related peptide (PTHrP) analogs revealed with constitutively active mutant PTH/PTHrP receptors’, *Endocrinology*, 137(9), pp. 3936–3941. doi: 10.1210/en.137.9.3936.

Gesty-Palmer, D. *et al.* (2006) 'Distinct β-Arrestin- and G Protein-dependent Pathways for Parathyroid Hormone Receptor-stimulated ERK1/2 Activation', *Journal of Biological Chemistry*. American Society for Biochemistry & Molecular Biology (ASBMB), 281(16), pp. 10856–10864. doi: 10.1074/jbc.m513380200.

Gesty-Palmer, D. *et al.* (2009) 'A beta-arrestin-biased agonist of the parathyroid hormone receptor (PTH1R) promotes bone formation independent of G protein activation.', *Science translational medicine*. American Association for the Advancement of Science (AAAS), 1(1), p. 1ra1. doi: 10.1126/scitranslmed.3000071.

Gesty-Palmer, D. and Luttrell, L. M. (2011) '"Biasing" the parathyroid hormone receptor: A novel anabolic approach to increasing bone mass?', *British Journal of Pharmacology*. Wiley, 164(1), pp. 59–67. doi: 10.1111/j.1476-5381.2011.01450.x.

Gilligan, P. J. *et al.* (2009) 'Synthesis and Structure−Activity Relationships of 8-(Pyrid-3-yl)pyrazolo[1,5-a]-1,3,5-triazines: Potent, Orally Bioavailable Corticotropin Releasing Factor Receptor-1 (CRF1) Antagonists', *Journal of Medicinal Chemistry*. American Chemical Society (ACS), 52(9), pp. 3084–3092. doi: 10.1021/jm900025h.

Gong, B., Murray, K. D. and Trimmer, J. S. (2016) 'Developing high-quality mouse monoclonal antibodies for neuroscience research – approaches, perspectives and opportunities', *New Biotechnology*. Elsevier BV, 33(5), pp. 551–564. doi: 10.1016/j.nbt.2015.11.007.

Grace, C. R. R. *et al.* (2004) 'NMR structure and peptide hormone binding site of the first extracellular domain of a type B1 G protein-coupled receptor.', *Proceedings of the National Academy of Sciences of the United States of America*, 101(35), pp. 12836–41. doi: 10.1073/pnas.0404702101.

Graham, F. L. *et al.* (1977) 'Characteristics of a human cell line transformed by DNA from human adenovirus type 5.', *The Journal of general virology*, 36(1), pp. 59–74. doi: 10.1099/0022-1317-36-1-59.

Granier, S. *et al.* (2012) 'Structure of the δ-opioid receptor bound to naltrindole', *Nature*. Springer Nature, 485(7398), pp. 400–404. doi: 10.1038/nature11111.

Grauschopf, U. *et al.* (2000) 'The N-Terminal Fragment of Human Parathyroid Hormone Receptor 1 Constitutes a Hormone Binding Domain and Reveals a Distinct Disulfide Pattern', *Biochemistry*. American Chemical Society (ACS), 39(30), pp. 8878–8887. doi: 10.1021/bi0001426.

Grauschopf, U. *et al.* (2000) 'The N-terminal fragment of human parathyroid hormone receptor 1 constitutes a hormone binding domain and reveals a distinct disulfide pattern.', *Biochemistry*, 39(30), pp. 8878–87. Available at: http://www.ncbi.nlm.nih.gov/pubmed/10913300 (Accessed: 16 June 2015).

Griffin, L. and Lawson, A. (2011) 'Antibody fragments as tools in crystallography', *Clinical & Experimental Immunology*. Wiley, 165(3), pp. 285–291. doi: 10.1111/j.1365-2249.2011.04427.x.

Grisshammer, R. (2009) *Chapter 36 Purification of Recombinant G-Protein-Coupled Receptors*. 1st edn, *Methods in Enzymology*. 1st edn. Elsevier. doi: 10.1016/s0076-6879(09)63036-6.

Groff, K., Brown, J. and Clippinger, A. J. (2015) 'Modern affinity reagents: Recombinant antibodies and aptamers', *Biotechnology Advances*. Elsevier BV, 33(8), pp. 1787–1798. doi: 10.1016/j.biotechadv.2015.10.004.

Guan, X. M., Tong Sun Kobilka and Kobilka, B. K. (1992) 'Enhancement of membrane insertion and function in a type IIIb membrane protein following introduction of a cleavable signal peptide', *Journal of Biological Chemistry*, 267(31), pp. 21995–21998. Available at: http://www.ncbi.nlm.nih.gov/pubmed/1331042 (Accessed: 21 November 2017).

Haga, K., Kruse, A. C., *et al.* (2012) 'Structure of the human M2 muscarinic acetylcholine receptor bound to an antagonist', *Nature*. Nature Publishing Group, 482(7386), pp. 547–551. doi: 10.1038/nature10753.

Haga, K., Kruse, A. C., *et al.* (2012) 'Structure of the human M2 muscarinic acetylcholine receptor bound to an antagonist.', *Nature*. Nature Publishing Group, 482(7386), pp. 547–51. doi: 10.1038/nature10753.

Hagemann, U. B. *et al.* (2014) 'Fully Human Antagonistic Antibodies against CCR4 Potently Inhibit Cell Signaling and Chemotaxis', *PLoS ONE*. Edited by M. Ho. Public Library of Science (PLoS), 9(7), p. e103776. doi: 10.1371/journal.pone.0103776.

Hamers-Casterman, C. *et al.* (1993) 'Naturally occurring antibodies devoid of light chains', *Nature*, 363(6428), pp. 446–448. doi: 10.1038/363446a0.

Hamm, H. E. (1998) 'The Many Faces of G Protein Signaling', *Journal of Biological Chemistry*. American Society for Biochemistry & Molecular Biology (ASBMB), 273(2), pp. 669–672. doi: 10.1074/jbc.273.2.669.

Han, M. *et al.* (2001) 'Crystal structure of beta-arrestin at 1.9 A: possible mechanism of receptor binding and membrane Translocation', *Structure*, 9(9), pp. 869–880. doi: S096921260100644X [pii].

Hansel, T. T. *et al.* (2010) 'The safety and side effects of monoclonal antibodies', *Nature Reviews Drug Discovery*. Nature Publishing Group, 9(4), pp. 325–338. doi: 10.1038/nrd3003.

Hanson, M. A. *et al.* (2008) 'A Specific Cholesterol Binding Site Is Established by the 2.8 Å Structure of the Human β2-Adrenergic Receptor', *Structure*. Elsevier BV, 16(6), pp. 897–905. doi: 10.1016/j.str.2008.05.001.

Hanson, M. A. *et al.* (2012) 'Crystal Structure of a Lipid G Protein-Coupled Receptor', *Science*. American Association for the Advancement of Science (AAAS), 335(6070), pp. 851–855. doi: 10.1126/science.1215904.

Hansson, M. M. D. *et al.* (2008) 'PCR-mediated deletion of plasmid DNA.', *Analytical biochemistry*. Elsevier BV, 375(2), pp. 373–5. doi: 10.1016/j.ab.2007.12.005.

Hanyaloglu, A. C. and von Zastrow, M. (2008) 'Regulation of GPCRs by endocytic membrane trafficking and its potential implications.', *Annual review of pharmacology and toxicology*, 48, pp. 537–568. doi: 10.1146/annurev.pharmtox.48.113006.094830.

Hauser, A. S. *et al.* (2017) 'Trends in GPCR drug discovery: new agents, targets and indications', *Nature Reviews Drug Discovery*. Springer Nature, 16(12), pp. 829–842. doi: 10.1038/nrd.2017.178.

Hauser, A. S. *et al.* (2018) 'Pharmacogenomics of GPCR Drug Targets', *Cell*. Elsevier BV, 172(1–2), p. 41–54.e19. doi: 10.1016/j.cell.2017.11.033.

He, Y. *et al.* (2017) 'Molecular assembly of rhodopsin with G protein-coupled receptor kinases', *Cell Research*. Springer Nature, 27(6), pp. 728–747. doi: 10.1038/cr.2017.72.

He, Y., Wang, K. and Yan, N. (2014) 'The recombinant expression systems for

structure determination of eukaryotic membrane proteins', *Protein & cell*. Springer, 5(9), pp. 658–672. doi: 10.1007/s13238-014-0086-4.

Heckman, K. L. and Pease, L. R. (2007) 'Gene splicing and mutagenesis by PCR-driven overlap extension', *Nature Protocols*. Springer Nature, 2(4), pp. 924–932. doi: 10.1038/nprot.2007.132.

Hino, T. *et al.* (2012) 'G-protein-coupled receptor inactivation by an allosteric inverse-agonist antibody', *Nature*. Springer Nature, 482(7384), pp. 237–240. doi: 10.1038/nature10750.

Hirsch, J. a *et al.* (1999) 'The 2.8 A crystal structure of visual arrestin: a model for arrestin's regulation.', *Cell*, 97(2), pp. 257–269. doi: 10.1016/S0092-8674(00)80735-7.

Ho, T. W. *et al.* (2008) 'Efficacy and tolerability of MK-0974 (telcagepant), a new oral antagonist of calcitonin gene-related peptide receptor, compared with zolmitriptan for acute migraine: a randomised, placebo-controlled, parallel-treatment trial', *The Lancet*. Elsevier BV, 372(9656), pp. 2115–2123. doi: 10.1016/s0140-6736(08)61626-8.

Hoare, S. R. J. (2007) 'Allosteric Modulators of Class B G-Protein-Coupled Receptors', *Current Neuropharmacology*. Bentham Science Publishers Ltd., 5(3), pp. 168–179. doi: 10.2174/157015907781695928.

HOARE, S. R. J. (2005) 'Mechanisms of peptide and nonpeptide ligand binding to Class B G-protein-coupled receptors', *Drug Discovery Today*. Elsevier BV, 10(6), pp. 417–427. doi: 10.1016/s1359-6446(05)03370-2.

Hofmann, B. A. *et al.* (2001) 'Functional and protein chemical characterization of the N-terminal domain of the rat corticotropin-releasing factor receptor 1', *Protein Sci*, 10(10), pp. 2050–2062. doi: 10.1110/ps.12101.

Hollenstein, K. *et al.* (2013) 'Structure of class B GPCR corticotropin-releasing factor receptor 1.', *Nature*. Springer Nature, 499(7459), pp. 438–43. doi: 10.1038/nature12357.

Hollenstein, K. *et al.* (2014) 'Insights into the structure of class B GPCRs', *Trends in Pharmacological Sciences*. Elsevier Ltd, 35(1), pp. 12–22. doi: 10.1016/j.tips.2013.11.001.

Hoogenboom, H. R. *et al.* (1998) 'Antibody phage display technology and its applications', *Immunotechnology*. Elsevier BV, 4(1), pp. 1–20. doi: 10.1016/s1380-2933(98)00007-4.

Hori, T. *et al.* (2018) 'Na + -mimicking ligands stabilize the inactive state of leukotriene B 4 receptor BLT1', *Nature Chemical Biology*, 14(3), pp. 262–269. doi: 10.1038/nchembio.2547.

Houde, D., Berkowitz, S. A. and Engen, J. R. (2011) 'The Utility of Hydrogen/Deuterium Exchange Mass Spectrometry in Biopharmaceutical Comparability Studies', *Journal of Pharmaceutical Sciences*, 100(6), pp. 2071–2086. doi: 10.1002/jps.22432.

Hua, T. *et al.* (2016) 'Crystal Structure of the Human Cannabinoid Receptor CB1', *Cell*, 167(3), p. 750–762.e14. doi: 10.1016/j.cell.2016.10.004.

Hua, T. *et al.* (2017) 'Crystal structures of agonist-bound human cannabinoid receptor CB1', *Nature*. Springer Nature, 547(7664), pp. 468–471. doi: 10.1038/nature23272.

Huang, Z. *et al.* (1996) 'The N-terminal Region of the Third Intracellular Loop of the Parathyroid Hormone (PTH)/PTH-related Peptide Receptor Is Critical for Coupling to cAMP and Inositol Phosphate/Ca2+Signal Transduction Pathways', *Journal of Biological Chemistry*.

American Society for Biochemistry & Molecular Biology (ASBMB), 271(52), pp. 33382–33389. doi: 10.1074/jbc.271.52.33382.

Huggins, D. J., Sherman, W. and Tidor, B. (2012) 'Rational Approaches to Improving Selectivity in Drug Design', *Journal of Medicinal Chemistry*. American Chemical Society (ACS), 55(4), pp. 1424–1444. doi: 10.1021/jm2010332.

Humphreys, D. P. *et al.* (2007) 'Alternative antibody Fab′ fragment PEGylation strategies: Combination of strong reducing agents, disruption of the interchain disulphide bond and disulphide engineering', *Protein Engineering, Design and Selection*, 20(5), pp. 227–234. doi: 10.1093/protein/gzm015.

Hunte, C. and Michel, H. (2002) 'Crystallisation of membrane proteins mediated by antibody fragments', *Current Opinion in Structural Biology*. Elsevier BV, 12(4), pp. 503–508. doi: 10.1016/s0959-440x(02)00354-8.

Hutchings, C. J. *et al.* (2017) 'Opportunities for therapeutic antibodies directed at G-protein-coupled receptors', *Nature Reviews Drug Discovery*. Nature Publishing Group, 16(11), pp. 787–810. doi: 10.1038/nrd.2017.91.

Hutchings, C. J., Koglin, M. and Marshall, F. H. (2010) 'Therapeutic antibodies directed at G protein-coupled receptors.', *mAbs*. Informa UK Limited, 2(6), pp. 594–606. doi: 10.4161/mabs.2.6.13420.

Iida-Klein, A. *et al.* (1995) 'Truncation of the carboxyl-terminal region of the rat parathyroid hormone (PTH)/PTH-related peptide receptor enhances PTH stimulation of adenylyl cyclase but not phospholipase C', *Journal of Biological Chemistry*, 270(15), pp. 8458–8465. doi: 10.1074/jbc.270.15.8458.

Iida-Klein, A. *et al.* (1997) 'Mutations in the second cytoplasmic loop of the rat parathyroid hormone (PTH)/PTH-related protein receptor result in selective loss of PTH-stimulated phospholipase C activity', *Journal of Biological Chemistry*. American Society for Biochemistry and Molecular Biology, 272(11), pp. 6882–6889. doi: 10.1074/jbc.272.11.6882.

Isberg, V. *et al.* (2015) 'GPCRdb: an information system for G protein-coupled receptors', *Nucleic Acids Research*. Oxford University Press (OUP), 44(D1), pp. D356–D364. doi: 10.1093/nar/gkv1178.

Ishihara, T. *et al.* (1991) 'Molecular cloning and expression of a cDNA encoding the secretin receptor.', *The EMBO journal*, 10(7), pp. 1635–41. Available at: http://www.pubmedcentral.nih.gov/articlerender.fcgi?artid=452832&tool=pmcentrez&rendertype=abstract.

Ismaili, A. *et al.* (2007) 'Production and characterization of anti-(mucin MUC1) single-domain antibody in tobacco (Nicotiana tabacum cultivar Xanthi).', *Biotechnology and applied biochemistry*, 47(Pt 1), pp. 11–9. doi: 10.1042/BA20060071.

Jaakola, V.-P. V.-P. *et al.* (2008) 'The 2.6 angstrom crystal structure of a human A2A adenosine receptor bound to an antagonist.', *Science (New York, N.Y.)*, 322(5905), pp. 1211–1217. doi: 10.1126/science.1164772.

Jaakola, V. P. *et al.* (2008) 'The 2.6 angstrom crystal structure of a human A2Aadenosine receptor bound to an antagonist', *Science*, 322(5905), pp. 1211–1217. doi: 10.1126/science.1164772.

Jakobovits, A. (1995) 'Production of fully human antibodies by transgenic mice', *Current Opinion in Biotechnology*. Elsevier Current Trends, 6(5), pp. 561–566. doi:

10.1016/0958-1669(95)80093-X.

Jamshad, M. *et al.* (2011) 'Surfactant-free purification of membrane proteins with intact native membrane environment.', *Biochemical Society transactions*. Portland Press Ltd., 39(3), pp. 813–8. doi: 10.1042/BST0390813.

Jamshad, M. *et al.* (2015) 'G-Protein-Coupled Receptor Solubilization and Purification for Biophysical Analysis and Functional Studies, in the Total Absence of Detergent.', *Bioscience reports*. Portland Press Ltd., 35(2), pp. 1–10. doi: 10.1042/BSR20140171.

Jazayeri, A., Dias, J. M. and Marshall, F. H. (2015) 'From G Protein-coupled Receptor Structure Resolution to Rational Drug Design', *Journal of Biological Chemistry*. American Society for Biochemistry & Molecular Biology (ASBMB), 290(32), pp. 19489–19495. doi: 10.1074/jbc.r115.668251.

Jeffrey Conn, P. *et al.* (2009) 'Allosteric modulators of GPCRs: a novel approach for the treatment of CNS disorders', *Nature Reviews Drug Discovery*. Springer Nature, 8(1), pp. 41–54. doi: 10.1038/nrd2760.

Jobert, A. S. *et al.* (1998) 'Absence of functional receptors for parathyroid hormone and parathyroid hormone-related peptide in Blomstrand chondrodysplasia.', *Journal of Clinical Investigation*. American Society for Clinical Investigation, 102(1), pp. 34–40. doi: 10.1172/jci2918.

Jones, D. T. and Cozzetto, D. (2014) 'DISOPRED3: precise disordered region predictions with annotated protein-binding activity', *Bioinformatics*. Oxford University Press (OUP), 31(6), pp. 857–863. doi: 10.1093/bioinformatics/btu744.

Jones, P. T. *et al.* (1986) 'Replacing the complementarity-determining regions in a human antibody with those from a mouse', *Nature*. Nature Publishing Group, 321(6069), pp. 522–525. doi: 10.1038/321522a0.

Jouishomme, H. *et al.* (1992) 'The protein kinase-C activation domain of the parathyroid hormone', *Endocrinology*, 130(1), pp. 53–60. doi: 066/17.

Kang, Y. *et al.* (2015) 'Crystal structure of rhodopsin bound to arrestin by femtosecond X-ray laser', *Nature*. Springer Nature, 523(7562), pp. 561–7. doi: 10.1038/nature14656.

Kashmiri, S. V. S. *et al.* (2005) 'SDR grafting - A new approach to antibody humanization', *Methods*, pp. 25–34. doi: 10.1016/j.ymeth.2005.01.003.

Kashyap, M. K. *et al.* (2015) 'Ulocuplumab (BMS-936564 / MDX1338): a fully human anti-CXCR4 antibody induces cell death in chronic lymphocytic leukemia mediated through a reactive oxygen species-dependent pathway', *Oncotarget*. Impact Journals, LLC, 7(3), pp. 2809–2822. doi: 10.18632/oncotarget.6465.

Katta, V., Chait, B. T. and Carr, S. (1991) 'Conformational changes in proteins probed by hydrogen-exchange electrospray-ionization mass spectrometry', *Rapid Communications in Mass Spectrometry*, 5(4), pp. 214–217. doi: 10.1002/rcm.1290050415.

Kazda, C. M. *et al.* (2016) 'Evaluation of Efficacy and Safety of the Glucagon Receptor Antagonist LY2409021 in Patients With Type 2 Diabetes: 12- and 24-Week Phase 2 Studies', *Diabetes Care*. American Diabetes Association, 39(7), pp. 1241–1249. doi: 10.2337/dc15-1643.

Kellermann, S. A. and Green, L. L. (2002) 'Antibody discovery: The use of transgenic mice to generate human monoclonal antibodies for therapeutics', *Current Opinion in Biotechnology*. Elsevier Current Trends, pp. 593–597. doi: 10.1016/S0958-1669(02)00354-3.

Kelley, L. P. and Kinsella, B. T. (2003) 'The role of N-linked glycosylation in determining the surface expression, G protein interaction and effector coupling of the alpha (α) isoform of the human thromboxane A2 receptor', *Biochimica et Biophysica Acta - General Subjects*, 1621(2), pp. 192–203. doi: 10.1016/S0304-4165(03)00059-X.

Kellner, C. *et al.* (2017) 'Modulating Cytotoxic Effector Functions by Fc Engineering to Improve Cancer Therapy', *Transfusion Medicine and Hemotherapy*. S. Karger AG, 44(5), pp. 327–336. doi: 10.1159/000479980.

Kempeni, J. (1999) 'Preliminary results of early clinical trials with the fully human anti-TNFalpha monoclonal antibody D2E7', *Annals of the Rheumatic Diseases*. BMJ, 58(Supplement 1), pp. i70–i72. doi: 10.1136/ard.58.2008.i70.

Kim, Y. J. *et al.* (2013) 'Crystal structure of pre-activated arrestin p44', *Nature*. Springer Nature, 497(7447), pp. 142–146. doi: 10.1038/nature12133.

Kingshury, G. A. *et al.* (1995) 'Screening of phage display immunoglobulin libraries by anti-M13 ELISA and whole phage PCR', *Nucleic Acids Research*. Oxford University Press (OUP), 23(13), pp. 2563–2564. doi: 10.1093/nar/23.13.2563.

Knowles, T. J. *et al.* (2009) 'Membrane Proteins Solubilized Intact in Lipid Containing Nanoparticles Bounded by Styrene Maleic Acid Copolymer', *Journal of the American Chemical Society*. American Chemical Society (ACS), 131(22), pp. 7484–7485. doi: 10.1021/ja810046q.

Köhler, G. and Milstein, C. (1975) 'Continuous cultures of fused cells secreting antibody of predefined specificity.', *Nature*. Springer Nature, 256(5517), pp. 495–497. doi: 10.1038/256495a0.

Kong, X. F. *et al.* (1994) 'The rat, mouse, and human genes encoding the receptor for parathyroid hormone and parathyroid hormone-related peptide are highly homologous.', *Biochemical and biophysical research communications*, 201(2), p. 1058. Available at: http://www.ncbi.nlm.nih.gov/pubmed/8002976 (Accessed: 16 June 2015).

Kontermann, R. E. and Brinkmann, U. (2015) 'Bispecific antibodies', *Drug Discovery Today*. Elsevier BV, 20(7), pp. 838–847. doi: 10.1016/j.drudis.2015.02.008.

Koole, C. *et al.* (2012) 'Second extracellular loop of human glucagon-like peptide-1 receptor (GLP-1R) has a critical role in GLP-1 peptide binding and receptor activation', *Journal of Biological Chemistry*. American Society for Biochemistry & Molecular Biology (ASBMB), 287(6), pp. 3642–3658. doi: 10.1074/jbc.M111.309328.

Koth, C. M. *et al.* (2012) 'Molecular basis for negative regulation of the glucagon receptor.', *Proceedings of the National Academy of Sciences of the United States of America*. Proceedings of the National Academy of Sciences, 109(36), pp. 14393–8. doi: 10.1073/pnas.1206734109.

Kristiansen, K. (2004) 'Molecular mechanisms of ligand binding, signaling, and regulation within the superfamily of G-protein-coupled receptors: molecular modeling and mutagenesis approaches to receptor structure and function', *Pharmacology & Therapeutics*. Elsevier BV, 103(1), pp. 21–80. doi: 10.1016/j.pharmthera.2004.05.002.

Kruse, A. C. *et al.* (2012) 'Structure and dynamics of the M3 muscarinic acetylcholine receptor', *Nature*, 482(7386), pp. 552–556. doi: 10.1038/nature10867.

Kruse, A. C. *et al.* (2013) 'Activation and allosteric modulation of a muscarinic acetylcholine receptor', *Nature*, 504(7478), pp. 101–106. doi: 10.1038/nature12735.

Kunishima, N. *et al.* (2000) 'Structural basis of glutamate recognition by a dimeric

metabotropic glutamate receptor.', *Nature*, 407(6807), pp. 971–977. doi: 10.1038/35039564.

Lagerström, M. C. and Schiöth, H. B. (2008) 'Structural diversity of G protein-coupled receptors and significance for drug discovery.', *Nature reviews. Drug discovery*. Nature Publishing Group, 7(4), pp. 339–57. doi: 10.1038/nrd2518.

Lambright, D. G. *et al.* (1996) 'The 2.0 Å crystal structure of a heterotrimeric G protein', *Nature*. Springer Nature, 379(6563), pp. 311–319. doi: 10.1038/379311a0.

Lane, J. R. *et al.* (2017) 'A kinetic view of GPCR allostery and biased agonism', *Nature Chemical Biology*. Springer Nature, 13(9), pp. 929–937. doi: 10.1038/nchembio.2431.

Lanske, B. *et al.* (1999) 'Ablation of the PTHrP gene or the PTH/PTHrP receptor gene leads to distinct abnormalities in bone development', *Journal of Clinical Investigation*. American Society for Clinical Investigation, 104(4), pp. 399–407. doi: 10.1172/jci6629.

Latorraca, N. R., Venkatakrishnan, A. J. and Dror, R. O. (2016) 'GPCR Dynamics: Structures in Motion', *Chemical Reviews*. American Chemical Society (ACS), 117(1), pp. 139–155. doi: 10.1021/acs.chemrev.6b00177.

Lawson, A. D. G. (2012) 'Antibody-enabled small-molecule drug discovery', *Nature Reviews Drug Discovery*. Springer Nature, 11(7), pp. 519–525. doi: 10.1038/nrd3756.

Leader, B., Baca, Q. J. and Golan, D. E. (2008) 'Protein therapeutics: a summary and pharmacological classification', *Nature Reviews Drug Discovery*. Springer Nature, 7(1), pp. 21–39. doi: 10.1038/nrd2399.

Lebesgue, D. *et al.* (1998) 'An agonist-like monoclonal antibody against the human β2-adrenoceptor', *European Journal of Pharmacology*. Elsevier BV, 348(1), pp. 123–133. doi: 10.1016/s0014-2999(98)00136-8.

Lebon, G. *et al.* (2011) 'Agonist-bound adenosine A2A receptor structures reveal common features of GPCR activation', *Nature*. Nature Publishing Group, 474(7352), pp. 521–5. doi: 10.1038/nature10136.

Leder, B. Z. *et al.* (2015) 'Effects of abaloparatide, a human parathyroid hormone-related peptide analog, on bone mineral density in postmenopausal women with osteoporosis', *Journal of Clinical Endocrinology and Metabolism*, 100(2), pp. 697–706. doi: 10.1210/jc.2014-3718.

Leder, B. Z. (2017) 'Parathyroid Hormone and Parathyroid Hormone-Related Protein Analogs in Osteoporosis Therapy', *Current Osteoporosis Reports*. Springer Nature, 15(2), pp. 110–119. doi: 10.1007/s11914-017-0353-4.

van der Lee, M. M. C. *et al.* (2013) 'β-Arrestin-biased signaling of PTH analogs of the type 1 parathyroid hormone receptor.', *Cellular signalling*. Elsevier Inc., 25(2), pp. 527–38. doi: 10.1016/j.cellsig.2012.11.012.

Lee, S. C. *et al.* (2016) 'A method for detergent-free isolation of membrane proteins in their local lipid environment', *Nature Protocols*. Springer Nature, 11(7), pp. 1149–1162. doi: 10.1038/nprot.2016.070.

Liang, X. *et al.* (2002) 'Transcriptionally active polymerase chain reaction (TAP). High throughput gene expression using genome sequence data', *Journal of Biological Chemistry*, 277(5), pp. 3593–3598. doi: 10.1074/jbc.M110652200.

Liang, Y.-L. *et al.* (2017) 'Phase-plate cryo-EM structure of a class B GPCR–G-protein complex', *Nature*. Springer Nature, 546(7656), pp. 118–123. doi: 10.1038/nature22327.

Liang, Y.-L. L. *et al.* (2018) 'Phase-plate cryo-EM structure of a biased agonistbound human GLP-1 receptor-Gs complex', *Nature*. Nature Publishing Group, 555(7694), pp. 121–125. doi: 10.1038/nature25773.

Lightwood, D. *et al.* (2013) 'The discovery, engineering and characterisation of a highly potent anti-human IL-13 fab fragment designed for administration by inhalation.', *Journal of molecular biology*. England, 425(3), pp. 577–593. doi: 10.1016/j.jmb.2012.11.036.

Lim, H.-H. H., Fang, Y. and Williams, C. (2011) 'High-Efficiency Screening of Monoclonal Antibodies for Membrane Protein Crystallography', *PLoS ONE*. Public Library of Science (PLoS), 6(9), p. e24653. doi: 10.1371/journal.pone.0024653.

Liu, J. K. H. (2014) 'The history of monoclonal antibody development – Progress, remaining challenges and future innovations', *Annals of Medicine and Surgery*. Elsevier BV, 3(4), pp. 113–116. doi: 10.1016/j.amsu.2014.09.001.

Liu, L. (2017) 'Pharmacokinetics of monoclonal antibodies and Fc-fusion proteins', *Protein & Cell*. Springer Nature, 9(1), pp. 15–32. doi: 10.1007/s13238-017-0408-4.

Liu, W. *et al.* (2012) 'Structural Basis for Allosteric Regulation of GPCRs by Sodium Ions', *Science*, 337(6091), pp. 232–236. doi: 10.1126/science.1219218.

Lohse, M. *et al.* (1990) 'beta-Arrestin: a protein that regulates beta-adrenergic receptor function', *Science*, 248(4962), pp. 1547–1550. doi: 10.1126/science.2163110.

Luttrell, L. M. *et al.* (1999) 'Beta-arrestin-dependent formation of beta2 adrenergic receptor-Src protein kinase complexes.', *Science (New York, N.Y.)*, 283(5402), pp. 655–61. Available at: http://www.ncbi.nlm.nih.gov/pubmed/9924018 (Accessed: 18 June 2015).

Luttrell, L. M. and Lefkowitz, R. J. (2002) 'The role of beta-arrestins in the termination and transduction of G-protein-coupled receptor signals.', *Journal of cell science*, 115(Pt 3), pp. 455–65. Available at: http://www.ncbi.nlm.nih.gov/pubmed/11861753 (Accessed: 31 May 2015).

Lyons, J. A. *et al.* (2016) 'Expression strategies for structural studies of eukaryotic membrane proteins', *Current Opinion in Structural Biology*. Elsevier BV, 38, pp. 137–144. doi: 10.1016/j.sbi.2016.06.011.

Macarron, R. (2006) 'Critical review of the role of HTS in drug discovery', *Drug Discovery Today*. Elsevier BV, 11(7–8), pp. 277–279. doi: 10.1016/j.drudis.2006.02.001.

Magnani, F. *et al.* (2008) 'Co-evolving stability and conformational homogeneity of the human adenosine A2a receptor', *Proceedings of the National Academy of Sciences*. Proceedings of the National Academy of Sciences, 105(31), pp. 10744–10749. doi: 10.1073/pnas.0804396105.

Mahon, M. J. *et al.* (2002) 'Na(+)/H(+) exchanger regulatory factor 2 directs parathyroid hormone 1 receptor signalling.', *Nature*. Springer Nature, 417(6891), pp. 858–861. doi: 10.1038/nature00816.

Mahon, M. J. and J. Mahon, M. (2012) 'The Parathyroid Hormone Receptorsome and the Potential for Therapeutic Intervention', *Current Drug Targets*. Bentham Science Publishers Ltd., 13(1), pp. 116–128. doi: 10.2174/138945012798868416.

Manglik, A. *et al.* (2012) 'Crystal structure of the μ-opioid receptor bound to a morphinan antagonist', *Nature*, 485(7398), pp. 321–326. doi: 10.1038/nature10954.

Manglik, A., Kobilka, B. K. and Steyaert, J. (2017) 'Nanobodies to Study G Protein–

Coupled Receptor Structure and Function', *Annual Review of Pharmacology and Toxicology*. Annual Reviews, 57(1), pp. 19–37. doi: 10.1146/annurev-pharmtox-010716-104710.

Marcus, R. *et al.* (2013) 'BMS-927711 for the acute treatment of migraine: A double-blind, randomized, placebo controlled, dose-ranging trial', *Cephalalgia*. SAGE Publications, 34(2), pp. 114–125. doi: 10.1177/0333102413500727.

Marvin, D. A. *et al.* (1994) 'Molecular models and structural comparisons of native and mutant class I filamentous bacteriophages Ff (fd, f1, M13), If1 and IKe.', *Journal of molecular biology*, 235(1), pp. 260–86. Available at: http://www.ncbi.nlm.nih.gov/pubmed/8289247 (Accessed: 2 October 2017).

Mary, S. *et al.* (2014) 'Amphipols in G Protein-Coupled Receptor Pharmacology: What Are They Good For?', *Journal of Membrane Biology*. Springer Nature, 247(9–10), pp. 853–860. doi: 10.1007/s00232-014-9665-9.

Matthews, J. E. *et al.* (2008) 'Pharmacodynamics, Pharmacokinetics, Safety, and Tolerability of Albiglutide, a Long-Acting Glucagon-Like Peptide-1 Mimetic, in Patients with Type 2 Diabetes', *The Journal of Clinical Endocrinology & Metabolism*, 93(12), pp. 4810–4817. doi: 10.1210/jc.2008-1518.

Mattle, D. *et al.* (2018) 'Ligand channel in pharmacologically stabilized rhodopsin', *Proceedings of the National Academy of Sciences*. National Academy of Sciences, 115(14), p. 201718084. doi: 10.1073/pnas.1718084115.

McCusker, E. C. *et al.* (2008) 'Heterologous GPCR Expression: A Bottleneck to Obtaining Crystal Structures', *Biotechnology Progress*. Wiley, 23(3), pp. 540–547. doi: 10.1021/bp060349b.

Mead, D. A. and Kemper, B. (1988) 'Chimeric single-stranded DNA phage-plasmid cloning vectors.', *Biotechnology (Reading, Mass.)*, 10, pp. 85–102. Available at: http://www.ncbi.nlm.nih.gov/pubmed/3061525.

Milić, D. *et al.* (2015) 'Large-scale production and protein engineering of G protein-coupled receptors for structural studies', *Frontiers in Pharmacology*. Frontiers Media SA, 6(March), pp. 1–24. doi: 10.3389/fphar.2015.00066.

Miraglia, S. *et al.* (1999) 'Homogeneous Cell- and Bead-Based Assays for High Throughput Screening Using Fluorometric Microvolume Assay Technology.', *Journal of biomolecular screening*, 4(4), pp. 193–204. doi: 10.1177/108705719900400407.

Mitchell, R. *et al.* (1998) 'Rhodopsin-family receptors associate with small G proteins to activate phospholipase D', *Nature*. Springer Nature, 392(6674), pp. 411–414. doi: 10.1038/32937.

Mitra, N. *et al.* (2013) 'Calcium-dependent ligand binding and g-protein signaling of family B GPCR parathyroid hormone 1 receptor purified in nanodiscs', *ACS Chemical Biology*. American Chemical Society (ACS), 8(3), pp. 617–625. doi: 10.1021/cb300466n.

Moore, C. A. C., Milano, S. K. and Benovic, J. L. (2007) 'Regulation of receptor trafficking by GRKs and arrestins.', *Annual review of physiology*, 69, pp. 451–482. doi: 10.1146/annurev.physiol.69.022405.154712.

Moraes, I. *et al.* (2014) 'Membrane protein structure determination — The next generation', *Biochimica et Biophysica Acta (BBA) - Biomembranes*. Elsevier BV, 1838(1), pp. 78–87. doi: 10.1016/j.bbamem.2013.07.010.

Morrison, K. A. *et al.* (2016) 'Membrane protein extraction and purification using

styrene-maleic acid (SMA) copolymer: effect of variations in polymer structure', *Biochemical Journal*. Portland Press Ltd., 473(23), pp. 4349–4360. doi: 10.1042/bcj20160723.

Mujić-Delić, A. *et al.* (2014) 'GPCR-targeting nanobodies: attractive research tools, diagnostics, and therapeutics', *Trends in Pharmacological Sciences*. Elsevier BV, 35(5), pp. 247–255. doi: 10.1016/j.tips.2014.03.003.

Mukund, S. *et al.* (2013) 'Inhibitory mechanism of an allosteric antibody targeting the glucagon receptor', *Journal of Biological Chemistry*. American Society for Biochemistry and Molecular Biology, 288(50), pp. 36168–36178. doi: 10.1074/jbc.M113.496984.

Murakami, M. and Kouyama, T. (2008) 'Crystal structure of squid rhodopsin', *Nature*. Nature Publishing Group, 453(7193), pp. 363–367. doi: 10.1038/nature06925.

Navratilova, I., Besnard, J. J. and Hopkins, A. L. (2011) 'Screening for GPCR Ligands Using Surface Plasmon Resonance', *ACS Medicinal Chemistry Letters*. American Chemical Society (ACS), 2(7), pp. 549–554. doi: 10.1021/ml2000017.

Neer, R. M. *et al.* (2001) 'Effect of Parathyroid Hormone (1-34) on Fractures and Bone Mineral Density in Postmenopausal Women with Osteoporosis', *New England Journal of Medicine*, 344(19), pp. 1434–1441. doi: 10.1056/NEJM200105103441904.

Neubig, R. R. *et al.* (2003) 'International Union of Pharmacology Commitee on Receptorn Nomenclature and Drug Classification.', *Pharmacological Reviews*, 55(4), pp. 597–606. doi: 10.1124/pr.55.4.4.and.

Nixon, A. E., Sexton, D. J. and Ladner, R. C. (2014) 'Drugs derived from phage display from candidate identification to clinical practice', *mAbs*, 6(1), pp. 73–85. doi: 10.4161/mabs.27240.

Noel, J. P., Hamm, H. E. and Sigler, P. B. (1993) 'The 2.2 A crystal structure of transducin-alpha complexed with GTP gamma S.', *Nature*, 366(6456), pp. 654–63. doi: 10.1038/366654a0.

Notredame, C., Higgins, D. G. and Heringa, J. (2000) 'T-coffee: a novel method for fast and accurate multiple sequence alignment 1 1Edited by J. Thornton', *Journal of Molecular Biology*. Elsevier BV, 302(1), pp. 205–217. doi: 10.1006/jmbi.2000.4042.

Oakley, R. H. *et al.* (2000) 'Differential affinities of visual arrestin, βarrestin1, and βarrestin2 for G protein-coupled receptors delineate two major classes of receptors', *Journal of Biological Chemistry*, 275(22), pp. 17201–17210. doi: 10.1074/jbc.M910348199.

Oldham, W. M. and Hamm, H. E. (2008) 'Heterotrimeric G protein activation by G-protein-coupled receptors', *Nature Reviews Molecular Cell Biology*. Springer Nature, 9(1), pp. 60–71. doi: 10.1038/nrm2299.

Olson, W. C. *et al.* (1999) 'Differential inhibition of human immunodeficiency virus type 1 fusion, gp120 binding, and CC-chemokine activity by monoclonal antibodies to CCR5', *Journal of virology*, 73(5), pp. 4145–4155.

Pal, K., Melcher, K. and Xu, H. E. (2012) 'Structure and mechanism for recognition of peptide hormones by Class B G-protein-coupled receptors.', *Acta pharmacologica Sinica*. Nature Publishing Group, 33(3), pp. 300–11. doi: 10.1038/aps.2011.170.

Palczewski, K. *et al.* (2000) 'Crystal Structure of Rhodopsin: A G Protein-Coupled Receptor', *Science*. American Association for the Advancement of Science (AAAS), 289(5480), pp. 739–745. doi: 10.1126/science.289.5480.739.

Parfitt, A. M. *et al.* (1996) 'Hypercalcemia due to constitutive activity of the parathyroid hormone (PTH)/PTH-related peptide receptor: Comparison with primary hyperparathyroidism', *Journal of Clinical Endocrinology and Metabolism*, 81(10), pp. 3584–3588. doi: 10.1210/jc.81.10.3584.

Park, S. H., Das, B. B., *et al.* (2012) 'Structure of the chemokine receptor CXCR1 in phospholipid bilayers', *Nature*. Springer Nature, 491(7426), pp. 779–783. doi: 10.1038/nature11580.

Park, S. H., Das, B. B., *et al.* (2012) 'Structure of the chemokine receptor CXCR1 in phospholipid bilayers', *Nature*. Nature Publishing Group, 491(7426), pp. 779–783. doi: 10.1038/nature11580.

Parthier, C. *et al.* (2009) 'Passing the baton in class B GPCRs: peptide hormone activation via helix induction?', *Trends in biochemical sciences*. Elsevier BV, 34(6), pp. 303–10. doi: 10.1016/j.tibs.2009.02.004.

Pierce, K. L., Premont, R. T. and Lefkowitz, R. J. (2002) 'Seven-transmembrane receptors', *Nature Reviews Molecular Cell Biology*. Springer Nature, 3(9), pp. 639–650. doi: 10.1038/nrm908.

Pioszak, A. A. *et al.* (2009) 'Structural basis for parathyroid hormone-related protein binding to the parathyroid hormone receptor and design of conformation-selective peptides.', *The Journal of biological chemistry*. American Society for Biochemistry & Molecular Biology (ASBMB), 284(41), pp. 28382–28391. doi: 10.1074/jbc.M109.022905.

Pioszak, A. A. *et al.* (2010) 'Dimeric arrangement of the parathyroid hormone receptor and a structural mechanism for ligand-induced dissociation', *Journal of Biological Chemistry*. American Society for Biochemistry & Molecular Biology (ASBMB), 285(16), pp. 12435–12444. doi: 10.1074/jbc.M109.093138.

Pioszak, A. A. and Xu, H. E. (2008) 'Molecular recognition of parathyroid hormone by its G protein-coupled receptor.', *Proceedings of the National Academy of Sciences of the United States of America*. Proceedings of the National Academy of Sciences, 105(13), pp. 5034–9. doi: 10.1073/pnas.0801027105.

Piserchio, A. *et al.* (2000) 'Characterization of Parathyroid Hormone/Receptor Interactions: Structure of the First Extracellular Loop†', *Biochemistry*. American Chemical Society (ACS), 39(28), pp. 8153–8160. doi: 10.1021/bi000196f.

Pitcher, J. A., Freedman, N. J. and Lefkowitz, R. J. (1998) 'G protein-coupled receptor kinases.', *Annual review of biochemistry*. Annual Reviews 4139 El Camino Way, P.O. Box 10139, Palo Alto, CA 94303-0139, USA, 67, pp. 653–92. doi: 10.1146/annurev.biochem.67.1.653.

Popot, J.-L. (2010) 'Amphipols, Nanodiscs, and Fluorinated Surfactants: Three Nonconventional Approaches to Studying Membrane Proteins in Aqueous Solutions', *Annual Review of Biochemistry*. Annual Reviews, 79(1), pp. 737–775. doi: 10.1146/annurev.biochem.052208.114057.

Postis, V. *et al.* (2015) 'The use of SMALPs as a novel membrane protein scaffold for structure study by negative stain electron microscopy', *Biochimica et Biophysica Acta - Biomembranes*. Elsevier B.V., 1848(2), pp. 496–501. doi: 10.1016/j.bbamem.2014.10.018.

Poyner, D. R. and Hay, D. L. (2012) 'Secretin family (Class B) G protein-coupled receptors - from molecular to clinical perspectives.', *British journal of pharmacology*. Wiley, 166(1), pp. 1–3. doi: 10.1111/j.1476-5381.2011.01810.x.

Prather, P. L. (2004) 'Inverse agonists: tools to reveal ligand-specific conformations of G protein-coupled receptors.', *Science's STKE : signal transduction knowledge environment*, 2004(215), p. pe1. doi: 10.1126/stke.2152004pe1.

Rabilloud, T. (2009) 'Membrane proteins and proteomics: Love is possible, but so difficult', *Electrophoresis*, pp. S174–S180. doi: 10.1002/elps.200900050.

Rahmeh, R. *et al.* (2012) 'Structural insights into biased G protein-coupled receptor signaling revealed by fluorescence spectroscopy', *Proceedings of the National Academy of Sciences*. Proceedings of the National Academy of Sciences, 109(17), pp. 6733–6738. doi: 10.1073/pnas.1201093109.

Rasmussen, S. G. F. *et al.* (2007) 'Crystal structure of the human beta2 adrenergic G-protein-coupled receptor.', *Nature*, 450(7168), pp. 383–7. doi: 10.1038/nature06325.

Rasmussen, S. G. F. *et al.* (2007) 'Crystal structure of the human β2adrenergic G-protein-coupled receptor', *Nature*. Nature Publishing Group, 450(7168), pp. 383–387. doi: 10.1038/nature06325.

Rasmussen, S. G. F. *et al.* (2011) 'Crystal structure of the β 2 adrenergic receptor-Gs protein complex', *Nature*. Nature Publishing Group, 477(7366), pp. 549–557. doi: 10.1038/nature10361.

Rasmussen, S. G. F. *et al.* (2011) 'Structure of a nanobody-stabilized active state of the β(2) adrenoceptor.', *Nature*. Nature Publishing Group, 469(7329), pp. 175–80. doi: 10.1038/nature09648.

Rawson, S. *et al.* (2016) 'The changing landscape of membrane protein structural biology through developments in electron microscopy', *Molecular Membrane Biology*. Taylor & Francis, pp. 12–22. doi: 10.1080/09687688.2016.1221533.

Regis, D. P. *et al.* (2008) 'Transcriptionally active PCR for antigen identification and vaccine development: In vitro genome-wide screening and in vivo immunogenicity', *Molecular and Biochemical Parasitology*. Elsevier BV, 158(1), pp. 32–45. doi: 10.1016/j.molbiopara.2007.11.009.

Reiter, E. and Lefkowitz, R. J. (2006) 'GRKs and β-arrestins: roles in receptor silencing, trafficking and signaling', *Trends in Endocrinology and Metabolism*, pp. 159–165. doi: 10.1016/j.tem.2006.03.008.

Rey, A. *et al.* (2006) 'Proline-rich Motifs in the Parathyroid Hormone (PTH)/PTH-related Protein Receptor C Terminus Mediate Scaffolding of c-Src with β-Arrestin2 for ERK1/2 Activation', *Journal of Biological Chemistry*. American Society for Biochemistry & Molecular Biology (ASBMB), 281(50), pp. 38181–38188. doi: 10.1074/jbc.m606762200.

Rief, N. *et al.* (1998) 'Production and characterization of a rabbit monoclonal antibody against human CDC25C phosphatase.', *Hybridoma*, 17(4), pp. 389–94. doi: 10.1089/hyb.1998.17.389.

Ring, A. M. *et al.* (2013) 'Adrenaline-activated structure of β 2-adrenoceptor stabilized by an engineered nanobody', *Nature*, 502(7472), pp. 575–579. doi: 10.1038/nature12572.

Ritter, S. L. and Hall, R. a (2009) 'Fine-tuning of GPCR activity by receptor-interacting proteins', *Nature Reviews Molecular Cell Biology*. Springer Nature, 10(12), pp. 819–830. doi: 10.1038/nrm2803.

Robertson, N. *et al.* (2011) 'The properties of thermostabilised G protein-coupled receptors (StaRs) and their use in drug discovery.', *Neuropharmacology*. Elsevier Ltd, 60(1),

pp. 36–44. doi: 10.1016/j.neuropharm.2010.07.001.

Robertson, N. *et al.* (2018) 'Structure of the complement C5a receptor bound to the extra-helical antagonist NDT9513727', *Nature*. Springer Nature, 553(7686), pp. 111–114. doi: 10.1038/nature25025.

Romero, G. *et al.* (2010) 'Parathyroid Hormone Receptor Directly Interacts with Dishevelled to Regulate β-Catenin Signaling and Osteoclastogenesis', *Journal of Biological Chemistry*. American Society for Biochemistry & Molecular Biology (ASBMB), 285(19), pp. 14756–14763. doi: 10.1074/jbc.m110.102970.

Rosenbaum, D. M. *et al.* (2007) 'GPCR Engineering Yields High-Resolution Structural Insights into 2-Adrenergic Receptor Function', *Science*. American Association for the Advancement of Science (AAAS), 318(5854), pp. 1266–1273. doi: 10.1126/science.1150609.

Rosenbaum, D. M. *et al.* (2011) 'Structure and function of an irreversible agonist-β(2) adrenoceptor complex.', *Nature*. Nature Publishing Group, 469(7329), pp. 236–40. doi: 10.1038/nature09665.

Rovati, G. E., Capra, V. and Neubig, R. R. (2007) 'The highly conserved DRY motif of class A G protein-coupled receptors: beyond the ground state.', *Molecular pharmacology*. American Society for Pharmacology & Experimental Therapeutics (ASPET), 71(4), pp. 959–964. doi: 10.1124/mol.106.029470.

Samaranayake, H. *et al.* (2009) 'Challenges in monoclonal antibody-based therapies', *Annals of Medicine*. Taylor & Francis, pp. 322–331. doi: 10.1080/07853890802698842.

Schiöth, H. B. and Fredriksson, R. (2005) 'The GRAFS classification system of G-protein coupled receptors in comparative perspective', *General and Comparative Endocrinology*. Elsevier BV, 142(1–2), pp. 94–101. doi: 10.1016/j.ygcen.2004.12.018.

Schipani, E. *et al.* (1997) 'Constitutive activation of the cyclic adenosine 3',5'-monophosphate signaling pathway by parathyroid hormone (PTH)/PTH-related peptide receptors mutated at the two loci for Jansen's metaphyseal chondrodysplasia.', *Molecular endocrinology (Baltimore, Md.)*. The Endocrine Society, 11(7), pp. 851–858. doi: 10.1210/me.11.7.851.

Schipani, E. *et al.* (2014) 'A Novel Parathyroid Hormone (PTH)/ PTH-Related Peptide Receptor Mutation in Jansen ' s Metaphyseal Chondrodysplasia *', *The Journal of clinical endocrinology and metabolism*, 84(9), pp. 3052–3057.

Schipani, E., Kruse, K. and Jüppner, H. (1995) 'A constitutively active mutant PTH-PTHrP receptor in Jansen-type metaphyseal chondrodysplasia.', *Science (New York, N.Y.)*, 268(5207), pp. 98–100. doi: 10.1126/science.7701349.

Schlüter, K.-D. (1999) 'PTH and PTHrP: Similar Structures but Different Functions.', *News in physiological sciences : an international journal of physiology produced jointly by the International Union of Physiological Sciences and the American Physiological Society*, 14, pp. 243–249. Available at: http://www.ncbi.nlm.nih.gov/pubmed/11390859 (Accessed: 16 June 2015).

Schwindinger, W. F. *et al.* (1998) 'Coupling of the PTH/PTHrP receptor to multiple G-proteins. Direct demonstration of receptor activation of Gs, Gq/11, and Gi(1) by [alpha-32P]GTP-gamma-azidoanilide photoaffinity labeling.', *Endocrine*, 8(2), pp. 201–209. doi: 10.1385/ENDO:8:2:201.

Seah, Y. F. S., Hu, H. and Merten, C. A. (2018) 'Microfluidic single-cell technology in

immunology and antibody screening', *Molecular Aspects of Medicine*. Pergamon, pp. 47–61. doi: 10.1016/j.mam.2017.09.004.

Seddon, A. M., Curnow, P. and Booth, P. J. (2004) 'Membrane proteins, lipids and detergents: not just a soap opera', *Biochimica et Biophysica Acta (BBA) - Biomembranes*. Elsevier BV, 1666(1–2), pp. 105–117. doi: 10.1016/j.bbamem.2004.04.011.

Serrano-Vega, M. J. *et al.* (2008) 'Conformational thermostabilization of the 1-adrenergic receptor in a detergent-resistant form', *Proceedings of the National Academy of Sciences*. Proceedings of the National Academy of Sciences, 105(3), pp. 877–882. doi: 10.1073/pnas.0711253105.

Shenoy, S. K. and Lefkowitz, R. J. (2003) 'Trafficking Patterns of β-Arrestin and G Protein-coupled Receptors Determined by the Kinetics of β-Arrestin Deubiquitination', *Journal of Biological Chemistry*. American Society for Biochemistry & Molecular Biology (ASBMB), 278(16), pp. 14498–14506. doi: 10.1074/jbc.m209626200.

Shi, L. *et al.* (2015) 'Pharmacologic Characterization of AMG 334, a Potent and Selective Human Monoclonal Antibody against the Calcitonin Gene-Related Peptide Receptor', *Journal of Pharmacology and Experimental Therapeutics*. American Society for Pharmacology & Experimental Therapeutics (ASPET), 356(1), pp. 223–231. doi: 10.1124/jpet.115.227793.

Shi, L. *et al.* (2016) 'Pharmacologic Characterization of AMG 334, a Potent and Selective Human Monoclonal Antibody against the Calcitonin Gene-Related Peptide Receptor', *J Pharmacol Exp Ther*, 356(1), pp. 223–231. doi: 10.1124/jpet.115.227793\rjpet.115.227793 [pii].

Shibata, Y. *et al.* (2009) 'Thermostabilization of the Neurotensin Receptor NTS1', *Journal of Molecular Biology*, 390(2), pp. 262–277. doi: 10.1016/j.jmb.2009.04.068.

Shimada, M. *et al.* (2002) 'Purification and Characterization of a Receptor for Human Parathyroid Hormone and Parathyroid Hormone-related Peptide', *Journal of Biological Chemistry*. American Society for Biochemistry & Molecular Biology (ASBMB), 277(35), pp. 31774–31780. doi: 10.1074/jbc.m204166200.

Shimamura, T. *et al.* (2011) 'Structure of the human histamine H1 receptor complex with doxepin.', *Nature*. Nature Publishing Group, 475(7354), pp. 65–70. doi: 10.1038/nature10236.

Shukla, A. K. *et al.* (2013) 'Structure of active β-arrestin-1 bound to a G-protein-coupled receptor phosphopeptide', *Nature*. Springer Nature, 497(7447), pp. 137–141. doi: 10.1038/nature12120.

Shukla, A. K. *et al.* (2014) 'Visualization of arrestin recruitment by a G-protein-coupled receptor', *Nature*. Nature Publishing Group, 512(7513), pp. 218–222. doi: 10.1038/nature13430.

Simon, M. I., Strathmann, M. P. and Gautam, N. (1991) 'Diversity of G proteins in signal transduction.', *Science (New York, N.Y.)*, 252(5007), pp. 802–808. doi: 10.1126/science.1902986.

Singh, A. T. K. *et al.* (2005) 'Gα12/Gα13Subunits of Heterotrimeric G Proteins Mediate Parathyroid Hormone Activation of Phospholipase D in UMR-106 Osteoblastic Cells', *Endocrinology*. The Endocrine Society, 146(5), pp. 2171–2175. doi: 10.1210/en.2004-1283.

Siu, F. Y. *et al.* (2013) 'Structure of the human glucagon class B G-protein-coupled

receptor.', *Nature*. Springer Nature, 499(7459), pp. 444–9. doi: 10.1038/nature12393.

Smith, A. J. (2015) 'New horizons in therapeutic antibody discovery: Opportunities and challenges versus small-molecule therapeutics', *Journal of Biomolecular Screening*, 20(4), pp. 437–453. doi: 10.1177/1087057114562544.

Smith, G. (1985) 'Filamentous fusion phage: novel expression vectors that display cloned antigens on the virion surface', *Science*, 228(4705), pp. 1315–1317. doi: 10.1126/science.4001944.

Smith, G. P. and Petrenko, V. A. (1997) 'Phage Display', *Chemical Reviews*. American Chemical Society (ACS), 97(2), pp. 391–410. doi: 10.1021/cr960065d.

Srivastava, A. *et al.* (2014) 'High-resolution structure of the human GPR40 receptor bound to allosteric agonist TAK-875.', *Nature*. Nature Publishing Group, 513(7516), pp. 124–7. doi: 10.1038/nature13494.

Stacey, M. *et al.* (2000) 'LNB-TM7, a group of seven-transmembrane proteins related to family-B G-protein-coupled receptors', *Trends in Biochemical Sciences*, pp. 284–289. doi: 10.1016/S0968-0004(00)01583-8.

Standfuss, J. *et al.* (2007) 'Crystal Structure of a Thermally Stable Rhodopsin Mutant', *Journal of Molecular Biology*, 372(5), pp. 1179–1188. doi: 10.1016/j.jmb.2007.03.007.

Starkie, D. O. *et al.* (2016) 'Generation of Recombinant Monoclonal Antibodies from Immunised Mice and Rabbits via Flow Cytometry and Sorting of Antigen-Specific IgG+ Memory B Cells', *PLOS ONE*. Public Library of Science (PLoS), 11(3), p. e0152282. doi: 10.1371/journal.pone.0152282.

Sun, C. *et al.* (2018) 'Structure of the alternative complex III in a supercomplex with cytochrome oxidase', *Nature*. Springer Nature, 557(7703), pp. 123–126. doi: 10.1038/s41586-018-0061-y.

Suzuki, Y. *et al.* (2018) 'Functional G-Protein-Coupled Receptor (GPCR) Synthesis: The Pharmacological Analysis of Human Histamine H1 Receptor (HRH1) Synthesized by a Wheat Germ Cell-Free Protein Synthesis System Combined with Asolectin Glycerosomes', *Frontiers in Pharmacology*. Frontiers Media SA, 9(FEB), p. 38. doi: 10.3389/fphar.2018.00038.

Syme, C. A., Friedman, P. A. and Bisello, A. (2005) 'Parathyroid hormone receptor trafficking contributes to the activation of extracellular signal-regulated kinases but is not required for regulation of cAMP signaling.', *The Journal of biological chemistry*. American Society for Biochemistry & Molecular Biology (ASBMB), 280(12), pp. 11281–11288. doi: 10.1074/jbc.M413393200.

Tan, Q. *et al.* (2013) 'Structure of the CCR5 chemokine receptor-HIV entry inhibitor maraviroc complex', *Science*, 341(6152), pp. 1387–1390. doi: 10.1126/science.1241475.

Tate, C. G. (2012) 'A crystal clear solution for determining G-protein-coupled receptor structures', *Trends in Biochemical Sciences*. Elsevier Ltd, 37(9), pp. 343–352. doi: 10.1016/j.tibs.2012.06.003.

Tawfeek, H. A. W., Qian, F. and Abou-Samra, A. B. (2002) 'Phosphorylation of the Receptor for PTH and PTHrP Is Required for Internalization and Regulates Receptor Signaling', *Molecular Endocrinology*. The Endocrine Society, 16(1), pp. 1–13. doi: 10.1210/mend.16.1.0760.

Tehan, B. G. *et al.* (2014) 'Unifying Family A GPCR Theories of Activation',

Pharmacology & Therapeutics. Elsevier BV, 143(1), pp. 51–60. doi: 10.1016/j.pharmthera.2014.02.004.

Tesmer, J. J. G. (2010) 'The quest to understand heterotrimeric G protein signaling', *Nature Structural & Molecular Biology*. Springer Nature, 17(6), pp. 650–652. doi: 10.1038/nsmb0610-650.

Thompson, A. A. *et al.* (2012) 'Structure of the nociceptin/orphanin FQ receptor in complex with a peptide mimetic', *Nature*. Nature Publishing Group, 485(7398), pp. 395–399. doi: 10.1038/nature11085.

Tickle, S. *et al.* (2009) 'High-Throughput Screening for High Affinity Antibodies', *Journal of the Association for Laboratory Automation*. SAGE Publications, 14(5), pp. 303–307. doi: 10.1016/j.jala.2009.05.004.

Tickle, S. *et al.* (2015) 'A fully automated primary screening system for the discovery of therapeutic antibodies directly from B cells.', *Journal of biomolecular screening*. SAGE Publications, 20(4), pp. 492–7. doi: 10.1177/1087057114564760.

Tribet, C., Audebert, R. and Popot, J.-L. L. (1996) 'Amphipols: Polymers that keep membrane proteins soluble in aqueous solutions', *Proceedings of the National Academy of Sciences*. Proceedings of the National Academy of Sciences, 93(26), pp. 15047–15050. doi: 10.1073/pnas.93.26.15047.

Umbhauer, M. *et al.* (2000) 'The C-terminal cytoplasmic Lys-Thr-X-X-X-Trp motif in frizzled receptors mediates Wnt/beta-catenin signalling', *The EMBO Journal*. Wiley, 19(18), pp. 4944–4954. doi: 10.1093/emboj/19.18.4944.

Unal, H. and Karnik, S. S. (2012) 'Domain coupling in GPCRs: the engine for induced conformational changes', *Trends in Pharmacological Sciences*. Elsevier BV, 33(2), pp. 79–88. doi: 10.1016/j.tips.2011.09.007.

Underwood, C. R. *et al.* (2009) 'Crystal Structure of Glucagon-like Peptide-1 in Complex with the Extracellular Domain of the Glucagon-like Peptide-1 Receptor', *Journal of Biological Chemistry*. American Society for Biochemistry & Molecular Biology (ASBMB), 285(1), pp. 723–730. doi: 10.1074/jbc.m109.033829.

Vadas, O. and Burke, J. E. (2015) 'Probing the dynamic regulation of peripheral membrane proteins using hydrogen deuterium exchange-MS (HDX-MS)', *Biochemical Society Transactions*, 43(5), pp. 773–786. doi: 10.1042/BST20150065.

Vaughn, J. L. *et al.* (1977) 'The establishment of two cell lines from the insect Spodoptera frugiperda (Lepidoptera; Noctuidae).', *In vitro*, 13(4), pp. 213–7. doi: 10.1007/BF02615077.

Venkatakrishnan, a J. *et al.* (2013) 'Molecular signatures of G-protein-coupled receptors.', *Nature*. Nature Publishing Group, 494(7436), pp. 185–94. doi: 10.1038/nature11896.

Vilardaga, J.-P. P. *et al.* (2010) 'Molecular basis of parathyroid hormone receptor signaling and trafficking: a family B GPCR paradigm', *Cellular and Molecular Life Sciences*. Springer Nature, 68(1), pp. 1–13. doi: 10.1007/s00018-010-0465-9.

Vinothkumar, K. R. and Henderson, R. (2016) 'Single particle electron cryomicroscopy: trends, issues and future perspective', *Quarterly Reviews of Biophysics*. Cambridge University Press (CUP), 49, p. e13. doi: 10.1017/s0033583516000068.

Voss, T. *et al.* (2016) 'A phase IIb randomized, double-blind, placebo-controlled trial of

ubrogepant for the acute treatment of migraine', *Cephalalgia*. SAGE Publications, 36(9), pp. 887–898. doi: 10.1177/0333102416653233.

Vroling, B. *et al.* (2013) 'GPCRDB: an information system for G protein-coupled receptors', *Nucleic Acids Research*. Oxford University Press (OUP), 42(D1), pp. D422–D425. doi: 10.1093/nar/gkt1255.

Wacker, D. *et al.* (2010) 'Conserved Binding Mode of Human β2Adrenergic Receptor Inverse Agonists and Antagonist Revealed by X-ray Crystallography', *Journal of the American Chemical Society*. American Chemical Society (ACS), 132(33), pp. 11443–11445. doi: 10.1021/ja105108q.

Wacker, D. *et al.* (2017) 'Crystal Structure of an LSD-Bound Human Serotonin Receptor', *Cell*. Elsevier BV, 168(3), p. 377–389.e12. doi: 10.1016/j.cell.2016.12.033.

Wajcberg, E. and Amarah, A. (2010) 'Liraglutide in the management of type 2 diabetes', *Drug Design, Development and Therapy*. Dove Medical Press Ltd., 4, p. 279. doi: 10.2147/dddt.s10180.

Wan, H. (2016) 'An Overall Comparison of Small Molecules and Large Biologics in ADME Testing', *Admet & Dmpk*, 4(1), p. 1. doi: 10.5599/admet.4.1.276.

Wang, C., Jiang, Y., *et al.* (2013) 'Structural Basis for Molecular Recognition at Serotonin Receptors', *Science*. American Association for the Advancement of Science (AAAS), 340(6132), pp. 610–614. doi: 10.1126/science.1232807.

Wang, C., Wu, H., Katritch, V., Han, G. W., Huang, X. P., *et al.* (2013) 'Structure of the human smoothened receptor bound to an antitumour agent', *Nature*. Nature Publishing Group, 497(7449), pp. 338–343. doi: 10.1038/nature12167.

Wang, C., Wu, H., Katritch, V., Han, G. W., Huang, X.-P., *et al.* (2013) 'Structure of the human smoothened receptor bound to an antitumour agent.', *Nature*. Nature Publishing Group, 497(7449), pp. 338–43. doi: 10.1038/nature12167.

Warne, T. *et al.* (2008a) 'Structure of a beta1-adrenergic G-protein-coupled receptor.', *Nature*, 454(7203), pp. 486–91. doi: 10.1038/nature07101.

Warne, T. *et al.* (2008b) 'Structure of a β1-adrenergic G-protein-coupled receptor', *Nature*. Springer Nature, 454(7203), pp. 486–491. doi: 10.1038/nature07101.

Waterhouse, A. M. *et al.* (2009) 'Jalview Version 2--a multiple sequence alignment editor and analysis workbench', *Bioinformatics*. Oxford University Press (OUP), 25(9), pp. 1189–1191. doi: 10.1093/bioinformatics/btp033.

Weber, J., Peng, H. and Rader, C. (2017) 'From rabbit antibody repertoires to rabbit monoclonal antibodies', *Experimental & Molecular Medicine*. Springer Nature, 49(3), pp. e305–e305. doi: 10.1038/emm.2017.23.

Weichert, D. *et al.* (2014) 'Covalent agonists for studying G protein-coupled receptor activation', *Proceedings of the National Academy of Sciences*. National Academy of Sciences, 111(29), pp. 10744–10748. doi: 10.1073/pnas.1410415111.

Wheatley, M. *et al.* (2012) 'Lifting the lid on GPCRs: The role of extracellular loops', *British Journal of Pharmacology*. Wiley, 165(6), pp. 1688–1703. doi: 10.1111/j.1476-5381.2011.01629.x.

White, J. F. *et al.* (2012a) 'Structure of the agonist-bound neurotensin receptor', *Nature*. Nature Publishing Group, 490(7421), pp. 508–513. doi: 10.1038/nature11558.

White, J. F. *et al.* (2012b) 'Structure of the agonist-bound neurotensin receptor.', *Nature*. Nature Publishing Group, 490(7421), pp. 508–513. doi: 10.1038/nature11558.

Whitfield, J. F. and Morley, P. (1995) 'Small bone-building fragments of parathyroid hormone: New therapeutic agents for osteoporosis', *Trends in Pharmacological Sciences*, pp. 382–386. doi: 10.1016/S0165-6147(00)89079-3.

Williams, C. (2004) 'cAMP detection methods in HTS: selecting the best from the rest', *Nature Reviews Drug Discovery*. Springer Nature, 3(2), pp. 125–135. doi: 10.1038/nrd1306.

Winter, T. A. *et al.* (2004) 'Intravenous CDP870, a PEGylated Fab′ fragment of a humanized antitumour necrosis factor antibody, in patients with moderate-to-severe Crohn's disease: An exploratory study', *Alimentary Pharmacology and Therapeutics*, 20(11–12), pp. 1337–1346. doi: 10.1111/j.1365-2036.2004.02285.x.

van der Woning, B. *et al.* (2016) 'DNA immunization combined with scFv phage display identifies antagonistic GCGR specific antibodies and reveals new epitopes on the small extracellular loops', *mAbs*. Taylor & Francis, 8(6), pp. 1126–1135. doi: 10.1080/19420862.2016.1189050.

Woolley, M. J. *et al.* (2017) 'Understanding the molecular functions of the second extracellular loop (ECL2) of the calcitonin gene-related peptide (CGRP) receptor using a comprehensive mutagenesis approach', *Molecular and Cellular Endocrinology*. Elsevier BV, 454, pp. 39–49. doi: 10.1016/j.mce.2017.05.034.

Wu, B. *et al.* (2010) 'Structures of the CXCR4 Chemokine GPCR with Small-Molecule and Cyclic Peptide Antagonists', *Science*. American Association for the Advancement of Science (AAAS), 330(6007), pp. 1066–1071. doi: 10.1126/science.1194396.

Wu, H. *et al.* (2012) 'Structure of the human κ-opioid receptor in complex with JDTic', *Nature*. Springer Nature, 485(7398), pp. 327–332. doi: 10.1038/nature10939.

Wu, H., Wang, C., Gregory, K. J., *et al.* (2014) 'Structure of a class C GPCR metabotropic glutamate receptor 1 bound to an allosteric modulator', *Science*. American Association for the Advancement of Science, 344(6179), pp. 58–64. doi: 10.1126/science.1249489.

Wu, H., Wang, C., Gregory, K. J., *et al.* (2014) 'Structure of a class C GPCR metabotropic glutamate receptor 1 bound to an allosteric modulator', *Science*, 344(6179), pp. 58–64. doi: 10.1126/science.1249489.

Xu, F. *et al.* (2011) 'Structure of an agonist-bound human A2A adenosine receptor', *Science*. NIH Public Access, 332(6027), pp. 322–327. doi: 10.1126/science.1202793.

Yan, H. *et al.* (2009) 'Fully Human Monoclonal Antibodies Antagonizing the Glucagon Receptor Improve Glucose Homeostasis in Mice and Monkeys', *Journal of Pharmacology and Experimental Therapeutics*. American Society for Pharmacology & Experimental Therapeutics (ASPET), 329(1), pp. 102–111. doi: 10.1124/jpet.108.147009.

Yang, D. *et al.* (2016) 'Structural Determinants of Binding the Seven- transmembrane Domain of the Glucagon-like Peptide-1 Receptor (GLP-1R)', *Journal of Biological Chemistry*, 291(25), pp. 12991–13004. doi: 10.1074/jbc.M116.721977.

Yang, L. *et al.* (2015) 'Conformational states of the full-length glucagon receptor', *Nature Communications*. Nature Publishing Group, 6(1), p. 7859. doi: 10.1038/ncomms8859.

Yeliseev, A., Zoubak, L. and Schmidt, T. G. M. M. (2017) 'Application of Strep-Tactin XT for affinity purification of Twin-Strep-tagged CB 2 , a G protein-coupled cannabinoid

receptor', *Protein Expression and Purification*. Elsevier BV, 131, pp. 109–118. doi: 10.1016/j.pep.2016.11.006.

Yin, J. *et al.* (2014) 'Crystal structure of the human OX2 orexin receptor bound to the insomnia drug suvorexant', *Nature*. Springer Nature, 519(7542), pp. 247–250. doi: 10.1038/nature14035.

Yu, X. *et al.* (2008) 'An optimized electrofusion-based protocol for generating virus-specific human monoclonal antibodies', *Journal of Immunological Methods*. Elsevier BV, 336(2), pp. 142–151. doi: 10.1016/j.jim.2008.04.008.

Zhang, C. *et al.* (2012) 'High-resolution crystal structure of human protease-activated receptor 1', *Nature*. Springer Nature, 492(7429), pp. 387–392. doi: 10.1038/nature11701.

Zhang, C. (2012) 'Hybridoma Technology for the Generation of Monoclonal Antibodies', *Methods in Molecular Biology*. Humana Press, pp. 117–135. doi: 10.1007/978-1-61779-931-0_7.

Zhang, H. H. *et al.* (2017) 'Structure of the full-length glucagon class B G-protein-coupled receptor', *Nature*. Nature Publishing Group, 546(7657), pp. 259–264. doi: 10.1038/nature22363.

Zhang, H. H. *et al.* (2018) 'Structure of the glucagon receptor in complex with a glucagon analogue', *Nature*. Springer Nature, 553(7686), pp. 106–110. doi: 10.1038/nature25153.

Zhang, J. *et al.* (2010) 'Fusion partners as a tool for the expression of difficult proteins in mammalian cells', *Current Pharmaceutical Biotechnology*, 11(3), pp. 241–245. doi: 10.2174/138920110791111898.

Zhang, K. *et al.* (2014) 'Structure of the human P2Y<inf>12</inf> receptor in complex with an antithrombotic drug', *Nature*, 508(7498), pp. 115–8. doi: 10.1038/nature13083.

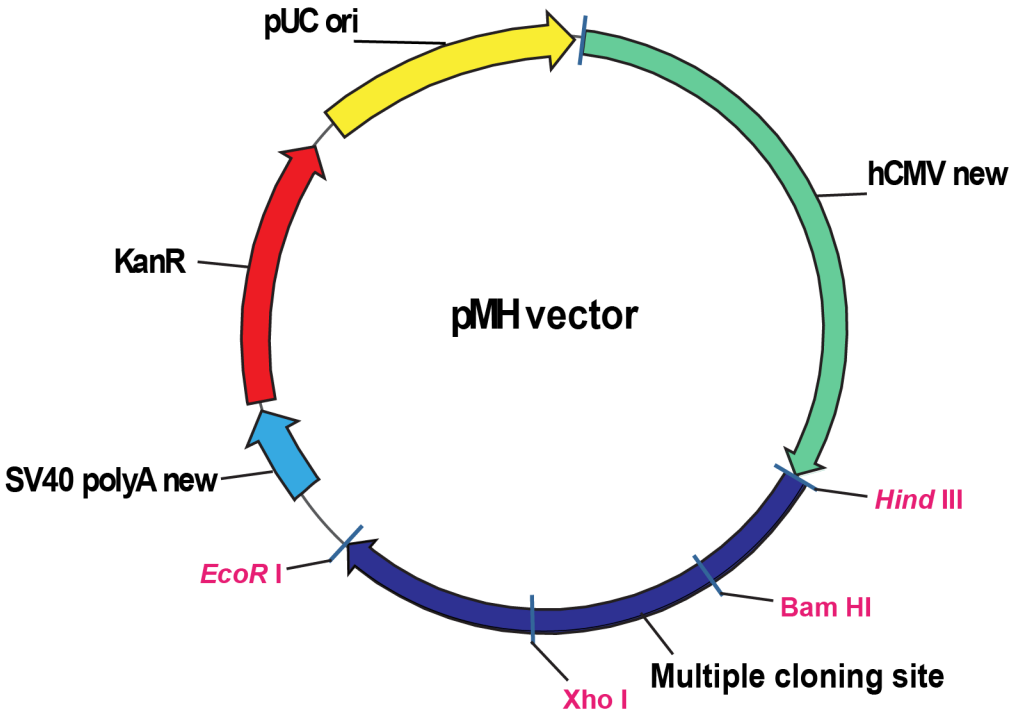
Zhang, P. *et al.* (1998) 'A Homozygous Inactivating Mutation in the Parathyroid Hormone/Parathyroid Hormone-Related Peptide Receptor Causing Blomstrand Chondrodysplasia', *Journal of Clinical Endocrinology & Metabolism*. The Endocrine Society, 83(9), pp. 3373–3376. doi: 10.1210/jc.83.9.3373.

Zhang, X. *et al.* (2010) 'Dynamics of the beta2-adrenergic G-protein coupled receptor revealed by hydrogen-deuterium exchange.', *Analytical chemistry*, 82(3), pp. 1100–8. doi: 10.1021/ac902484p.

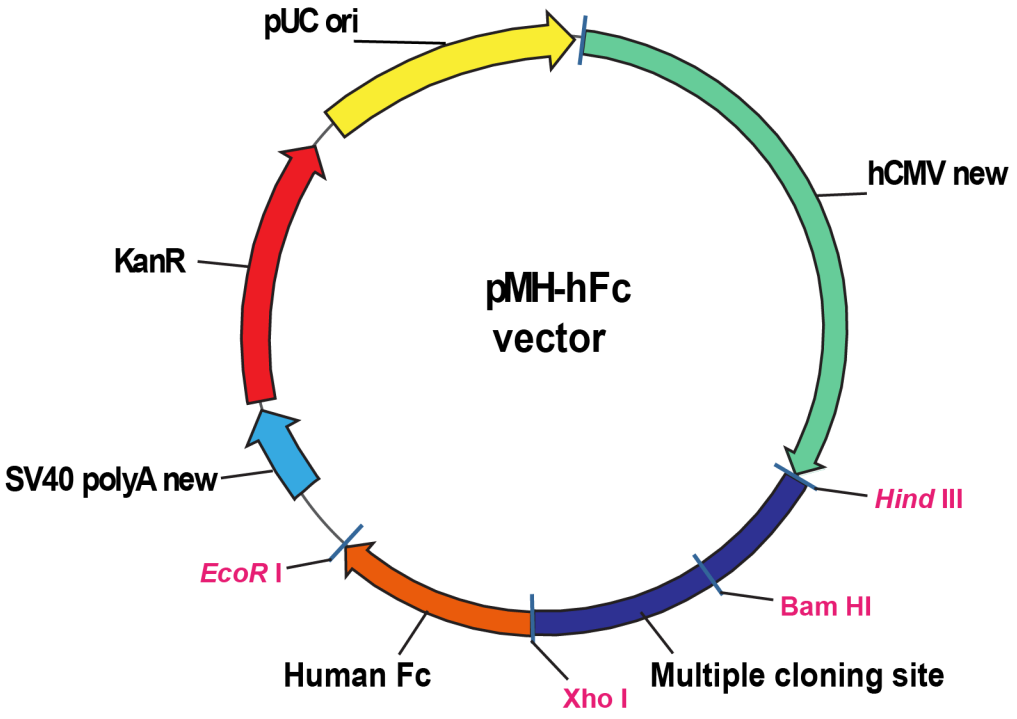
Zhang, Y. *et al.* (2017) 'Cryo-EM structure of the activated GLP-1 receptor in complex with a G protein', *Nature*. Nature Publishing Group, 546(7657), pp. 248–253. doi: 10.1038/nature22394.

Zou, Y., Weis, W. I. and Kobilka, B. K. (2012) 'N-Terminal T4 Lysozyme Fusion Facilitates Crystallization of a G Protein Coupled Receptor', *PLoS ONE*. Edited by R. Seifert, 7(10), p. e46039. doi: 10.1371/journal.pone.0046039.

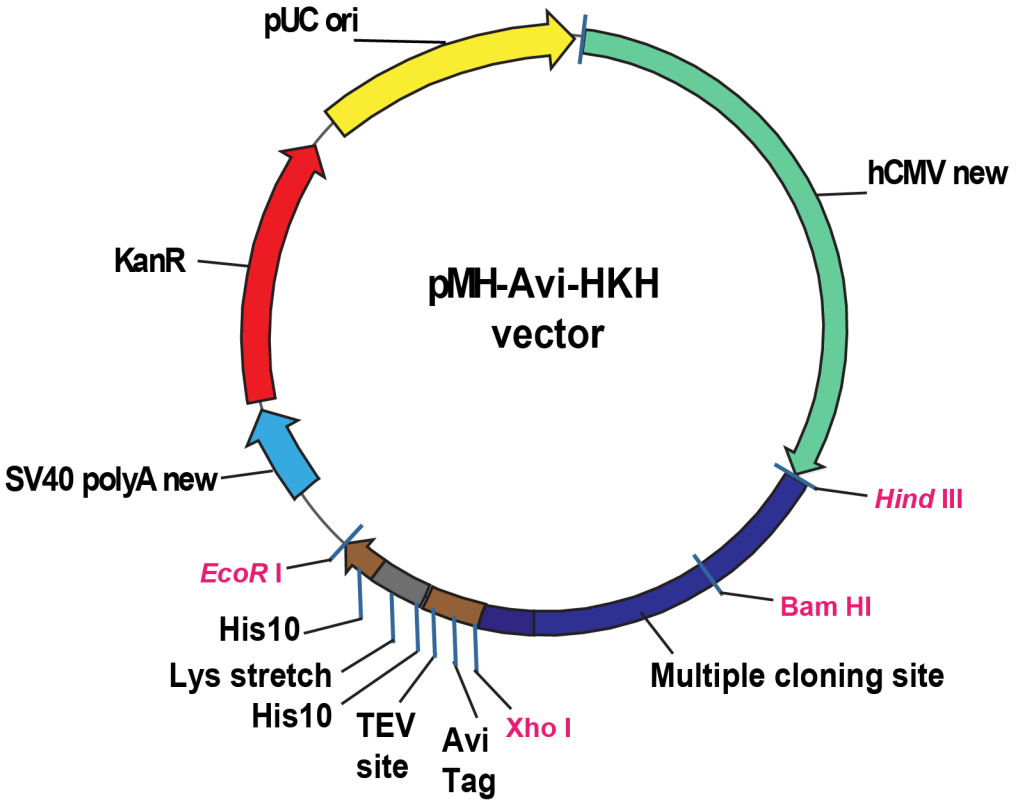
Supplementary data



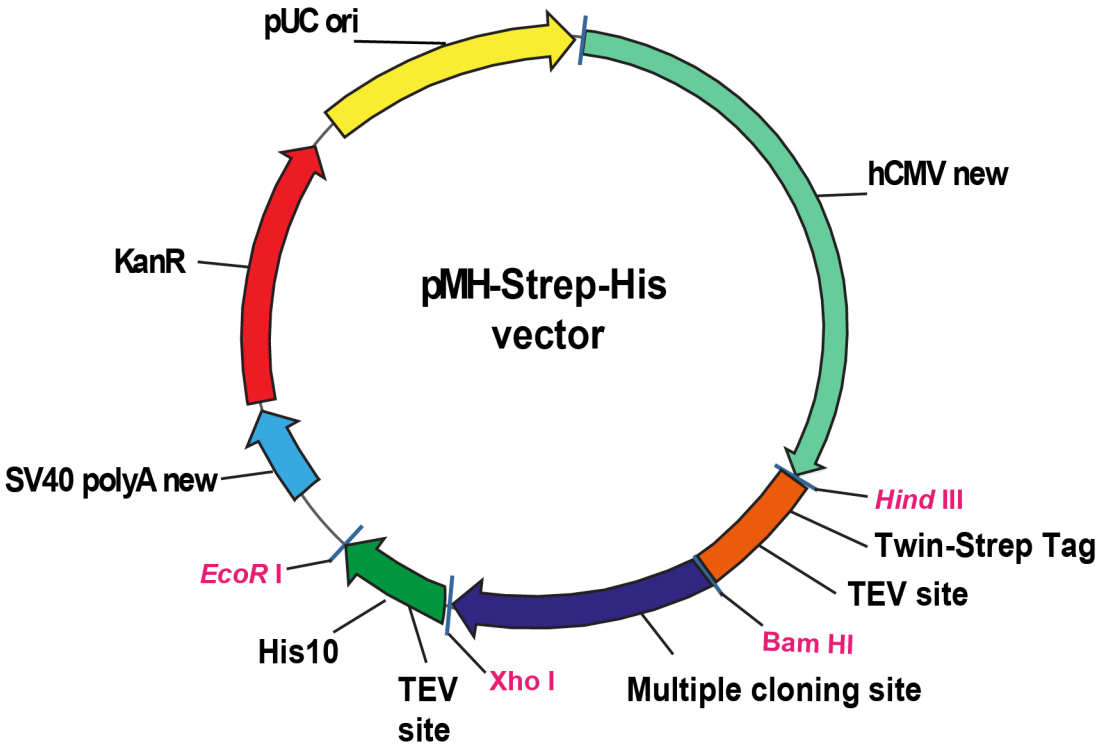
Supplementary Data 1: A schematic of pMH plasmid map



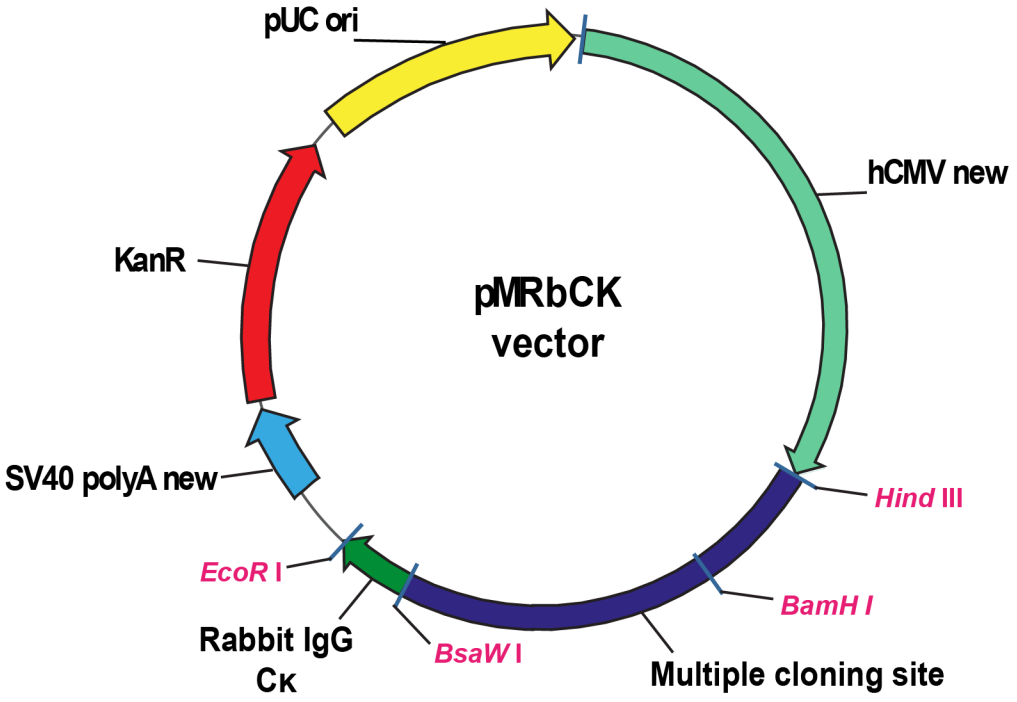
Supplementary Data 2: A schematic of pMH-hFc plasmid map



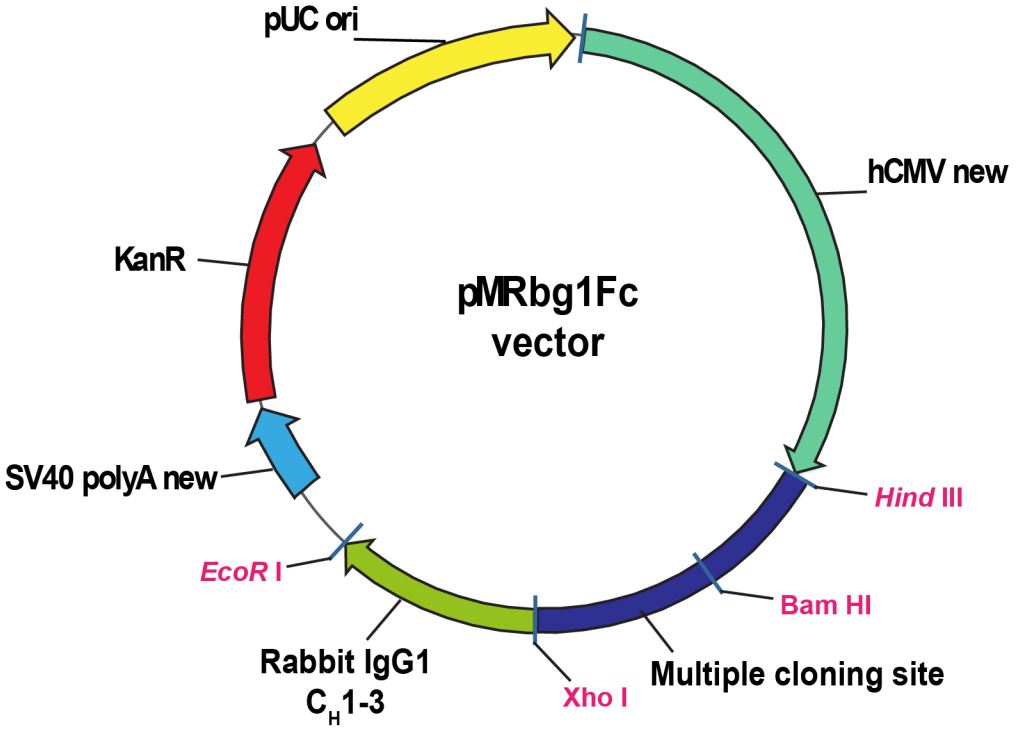
Supplementary Data 3: A schematic of pMH-Avi-HKH plasmid map



Supplementary Data 4: A schematic of pMH-Strep-His plasmid map



Supplementary Data 5: A schematic of pMRbCK plasmid map.



Supplementary Data 6: A schematic of pMRbg1Fc plasmid map.

RB1TAP (KOD 1)
Close cycler lid to 250N
Heat lid to 105°C for 2 min 0 sec
Hold 96°C for 2 min 0 sec
Start cycle loop (40 cycles)
Hold 96°C for 0 min 15 sec
Hold 55°C for 0 min 15 sec
Hold 68°C for 1 min 0 sec
End cycle loop
Hold 68°C for 5 min 0 sec
Hold 10°C for 1 min 0 sec
Open cycler lid
Deactivate lid heating

Supplementary Data 7: PCR cycle details for RB1TAP (KOD1).

RB2TAPH
Close cycler lid to 250N
Heat lid to 105°C for 2 min 0 sec
Hold 96°C for 2 min 0 sec
Start cycle loop (40 cycles)
Hold 96°C for 0 min 15 sec
Hold 60°C for 0 min 15 sec
Hold 68°C for 0 min 50 sec
End cycle loop
Hold 68°C for 3 min 0 sec
Hold 10°C for 1 min 0 sec
Open cycler lid
Deactivate lid heating

Supplementary Data 8: PCR cycle details for RB2TAPH

RB2TAPK
Close cycler lid to 250N
Heat lid to 105°C for 2 min 0 sec
Hold 96°C for 2 min 0 sec
Start cycle loop (40 cycles)
Hold 96°C for 0 min 15 sec
Hold 55°C for 0 min 15 sec
Hold 68°C for 0 min 50 sec
End cycle loop
Hold 68°C for 3 min 0 sec
Hold 10°C for 1 min 0 sec
Open cycler lid
Deactivate lid heating

Supplementary Data 9: PCR cycle details for RB2TAPK

TAPOPT
Close cycler lid to 250N
Heat lid to 105°C for 2 min 0 sec
Hold 98°C for 2 min 0 sec
Start cycle loop (25 cycles)
Hold 98°C for 0 min 30 sec
Hold 66°C for 3 min 0 sec
End cycle loop
Hold 66°C for 10 min 0 sec
Hold 4°C for ever
Open cycler lid
Deactivate lid heating

Supplementary Data 10: PCR cycle details for TAPOPT

TAP1
Close cycler lid to 250N
Heat lid to 105°C for 2 min 0 sec
Hold 98°C for 1 min 0 sec
Start cycle loop (29 cycles)
Hold 98°C for 0 min 30 sec
Hold55°C for 0 min 30 sec
Hold 68°C for 0 min 30 sec
End cycle loop
Hold 68°C for 5 min 0 sec
Hold 4°C for ever
Open cycler lid
Deactivate lid heating

Supplementary Data 11: PCR cycle details for TAP1

TAP2
Close cycler lid to 250N
Heat lid to 105°C for 2 min 0 sec
Hold 98°C for 1 min 0 sec
Start cycle loop (29 cycles)
Hold 98°C for 0 min 30 sec
Hold 61°C for 0 min 30 sec
Hold 68°C for 3 min 0 sec
End cycle loop
Hold 68°C for 10 min 0 sec
Hold 4°C for ever
Open cycler lid
Deactivate lid heating

Supplementary Data 12: PCR cycle details for TAP2

ECL-mAb Fab Heavy chain

QCQSVEESGGRLVTPGTPLTLACTAS**GIDLSSHAMT**WVRQAPGEGLEYIG**LIGASSETWY**
ADWAKGRFTISKTSTTVDLKIAGPTIEDTATYFCAS**HGSSPYWWAANI**WGPGTLVTVSSGQ
PKAPSVFPLAPCCGDTPSSTVTLGCLVKGYLPEPVTVTWNSGTLTNGVRTFPSVRQSSGLY
SLSSVVSVTSSSQPVTCNVAHPATNTKVDKTVAPSTCSKP
ECL-mAb Fab Light chain

QVLTQTTSPVSAAVGGTVSISC**QASESVVNKNRLA**WFQQKPGQSPKLLIY**LASTLDS**GVPS
RFKGSGSGTEFTLIISDLECDDAATYYC**AGAYKNNIFV**FGGGTEVVVKRTPVAPTVLIFPPAA
DQVATGTVTIVCVANKYFPDVTVTWEVDGTTQTTGIENSKTPQNSADCTYNLSSTLTLTSTQ
YNSHKEYTCKVTQGTTSVVQSFNRGDC
CDRs in RED

Supplementary Data 13: Amino acid sequence of ECL-mAb

ECD-mAb Heavy chain

QVQLVQSGGGLVQPGGSLRLSCAVS**GFTFSSYEM**NWVRQAPGEGPEWVA**YISSSSSTIYY**
ADSVKGRFTISRDNAKNSLYLQMNSLRAEDTAVYYCAR**RGLGISGFDY**WGQGTLVTVSSA
STKGPSVFPLAPSSKSTSGGTAALGCLVKDYFPEPVTVSWNSGALTSGVHTFPAVLQSSGL
YSLSSVVTVPSSSLGTQTYICNVNHKPSNTKVDKKVEPKSC
ECD-mAb Light chain

QSALTQPPSASGSPGQSVTISC**TGTSSDVGGYKYVS**WYQQHPGKAPKLMIS**EVSKRP**SGV
PDRFSGSKSDNTASLTITGLQPEDEADYYC**CSYADTYSGYV**FGSGTKVTVLRTVAAPSVFIF
PPSDEQLKSGTASVVCLLNNFYPREAKVQWKVDNALQSGNSQESVTEQDSKDSTYSLSST
LTLSKADYEKHKVYACEVTHQGLSSPVTKSFNRGEC
CDRs in RED

Supplementary Data 14: Amino acid sequence of ECD-mAb